The Development and Characterisation

of

Some Novel Amperometric Sensors

by

Dónal Patrick Leech

A thesis submitted for the Degree

of

Doctor of Philosophy

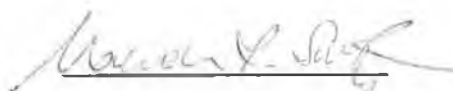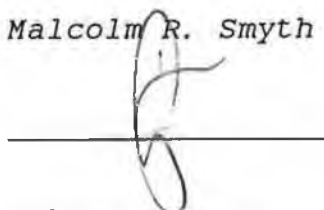Dublin City University   August 1991

Declaration

*I hereby declare that the contents of this thesis,
except where otherwise stated, are based entirely on my
own work, which was carried out in the School of
Chemical Sciences, Dublin City University, Dublin and
in the Department of Chemistry, New Mexico State
University, Las Cruces, New Mexico, U.S.A.*

Donal Leech

Malcolm R. Smyth

Johannes G. Vos

(Supervisors)

(ii)

To Elaine and my parents

Acknowledgements

I wish to acknowledge the following people and to thank them sincerely for their help and encouragement throughout my postgraduate studies,

The staff at D.C.U., School of Chemical Sciences, especially the technical staff, Teresa, Ita, Mick, Peig, Veronica, Fintan and Maurice,

All my fellow postgraduates especially Alan, Paula, Eleanor, Boris, Kieran, Andrew and all the lads in Dublin and Dr. Ozsoz, Dr. Li, Teddy, Bert and Sandra in Las Cruces,

Dr. Robert Forster for his advice, guidance and stimulating conversations,

Prof. Joe Wang for giving me the opportunity to work with him in New Mexico,

My family for encouragement and support throughout my time in college,

My supervisors, Dr. Malcolm Smyth, for his guidance, support and humour, and Dr. Han Vos for his encouragement and advice,

and finally, Elaine, for her being there.

Contents

(ix)

Abstract

THE DEVELOPMENT AND CHARACTERISATION OF SOME
NOVEL AMPEROMETRIC SENSORS

Dónal Leech

Chapter 1 of this thesis serves as a general
introduction to electrode processes and to some of the
electrochemical techniques used for the
characterisation and development of amperometric
sensors. A brief review of recent applications of
modified electrodes in the field of electroanalysis is
also presented.
The remainder of the thesis is divided into three
sections. The first of these comprises chapters 2 and
3. Chapter 2 describes the synthesis and
characterisation of a series of polymers based
on ruthenium-bound 4-vinylpyridine/styrene copolymers.
An investigation into factors that affect charge
transport rates and processes through thin films of
these polymers on glassy carbon electrodes, using
cyclic voltammetry, chronoamperometry and sampled
current voltammetry, is also presented. Chapter 3
describes the optimisation of the performance of these
polymer modified electrodes as sensors for the nitrite
ion, using the rotating disk electrode and
flow-injection amperometric detection techniques.
The second section of this thesis comprises the
development of ruthenium dioxide-based modified
electrodes for the electrocatalytic detection of
alcohols and selected saccharide antibiotics. The
ruthenium dioxide modifier is also confined in a
graphite-epoxy matrix to yield a stable, polishable
sensor for the saccharide antibiotics.
Finally, chapter 5 describes the development of,
and investigation into, two sensors for the detection
of glucose. The first of these is based on the
electrocatalytic oxidation of glucose at a ruthenium
dioxide-modified graphite-epoxy electrode surface,
while the second involves a novel one-step fabrication
of a glucose sensor based on the entrapment of the
enzyme glucose oxidase within a poly(ester sulfonic
acid) coating.

CHAPTER 1

The Theory and Analytical Applications

of Modified Electrodes

1

1.1. INTRODUCTION

The development of electrochemical analysis based on amperometric techniques has, until recently, been restricted by the range of electrode materials available; namely the limitation of using either the dropping mercury and hanging mercury drop electrode or a solid metal or carbon electrode. The deliberate modification of electrode surfaces can be considered as the start of a new era in electroanalysis. By utilising a modified electrode one tries to exert greater control over the electrode characteristics and the surface reactivity. The modifying material is selected such that it is either selective for a particular analyte, or is capable of mediating redox reactions that are slow or not possible at a bare unmodified electrode. The application of modified electrodes is potentially very widespread, and already their unique features are exploited in diverse areas such as energy storage [1], electrochromics [2-4], redox catalysis [5-11], solar energy conversion [12-14] and information storage [15,16]. In all of these applications, the observed response of the device is directly related to the properties of the modifier used. In particular, in the case of electroanalysis, the redox process occurring between a modified electrode and the analyte in solution is mediated by the modifier. The range of modifying species is vast, varying from metal deposits and metal oxide layers to the use of organic materials, enzymes and polymers. It is the availability of such a variation of modifying materials which allows the properties of traditional electrode materials to be tailored to meet the requirements of a particular application.

Electrochemical communication between the underlying electrode material and the contacting solution containing the analyte is most frequently achieved via an electroactive group within the layer, such as quinones [17], iridates [18,19] hexacyano compounds [20,21] and other transition metal complexes [22-24], as well as by utilising electronically conducting

2

polymers [25,26]. The physical method of implementing the techniques above can be by a number of electrode modification procedures. Over the past decade and a half, a variety of approaches for the modification of electrode surfaces has been developed and investigated, since the early work of Lane and Hubbard [27,28] on the adsorption of unsaturated monomers at electrodes. Subsequent methods for the direct covalent attachment of mediators to the electrode surface have been developed by Murray's group [29,30] and others [31-33]. These methods were most frequently employed to produce monolayer coverages, although, by judicious control of the conditions, adaption for multilayer coverage has been attempted [34]. Multilayer coverage of electrode surfaces is most frequently achieved by modification of the electrode with a polymer layer. Methods available to achieve this include electrochemical polymerisation of suitable monomers [35,36], electrochemical precipitation of a preformed polymer [37], drop, dip or spin-coating of preformed polymers onto the electrode surface [38,39] and the gas phase polymerisation of monomers onto the electrode surface [38,39]. Another modification technique which is frequently utilised is the incorporation of the modifier into the carbon paste matrix [39].

Most of the applications discussed in this chapter are based on either the activation or passivation of particular electrochemical reactions. The protection of the electrode/electrolyte interface so as to avoid the problems of surface passivation and so permit the amperometric determination of an analyte is also considered. Electroanalytical applications of modified electrodes are mostly based on achieving a certain degree of selectivity, which can then be coupled with the high sensitivity achievable using modern voltammetric techniques. This selectivity can be obtained by either an analyte selective preconcentration effect or by selecting the properties of the layer so as to catalyse a specific reaction. This analyte selective catalysis is the basis of the well documented glucose

3

electrode, where the presence of a surface immobilised enzyme catalyses the oxidation of glucose, in the presence of oxygen, to yield hydrogen peroxide, which can be oxidatively detected at the electrode surface and thus permit the determination of glucose levels [39].

This chapter consists of, firstly, a general overview of voltammetric electrode process, followed by an introduction to the two principal electrochemical techniques that will be utilised throughout the remainder of this thesis; cyclic voltammetry and amperometry in flowing streams. The electrochemical techniques that are unique to each chapter, such as chronoamperometry (chapter 2) and rotating disk voltammetry (chapter 3) are introduced in their corresponding chapters. Finally, the electroanalytical applications of different types of modified electrodes are explored. In recent years some excellent general reviews dealing with modified electrodes have appeared in the literature including those by Murray [38], Hillman [39], Albery [40] and others [41-43]. The aim of the review of the analytical applications of modified electrodes is by no means to present a complete literature survey covering the whole of the modified electrode area, but to survey and present the most interesting and representative examples of amperometric electroanalysis which currently exploit modified electrodes.

1.2.   VOLTAMMETRIC AND AMPEROMETRIC ELECTRODE PROCESSES

Voltammetry involves the measurement of current as a function of potential applied to a working electrode with regard to a reference electrode in a 3-electrode cell, the auxiliary (or counter) electrode being the third component of the cell. A plot of current versus applied potential is known as a voltammogram, and is utilised for the investigation of analyte species. Amperometric measurements are made by recording the current flow in the cell at a fixed applied potential. The working electrode, in both cases, can function as either a cathode or anode and may be a solid or dropping mercury electrode. In general, voltammetric techniques are considered to be more effective for examining the electrochemical behaviour of a system. However, the application of sensors based on this technique is limited, due, in part, to the complicated electronic circuitry needed for scanning the applied potential. Thus, the majority of sensors have utilised the electrochemical cell in an amperometric mode. Both techniques are, however, essential in the design and application of operational electrochemical sensors [44] and will be discussed in the following sections. Before the discussion of these techniques is considered, however, some general features of electrolysis need to be introduced. The theories outlined below are treated in greater depth in several available texts [45-47].

1.2.1.   Basic Features of Electrochemical Processes

Electrochemical reactions that involve the transfer of charge at the solution/electrode interface are classed as heterogeneous processes. The rate of the electrochemical reaction is determined by a series of steps, involving transport of electroactive species to the electrode surface and then charge transfer at the interface. Consider a simple electrochemical reaction of the type:

5

$$Ox + ne^- \iff Red \qquad (1.1)$$

Conversion of Ox to Red involves the folowing steps:

- diffusion of Ox from bulk solution to the electrode surface;

- transfer of electrons at the electrode surface to form Red;

- diffusion of Red from the electrode surface into the bulk solution.

In addition, the overall electrode reaction can often involve homogeneous chemical reactions, which can either precede or follow the electron transfer step. Furthermore, heterogeneous processes, such as adsorption or desorption of reactants or products, or surface-mediated recombination of atoms or radicals, may be coupled with the electrode reaction [45]. The overall rate of the electrode reaction will be determined by the slowest of all of the reactions involved in that process, which is thus called the rate-determining step.

1.2.1.1. Faradaic and Charging Currents

The observed current in an electrochemical process arises from two different processes at the electrode surface. The first process involves electron transfer across the electrode/solution interface and gives rise to the faradaic current. Faradaic currents result when either oxidation or reduction of electroactive species occurs, with the amount of chemical reaction caused by the flow of current being proportional to the amount of electricity passed. The magnitude of the faradaic current is determined by the mass transfer process, the technique being used, and whether the electrolysis is controlled by diffusion, electron transfer, chemical kinetics or adsorption effects [45].

6

The second electrode process gives rise to a charging (or capacitive) current, and results from the changing structure of the electrode/solution interface with changing potential (and electrode surface area for the dropping mercury electrode). The electrode/solution interface has been shown experimentally to behave like a capacitor [45], with the interfacial region being known as the electrical double layer. A widely accepted model of the double layer is shown in Figure 1.1. The solution side of the double layer is thought to be made up of several layers. The layer closest to the electrode contains solvent molecules and other species, such as non-solvated ions, said to be specifically adsorbed. The second layer involves the non-specific adsorption of solvated ions, involving long-range electrostatic forces. These ions are distributed, because of thermal motion, throughout an area which extends into the bulk of the solution, called the diffuse layer.

In voltammetric and amperometric studies, apart from those concerned with the investigation of the double layer, only faradaic currents are of analytical interest. Many methods are currently available which can discriminate against the charging current [45,46].

1.2.1.2. Modes of Mass Transfer

During electrolysis, three modes of mass transfer are generally important [45]:

- migration, which involves movement of a charged species under the influence of an electric field;

- diffusion, which is movement of a species under the influence of a concentration gradient;

- convection, from stirring or hydrodynamic transport.

7
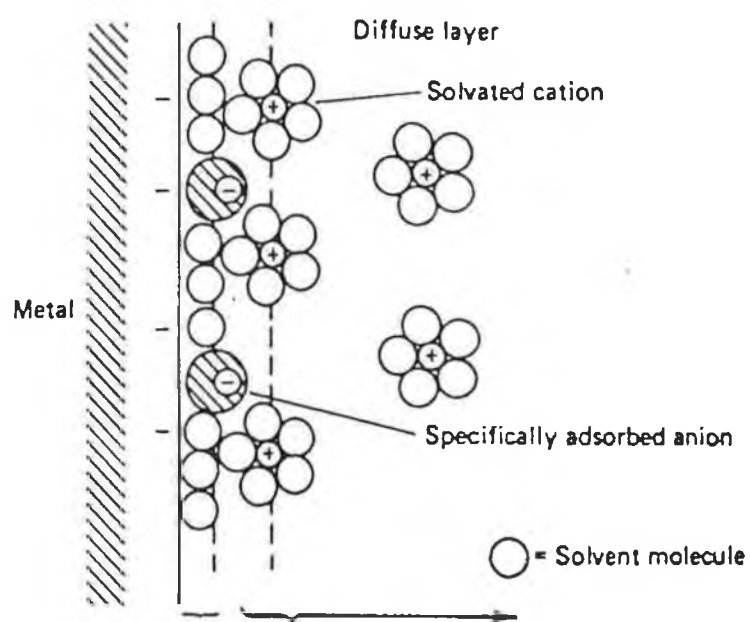
Figure 1.1: Proposed model of the electrode/solution, double-layer region.

Reduction or elimination of the migrational mode of mass
transfer of electroactive species in solution can be
accomplished by addition of excess of a supporting electrolyte,
whose ions can not be oxidised or reduced in the potential
window of interest. The ions of the supporting electrolyte can
thus carry practically the total charge within the analyte
solution, leading to negligible migration currents in the
system.

Convective mass transfer occurs under the influence of
stirring, flow or temperature gradients in the solution.
Although this mode of mass transfer is commonly utilised in
techniques such as rotating disk voltammetry and stripping
voltammetry, it is generally undesirable in voltammetric studies
as it causes non-linear responses. A discussion of mass
transport under hydrodynamic conditions will be presented in
section 1.3.2.1. Elimination of convective mass transfer is
achieved in quiescent solutions.

Probably the most important mass transfer mechanism is
diffusion. Diffusion occurs when a concentration gradient
develops, normally at the electrode surface. Consider a
reversible electrochemical reaction which occurs upon
application of a potential step. The surface concentration of
the electroactive species drops to zero, resulting in a gradient
being formed that extends into the bulk of the solution. The
portion of the solution in which this gradient occurs is known
as the diffusion layer. The initial diffusion layer thickness
upon application of the potential step is thin, but gradually
the diffusion layer extends further out into the bulk solution.
Thus time is an important parameter in an electrochemical
measurement (as will be shown in chapter 2).

1.3. VOLTAMMETRIC AND AMPEROMETRIC TECHNIQUES

This section of the chapter will concentrate on the theory
associated with the technique of cyclic voltammetry (CV) and

amperometry only. These techniques represent the bulk of
experimental techniques carried out throughout the remainder of
the theses. Further details on both of these techniques and
other voltammetric methods are available [45-48]. Techniques
that are unique to the various chapters, such as CV and
chronoamperometry for the determination of the charge transfer
diffusion coefficient, and rotating disk voltammetry for
investigation of mediating reactions, are presented in their
respective chapters (chapter 2 and 3, respectively).

1.3.1.   Cyclic Voltammetry

Cyclic voltammetry consists of cycling the potential applied
at the working electrode in an unstirred solution and measuring
the resulting current, with the potential of the working
electrode controlled versus a reference electrode. Since its
introduction, CV has become perhaps the most effective technique
for the mechanistic study of redox systems [49-51]. A redox
system can be characterised from the potentials of the peaks on
the cyclic voltammogram and from changes caused by variations in
scan rate.

The potential waveform that is applied across the
electrode/solution interface for cyclic voltammetry is
illustrated in Figure 1.2. Single or multiple scans may be used,
and the potential ramp (scan rate) can also be varied. The
current evolved at the working electrode is measured during the
potential scan. A typical cyclic voltammogram for a solution
species, with the important diagnostic features given in the
diagram, is shown in Figure 1.3. The important parameters in a
cyclic voltammogram include the cathodic (E_{pc}) and anodic
(E_{pa}) peak potentials and cathodic (i_{pc}) and anodic (i_{pa})
peak curents. The establishment of a correct baseline is
essential for the accurate measurement of peak curents. This is
not always easy, particularly for more complicated or
multicomponent systems. Difficulty in obtaining accurate peak
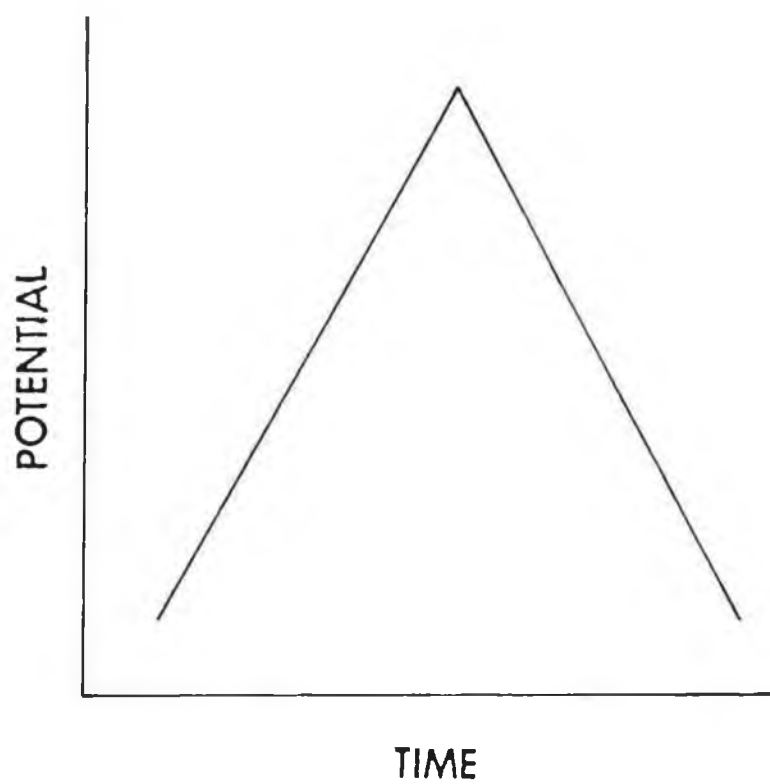
Figure 1.2: Potential excitation waveform for cyclic voltammetry

11
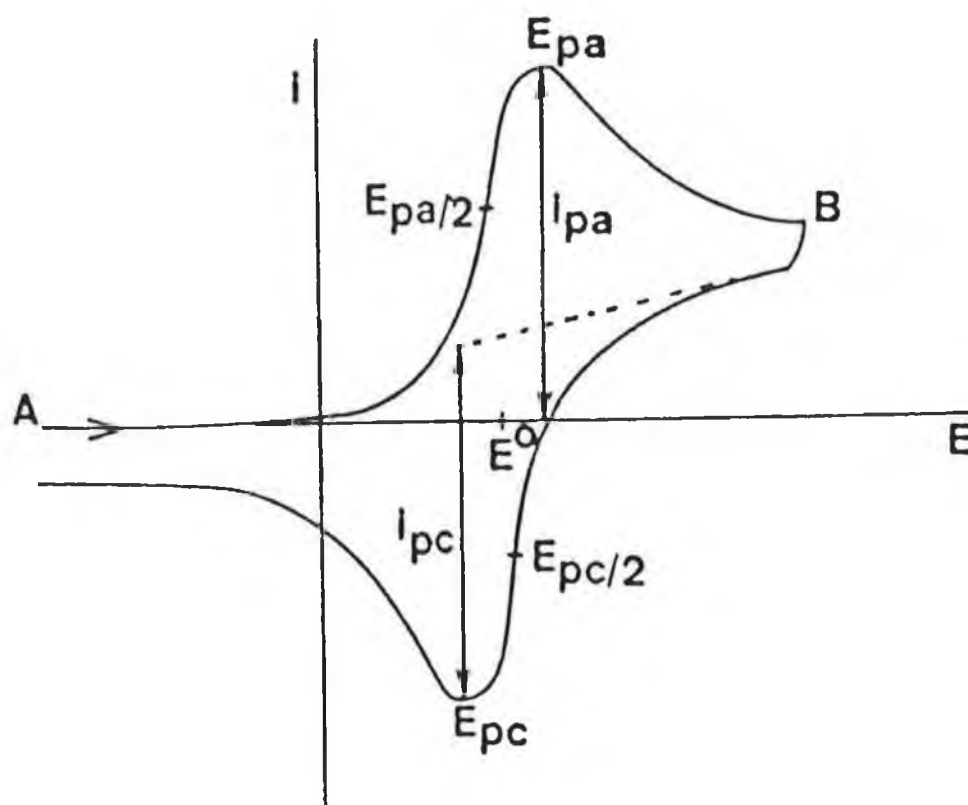
Figure 1.3: Diagnostic features of a cyclic voltammogram. E_{pa}, i_{pa}, E_{pc} and i_{pc} represent the anodic and cathodic peak potentials and currents respectively. $E_{pa/2}$ and $E_{pc/2}$ are the anodic and cathodic half peak potentials, respectively, and E^O is the formal reduction potential for the electroactive species. A is the start of the potential scan with B being the switching potential. (From reference 44, ch. 8).

currents has been suggested to be perhaps one of the biggest problems in CV [52].

Having established a correct baseline, the peak current measured depends on both the rate of mass transfer and the rate of the electron transfer reaction. The rate of electron transfer for a reduction process is a function of potential and can be described by the Butler-Volmer equation [45] below:

$$k_f = k^o \exp[-\alpha n F / RT (E-E^o)] \qquad (1.2)$$

where k^o is the standard heterogeneous electron transfer rate constant, α is the transfer coefficient, E^o is the formal reduction potential, n is the number of electrons transferred in the electrode process, F is the Faraday constant and R is the universal gas constant. Similarly, the electron transfer rate constant for the reverse process, k_b, can be described by:

$$k_b = k^o \exp[(1-\alpha) n F / RT (E-E^o)] \qquad (1.3)$$

When the electron transfer process is reversible, the difference between anodic and cathodic peak potentials is equal to 59/n mV. This separation of peak potentials is independent of scan rate for a reversible process, but is slightly dependent on switching potential and cycle number [45]. Under reversible conditions, the electron transfer reaction at the electrode surface is rapid enough to maintain the concentrations of the oxidised and reduced forms of the electroactive species in equilibrium with each other. The equilibrium ratio for a given potential at the electrode surface is determined by the Nernst equation:

$$E = E^o + RT/nF \ln([Ox]/[Red]_{x=o}) \qquad (1.4)$$

where Ox and Red are the oxidised and reduced forms respectively and x is the distance from the electrode surface.

Electrochemical irreversibility is caused by slow electron

13

exchange of the redox species with the working electrode. It is characterised by a peak potential separation of greater than 59/n mV, which is dependent on the scan rate. This is due to the non-equilibrium (non-Nernstian) conditions at the electrode surface.

The peak current of a cyclic voltammogram for a reversible redox system can be given by the Randles-Sevcik equation below [45]:

$$i_p = [0.4463(nF)^{3/2}AD^{1/2}v^{1/2}C^*]/[(RT)^{1/2})] \quad (1.5)$$

where A is the electrode area, D is the diffusion coefficient, v is the scan rate and C^* is the bulk solution concentration of electroactive species. Thus the dependence of the peak current on the square root of the sweep rate is a further characteristic identifying a reversible system.

CV has become increasingly popular in all fields of chemistry for the investigation of redox species [51]. The technique enables a wide potential range to be rapidly scanned for reducible or oxidisable species. This capability, together with the ability to use a variable time scale, make this one of the most versatile electroanalytical techniques available today.

1.3.2. Hydrodynamic Amperometry

As with CV, hydrodynamic amperometry involves the measurement of the current produced under the influence of an applied potential. In this case, however, the working electrode is held at a fixed potential with the analyte being forced to flow past the electrode. The current signal at these electrodes will be dependent on the mass transfer process.

1.3.2.1 Mass Transfer Processes for Hydrodynamic Conditions

The most commonly used theory concerning the kinetics of

14

heterogeneous chemical reactions in stirred solution is that of Nernst [53]. According to this theory, there is a thin layer of static liquid immediately adjacent to the surface of the electrode through which diffusion of the reacting species occurs. Beyond this layer, known as the diffusion layer, of thickness , the analyte is transported by convection. Inside the diffusion layer, the solution is assumed to be unstirred with the concentration distribution within the layer being linear. However, the experimental observations do not support the Nernst assumptions, with the concentration distribution being non-linear and the liquid not being stationary in the vicinity of the electrode surface.

The exact treatment of mass transport involving convection and diffusion has been given by Levich [48]. In this case Levich assumed that the transport of a solute is governed by two mechanisms. First, there is molecular diffusion as a result of concentration differences, and second, solute particles are entrained by the moving liquid and are transported with it. The combination of these processes is called convective diffusion of a solute in a liquid. In the vicinity of a solid electrode surface both of these processes can play a role. The overall concentration distribution relating to a heterogeneous chemical reaction can be given as follows:

$$dC_i = (D_i \nabla C_i) - V \nabla C_i + z_i F \nabla (u_i C_i \Phi) + R_i \qquad (1.6)$$

where D_i is the diffusion coefficient of species i, C_i is the concentration of i, V is the flow velocity vector, z_i is the number of charges transported by i, u_i is the ionic mobility, is the electric field strength and R_i is the rate of the homogeneous chemical reaction. The first term on the right hand side of equation (1.6) above relates to the concentration gradient of species i; the second to the macroscopic fluid flow velocity and the concentration of i, with the third term relating to the migration and fourth to the rate

of homogeneous chemical reaction. This equation can only be solved in a few cases, usually for systems with very simple electrode geometries.

Equation (1.6) has been solved by Levich [48] for a variety of geometries, namely; rotating disk electrodes, tubular electrodes, flat surfaced electrodes and conical microelectrodes. Equation (1.7) below describes the limiting current obtained at flat-surfaced electrodes:

$$i_L = 0.63nFD^{2/3}v^{-1/6}(W_L V)^{1/2}W_e C^* \qquad (1.7)$$

where V is the laminar flow velocity of the fluid, with the length, W_L, and width, W_e, of the electrode being greater than the thickness of the hydrodynamic boundary layer. The steady-state current response of an electrode on one wall of a planar thin-layer flow cell has been described, for a rectangular electrode, by Weber and Purdy [54] as:

$$i_{ss} = 1.467nFW_e(W_L D/b)^{2/3}(V/W_c)^{1/3}C^* \qquad (1.8)$$

when the diffusion is thin relative to the channel height b, and where W_c is the channel width perpendicular to the fluid flow. This equation has recently been modified by Ou and Anderson [55], to account for the steady-state current response at circular solid electrodes in a planar thin-layer detector, to equation (1.9) below:

$$i_{ss} = 1.234nFW_L^{5/3}(D/b)^{2/3}(V/W_c)^{1/3}C^* \qquad (1.9)$$

with this equation valid only when the diameter of the circular electrode does not exceed the channel width and the sample injection volume is much larger than the dead volume between the injector and the detector, as is the case for the thin-layer electrode cells utilised in the following chapters.

16

1.4. ANALYTICAL APPLICATIONS OF MODIFIED ELECTRODES

The focus of this review will be on electroanalytical
applications of modified electrodes. Several other important
applications of modified electrodes are also under
investigation. Electrochromic devices, photoelectrochemical
applications and devices which mimic electronic components are
important areas of research in the field of modified electrodes.
Applications of these electrodes has been treated in several
reviews [39,56,57]. The vast area of bioelectrochemistry,
including enzyme and tissue modified electrodes, is largely
ignored in this review. Several excellent reviews on the
applications of such electrodes are available [58-60]. The
specific area of glucose electrode development will be briefly
reviewed in the introduction to chapter 5.

The analytical application of chemically modified
electrodes usually has one or all of three objectives: enhanced
signals over unmodified electrode surfaces, increased stability
and reproducibility, and/or freedom from interferences. The
principal materials employed in the field of modified electrodes
are modifiers with electrocatalytic, preconcentrating or barrier
properties. The field of electroanalysis using modified
electrodes is only recently producing "operational" sensors
where factors such as calibration ranges and interferences have
been considered. The area has been the subject of a number of
recent reviews [61-63].

1.4.1. Analysis by Redox Catalysis at Modified Electrodes

Amperometric detection of a solute species is dependent on
the analyte of interest undergoing a redox reaction. Frequently,
however, the electrode kinetics are such that the species of
interest will only undergo such a redox reaction at a potential
which is either much more negative or positive than that
expected on the basis of thermodynamics. Surface modification

can frequently reduce or possibly eliminate overpotentials, or bring the redox potential into a domain where the species of interest can be determined free from possible interferences. As well as this shift in the operational formal potential, the redox reaction often occurs at a rate which is greater than those experienced at an unmodified surface. The nature of such modifying layers differs greatly between applications, but deposited metallopolymer layers find frequent application. Such metallopolymer layers possess the essential feature of all catalytic modified electrodes, that of a strongly bound mediating centre. The metal complex can be chosen to catalyse a given reaction of interest from a knowledge of the homogeneous solution kinetics. The loading of the active site within the modifying layer can also be varied greatly in the initial synthetic procedure.

The theory of catalytic modified electrodes has been developed to a considerable extent, as reviewed in chapter 3, and allows definition of performance criteria and optimisation of response. Despite the elegance and interest in this theory, its exploitation to optimise modified electrode response is limited.

Where attempts to quantify species of interest based on a catalytic system have been successful, the approaches used have typically centred on polymer-bound metal complexes, notably ruthenium. Geraty et al. [64] have utilised a $[Ru(bpy)_2(PVP)_5Cl]Cl$ modified electrode, where bpy is 2,2'-bipyridyl and PVP is poly-4-vinylpyridine, for the determination of Fe(II) and obtained a linear range from $5x10^{-6}$ up to 10^{-2} M. Electrodes modified with this metallopolymer also exhibited improved sensitivity in the determination of nitrite and nickel bis(2-hydroxyethyl) dithiocarbamate $[Ni(HDTC)_2]$ in flow systems [65]. The use of this metallopolymer in flow systems was restricted because of loss of electroactive material from the modified surface, due to abrasion by the mobile phase. Other metallopolymer coatings used

18

to perform electroanalysis include a poly(vinylferrocene-4-methyl-4'-vinyl-2,2'bipyridyl) copolymer. This material was deposited onto Pt wire to determine Fe(II) at pH 2.1, giving a linear calibration range of 50 nM – 5 μM Fe [66]. Using a viologen based polymer and antipyrylazo (3,6 bis(antipyrylazo) chromotropic acid), Ca(II) was determined in aqueous solution (pH 9.5) with a linear response over 3 orders of magnitude and a sub nM detection limit [66]. Interferences such as Mg(II) were considered. Platinum particles deposited within Nafion films on glassy carbon by potential cycling in chloroplatinic acid gave rise to an analytic response for H_2O_2 which could be used in a flow cell [67]. The response was linear for 1 μM – 50 mM, when the Pt particle density was greater than 150 μg cm^{-2}. Belanger et al. [68] have demonstrated the use of a polypyrrole-modified electrode containing Pt microparticles for enhanced detection of peroxide, generated enzymatically by the glucose oxidase enzyme incorporated into the polypyrrole film, to yield an improved glucose sensor. Polyvinylferrocene modified electrodes have been shown to catalyse the ascorbic acid oxidation over a wide pH range [69]. These catalytic currents have been used to determine ascorbic acid concentration over the $6 \times 10^{-6} - 6 \times 10^{-2}$ M range. By electrostatically binding hexachloroiridate$^{2-/3-}$ into quaternised PVP, Cox et al. [70] demonstrated the ability of these electrodes to mediate the determination of NO_2^- in a flow injection system, with a detection limit of 0.07ppm and a linear working curve from $1 \times 10^{-5} - 1 \times 10^{-3}$ M NO_2^-. Surface poisoning of SCN$^-$ was prevented and interference from Pb(II), Mn(II) and Fe(II) was lowered. Further work with electrostatically bound $[IrCl_6]^{2-/3-}$ within quaternised polyvinylpyridine for NO_2^- oxidation has been explored, giving a larger working range, i.e. $8 \times 10^{-6} - 4 \times 10^{-3}$ M [71]. The ability of $[IrCl_6]^{2-}$ to mediate the electron transfer was shown.

The use of ruthenium- and osmium-bridged dimers, i.e. $[(bpy)_2(H_2O)M(III)]_2O^{4-}$, where M represents Ru or Os

metal centres, in a cation exchange resin (p-chlorosulfonated polystyrene) to give catalytic currents for Cl^- oxidation at a rotating disk electrode has been reported as a method for Cl^- determination [72]. An electrocatalytic chloride modified electrode for the determination of epinephrine following liquid chromatographic separation has also been reported [73]. A polycrystalline gold electrode was electroplated in 1M HCl to give rise to smooth, glassy, copper coloured films. In liquid chromatography, the peak height obtained at the modified surface was 25 times that obtained at a gold electrode.

The nature of the supporting medium in which the catalytic centre is bound has been varied from polymer layers on electrode surfaces to carbon paste. Santos and Baldwin have successfully detected carbohydrates [74] and sulfhydryl [75] compounds at a cobalt phthalocyanine- modified carbon paste electrode, in combination with liquid chromatography and flow injection systems. Detection limits varied from 100 pmol for glucose to 500 pmol for fructose. Other groups, most notably those of Baldwin and Wang, have extensively used the carbon paste matrix for construction of modified electrodes. Geno et al. [76] have ion exchanged $[Fe(CN)_6]^{4-}$ into PVP which was incorporated into the carbon paste matrix to yield a modified electrode for ascorbic acid oxidation, while Wang and Taha [77] have demonstrated the electrocatalytic oxidation of carbohydrates at a RuO_2-modified carbon paste electrode. Other electrocatalytic applications of carbon paste modified electrodes can be found in a recent review [78].

Purely inorganic modifications of the electrode surface were amongst the first to be used for analysis [79]. An enhanced response for ascorbic acid oxidation has been obtained at a platinum electrode modified by Prussian Blue [80]. The anodic peak for ascorbic acid appeared at almost the same potential as the modifying film, with the peak current being enhanced 28 times. The electronically conducting polymer, polypyrrole, has also been shown to enhance the rate of ascorbic acid oxidation

[81]. An inorganic catalytic system which has shown considerable promise is that developed by Gorton et al. [82] and used in a flow injection system. Gorton's method for the determination of hydrogen peroxide relied on vacuum deposited gold and palladium on graphite or carbon to give a catalytic system for peroxide. The modified electrode gave rise to considerably reduced overpotentials and an amperometric response which was linear with respect to hydrogen peroxide concentration between 10^{-7} and 10^{-3} M. By depositing an inorganic Ru-containing film from a $[RuCl_3]$ and $[K_4Ru(CN)_6]$-containing solution onto carbon, Cox et al. [83] have created a modified electrode for the determination of As(III) over the 5 μM – 2 mM concentration range, using cyclic voltammetry peak currents. A typical response at this modified electrode for As(III) is shown in Figure 1.6. The modified electrode was mechanically stable for periods greater than 10 weeks [83,84]. These Ru films were also used by Cox et al. [85] for the amperometric detection of SCN$^-$ in flowing solutions. A linear dynamic range of $2 \times 10^{-7} - 4 \times 10^{-6}$ M SCN$^-$ was observed, with electrode stability of the order of months rather than days. Platinum electrodes modified by adsorption of iodine and coated with a layer of cellulose acetate also yielded stable SCN$^-$ oxidation currents in flow injection analysis, with a broader linear range extending to 1×10^{-4} M [85]. Wang et al. [86] have modified glassy carbon electrodes with alumina to give a stable modified electrode for use in a thin layer cell. This electrode avoided the problems of protein adsorption in complex biological matrices, thus allowing ascorbic acid determinations in untreated urine samples, and was used as an amperometric detector following high performance liquid chromatography, with ascorbic and oxalic acids and epinephrine capable of being detected at the nanogram level.

Other examples of neurologically important analytes which have been studied using a modified electrode include dopamine, ascorbic acid and NADH. The kinetics of NADH oxidation at an unmodified carbon electrode are slow, with the electrochemical

21
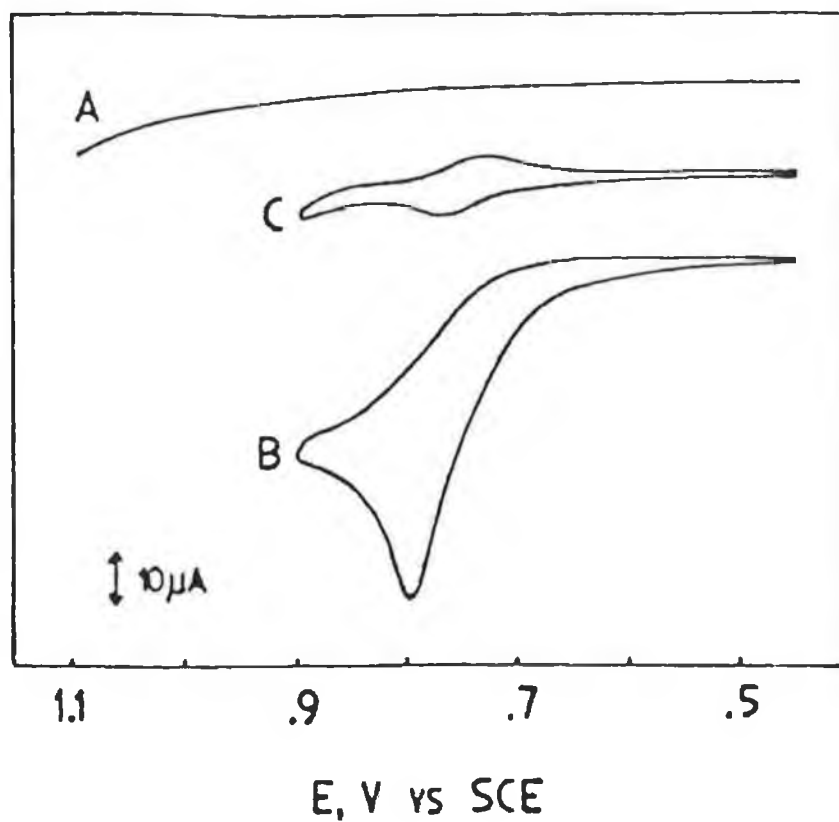
Figure 1.6: Cyclic voltammograms for (A) bare glassy carbon and (B) the ruthenium-coated glassy carbon electrode in 2 mM NaAsO$_2$ in 0.5 M NaCl at pH 2. Curve C is a cyclic voltammogram of the modified electrode in blank electrolyte solution. Scan rate was 50 mV s^{-1}. (From reference 83).

22

determination being further hampered by strong adsorption of its
oxidation products. Kuwana and co-workers [87,88], have solved
this problem by a systematic approach, firstly examining the
homogeneous solution kinetics and then identifying a strong
catalytic mediator, o-quinone. In their modified electrode,
3,4-dihydroxy-benzylamine was first confined on a glassy carbon
electrode and a condensation reaction with the quinone was then
carried out. The oxidation of NADH at such modified electrodes
was mediated with reduced overpotentials (see Figure 1.7).
Miller et al. [89] isolated the same quinone moiety in a
polymeric matrix to give the NADH redox reaction at a potential
near the o-quinone potential. Yon et al. [90] have developed a
modified electrode based on the electrodeposition of
hexacyanoferrate$^{4-/3-}$ on porous nickel electrodes, which can
catalyse the oxidation of reduced NAD (NADH) with a 150 mV
reduction in overpotential. The nickel hexacyanoferrate films
are capable of reoxidising enzymatically generated NADH and show
many features desirable for use as an analytical sensor for
oxidoreductase substrates [90]. A similar system, based on a
nickel hexacyanoferrate-modified glassy carbon electrode, has
been used as a catalytic modifying layer in the high performance
liquid chromatographic determination of Fe(III), without the
need for oxygen removal from the mobile phase [91]. A linear
working range of 2 x 10^{-7} - 9 x 10^{-7} M was established, with
a detection limit of 2.3 ng cm^{-3} Fe(III).

1.4.2.   Preconcentration and Complexation Schemes at Modified Electrodes

The dropping mercury and mercury film electrodes have found
frequent application in the determination of many species
including metals, proteins and inorganic complexes [92,93]. The
technique of adsorptive stripping voltammetric analysis, which
involves preconcentration of the analyte into a stationary phase
prior to amperometric determination, has a parallel in the field
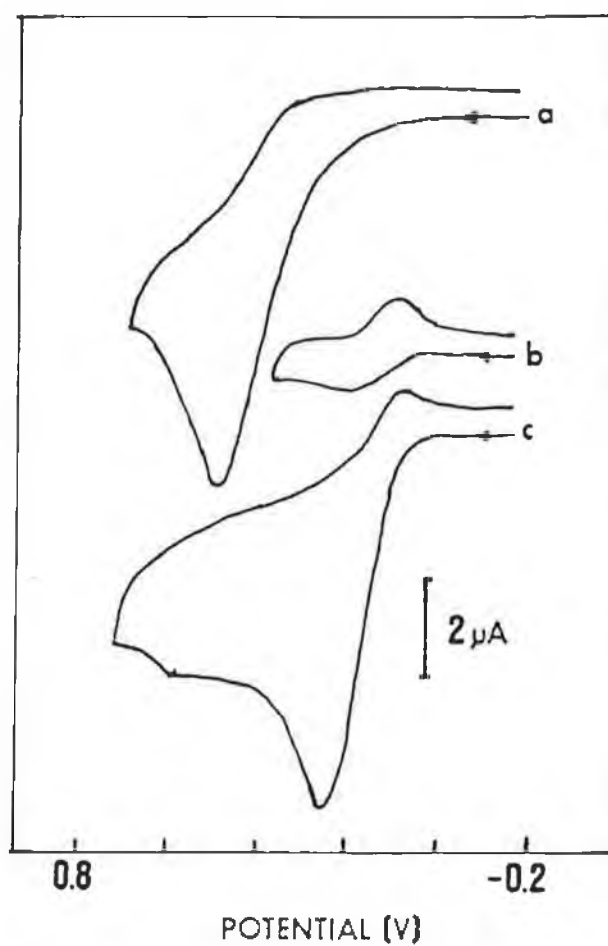
Figure 1.7: Catalytic oxidation of 0.5 mM NADH at (a) the bare glassy carbon electrode and (c) the modified electrode with a surface coverage of 7.5 x 10^{-10} mol cm^{-2} in 0.1 M KCl at pH 7. Curve (b) represents the response of the modified electrode in blank solution electrolyte. (From reference 89).

of modified electrodes. Modified electrodes have advantages over previous systems, in that they can extract a specific species of interest from complex matrices on the basis of electrostatics, chemical functionality, stereochemistry, selective binding or size. Highly charged species can be extracted from very dilute solutions and then reduced or oxidised in a subsequent electrode potential step or sweep, giving rise to an amperometric response. In particular, polymer modified electrodes are widely exploited for their preconcentration properties. These coatings are often ionomers and achieve high sensitivity by exploiting the inherent thermodynamic driving force of ion exchange reactions to preconcentrate a cation into a small volume ionomer film, frequently Nafion. One alternative to a coating consisting purely of a polymeric species is to bind a strong coordinating ligand within the polymer matrix, with the polymer backbone affording the chemical stability and mechanical strength which is essential for the successful application of the electrode, while the incorporated ligand can be varied according to the analyte of interest.

Perhaps the single most exciting idea forwarded for the analysis of metal ions is that proposed by Abruna and co-workers [94-96]. The modifying film consists of a copolymer film which incorporates an electroactive centre and an analyte selective ligand. The ligand is chosen to be analyte selective, and the electroactive centre induces electropolymerisation and acts as an internal standard. For example, sulfonated 2,9-dimethyl bathophenanthroline was employed for selective measurements of Cu(I) in the presence of Fe(II) [94]. Unmethylated sulfonated bathophenanthroline can however, be utilised for the determination of Fe(II) [97]. Submicromolar levels of Cu(I) have been selectively detected in the presence of a 100-fold excess of Fe(II) by the use of an electrode of sulfonated bathocuproine immobilised in a quaternised vinylpyridine/vinylferrocene copolymer [95]. In a recent publication, Cha and Abruna [98] have systematically investigated the determination of copper by

25

incorporating seven different ligands of varying coordination strength into an electropolymerised film of $[Ru(v-bpy)_3]^{2+}$, where v-bpy is 4-vinyl,4'-methyl, 2,2'-vinylpyridine. The relevance of this work to speciation studies was discussed. In a separate publication, Cha et al. [99] have employed platinum and glassy carbon electrodes, modified with the ligand Chromotrope 2B incorporated by ion exchange into films of electropolymerised $[Ru(v-bpy)_3]^{2+}$, for the amperometric determination of Cu(I) in the concentration range $7 \times 10^{-8} - 1 \times 10^{-4}$ M. The effects of competitive binding of competing ligands, such as chloride, bromide and oxalate, and competing metal ions, such as Ni(II) and Co(II), on the response for Cu(I) was investigated, with a diminution in the analytical signal for Cu(I) in all cases.

The technique of preconcentration within a polymeric film has wide application and has been used in the determination of U(VI) for concentrations greater than 10^{-8}M [100]. In this case the two step procedure adopted involved preconcentration at 0 V vs SCE into surface immobilised trioctylphosphine oxide (TOPO) and subsequent amperometric detection in a cathodic stripping scan. A representative voltammogram at this modified electrode, for the detection of U(VI), is given in Figure 1.8. Oxidising agents cause interference, but some tests on seawater have been reported [101,102]. Mercury film electrodes, modified with this compound in a PVC matrix, have been utilised for the determination of Bi(III) in copper and copper alloys [103]. By varying the thickness of the modifying layer, modifier to matrix ratio, and base electrolyte, these electrodes permit selective and sensitive determination of many metals [103].

Other systems which have been studied are those based on polypyrrole and substituted polypyrroles. O'Riordan and Wallace [104-106] have used N-carbodithioate polypyrrole to concentrate Cu(II) giving a surface concentration of 6×10^{-3} M, the Cu(II) being accumulated at a rate of 10^{-7} mol min^{-1}. This accumulated copper is subsequently determined voltammetrically.

26
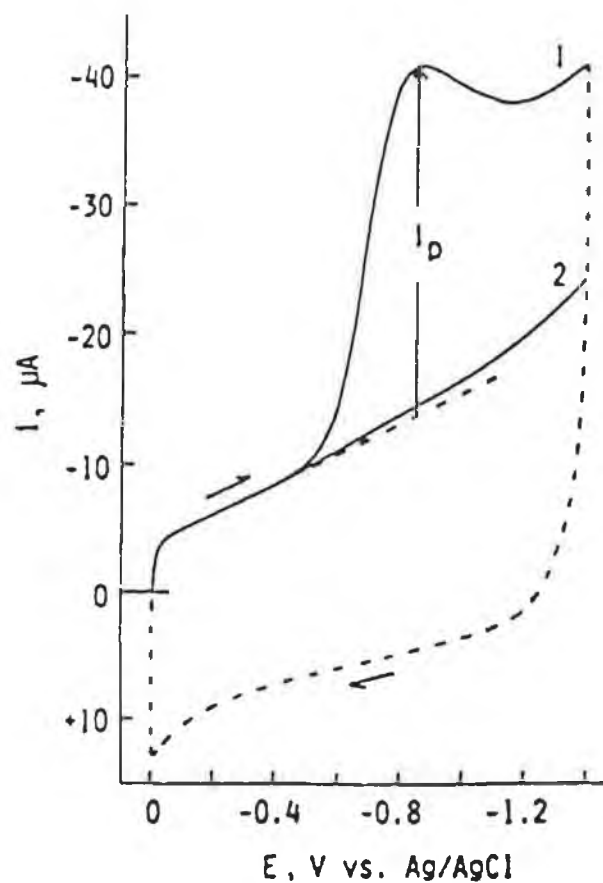
Figure 1.8: Voltammograms at a TOPO-modified glassy carbon electrode following 10 min preconcentration at 0.0 V, (1) in the presence of 1 x 10^{-7} M UO_2^{2+} and (2) in the absence of UO_2^{2+}. (From reference 100).

27

The immobilisation of 3-aminopropyltriethoxysilane onto carbon electrodes via condensation with surface alcohol functionalities gives rise to a highly sensitive sensor for Cu(II), with a linear range of 0.01 - 1.0 ng cm^{-3} [107].

Cox and Majda [108] have irreversibly adsorbed adenosine 5-monophosphate onto Pt and subsequently plated the modified electrode with a non labile Fe(III) complex, from Fe(III) initially present in the solution or from the oxidation of Fe(II). Short deposition times (60s) yielded a stripping peak current which was proportional to the sum of Fe(II) and Fe(III) in the test solution. Oxalate was used to remove Fe(III) from solution thus permitting Fe(II) determination. The method was shown to be applicable to the determination of Fe(III) and Fe(II) in the concentration range 10^{-8} - 10^{-6} M. PVP-coated electrodes have been used by Cox et al. [109] to preconcentrate Cr(VI). This permitted the study of an irreversible system at an ionomer-coated electrode. Excellent sensitivity for copper determination can be achieved using surface bound-((carboxyamido)propyl)trioxysilylidine) groups on glassy carbon. Cu(II) was electrochemically deposited from Cu(II)-containing solutions [110]. This coating was then anodically stripped in the same solution, with a current-potential curve being recorded by a differential pulse technique. The modified electrode showed increased sensitivity, precision and selectivity compared to unmodified surfaces. In 0.1M oxalic acid at pH 1.6, ng and subng amounts could be detected.

The exploitation of standard chelating agents with well understood and documented responses as electrode modifiers has also been reported [111]. By oxidising a glassy carbon surface with KMnO$_4$, the resulting surface functionalities have been coupled with iminodiacetic acid using dicyclohexylcarbodiimide as dehydrating agent. The extensively exploited chelate EDTA, as well as 3,6 dioxaoctane-1,8 diamine-NNN'N'-tetracetic acid have been surface bound. Such modified electrodes have been shown to preconcentrate Ag(I). Evaluation of the charge under the silver

28

redox peak in a cyclic voltammetric sweep was proportional to Ag(I) concentration over the range $1.1 - 11 \times 10^{-6}$ M in 0.1 M KNO_3 with added chloride [111].

The ability of the ionomer Nafion to inhibit interferences and surface passivation has lead to a modified mercury film electrode for determination of trace metals in body fluids [112,113]. The effect of film properties on the analytic response of such modified mercury film electrodes has been considered using $[Ru(NH_3)_6]^{3+}$ as a test analyte. This type of investigation into parameters such as film thickness should permit further optimisation of electrode response [115]. A regeneration of the modified electrode after analyte determination has also been reported [115]. Transition metal cations have been successfully analysed by preconcentration into a Nafion 117 modified mercury film for 10 minutes to give a linear response between 25 nM and 1 µM for Cd(II), Pd(II) and Zn(II) [116].

A modified surface has been prepared by oxidising a graphite electrode with $HNO_3:H_2SO_4$ (1:1) and then coating with polyacrylonitrile, followed by reaction of this adsorbed layer with NH_4SCN. By presoaking for 15 minutes, Au(III) could be preconcentrated and then determined by peak current measurement from cyclic voltammetry [117]. The reduction current was proportional to Au(III) concentration over the range 4.8×10^{-5} to 1.2×10^{-3} M. No interference from Ag, Ru, Ir and Pt was observed. The use of preconcentration into a modified matrix has been further developed by Wang et al. [118]. Modifiers (cation exchange resins) have been incorporated into epoxy-bonded graphite loaded resins to form modified electrodes of high mechanical stability with a surface which can be renewed by polishing. It has been proposed that several modifiers could be incorporated [118].

Recently the modification of electrodes with lipid layers has been investigated for the accumulation and subsequent stripping analysis of hydrophobic species [119-121]. Chastel et

al. [119] have described the detection of the anti-tumour drug, marcellomycin, at a glassy carbon electrode modified with a lipid layer of either asolectin or phosphatidylcholine [119]. Phosphatidylcholine-modified glassy carbon electrodes have also been utilised by Wang et al. [120,121] for the detection of analytes such as the antihypertensive agent reserpine [120], and antidepressants such as desipramine [121]. An added advantage of these lipid-modified electrodes was that hydrophilic electroactive interferents, such as ascorbic and uric acid and ferrocyanide, were rejected by the hydrophobic lipid layer. Nelson et al. [114] have demonstrated the use of a mercury film electrode modified with a layer of di-oleoyl lecithin for the determination of polynuclear aromatic hydrocarbons.

Modified carbon paste electrodes also exploit the preconcentration technique to achieve a sensitive response. The incorporation of exchange resins into such media has been widely exploited. Metal determination via the carbon paste medium is popular because of the near universal applicability of the technique. Commercially available exchange resins can be readily incorporated into the graphite/oil mix usually used to construct the carbon paste electrode. Amberlite LA2, an anion exchange resin, was incorporated by Kalcher into a carbon paste and $[AuCl_4]^-$ and $[AuBr_4]^-$ preconcentrated into the modified paste. Using these modified electrodes, detection limits for Au(III) salts of 100-300 ng cm^{-3} were obtained [122]. Wang et al. have incorporated a cation exchange resin, Dowex CGC 241 sulphonated polystyrene crosslinked to 8%, into the carbon paste matrix and preconcentrated ionic analytes. The procedure exhibited good linearity for 6.25 x 10^{-5} - 3 x 10^{-4} M Cu(II), and the peak current varied linearly with a preconcentration time of between 1 and 7 minutes [123]. Ag(I) determinations at the sub μg cm^{-3} level was possible by incorporating a zeolite into the carbon paste mull [124]. By judicious choice of the incorporated resin the modified electrode can achieve both high sensitivity and selectivity.

Bi(III) has been quantified at low concentrations (0.02 - 4 μg cm^{-3}) in acidic conditions by incorporating decyl- or dodecylmercaptan into the carbon paste [125]. Au(III) has also been determined successfully by the incorporation of dithizone in a carbon paste to give a linear response over 10 - 1000 ng cm^{-3} [126]. The effect of other ions which form dithizonates in acidic medium was also investigated. Mercury (II) has been quantified by the incorporation of a zeolite into the initial carbon paste mix. Trace amounts of Hg(II) were accumulated and then cyclic voltammetry used to determine the Hg concentration, with the peak current being linear with respect to the Hg concentration over the range 0.11 - 2.2 μg cm^{-3} [127].

The stability of nickel-dimethylglyoxime complexes has permitted the development of a modified electrode capable of determining Ni(II) levels with a linear region of 0.05 - 5 μM [128]. Multiple use of the electrodes could be achieved by acid treatment. This modified electrode has also been utilised in a flow system, with a breakdown of linearity observed with a preconcentration time of 60 s for the detection of 8 μm of nickel [129]. Direct calibration versus known Ni(II) standards was possible. Materials which have been used as direct surface modifiers have also shown utility for modifying carbon pastes. TOPO-modified carbon paste electrodes can extract, and therefore preconcentrate, Au(III), thus allowing quantitation in solution using differential pulse voltammetry (DPV) [130].

Copper sensitive modified carbon paste electrodes have been constructed by incorporating 2,9-dimethyl-1,10-phenanthroline into a conventional carbon paste mix of graphite powder and nujol oil. Chemical deposition of Cu(I) was achieved by immersion in a Cu(I) solution. The area under the resulting anodic wave in CV or DPV gave quantitative results for Cu(I) up to 10 uM with a detection limit of 0.3 μM. Ag(I) interfered minimally but no response was observed for Cu(II), Zn(II), Co(II), Pb(II), Ni(II) or Fe(III), although at large concentrations these did cause suppression of the CV peak [131].

31

The use of naturally available material rather than a synthesised product has also been used as a carbon paste modifier. Cu(II) has been determined using a carbon paste with incorporated algae. The modified electrodes are free from interference, exhibit short accumulation times and can be regenerated by acid exposure [132,133].

The other major area where modified carbon paste electrodes are widely exploited is in the determination of naturally occurring and common organic compounds. The determination of biologically important molecules such as dopamine can be achieved by modified carbon paste electrodes. The modification of carbon paste with N,N,N,'N'-tetramethyl-p-phenylenediamine yielded an electrode which could determine ascorbic acid concentrations in the $5x10^{-5}$ to $5x10^{-3}$M range in the presence of dopamine [134].

1.4.3. Permselective Modified Electrodes

Permselective films on electrodes provide routes for the separation of the analyte from co-existing interferences. This separation can be achieved via the permeability of polymeric films, which act as membrane barriers on the electrode surface. The selective permeability can be produced on the basis of size, charge and polarity.

An early example of the permselective function of polymer films was the blocking of large protein molecules from the surface of a gold electrode by the placement of thick polyethylene membranes onto the electrode surface [56]. These devices were utilised for the monitoring of blood oxygen levels. The cellulose acetate (CLA) films popularised by Wang and co-workers [135-137] is another example of a successful membrane barrier. Base hydrolysis of CLA results in uniform pinholes through the film, the size of which can be controlled by the hydrolysis time. This CLA film has been used to prevent surfactant fouling of the electrode surface in anodic stripping

32

voltammetry [137].

The use of Nafion as an effective charge-exclusion film has been investigated for the selective determination of the cationic neurotransmitter, dopamine, in the presence of interferents such as ascorbic acid and dihydroxyphenylacetic acid [138,139]. A 200-fold selectivity for dopamine over ascorbic acid was observed using this approach. Nafion-coated glassy carbon electrodes have also been used by Ji and Wang [140] for the detection of neurotransmitters following liquid chromatographic separation. High selectivities for the cations dopamine, norepinephrine and epinephrine over ascorbic and uric acids were obtained.

The coupling of size and charge-exclusion effects of polymer films with active functions such as ion exchange, complexation or electrocatalysis of other modifiers has been investigated. The detection of dopamine in the presence of larger neurotransmitter cations, such as epinephrine and norepinephrine, has been accomplished by the use of a bilayer electrode system consisting of a CLA layer on top of a Nafion film [141] (Figure 1.9). Using this modified electrode arrangement, Wang et al. [142] have determined norepinephrine and epinephrine (cationic neurotransmitters) in a flow system. The response time was approximately 2 s, with a linear response of 20 - 160 μM and detection limits of 0.04 and 0.1 ng, respectively. Surfactants, such as gelatin, were found to be non-passivating, and the bilayer arrangement was selective in the presence of ascorbic and uric acid. Bilayer modified electrodes employing films of CLA over PVP have been used for the selective determination of small electroactive organic molecules in urine [143]. Cobalt phthalocyanine modified electrodes coated with CLA films have effectively coupled size exclusion with electrocatalysis [144]. These electrodes demonstrated the selective catalytic determination of compounds of varying sizes, by controlling the size exclusion effect of the outer CLA layer.
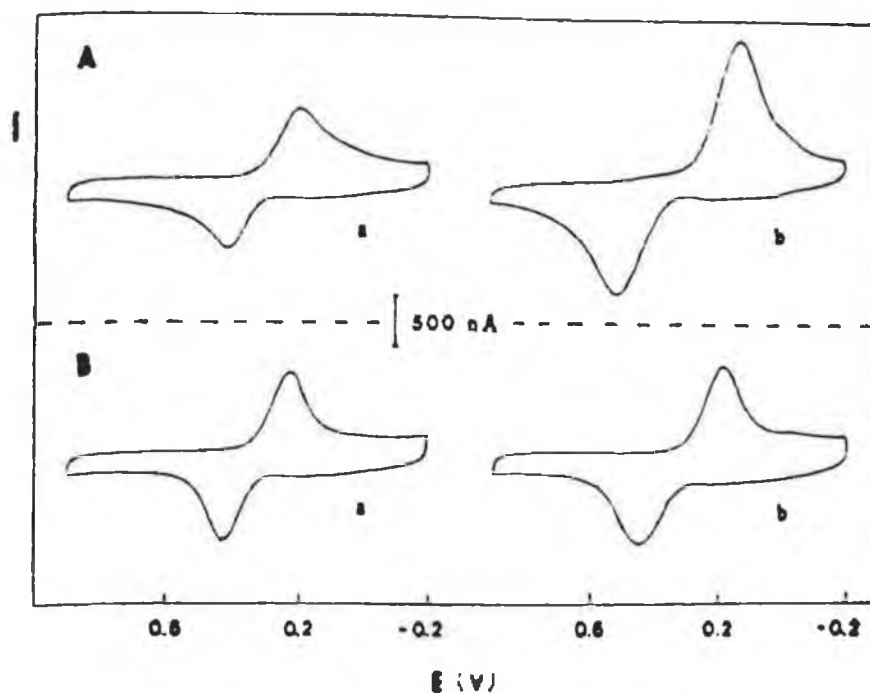
Figure 1.9: Cyclic voltammograms at Nafion (A) and bilayer (B) coated glassy carbon electrodes of (a) 5 μM dopamine and (b) same as in (a), but after addition of 20 μM epinephrine. Hydrolysis time of CLA film of 30 min. Scan rate was 50 mV s^{-1} and electrolyte was 0.05 M phosphate buffer at pH 4. (From reference 141).

34

Other permselective polymers have proved to be effective. Eastman-AQ poly(ester sulfonic acid) films have been shown to selectively retard anionic species, such as ascorbic and dihydroxyphenylacetic acid, while allowing detection of cations such as dopamine and catechols at the underlying glassy carbon electrode surface [145]. Electropolymerised films of poly(2,6-dimethyl,1,4-phenyleneoxide) were shown to be selective towards hydrogen ions [146]. Several electropolymerised conducting polymer films have been investigated for use as permselective membranes. Fine molecular weight cut-offs were obtained for electropolymerised films of polyaniline, polypyrrole and polyphenol on glassy carbon electrodes, by variation of the electropolymerisation time or monomer concentration [26]. The application of these films for the selective determination of catechol, hydrazine, hydrogen peroxide and acetaminophen in the presence of ascorbic acid, uric acid, chlorpromazine and ferrocyanide interferents was demonstrated. Glassy carbon electrodes modified with electropolymerised films of poly(3-methylthiophene) have been reported to allow the stable detection of phenolic compounds, which would normally passivate the unmodified electrode surface [147].

Gelbert and Curran [148] have suggested the use of a stearate modified carbon paste electrode for the determination of dopamine in the presence of ascorbic acid. The modified electrode was capable of separating the dopamine and ascorbic acid peaks allowing quantitation of dopamine based on CV. The response of these electrodes was such that dopamine could be quantified in freely moving rats despite large changes in ascorbate and DOPAC concentrations.

1.5. CONCLUSION

The chemical modification of electrode surfaces will
continue into the future, with interest spurred on by the
undoubted analytical applications which this new area of
electrochemistry offers. The fundamental understanding of the
modified electrode has only been examined extensively and
profitably in more recent times. This continued research into
the theoretical aspects of modified electrodes will help clarify
the responses obtained for the electrodes discussed above.
Mechanistic examinations of charge transport, analyte
intercalation rates or the fundamental reaction upon which the
sensor is based cannot be ignored in the design of an
"operational" sensor.

1.6. REFERENCES

1. T. Osaka, K. Naoi, S. Ogano and S. Nakamura, J. Electrochem. Soc., (1987), 134, 2096.

2. K. Itaya, H. Akahoshi and S. Toshima, J. Electrochem. Soc., (1982), 129, 762.

3. G.F. Kirkbright, R. Narayanaswamy and N.A. Welti, Analyst, (1984), 109, 15.

4. Z. Zhujun and W. R. Seitz, Anal. Chim. Acta., (1984), 160, 47.

5. F.C. Anson, J. Phys. Chem., (1980), 84, 3336.

6. R.W. Murray, Acc. Chem. Res., (1980), 13, 135.

7. D.A. Buttry and F.C. Anson, J. Am. Chem. Soc., (1984), 106, 59.

8. W.R. Heinemann and P.T. Kissinger, Anal. Chem., (1980), 52, 138R.

9. A.R. Guadalupe, D.A. Usifer, K.T. Potts, H.C. Hurrell, A. E. Mogstad and H.D. Abruna, J. Am. Chem. Soc., (1988), 110, 3462.

10. T.D. Cabelka, D.S. Austin and D.C. Johnson, J. Electrochem. Soc., (1985), 132, 359.

11. R.W. Murray, Annu. Rev. Mater. Sci., (1984), 14, 145.

12. N. Oyama, S. Yamaguchi, M. Kaneko and A Yamada, J. Electroanal. Chem., (1982), 139, 215.

13. D.C. Bookbinder and M.S. Wrighton, J. Am. Chem. Soc., (1980), 102, 5123.

14. H.D. Abruna and A.J. Bard, J. Am. Chem. Soc., (1981), 103, 6898.

15. C.E.D. Chidsey and R.W. Murray, J. Phys. Chem., (1986), 90, 1479.

16. P.G. Pickup and R.W. Murray, J. Am. Chem. Soc., (1983), 105, 4510.

17. H. Gomathi and G.P. Rao, J. Electroanal. Chem., (1985), 190, 85.

18. T. Ikeda, H. Hamada, K. Miki and M. Senda, Agric. Biol.

Chem., (1985), 49, 541.

19.   R.D. Armstrong, B. Lindholm and M. Sharp, J. Electroanal.
       Chem., (1986), 202, 69.

20.   N. Oyama, T. Ohsaka and T. Okajima, Anal. Chem., (1986),
       58, 979.

21.   B. Lindholm, M. Sharp and R D. Armstrong, J. Electroanal.
       Chem., (1987), 235, 169.

22.   H. Daifuku, K. Aoki, K. Tokuda and H. Matsuda, J.
       Electroanal. Chem., (1985), 183, 1.

23.   J. Leddy and A.J. Bard, J. Electroanal. Chem., (1983),
       153, 223.

24.   B.A. White and R.W. Murray, J. Am. Chem. Soc., (1987),
       109, 2576.

25.   T. Ohsaka, T. Okajima and N. Oyama, J. Electroanal.
       Chem., (1986), 215, 191.

26.   J. Wang, S. Chen and M.S. Lin, J. Electroanal. Chem.,
       (1989), 273, 231.

27.   R.F. Lane and A.T. Hubbard, J. Phys. Chem., (1973), 77,
       1401.

28.   R.F. Lane and A.T. Hubbard, J. Phys. Chem., (1973), 77,
       1411.

29.   P.R. Moses, L. Wier and R.W. Murray, Anal. Chem., (1975),
       47, 1882.

30.   J.R. Lenhard and R.W. Murray, J. Electroanal. Chem.,
       (1977), 78, 195.

31.   M.S. Wrighton, R.G. Austin, A.B. Bocarsly, J.M. Bolts, P.
       Haas, K.D. Legg, L. Nadjo and M.C. Palazatto, J.
       Electroanal. Chem., (1978), 87, 429.

32.   M.S. Wrighton, M.C. Palazzatto, A.B. Bocarsly, J.M.
       Bolts, A.B. Fischer and L. Nadjo, J. Am. Chem. Soc.,
       (1978), 100, 7264.

33.   A.W.C. Lin, P. Yeh, A.M. Yacynych and T. Kuwana, J.
       Electroanal. Chem., (1977), 84, 411.

34.   J.M. Bolts and M.S. Wrighton, J. Am. Chem. Soc., (1979),
       101, 6179.

35. A. Bettelheim, B.A. White, S.A. Raybuck and R.W. Murray, Inorg. Chem., (1987), 26, 1009.

36. J.M. Calvert, R.H. Schmehl, B.P. Sullivan, J.S. Facci, T.J. Meyer and R.W. Murray, Inorg. Chem., (1983), 22, 2151.

37. A. Merz and A.J. Bard, J. Am. Chem. Soc., (1978), 100, 3222.

38. R.W. Murray, Electroanalytical Chemistry, A.J. Bard (Ed.), M. Dekker, New York (1984), Vol 13.

39. A.R. Hillman, Electrochemical Science and Technology of Polymers, R.G. Linford (Ed.), Elsevier, Amsterdam (1981), Ch.s 5 & 6.

40. W.J. Albery and A.R. Hillman, R.S.C. Annual Report, (1981), 78, 377.

41. K.D. Snell and A.G. Keenan, Chem. Soc. Rev., (1979), 8, 259.

42. P. N. Bartlett, Biosensors, Fundamentals and Applications, A.P.F. Turner, G.S. Wilson and I. Karube (Eds.), Oxford University Press, New York (1987), Ch. 13.

43. H.D. Abruna, Coord. Chem. Rev., (1988), 86, 135.

44. T.E Edmonds, Chemical Sensors, Blackie & Son, London (1988), Ch. 8.

45. A.J. Bard and L.R. Faulkner, Electrochemical Methods: Fundamentals and Applications, Wiley, New York (1980).

46 P.T. Kissinger and W.R. Heineman, Laboratory Techniques in Electroanalytical Chemistry, M. Dekker, New York (1984).

47. D.T. Sawyer and J.L. Roberts, Experimental Electrochemistry for Chemists, Wiley, New York (1974).

48. V.G. Levich, Physicochemical Hydrodynamics, Prentice-Hall, Englewood Cliffs, N.J. (1962).

49. R.S. Nicholson and I. Shain, Anal. Chem., (1964), 36, 706.

50. D.H. Evans, Acc. Chem. Res., (1977), 10, 313.

51. W.R. Heineman and P.T. Kissinger, Am. Lab., (1982), 14,

29.

52. R.N. Adams, <u>Electrochemistry at Solid Electrodes</u>, M. Dekker, New York (1969).

53. W. Nernst, <u>Z. Phys. Chem.</u>, (1904), <u>47</u>, 52.

54. S.G. Weber and W.C. Purdy, <u>Anal. Chim. Acta.</u>, (1978), <u>100</u>, 531.

55. T. Ou and J.L. Anderson, <u>J. Electroanal. Chem.</u>, (1991), <u>302</u>, 1.

56. A.J. Bard, <u>J. Chem. Ed.</u>, (1983), <u>60</u>, 302.

57. C.E.D. Chidsey and R.W. Murray, <u>Science</u>, (1986), <u>231</u>, 25.

58. A.P.F. Turner, G.S. Wilson and I. Karube, <u>Biosensors, Fundamentals and Applications</u>, Oxford University Press, New York (1987).

59. G.A. Rechnitz, <u>Tr. Anal. Chem.</u>, (1986), <u>5</u>, 172.

60. F. Scheller, F. Schubert, D. Pfeiffer, R. Hintsche, I. Dransfeld, R. Renneberg, U. Wollenberger, K. Riedel, M. Pavlova, M. Kuhn, H.G. Muller, P. Tan, W. Hoffman and W. Moritz, <u>Analyst</u>, (1986), <u>114</u>, 653.

61. S. Dong and Y. Wang, <u>Electroanalysis</u>, (1989), <u>1</u>, 99.

62. M.P. Imisides, G.G. Wallace and E.A. Wilke, <u>Tr. Anal. Chem.</u>, (1988), <u>7</u>, 143.

63. R.P. Baldwin and K.N. Thomsen, <u>Talanta</u>, (1991), <u>38</u>, 1.

64. S.M. Geraty, D.W.M. Arrigan and J.G. Vos, <u>Electrochemistry, Sensors and Analysis</u>, M.R. Smyth and J.G. Vos (Eds.), Elsevier, Amsterdam (1986), 303.

65. J.N. Barisci, G.G. Wallace, E.A. Wilke, M. Meaney, M.R. Smyth and J.G. Vos, <u>Electroanalysis</u>, (1989), <u>1</u>, 245.

66. H C. Hurrell and H.D. Abruna, <u>Anal. Chem.</u>, (1988), <u>60</u>, 254.

67. B.T. Tay, K.P. Ang and H. Gunasingham, <u>Analyst</u>, (1988), <u>113</u>, 617.

68. D. Belanger, E. Brassard and G. Fortier, <u>Anal. Chim. Acta.</u>, (1990), <u>228</u>, 311.

69. Z. Lu and S. Dong, <u>Acta Chim. Sin.</u>, (1986), <u>44</u>, 32.

70. J.A. Cox and·K.R. Kulkarni, <u>Analyst</u>, (1986), <u>111</u>, 1219.

71. J.A. Cox and P.J. Kulesza, *J. Electroanal. Chem.*, (1984), 175, 105.

72. W.J. Vinning and T.J. Meyer, *Inorg. Chem.*, (1986), 25, 2023.

73. M.S. Tunuli and L. Arnendariz, *J. Electrochem. Soc.*, (1987), 134, 2641.

74. L.M. Santos and R.P. Baldwin, *Anal. Chem.*, (1987), 59, 1766.

75. M.K. Halbert and R.P. Baldwin, *Anal. Chem.*, (1987), 59, 591.

76. P.W. Geno, K. Ravichandran and R.P. Baldwin, *J. Electroanal. Chem.*, (1985), 183, 155.

77. J. Wang and Z. Taha, *Anal. Chem.*, (1990), 62, 1413.

78. K. Kalcher, *Electroanalysis*, in press.

79. R.F. Lane and A.T. Hubbard, *Anal. Chem.*, (1976). 48, 1287.

80. F. Li and S. Dong, *Electrochim. Acta*, (1987), 32, 1511.

81. K.K. Kanazawa, A.F. Diaz, R.H. Geiss, W.D. Gill, J.F. Kwak, J.A. Logan, J.F. Rabolt and G.B. Street, *J. Chem. Soc. Chem. Comm.*, (1979), 854.

82. L. Gorton and T. Svensson, *J. Mol. Catal.*, (1986), 38, 49.

83. J.A. Cox and P.J. Kulesza, *Anal. Chem.*, (1984), 56, 1021.

84. J.A. Cox and K.R. Kulkarni, *Talanta*, (1986), 33, 911.

85. J.A. Cox, T. Gray and K.R. Kulkarni, *Anal. Chem.*, (1988), 60, 1710.

86. J. Wang and B. Freiha, *Anal. Chem.*, (1984), 56, 2266.

87. D.C. Tse and T. Kuwana, *Anal. Chem.*, (1978), 50, 1315.

88. C. Ueda, D.C. Tse and T. Kuwana, *Anal. Chem.*, (1982), 54, 850.

89. A.N.K. Lau and L.L. Miller, *J. Am. Chem. Soc.*, (1983), 105, 5271.

90. H.B. Yon and C.R. Lowe, *Anal. Chem.*, (1987), 59, 2111.

91. P.J. Kulesza, K. Bratjer and E.D. Zlotorzynska, *Anal. Chem.*, (1987), 59, 2776.

92.   J. Wang, *Am. Lab.*, (1985), <u>19</u>, 41.

93.   K.Z. Brainina, *Talanta*, (1971), <u>18</u>, 513.

94.   A.R. Guadalupe and H.D. Abruna, *Anal. Chem.*, (1985), <u>57</u>, 142.

95.   L.M. Wier, A.R. Guadalupe and H.D. Abruna, *Anal. Chem.*, (1985), <u>57</u>, 2009.

96.   A.R. Guadalupe, L.M. Wier and H.D. Abruna, *Am. Lab.*, (1986), <u>18</u>, 102.

97.   M.J. Gehron and A. Bratjer-Toth, *Anal. Chem.*, (1986), <u>58</u>, 1488.

98.   S.K. Cha and H.D. Abruna, *Anal. Chem.*, (1990), <u>62</u>, 274.

99.   S.K. Cha, K.K. Kasem and H.D. Abruna, *Talanta*, (1991), <u>38</u>, 89.

100. K.H. Lubert and M. Schnurrbusch, *Anal. Chim. Acta.*, (1986), <u>186</u>, 57.

101. K.H. Lubert, M. Schnurrbusch and A. Thomas, *Anal. Chim. Acta.*, (1982), <u>144</u>, 123.

102. K. Izutsu, T. Nakamura, R. Takizawa and H. Hanawa, *Anal. Chim. Acta.*, (1983), <u>152</u>, 285

103. J. Lexa and K. Stulik, *Talanta*, (1985), <u>32</u>, 1027.

104. D.M.T. O'Riordan and G.G. Wallace, *Anal. Proc.*, (1985), <u>22</u>, 199.

105. D.M.T. O'Riordan and G.G. Wallace, *Anal. Proc.*, (1986), <u>23</u>, 14.

106. D.M.T. O'Riordan and G.G. Wallace, *Anal. Chem.*, (1986), <u>58</u>, 128.

107. L. Jin, J. Xu and Y. Fang, *Fenxi Huaxue*, (1986), <u>14</u>, 513.

108. J.A. Cox and M. Majda, *Anal. Chim. Acta.*, (1981), <u>118</u>, 271.

109. J.A. Cox and P.J. Kulesza, *Analyst*, (1984), <u>109</u>, 927.

110. T.J. Miwa, L.T. Jin and A. Mizuiki, *Anal. Chim. Acta.*, (1984), <u>160</u>, 135.

111. J. Wang, T. Peng and T. Golden, *Anal. Chim. Acta.*, (1987) <u>194</u>, 129.

112. B. Hoyer, T.M. Florence and G.E. Batly, *Anal. Chem.*,

(1987), <u>59</u>, 1608.

113. B. Hoyer and T.M. Florence, <u>Anal. Chem.</u>, (1987), <u>59</u>, 2839.

114. A. Nelson, N. Auffret and J. Readman, <u>Anal. Chim. Acta.</u>, (1988), <u>207</u>, 47.

115. L.D. Whitely and C.R. Martin, <u>Anal. Chem.</u> (1987), <u>59</u>, 1746.

116. R.D. Guy and S. Namaratne, <u>Can. J. Chem.</u>, (1987), <u>65</u>, 1133.

117. X. Su, H. Li, Y. Zang and Z. Li, <u>Fenxi Huaxue</u>, (1986), <u>14</u>, 886.

118. J. Wang, T. Golden, K. Varughese and I. El-Rayes, <u>Anal. Chem.</u>, (1989), <u>61</u>, 508.

119. O Chastel, J.M. Kauffmann, G.J. Patriarche and G.D. Christian, <u>Anal. Chem.</u>, (1989), <u>61</u>, 170.

120. J. Wang and M. Ozsoz, <u>Analyst</u>, (1990), <u>115</u>, 831.

121. J. Wang and M. Ozsoz, <u>Biolelectrochem. Bioenerg.</u>, (1990), <u>23</u>, 217.

122. K. Kalcher, <u>Anal. Chim. Acta.</u>, (1985), <u>177</u>, 175.

123. J. Wang, B. Greene and C. Morgan, <u>Anal. Chim. Acta.</u>, (1984), <u>158</u>, 15.

124. J. Wang and T. Martinez, <u>Anal. Chim. Acta.</u>, (1988), <u>207</u>, 95.

125. K. Kalcher, <u>F. Z. Anal. Chem.</u>, (1986), <u>325</u>, 186.

126. K. Kalcher, <u>F. Z. Anal. Chem.</u>, (1986), <u>325</u>, 181.

127. P.A.E. Hernandez, E. Alda and L. Hernandez, <u>F. Z. Anal. Chem.</u>, (1986), <u>327</u>, 676.

128. R.P. Baldwin, J.K. Christensen and L. Kryger, <u>Anal. Chem.</u>, (1986), <u>58</u>, 1790.

129. K.N. Thomsen, L. Kryger and R.P. Baldwin, <u>Anal. Chem.</u>, (1988), <u>60</u>, 151.

130. K. Kalcher, H. Greschonig and R. Pietsch, <u>F. Z. Anal. Chem.</u>, (1987), <u>327</u>, 513.

131. S.V. Prabhu, R.P. Baldwin and L. Kryger, <u>Anal. Chem.</u>, (1987), <u>59</u>, 1074.

132. J. Gardea-Torresdey, D. Darnell and L. Kryger, Anal. Chem., (1988), 60, 151.

133. K.M. Korfhage, K. Ravichandran and R.P. Baldwin, Anal. Chem., (1984), 56, 1514.

134. K. Ravichandran and R.P. Baldwin, Anal. Chem., (1983), 55, 1586.

135. J. Wang and P. Tuzhi, J. Electrochem. Soc., (1987), 134, 586.

136. J. Wang and L.D. Hutchins, Anal. Chem., (1985), 57, 1536.

137. J. Wang and L.D. Hutchins, Anal. Chem., (1986), 58, 402.

138. G.A. Gerhardt, A.F. Oke, G. Nagy, B. Moghaddun and R.N. Adams, Brain Res., (1984), 290, 390.

139. G. Nagy, G.A. Gerhardt, A.F. Oke, M.E. Rice, R.N. Adams, R.B. Moore, M.N. Szentirmay and C.R. Martin, J. Electroanal. Chem., (1985(, 188, 85.

140. H. Ji and E. Wang, J. Chromatog., (1987), 410, 111.

141. J. Wang and P. Tuzhi, Anal. Chem., (1986), 58, 3257.

142. J. Wang, M. Bonakder and M.M. Pack, Anal. Chim. Acta., (1987), 192, 215.

143. J. Wang, T. Golden and P. Tuzhi, Anal. Chem., (1987), 59, 740.

144. J. Wang, T. Golden and P. Tuzhi, Anal. Chem., (1988), 60, 1642.

145. J. Wang and T. Golden, Anal. Chem., (1989), 61, 1397.

146. T. Ohsaka, T. Hirokawa, H. Migamoto and N. Oyama, Anal. Chem., (1987), 59, 1758.

147. J. Wang and R. Li, Anal. Chem., (1989), 61, 2809.

148. M.B. Gelbert and D.J. Curran, Anal. Chem., (1986), 58, 1028.

CHAPTER 2

The Synthesis, Characterisation and

Electrochemical Properties of

Ruthenium bis(2,2'-bipyridyl)-containing

4-Vinylpyridine/Styrene Copolymers

2.1. INTRODUCTION

Redox polymer modified electrodes have been the object of active investigation in recent years because of their potential application in catalysis [1,2], photoelectrochemistry [3,4] and molecular electronics [5]. The main interest in these electrodes is as redox catalysts, where the polymer layer offers several advantages over monolayers, such as high local concentration of catalytic sites and a three dimensional reacting layer for homogeneous catalysis. A large theoretical background has been amassed concerning the mode of operation of redox polymer modified electrodes, including the mode of charge transport [6], mediation reactions [7] and the effect of external factors such as the synthetic procedure [8] and electrolyte effects [9]. What has emerged from these studies is the requirement of a detailed understanding of the rates and mechanisms of charge propagation. It is generally accepted that the fundamental charge transport mechanism in the redox polymer film is electron hopping between reduced and oxidised sites [10-12], as depicted in Figure 2.1. It has become apparent recently, however, that for some systems the rate determining step for charge transport is not necessarily the aforementioned self-exchange reaction. In many cases, ion transport processes, such as permeation and the availability of counter-ions, and polymer motions have been shown to limit the charge transport process [7,13-15].

Ruthenium- and osmium-containing metallopolymers have received particular attention because of their potential photoelectrochemical and catalytic applications [16-23]. However, relatively little attention has been paid thus far to the effects of systematic structural variations in the polymer backbone on the charge propagation rate and mechanism within polymeric coatings [23,24].

In this chapter, the synthesis and characterisation of 4-vinylpyridine/styrene copolymers containing $[Ru(bpy)_2Cl]^+$,
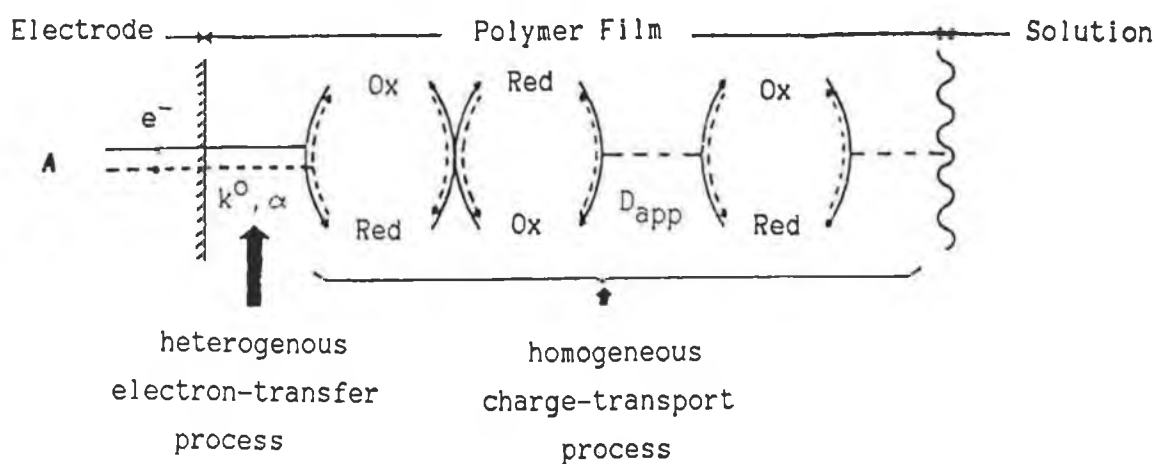
Figure 2.1: Charge transport process through redox polymer modified electrodes. k^0 and α represent the standard rate constant and transfer coefficient, respectively, for the heterogeneous charge transport process. D_{app} is the diffusion coefficient for the homogeneous charge transport within the film with Red and Ox indicating the reduced and oxidised form of the redox couple. (_____) represents the anodic process while (-----) represents the cathodic process.

47

where bpy is 2,2'-bipyridyl, is described. The structure of the corresponding metallopolymers, [Ru(bpy)$_2$(Pol)$_{10}$Cl]Cl, where Pol refers to one monomer unit of the polymer, is depicted in Figure 2.2.

A recent study of the analytical application of the [Ru(bpy)$_2$(PVP)$_5$Cl]Cl polymer films for the electrocatalytic detection of Fe(II), NO$_2^-$ and metal dithiocarbamate complexes [25] found that these films were not sufficiently stable in the flowing solutions used (half-life of approximately 8 hours), and further attempts to improve this stability, with coatings of both conducting and non-conducting polymers on top of the film, were not fully successful [26]. The incorporation of styrene into the poly(4-vinylpyridine) (PVP) backbone was expected to alleviate this problem. A study of the analytical applications of the copolymer modified electrodes is presented in Chapter 3. In this Chapter, a study of the charge transport process for the Ru(II/III) oxidation for glassy carbon electrodes modified with thin films of these metallopolymers is reported. Both potential step techniques and cyclic voltammetry (CV) were utilised to probe the charge transport process throughout the whole of the layer, rather than just close to the electrode/layer interface. Activation parameters for the charge transport process were also determined to help distinguish between the different limiting processes. The results obtained are discussed with particular reference to the composition of the polymer backbone and are of fundamental importance in polymer modified electrodes. The use of sampled current voltammetry (SCV) to determine k^o, the standard rate constant of heterogeneous electron transfer, is also described, with the results obtained discussed with reference to the rate limiting process for charge transport through the polymer modified electrodes.

A brief overview of the principles and theory of the study of charge transport through polymer modified electrodes, using the electrochemical techniques in this chapter, is presented
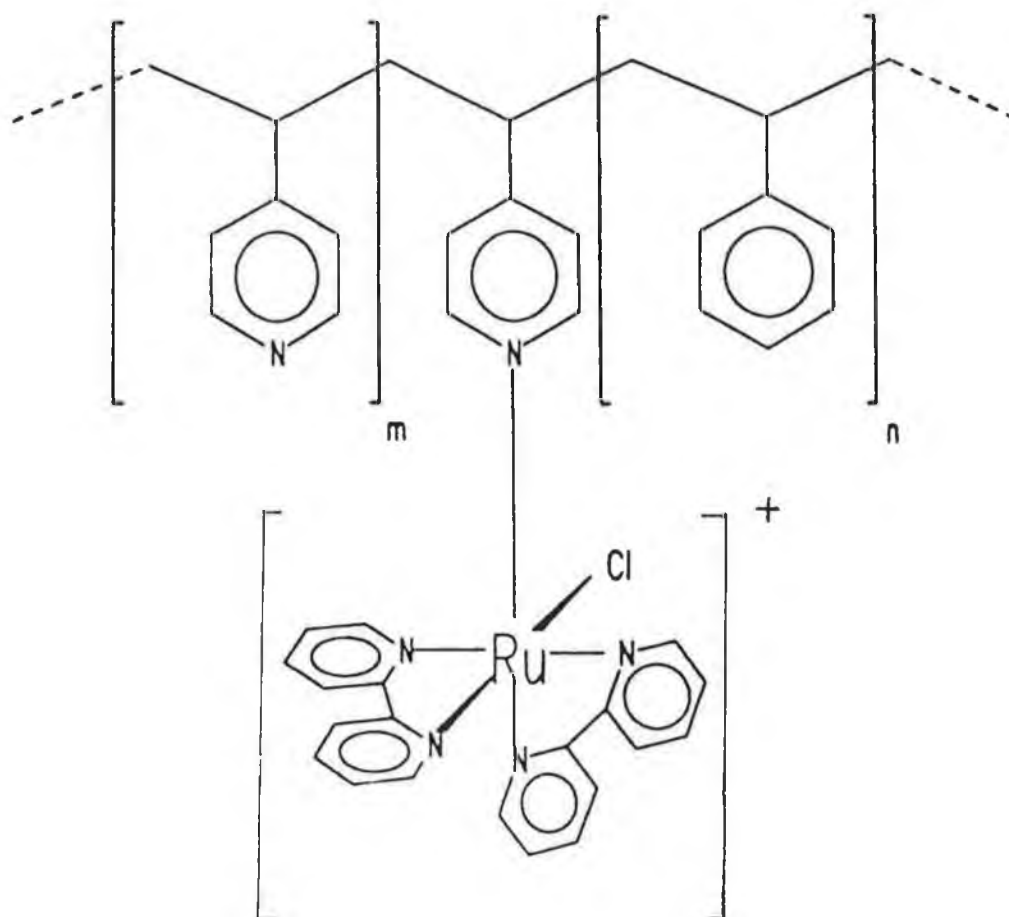
Figure 2.2: Chemical structure of the metallopolymers investigated in this study. The sum of m and n in this structure is 9, in order to give a constant polymer unit-to-metal centre ratio of 10 to 1.

followed by a short summary on the relevant literature.

2.1.1. Electrochemical Methods for the Determination of Charge Transport in Polymer Modified Electrodes

It is not the purpose of this section to conduct an in-depth review of all the methods and principles in the evaluation of charge transport through polymer films. Only the principles of the techniques utilised in this chapter will be discussed. For more comprehensive treatments the reader may consult several excellent papers on the subject [27-30].

2.1.1.1. Cyclic Voltammetry

Cyclic voltammetry (CV) has been extensively used to characterise the electroactivity of polymer modified electrodes and for the elucidation and the evaluation of charge transport rates. This electrochemical method gives a wide variety of information over a wide potential range without the need for specialised experimental conditions. Much of the CV studies have focussed on qualitative data and utilised other techniques, such as chronoamperometry, to quantitatively determine the charge transfer diffusion coefficient (D_{ct}). However, several authors have now used the following approaches successfully.

Quantitative data regarding charge transport have been largely obtained from examining the modifying layer at high sweep rates, where semi-infinite diffusion conditions prevail. The characteristic equations of the cyclic voltammogram in the case of a reversible electrode reaction within a semi-infinite diffusion regime are:

$$i_p = [0.4463(nF)^{3/2}AD_{ct}^{1/2}v^{1/2}c^*]/[(RT)^{1/2}] \quad (2.1)$$

$$E_p = E_{pa} - E_{pc} = 0.059/n \text{ V at } 25^{o}C \quad (2.2)$$

$$i_{pa}/i_{pc} = 1 \qquad\qquad (2.3)$$

where i_p is the peak current, n the number of electrons passed, T the temperature, A the area of the electrode. C^* the concentration of electroactive species, v the sweep rate and E_{pa} and E_{pc}, i_{pa} and i_{pc} the anodic and cathodic peak potentials and peak currents, respectively [31]. When there is no diffusional limitation (at slow sweep rates), the peak current varies linearly with v. Thus the variation of peak current height with sweep rate is a simple diagnostic tool for the behaviour of the modified electrode and, in certain circumstances, a changeover from v to $v^{1/2}$ dependence can be observed with increasing sweep rate. For the modified electrodes studied here, semi-infinite diffusion prevails at sweep rates above 100 mV s^{-1}.

At slow sweep rates, when all of the modifying layer is oxidised or reduced, the surface, or thin-layer, situation arises [32], which can be described by the equations shown below:

$$i_p = [n^2F^2\Gamma_Tv]/[4RT] \qquad\qquad (2.4)$$

$$E_{pa} = E_{pc} \qquad\qquad (2.5)$$

$$FWHH = 90.6n \text{ mV} \qquad\qquad (2.6)$$

where Γ_T is the total amount of electroactive material on the electrode surface. This can be readily obtained from slow scan cyclic voltammograms from the relation $\Gamma_T = Q/nFA$, where Q is the total charge passed upon oxidation or reduction of the entire film (see Figure 2.3). FWHH represents the full peak width at half height.

It is often found that the diffusion layer spreads up to the film/solution interface in a timescale of measurement. This

51
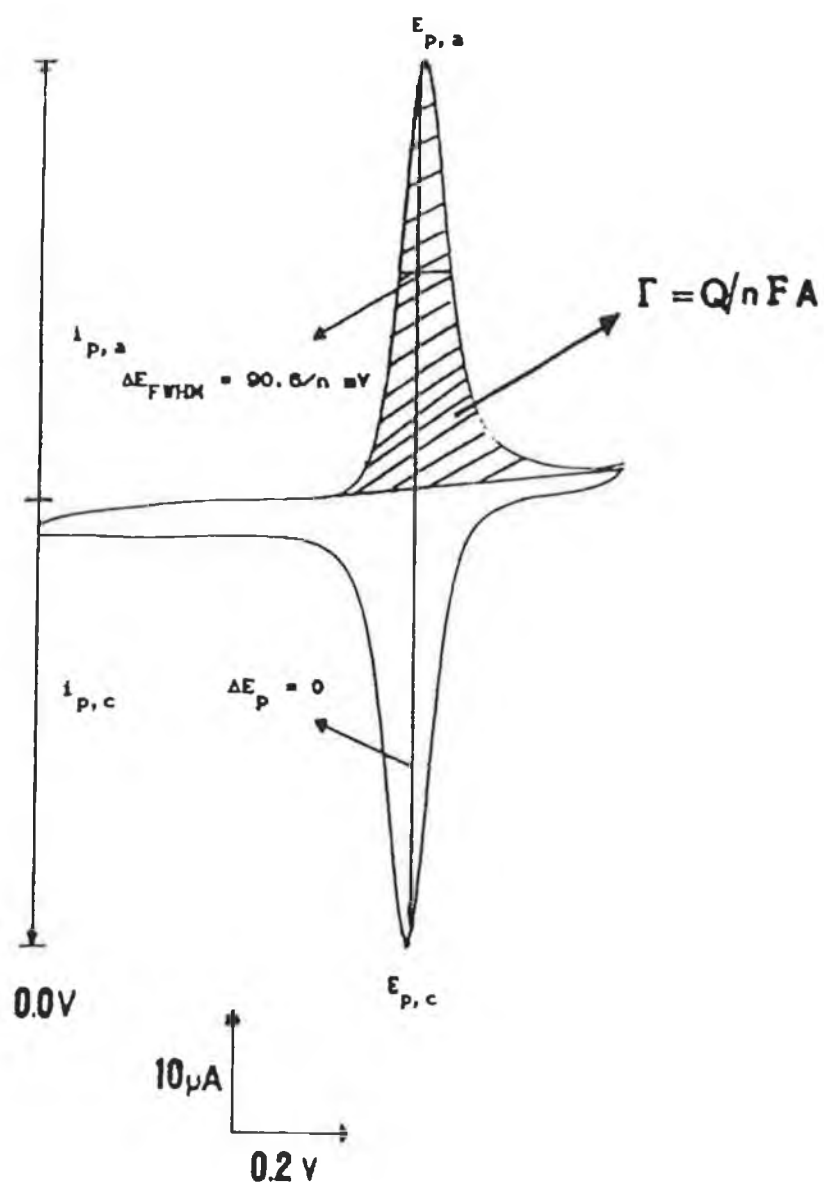
Figure 2.3: Slow sweep (1 mV s^{-1}) cyclic voltammogram obtained for [Ru(bpy)$_2$(PVP)$_{10}$Cl]Cl in 1.0 M NaNO$_3$ electrolyte. Surface coverage of ruthenium centres is 6.0 x 10^{-8} mol cm^{-2}.

concept of a finite diffusion space for linear sweep voltammetry
has been examined by Aoki et al. [33] for reversible kinetics
with the following assumptions:

- mass transfer of both species is only subject to the
  diffusion that is described by Fick's second law (equation
  2.7);

$$\delta C^*(x,t)/\delta t = D\delta^2 C^*(x,t)/\delta x^2 \qquad (2.7)$$

- the solution initially contains R with concentration C^*;

- diffusion coefficients of both oxidised and reduced forms of
  the redox couple have the common value D;

- electroactive species cannot pass through the interface
  between the film and solution;

- the electrode reaction is sufficiently rapid to ensure a
  Nernstian response.

The boundary conditions at the electrode are given by:

$$C_o(0,t)/C_r(0,t) = \exp[nF(E_i + vt - E^{o\prime})/RT] \qquad (2.8)$$

$$i/nF = D(\delta C_r/\delta x)_{x=0} = -D(\delta C_o/\delta x)_{x=0} \qquad (2.9)$$

where C_o and C_r represent the concentration of O and R,
respectively, at time t. The theta function has been used by
Aoki to evaluate the i-E curve, this being described by:

$$i = nFC^*[Dv(nF/RT)]^{1/2}f(w,\xi) \qquad (2.10)$$

where $f(w,\xi) = w^{1/2}\int_o^\infty \Theta_2(0/z)e^{wz-\xi}/(1 + e^{wz-\xi})^2 dz$, and
with $W = (nF/RT)vd^2/D$, the square root of which denotes the

ratio of the thickness of diffusion space, d, to the diffusion layer thickness. The approximate solution of the finite diffusion space equation is given by Simpson's rule as:

$$i_p/nF = 0.446(C^*D/d)W^{1/2}\tanh(0.56W^{1/2} + 0.05W) \quad (2.11)$$

This theory allows the evaluation of the charge transfer diffusion coefficient over large sweep rate ranges simply from a knowledge of the surface coverage and the peak current. For solution type behaviour (i.e. when W is large) this equation reduces to the semi-infinite diffusion equation of Randles-Sevcik (equation (2.1), while if W is less than 1 the Langmuir surface equation (2.4) is obtained. Aoki has also introduced kinetic limitation theory and the theory of quasi-reversible and totally irrevsible redox waves into the finite diffusion space equation [34], the scope of which is not covered in this thesis.

2.1.1.2. Chronoamperometry

Most workers, when using chronoamperometry to evaluate D_{ct}, tend to neglect the finite diffusion space equation [35] and manipulate the timescale of the potential step to remain within a semi-infinite diffusion space, where the current decay conforms to the Cottrell equation shown below [29]:

$$i_t = [nFAD_{ct}^{1/2}C^*]/[(\pi t)^{1/2}] \quad (2.12)$$

Chronoamperometric experiments generally reflect a measure of electron hopping as well as other limiting processes such as counterion or polymer chain motions in redox polymer films.

2.1.1.3. Sampled Current Voltammetry

The potential waveform that is utilised in sampled current voltammetry is depicted in Figure 2.4. The rate of charge propagation in the modifying layer can be examined by SCV to give essentially the same results as chronoamperometry. Plots of the sampled anodic currents at different times versus the reciprocal square root of the sampling time are linear and obey the Cottrell relation shown in equation (2.12). SCV is utilised in this chapter, however, to determine the standard rate of heterogeneous electron transfer between the electrode material and the modified electrode film.

The current-potential relationship for the SCV for the simple process, red = ox + ne$^-$, has been derived by Matsuda et al. [36] and is given by equation (2.13) below:

$$E = E^* + \frac{RT}{\alpha nF} \ln \left[x \left(\frac{1.75 + x^2 (1 + \exp(\pm\zeta))^2}{1 - x(1 + \exp(\pm\zeta))} \right)^{1/2} \right] \qquad (2.13)$$

with

$$E^* = E_{1/2} \pm \frac{RT}{\alpha nF} \ln \left[\frac{4 \, k^o (\tau)^{1/2}}{(3)^{1/2} (D_{ct})^{1/2}} \right] \qquad (2.14)$$

where E is the electrode potential, $E_{1/2}$ the reversible half wave potential, k^o the standard rate constant, τ the sampling time, R the gas constant, ζ a dimensionless parameter expressed as $[(nF/RT)(E-E_{1/2})]$, D_{ct} the homogeneous charge transfer diffusion coefficient as determined by potential step methods, and x the ratio of the current at potential E to the anodic limiting current (Cottrell current). A plot of the right hand side of equation (2.13) against E is linear with a slope of $((RT/nF)^{-1})$ and intercept E^*. Thus k^o may be evaluated with the assumption that $D_{ct}{}^a = D_{ct}{}^c$ and using the value of the formal potential obtained from cyclic voltammetry.

55
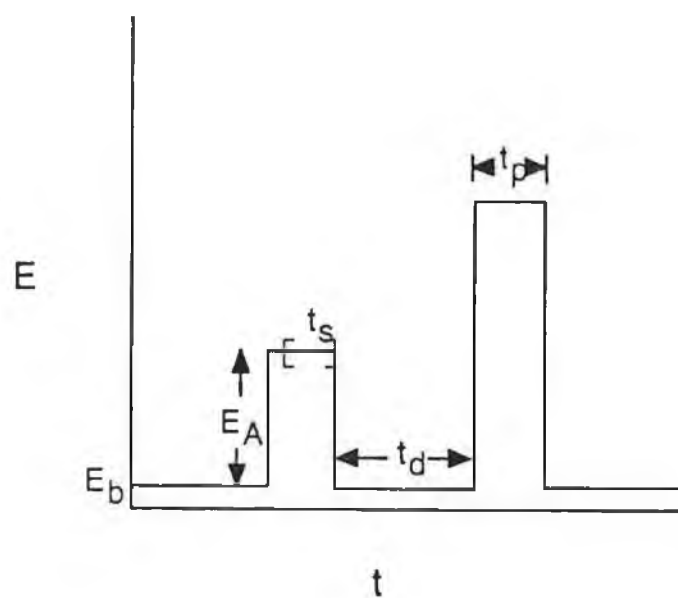
Figure 2.4: Potential waveform utilised in SCV, where E_b is the base potential, E_A is the pulse amplitude, t_p the pulse width, t_d the delay between pulses and t_s the time over which the current is sampled.

2.1.2. Activation parameters

The evaluation of activation parameters for the charge transport process can be helpful in the specification of the rate determining step in redox polymer films [14-16]. As discussed earlier, the mechanism of charge transfer in these films is thought to involve electron hopping between fixed redox sites accompanied by counterion diffusion to maintain electroneutrality. Both processes are described by Fick's laws of diffusion and can be described by the Arrhenius equation for activated diffusion or chemical reaction [16]:

$$D_{ct} = D_{ct}{}^{O}\exp(-E_a/RT) \qquad (2.15)$$

with the Eyring equation being used to calculate entropies.

$$D_{ct}{}^{O} = e\delta^2(k_BT/h)\exp(\Delta S^{\neq}/R) \qquad (2.16)$$

In the equations shown above, E_a refers to the activation energy, δ denotes the mean separation of the fixed redox sites, e is the base of the natural log, k_B is the Boltzmann constant and h is the Planck constant. A discussion on the use of activation parameters in the elucidation of the rate limiting charge transport process will be presented with the results.

2.1.3. Review of Charge Transport Through Polymer Films on Electrodes

The success of any attempt to exploit chemically modified electrodes (CMEs) for electrocatalytic detection of substrates lies in a detailed understanding of charge transport rates and mechanisms, so that charge transport does not severely limit the electrode performance. This section of the chapter reviews the relevant literature on the investigation and determination of charge transport processes and rates for polymer modified electrodes.

The investigation of charge transport rates and mechanisms through polymeric matrices has been carried out by many workers. A feature of the earlier publications, however, was the absence of actual quantitative data regarding ion and electron movement within the films. What is more commonly exploited are parameters such as wave shape and position to broadly discuss possible mechanisms. An excellent early paper by Kaufmann et al. [37] discussed ion and electron transport in tetrathiafulvalene polymer films using a combination of CV and potential step techniques. Khoo et al. [13] have examined the effect of the electrolyte type on the charge transport diffusion coefficient in tetracyanoquinodimethane (TCNQ) and tetracyanoethylene (TCNE) modified electrodes using the Randles-Sevcik equation for cyclic voltammetry, and have attributed changes in D_{ct} to the ion-pairing effect of the perchlorate anion in these films. Inzelt et al. [38,39] have also studied the effect of the nature and concentration of the counterion on the wave-shape of the CV behaviour of the TCNQ polymer films, and have concluded that salt or ion pair formation between the reduced forms of the redox films and the counterions contribute to the variabilities observed with different electrolyte types and concentrations.

Inzelt and Szabo [9] have shown that the nature and concentration of electrolyte can also affect the response for polyvinylferrocene (PVF) films. Daum et al. [15] have

interpreted charge transport through radiofrequency plasma polymerised PVF as controlled by both polymer chain motions and counterion diffusion. Activation energies and entropies of approximately 16 $kJmol^{-1}$ and -140 $Jmol^{-1}K^{-1}$, respectively, corresponding to rate limiting diffusion of counterions have also been determined for these films [15]. Bowden et al. [40-42], in a significant series of papers, considered the thermodynamics of PVF modified electrodes. In this study, controlled potential coulometry and CV were utilised to examine the reversibility of the redox reactions. A model was developed to explain the observed response in terms of forced inclusion of charge compensating counterions into the film during redox cycling. Electrolyte effects of this type will be discussed in the results section of this chapter for the ruthenium redox polymers investigated.

Other workers have reported effects of electrolyte size on the rate of charge propagation. Albery et al. [43] have shown that the rate of charge propagation is dependent on the size of the counterion, in a study of thionine-coated electrodes. Ohsaka et al. [44] reported that the rate determining process for charge transport through poly(methylviologen) films was not the electron hopping process between adjacent viologen sites, but rather the process of charge compensating counterion motions and/or polymer film motions, based on the variations observed in D_{ct} values with varying electrolyte types and concentrations.

For most of the polymer films studied, an increase in redox site loading within films of equal thicknesses results in an increase in the rate of charge propagation through the film. The variation of the homogeneous charge transport diffusion coefficient with fixed site loading has been studied for osmium redox centres bound to films prepared from electropolymerised bis(bpy)bis(N-4-pyridylcinnamamide)osmium(II) hexa-fluorophosphate [45,46]. Facci et al. [46], in a well constructed experiment, used ruthenium redox centres to dilute the osmium metal sites in the film while keeping the overall

redox loading constant, with three regions of behaviour being observed depending on the site-to-site distances.

In the more popular ion exchange type membranes, several papers investigating the loading have been published [35,47-49]. Oh and Faulkner [49] have varied the loading of $[Fe(CN)_6]^{3-/4-}$ within partially quaternised PVP films and have concluded that counterion motions are not limiting in these films because of similarities in D_{ct} determined by both steady-state and transient methods, although D_{ct} was shown to decline with increased loading because of increased crosslinking of the film. These workers have also investigated effects of crosslinking on the charge transport through films of PVP bound $[Ru(bpy)_2Cl]^+$, and have found that the activation energies were linearly dependent on the degree of crosslinking. It was also concluded that the anion dependence observed in D_{ct} values for these films was a structural effect and that polymer segmental motions controlled the diffusion process [23].

In a significant series of papers, the theory and application of sampled current voltammetry to the determination of charge transport parameters in polymer modified electrodes was treated [44,48,50]. Homogeneous charge transfer rates for PVP films incorporating $[W(CN)_8]^{3-/4-}$ and $[IrCl_6]^{2-/3-}$ were shown to vary with electrolyte and redox site loading. SCV has also been used by Chiba et al. [51] for the study of electrode kinetics in electropolymerised electroactive films. Several other workers have now successfully utilised the SCV approach for the investigation of charge transport kinetics in polymer modified electrodes [52,53].

Perhaps more closely related to this work is the investigation of charge propagation through polymers where the redox centre is an immobilised metal complex. Pickup and Osteryoung [54] have observed a 2.6 fold decrease in the charge transport rate through a poly-$[Ru(bpy)_2(4-vinylpyridine)_2]^{2+3+}$ film in chloride molten salts in comparison with acetonitrile electrolytes. This was discussed in

terms of solvent effects and/or polymer swelling contributions to the determined D_{ct} value. In a series of contributions, Forster et al. [7,14,55,56] have systematically studied the dependence of D_{ct} in $[Os(bpy)_2(Pol)_nCl]Cl$ films, where Pol can be either PVP or poly(N-vinylimidazole), on various factors such as electrolyte type and concentration, temperature and redox site loading. Increases in D_{ct} with increasing electolyte concentrations were observed for all but the perchlorate electrolytes. The decrease in D_{ct} with increasing perchloric acid concentration was attributed to ion pairing effects of this counterion. The rate limiting step for charge transport through these polymers was shown to be counterion diffusion for most of the systems, with all of the polymers showing variations in D_{ct} and activation parameters with electrolyte concentration and type. Differences, similar to those reported in the next section, between charge transport rates determined by both cyclic voltammetric and potential step methods were also reported for these polymers [7,14,55,56] and were attributed to the differing timescales for both electrochemical techniques.

2.2. EXPERIMENTAL

2.2.1. Materials

Bulk polymerisation of the polymers and copolymers was carried out without regard for reactivity ratios in order to achieve the highest molecular weight materials.

Poly(4-vinylpyridine): poly(4-vinylpyridine) was prepared by bulk polymerisation of freshly distilled 4-vinylpyridine under nitrogen atmosphere using 2,2'-azobisisobutyronitrile as a free radical initiator at 70°C. The resulting polymer was fractionated by partial precipitation from methanol solution and the precipitant was dried at 60°C in vacuo overnight.

co-Poly(4-vinylpyridine-styrene): copolymers of 4-vinylpyridine and styrene were prepared as above, with the freshly distilled monomers mixed in the desired molar ratios. The resulting polymers were purified by repeated precipitation in diethyl ether from 2-methoxyethanolic solution and dried in vacuo at 60°C overnight. Microanalytical results for the series of copolymers are shown in Table 2.1. Theoretical values allowing for 0.5 H_2O molecules per pyridine unit were used, as samples of PVP have been known to retain water even upon rigorous drying [17,18]. Also shown in Table 2.1 are the abbreviations used throughout the text for the polymers and those that will be used for the ruthenium metallopolymers (the subscripts refer to the approximate 4-vinylpyridine percentage compositions of the polymer backbone).

[Ru(bpy)$_2$Cl$_2$].2H$_2$O: commercial RuCl$_3$.3H$_2$O (Johnson Matthey, 7.8 g, 29.8 mmol), 2,2'-bipyridyl (9.36 g, 60 mmol) and LiCl (0.8 g, 2 mmol) were heated at reflux in reagent grade dimethylformamide (50 cm ^{3}) for 8 hours. The reaction was stirred magnetically throughout this period. After the reaction

62

Table 2.1: Microanalytical results for the synthesised unbound copolymers, together with the abbreviations that will be used for the metallopolymers throughout the text.

	Theory			Found			Ru-polymer
% PVP	% C	% H	% N	% C	% H	% N	abbreviation
75	78.03	7.17	9.42	77.69	6.82	9.66	Ru–PVP$_{75}$
67	79.52	7.23	8.43	79.63	6.91	8.91	Ru–PVP$_{67}$
50	82.60	7.34	6.42	82.38	7.13	6.88	Ru–PVP$_{50}$
33	85.70	7.45	4.35	85.91	7.33	4.63	Ru–PVP$_{33}$

mixture was cooled to room temperature, 250 cm^3 of reagent grade acetone was added and the resulting solution cooled at 0°C overnight. Filtering yielded a red to red-violet solution and a dark green-black microcrystalline product. The solid was washed three times with 25 cm^3 portions of water followed by three 25 cm^3 portions of diethyl ether, and then it was dried by suction. The purity of the product was checked by high performance liquid chromatographic separation (HPLC) on a cation exchange resin with subsequent uv-visible detection using a photodiode array detector. The chromatogram obtained showed only one peak eluting at a retention time of 2.5 min. The maxima observed for this peak in the uv-visible region at 365 nm and 524 nm, respectively, correspond well with reported values for [Ru(bpy)$_2$Cl$_2$].

Yield: 68% based on starting ruthenium.

[Ru(bpy)$_2$(Pol)$_{10}$Cl]Cl: the copolymer (100 mg, 1 mmol) and the required weight of the [Ru(bpy)$_2$Cl$_2$].2H$_2$O (51 mg, 0.1 mmol) were heated at reflux for 72 hours, with the course of the reaction being monitored by uv-visible spectroscopy and cyclic

voltammetry. The product was isolated by precipitation into hexane and purified by repeated precipitation into diethyl ether from dichloromethane.

2.2.2. Apparatus

Uv-visible spectra were recorded on either a Hewlett-Packard 342A diode array or Shimadzu UV 240 spectrophotometers. A Waters 990 photodiode array HPLC system in conjunction with a NEC APC III computer, a Waters Model 6000A pump and a Partisil SCX radial PAK cartridge column were utilised with an 80:20 acetonitrile:water mobile phase containing 0.08 M $LiClO_4$ to check the purity of the synthesised [$Ru(bpy)_2Cl_2$]. Emission spectra were recorded using a Perkin-Elmer LS-5 luminescence spectrometer equipped with a red-sensitive Hamamatsu R928 detector. Spectra were recorded using an emission slit width of 10 nm at room temperature and 2.5 nm at 77 K, and were not corrected for photomultiplier response. Infrared spectra, obtained as either KBr disks, or from thin films on NaCl disks were recorded using a Perkin-Elmer 599 spectrophotometer. Differential scanning calorimetry (DSC) was performed on vacuum dried samples using a Stanton Redcroft CPC 706 Temperature Programmer, a DSC lineariser and a DC amplifier. Experiments were carried out in static air at a heating rate of $5^{o}C$ min^{-1} up to a temperature of $350^{o}C$. Electrochemical measurements were performed using an EG & G PAR 273 potentiostat/galvanostat, with a Philips 311 digital oscilloscope interfaced to a BBC microcomputer being used for data capture and interrogation for the potential step experiments. All potentials are quoted versus a saturated calomel electrode (SCE) without regard for liquid junction potentials. Elemental analyses were carried out at the Microanalytical Department of University College Dublin.

2.2.3. Procedures

Glassy carbon electrodes of 7 mm diameter were polished with a 0.3 m alumina slurry on a felt cloth and then dipped in methanol to remove any residual alumina. The electrodes were modified by pipetting the required quantity of a methanolic or 2-methoxyethanolic (0.1% w/v) solution of the metallopolymer directly onto their surface. The solvent was then allowed to evaporate slowly in a solvent saturated chamber, to ensure film homogeneity, followed by air drying. Surface coverages of the ruthenium for the metallopolymers were determined from the integration of the charge under slow scan (1 mV s^{-1}) cyclic voltammetric peaks. Surface coverages of 4-8 x 10^{-8} mol cm^{-2} were utilised throughout this study in order to minimise variations in the determination of charge transport rates caused by varying coverages. Potential step chronoamperometry was used to determine Ru(II/III) charge transport rates by stepping from 0.0 V to 1.2 V (approximately 500 mV past the formal potential of the redox couple) over the time range 0 to 10 ms using signal averaging. Potential steps for background correction were made between 0 V and 0.2 V, where no redox reaction occurred, and linearly extrapolated. Positive feedback circuitry was used for these experiments to minimise IR drops in the film, with 85-90% of the resistance normally being compensated for. Cell time constants of, normally, between 50-200 μs, after IR correction, were thus obtainable.

The experimentally determined variable for the charge transport determinations is $D_{ct}^{1/2}C$ (where C is the concentration in mol cm^{-3} of electroactive species on the electrode surface). This concentration, and thus the polymer layer thickness, may be estimated from the individual densities of the dry metallopolymers as measured by flotation in non-swelling solvents (carbon tetrachloride and hexane in this case). The concentrations determined for the polymers studied here were 0.82, 0.81, 0.80, 0.79 and 0.78 mol dm^{-3} for the

65

Ru-PVP$_{100}$, Ru-PVP$_{75}$, Ru-PVP$_{67}$, Ru-PVP$_{50}$ and Ru-PVP$_{33}$ metallopolymers, respectively. These values were used to calculate the D_{ct} values from $D_{ct}^{1/2}C$.

In the studies where electrolyte type and concentrations were varied, all experiments were carried out on fresh coatings in order to minimise possible problems from "memory effects", where the rate of charge transport through the films would be dependent on the electrolytes to which it had been previously exposed. Light was excluded from the electrochemical cell for all of the electrochemical experiments to prevent the photosubstitution of the coordinated Cl$^-$ with solvent (H_2O) [22].

2.3.   RESULTS AND DISCUSSION

2.3.1. Characterisation of the Polymers

The synthetic approach used was to react the preformed polymers with [Ru(bpy)$_2$Cl$_2$]. This allowed the metallopolymers to be characterised both in solution and as thin films on the electrode surface. The formation of the metallopolymers was based on the well documented lability of the chloride ions in the [Ru(bpy)$_2$Cl$_2$] complex. Extensive studies have shown that the first chloride ion is easily removed by refluxing in methanol or ethanol leading to substitution by polymer molecules (see reactions (2.17) and (2.18) below, S = solvent) [17,21,57,58]. The solvent used in this study was 2-methoxyethanol, which is a better solvent for the copolymers than the lower alcohols [59].

$$[Ru(bpy)_2Cl_2] + S \longrightarrow [Ru(bpy)_2(S)Cl]^+ + Cl^- \quad (2.17)$$

$$[Ru(bpy)_2(S)Cl]^+ + Pol_n \longrightarrow [Ru(bpy)_2(Pol)_nCl]^+ + S \quad (2.18)$$
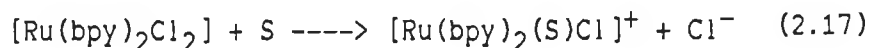
The metal loading of the metallopolymers was based on the

quantity of starting material employed, assuming complete reaction. The validity of this asumption is supported by continuous monitoring of the reaction using spectroscopic and electrochemical techniques (vide infra). A constant loading of 10:1 polymer unit:metal centre (where the polymer unit can be either that of styrene or 4-vinylpyridine) was used to maintain an approximately constant mean metal-to-metal intersite distance to enable comparison of entropy values (determined from equation 2.16). In the present case this separation has been approximated using crystal structure data for the poly(4-vinylpyridine) backbone [60]. This gives a separation of 0.25 nm between adjacent monomers and thus, assuming a rigid rod structure in the metallopolymers, the ruthenium metal centres are assumed to be separated by 2.5 nm, when n = 10. The characterisation of the polymers and the metallopolymers was accomplished by applying several techniques to each sample and will be detailed below.

2.3.1.1. Glass Transition Temperature

The effect of varying the percentage concentration of styrene in the copolymer backbone on the glass transition temperature (T_g) of both the copolymers and the metallopolymers has been examined and is presented in Table 2.2. Thoroughly dried PVP has a T_g of approximately 142°C, while polystyrene (PS) has a T_g of approximately 100°C, both of which are largely independent of molecular weight [61]. The linear increase in the determined T_g values for the copolymers with increasing PVP content supports and reflects the experimentally determined copolymer composition.

The much higher glass transition temperatures for the metallopolymers most likely reflect the greater difficulty in obtaining fluid-like motion because of a decrease in mobility upon coordination of the bulky metal centres. This increase in T_g upon metalation has also been reported for osmium analogues of the PVP homopolymer [62]. The trend in the T_g values

67

Table 2.2: Glass transition temperatures determined by differential scanning calorimetry for the copolymers and their respective metallopolymers.

% PVP in	T_g (°C)	
copolymers	Copolymer	Metallopolymer
100	140 ($\pm$2)	224 ($\pm$5)
75	133 ($\pm$4)	216 ($\pm$5)
67	131 ($\pm$3)	210 ($\pm$5)
50	126 ($\pm$3)	209 ($\pm$5)
33	119 ($\pm$3)	208 ($\pm$5)

determined for the metallopolymers, with increasing PVP content in the polymeric backbone, reflects the trend associated with the increasing PVP content observed for the free copolymers. It has been shown that, for the osmium analogues of the $Ru-PVP_{100}$ homopolymer studied here, the glass transition temperature for these metallopolymers is sensitive to the metal loading, with T_g increasing from 180°C to 230°C upon altering the metal to polymer subunit loading from 1:25 to 1:5 [62]. Thus the relatively small differences in transition temperatures obtained for the ruthenium metallopolymers studied here are an indication of a similar metal-to-polymer unit ratio for the whole series. The slight variations in T_g for the metallopolymers is thought to be because of the changes in PVP content in the polymer backbone and not due to variations in the metal-to-polymer unit ratios. This assumption is supported by the spectroscopic evidence presented below and thus allows the calculation and comparison of entropy values for charge transport through these metallopolymers based on constant metal-to-polymer unit distances (vide infra).

PVP is thermallly stable in a nitrogen atmosphere up to 300°C. On conversion to the acid salt or 1-alkylpyridinium salt, the thermal stability decreases, the decrease being a function of the extent of quaternisation. For the materials described here, however, no loss in thermal stability via DSC measurements was observed, and both spectroscopic and electrochemical measurements suggest that the metallopolymers do not decompose at temperatures of up to 300°C. The degradation in the polymeric 1-alkylpyridinium salts is generally accepted as occuring in two stages: loss of the 1-alkyl group and scission of the polymer backbone [63]. That these metal containing polymers remain stable suggests a strong coordination between the metal and polymer nitrogen.

2.3.1.2. Infrared Spectroscopy

The spectra of the copolymers were a combination of all the bands present in poly(4-vinylpyridine) and polystyrene spectra. Furthermore, a linear correlation between the ratio of the percentage transmission of the poly(4-vinylpyridine) band at 1550 cm^{-1} to the percentage transmission of the $-CH_2-$ polymer backbone stretching frequency at 2931 cm^{-1} and the molar ratio of poly(4-vinylpyridine) in the polymer backbone was found. This result confirms and reflects the experimentally detemined polymer composition.

For all of the metallopolymers, the presence of the chloride ligand was confirmed by a M-Cl stretching vibration at 330 cm^{-1}.

2.3.1.3. Absorption and Emission Spectroscopy

The electronic spectra in 2-methoxyethanol for the homopolymers of styrene and 4-vinylpyridine both show strong overlapping $\pi -> \pi^*$ transitions at approximately 220 nm and 256 nm. The ratio between the absorbance of the copolymers at 256 nm

69

and the absorbance obtained at this wavelength upon protonation of the pendant pyridines with hydrochloric acid gives an estimate of the 4-vinylpyridine content, with the results obtained in good agreement with the expected 4-vinypyridine content.

The electronic spectra obtained for ruthenium 2,2'-bipyridyl complexes have been well documented [17-19] and have proved to be a useful tool in the characterisation of such compounds. In particular, the energy of the lowest absorption maxima and the wavelength of emission are characteristic for a particular ruthenium moiety. According to the literature [64], the visible absorption spectrum of Ru(II)-diimine compounds is assigned to a spin allowed metal-to-ligand charge transfer transition ([1]MLCT) from the metal d-orbitals to the π^*-orbital of the bipyridyl ligand, while the emission is thought to occur from a ligand-based [3]MLCT orbital. The metallopolymers studied here show two intense absorptions in the visible region, at 356 nm and 502 nm. The uv-visible spectrum of a model monomeric compound, [Ru(bpy)$_2$(py)Cl]Cl (where py represents a pyridine unit) [65], shows two absorptions at 352 nm and 496 nm in ethanol. The slight red shifts for the polymeric compounds can be attributed to various factors, such as the steric effect of the polymeric ligand having a methylene chain as the backbone, or solvent effects. Slight variations in extinction coefficients calculated for the copolymer metallopolymers were observed and could be because of the problems caused by varying degrees of hydration of the polymers. The extinction coefficient calculation does, however, remain a useful tool in the examination and confirmation of metal centre to polymer unit ratios. An extinction coefficient of 8500 $M^{-1}cm^{-1}$ has been given for the lowest energy [1]MLCT band of the model monomeric compund [65]. The extinction coefficients calculated for all of the metallopolymers were equal to this, within experimental error, confirming the metal-to-polymer subunit loading of 1:10 calculated from the initial reaction concentrations of polymer

and $[Ru(bpy)_2Cl_2]$.

The presence of an emission maximum for the metallopolymers, upon excitation at 500 nm, at 712 ± 9 nm at room temperature and at 671 ± 3 nm at 77 K are consistent with the presence of the $[RuN_5Cl]$ moiety [66].

2.3.1.4. Electrochemistry

The formal potentials for the Ru(II/III) oxidation in perchloric acid and sodium nitrate (pH 3.0) electrolytes (0.1 M and 1.0 M concentrations) were determined from the slow sweep (1 mV s^{-1}) cyclic voltammetric waves. For the Ru-PVP$_{100}$ metallopolymer, formal potentials of 655 mV and 600 mV were obtained in 0.1 M and 1.0 M $HClO_4$, respectively, while formal potentials of 690 mV and 655 mV were obtained in 0.1 M and 1.0 M $NaNO_3$, respectively. These formal potentials were shifted positively in all electrolytes upon incorporation of styrene in the polymers, to a maximum shift of 30 mV for the Ru-PVP$_{33}$ metallopolymers. This shift may be explained in terms of the increasing hydrophobic nature of the films upon increasing the styrene content.

2.3.1.5. Conclusions

All of the above results point to the fact that the polymer backbone may be altered by the addition of styrene with little subsequent varations in the spectroscopic data or electrochemical formal potentials for the metallopolymers. The next section of this chapter involves the investigation of charge transport processes and mechanisms in these metallopolymers, and the effect various parameters can have on the rate of charge transport and the rate limiting step for the charge transport process with a view to optimisation of sensor response.

2.3.2. Investigation of Charge Transfer Processes

This section of the chapter involves the systematic investigation of some parameters which affect the rate of charge propagation through thin films of the materials prepared on electrode surfaces. Factors such as electrolyte type and concentration and temperature, as well as the 4-vinylpyridine mole ratio in the polymer backbone, have been varied. These variations are such that they enable information to be obtained as to the charge transport mechanism and the factors which affect its rate. The results obtained are of a fundamental importance to the development of a complete understanding of the charge transport processes in polymer films. The identification of the rate limiting process for charge transport in these films can help in the optimisation of sensor response, for instance with respect to charge transport rates or formal potentials. This is extremely important for polymer modified electrodes, as rapid charge transport is frequently a requirement for sensor applications.

Potential step chronoamperometry (CA) was employed in conjunction with the Cottrell equation (2.12) to estimate charge transport rates for the Ru(II/III) oxidation as an apparent diffusion coefficient, $D_{ct}(CA)$. In general, linear Cottrell plots were obtained for times up to about 10 ms, these plots exhibiting zero current intercepts in all cases, suggesting that the current response is under semi-infinite diffusion/migration control.

In the CV experiments, sweep rates between 100 and 500 mV s^{-1} were utilised, giving linear peak-current versus square root of sweep-rate plots, again suggesting semi-infinite diffusion/migration conditions. It was therefore anticipated that both the Randles-Sevcik and Aoki analysis presented in section 2.1.1.1. were applicable for the evaluation of $D_{ct}(CV)$. Both approaches gave the same value within experimental error for $D_{ct}(CV)$. At slow sweep rates ideal

72

surface or finite diffusion behaviour was observed, as
illustrated on page 52.

The evaluation of activation parameters for the charge
transport process can be helpful in the identification of the
rate limiting step in redox polymer films [14-16]. It is
recognised that the absolute values of the activation parameters
determined are somewhat limited by the assumptions made in their
calculation, such as intersite separation. However, the ability
to distinguish between rate determining cases such as ion
diffusion or polymer motions is unlikely to be affected and the
observed trends should remain valid [67]. In the analysis of
these parameters, the interpretation of Murray and co-workers
[15] was followed. These workers suggested that a negative
entropy value was associated with either electron hopping or ion
movement as rate determining step, while a positive entropy term
indicated rate limiting polymer chain movement. The activation
energies for charge transport within the
$[Ru(bpy)_2(PVP)_5Cl]Cl$ polymer have been previously reported
as being approximately 40 kJ mol^{-1} for ion movement control,
while for polymer segmental chain motions activation energies of
approximately 120 kJ mol^{-1} have been reported [16]. These
values are, however, electrolyte dependent.

As discussed previously, homogeneous charge transport
through metallopolymer films is now widely accepted as occuring
through electron self exchange (by a hopping mechanism) between
reduced/oxidised redox couples [10-12]. The rate determining
step for charge propagation can be limited by the intrinsic
barrier to electron self exchange, the transport of charge
compensating counterion into/out of the modifying film during
redox, or the rate of segmental polymer chain motion required
for redox site juxtaposition.

Electron self exchange rates through electropolymerised
osmium-containing polymers [6] have been measured independently
of ion or polymer chain motion using steady state techniques.
The resulting values of D_E are frequently higher (10^{-8}-

73

10^{-6} cm^{2}s^{-1}) than those reported in this chapter. This, taken together with the observed dependence of the charge transport rate on the electrolyte type and concentration (vide infra), strongly suggests that in these materials electron self exchange is unlikely to be the rate determining step.

The accurate determination of charge transport rates using the models employed in this study requires that the response be diffusional in character and that migrational effects be absent. The examination of migration within metallopolymers of this type has recieved considerable attention and diagnostic criteria have been established [68,69]. Perturbation of the diffusion current by other components is indicated by a non-zero intercept of the short time portion of the Cottrell plot or, by a peak in the $it^{1/2}$ versus $t^{1/2}$ plot [70]. Typical Cottrell plots for the metallopolymers studied here are shown in Figure 2.5. These plots all gave zero current intercepts, within experimental error, indicating the absence of migration effects. The effect of redox site loading on D_{ct} can also reveal migration. Andrieux and Saveant [69] have demonstrated that in the presence of migration, the dependence of D_{ct} on redox site loading goes beyond simple proportionality, eventually reaching a cubic dependence when the mobility of counterions is much lower that the mobility of electrons. Although the variation in redox site loading was not investigated here, previous studies on osmium analogues of the Ru-PVP$_{100}$ homopolymer have shown that such a relationship does not arise for these polymers [56]. The reduction/oxidation current ratio is also expected to be non-unity in the presence of migration [68]. In all cases the i_{pa}/i_{pc} ratio is unity (Figure 2.3) and identical current responses were obtained for fully oxidised and reduced films.

An increased supporting electrolyte concentration is, in the case of electrolytes which swell the film, likely to increase the ion availability within the film and hence suppress migration. Therefore, in circumstances where migration makes a significant contribution to the observed current, an increasing
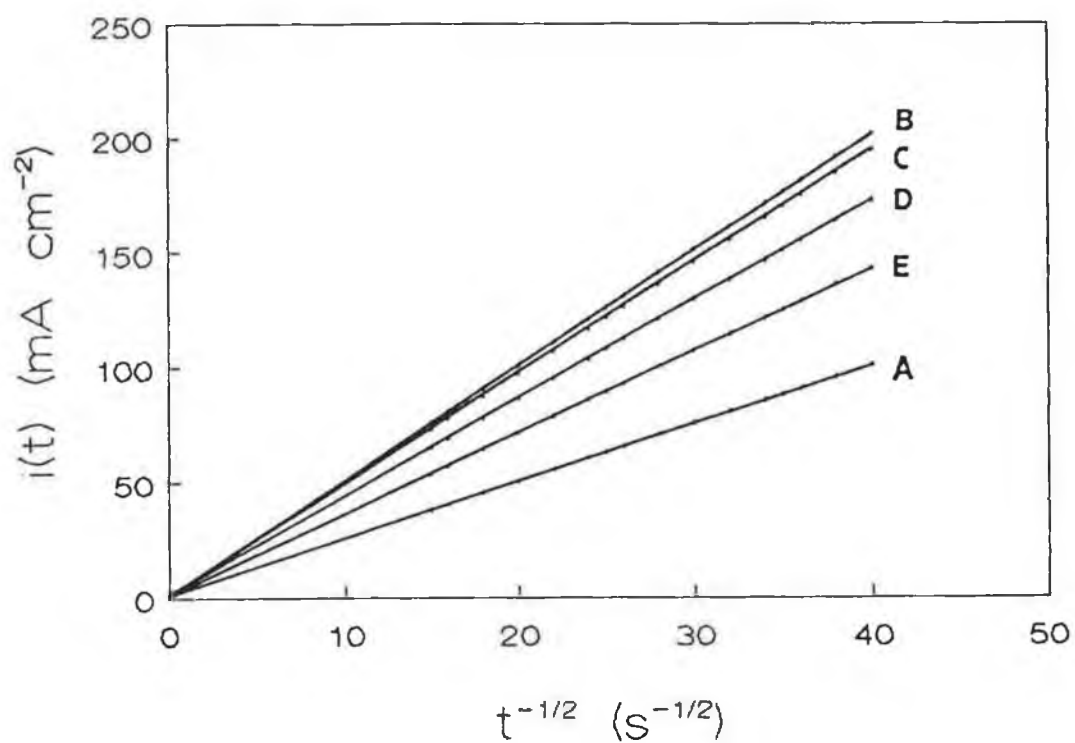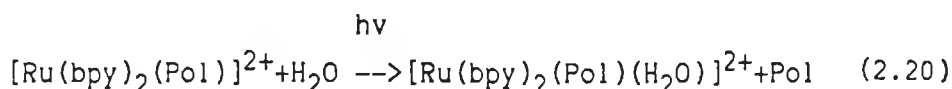
Figure 2.4: Cottrell plots for the short time
chronoamperometric experiments in 1.0 M NaNO$_3$ electrolyte for
Ru-PVP$_{100}$ (A), Ru-PVP$_{75}$ (B), Ru-PVP$_{67}$ (C), Ru-PVP$_{50}$ (D)
and Ru-PVP$_{33}$ (E) metallopolymers.

75

electrolyte concentration would be expected to decrease migration and hence decrease D_{ct}. Such behaviour was observed only for the case of D_{ct}(CV) in perchloric acid (vide infra). However, in this case, none of the other diagnostic criteria for migration were observed, and other possible explanations of this behaviour are discussed later. The fact that no evidence of significant migration was observed suggests, where counterion movement represents the rate determining step, that this response is diffusional in character, and occurs as a result of a Ru(II/III) concentration gradient within the film and not due to a potential gradient.

Charge transfer diffusion coefficients and activation parameters for the charge transport process have been determined in both 0.1 M and 1.0 M sodium nitrate (pH 3.0) and perchloric acid. Perchloric acid as an electrolyte is of interest because of the insolubility of the perchlorate salts of the metallopolymers, and also because of the reported ion-pairing associations of the perchlorate anion, which can act as a crosslink, in polyvinylferrocene- [9,15] and $[Os(bpy)_2(PVP)_{10}Cl]Cl$-coated [14] electrodes. A study of charge transport through the films in sodium nitrate electrolytes was undertaken because of the use of this electrolyte in previously published analytical investigations of electrocatalysis at $[Ru(bpy)_2(PVP)_5Cl]Cl$ modified electrodes in flowing solutions [25,26].

In general, the errors in the charge transfer diffusion coefficient values and in the activation parameters for the charge transport process are quite large (vide infra). The large errors arise, possibly, because of the inhomogeneity of the polymer films. This problem is possibly further aggravated by a photosubstitution process at the modified electrodes. Photochemical investigations of glassy carbon electrodes modified with $[Ru(bpy)_2(Pol)Cl]Cl$ [22] and $[Ru(bpy)_2(Pol)]Cl_2$ [71] films, where Pol represents

76

poly(4-vinylpyridine) or poly(N-vinylimidazole), have reported
the exchange of the coordinated Cl⁻ (or Pol in the case of the
bis polymer) with H_2O as shown below.

$$[Ru(bpy)_2(Pol)Cl]^+ + H_2O \xrightarrow{h\nu} [Ru(bpy)_2(Pol)(H_2O)]^{2+} + Cl^- \quad (2.19)$$

$$[Ru(bpy)_2(Pol)]^{2+} + H_2O \xrightarrow{h\nu} [Ru(bpy)_2(Pol)(H_2O)]^{2+} + Pol \quad (2.20)$$
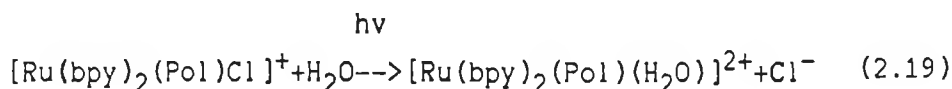
It is to be expected that the presence of even small amounts of
the aquo complex will seriously affect D_{ct} values. Values
obtained for D_{ct} are, however, still useful to study the
trends observed when different parameters are varied.

Sodium nitrate electrolytes were adjusted to a pH of 3.0 in
order to protonate the pendant pyridine units (pK_a 3.5) and
thus enhance ion permeation and transport. Interestingly a
polymer "break-in" effect was observed for the low styrene
content polymers. Figure 2.6 shows repeated cyclic voltammograms
(1 minute delay between scans) for the Ru-PVP$_{100}$
metallopolymer in 0.6 M NaNO$_3$. This effect is attributable to
polymer swelling upon protonation, as it was not observed for
the Ru-PVP$_{33}$ metallopolymers, and indeed the time required for
stable cyclic voltammetric waves to be observed decreased with
increasing styrene content in the polymer backbone. All
measurements for the determination of charge transfer diffusion
coefficients and activation parameters for charge transport were
therefore performed on films that had been previously
"broken-in". No "break-in" effects were observed for the films
in perchloric acid electrolytes. This is attributed to the
compact dehydrated nature of the metallopolymer films in this
electrolyte and will be discussed in the following sections.
    The effect of electrolyte concentration and styrene content
on the magnitude of D_{ct} evaluated from both potential step
chronoamperometry and cyclic voltammetry is presented in Table

77
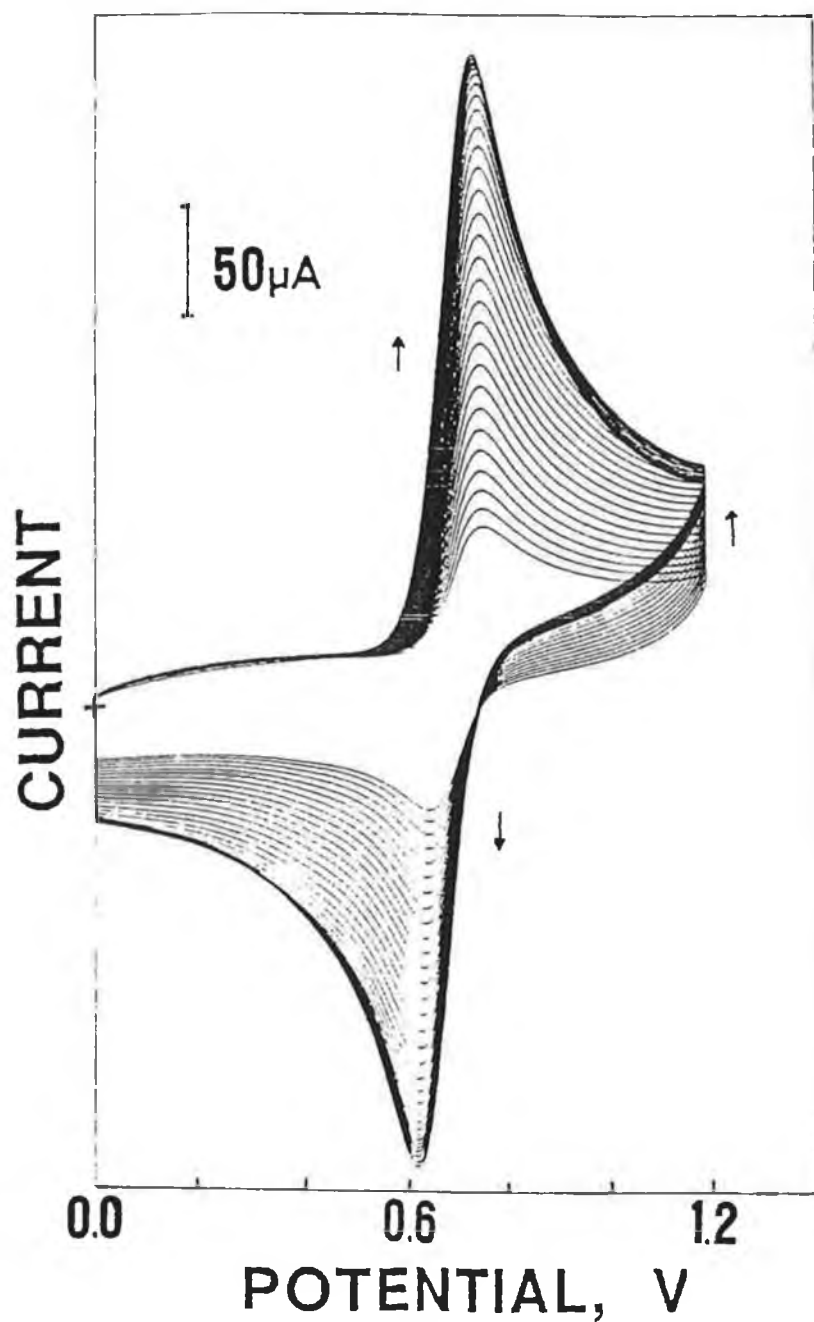
Figure 2.6: Repeated cyclic voltammograms for the Ru-PVP$_{100}$ metallopolymer film in 0.6 M NaNO$_3$ electrolyte. Surface coverage of 4.5 x 10^{-8}mol cm^{-2} ruthenium, scan rate 100 mV s^{-1} and 1 minute delay between repeated scans. The arrows show the direction of wave growth.

2.3 for the sodium nitrate electrolyte and in Table 2.4 for the perchloric acid electrolyte, while the activation parameters associated with the charge transport process are presented in Table 2.5 and Table 2.6 for the sodium nitrate electrolyte and Table 2.7 and Table 2.8 for the perchloric acid electrolyte, respectively.

Table 2.3: The effect of electrolyte concentration and styrene content on the charge transfer diffusion coefficient for the metallopolymer modified electrodes in sodium nitrate electrolytes (pH 3.0).

Polymer	Conc. (M)	$D_{ct}(CV)^a$ *10^{11} cm^2s^{-1}	$D_{ct}(CA)^b$ *10^9 cm^2s^{-1}
Ru-PVP$_{100}$	0.1	3.4 (1.4)^c	1.0 (0.4)^c
	1.0	14.3 (5.0)	3.2 (1.2)
Ru-PVP$_{75}$	0.1	3.8 (1.8)	1.0 (0.5)
	1.0	25.1 (1.3)	13.1 (3.1)
Ru-PVP$_{67}$	0.1	3.5 (1.2)	1.2 (0.5)
	1.0	30.0 (10.1)	12.5 (4.5)
Ru-PVP$_{50}$	0.1	3.8 (2.1)	1.5 (0.9)
	1.0	22.6 (6.6)	10.1 (5.8)
Ru-PVP$_{33}$	0.1	4.1 (0.9)	1.7 (0.5)
	1.0	12.6 (5.0)	7.1 (3.1)

^{a}Evaluated from cyclic voltammetry using the anodic peak current and the Randles-Sevcik equation.
^{b}Evaluated from chronoamperometry using the Cottrell equation.
^{c}Errors calculated as standard deviation from the mean of, usually, determinations on 3 different films.

Table 2.4: The effect of electrolyte concentration and styrene content on the charge transfer diffusion coefficient for the metallopolymer modified electrodes in perchloric acid electrolytes.

Polymer	Conc. (M)	$D_{ct}(CV)^a$ $*10^{11}$ cm^2s^{-1}		$D_{ct}(CA)^b$ $*10^9$ cm^2s^{-1}	
Ru-PVP$_{100}$	0.1	1.6	(0.7)[c]	0.6	(0.2)[c]
	1.0	1.2	(0.9)	1.8	(0.9)
Ru-PVP$_{75}$	0.1	2.2	(1.3)	1.8	(0.5)
	1.0	1.2	(1.0)	5.0	(3.4)
Ru-PVP$_{67}$	0.1	1.6	(0.8)	1.2	(0.8)
	1.0	1.2	(0.6)	6.7	(2.4)
Ru-PVP$_{50}$	0.1	2.9	(1.5)	1.3	(0.6)
	1.0	1.6	(0.9)	2.7	(1.1)
Ru-PVP$_{33}$	0.1	4.5	(2.2)	0.9	(0.2)
	1.0	3.0	(0.8)	3.1	(2.0)

[a]Evaluated from cyclic voltammetry using the anodic peak current and the Randles-Sevcik equation.
[b]Evaluated from chronoamperometry using the Cottrell equation.
[c]Errors calculated as standard deviation from the mean of, usually, determinations on 3 different films.

Table 2.5: Activation parameters determined by cyclic voltammetric methods, for charge transport through the metallopolymer films in sodium nitrate electrolytes (pH 3.0).

Electrolyte/ Polymer	E_a (CV) kJ mol^{-1}	$S^{\neq}$ (CV) Jmol^{-1}K^{-1}	$G^{\neq}$ (CV) kJ mol^{-1}
0.1 M NaNO$_3$			
Ru-PVP$_{100}$	14 (2)[a]	-158 (10)[a]	58 (2)[a]
Ru-PVP$_{75}$	20 (3)	-140 (11)	59 (2)
Ru-PVP$_{67}$	27 (3)	-114 (8)	59 (2)
Ru-PVP$_{50}$	28 (3)	-105 (12)	57 (2)
Ru-PVP$_{33}$	25 (6)	-115 (9)	57 (3)
1.0 M NaNO$_3$			
Ru-PVP$_{100}$	55 (6)	-11 (9)	53 (4)
Ru-PVP$_{75}$	46 (3)	-33 (7)	53 (3)
Ru-PVP$_{67}$	60 (5)	20 (8)	52 (4)
Ru-PVP$_{50}$	58 (5)	7 (9)	58 (5)
Ru-PVP$_{33}$	57 (8)	4 (16)	54 (3)

[a]Errors, ±, calculated from the standard deviation from the slope and the intercept of the best fit line of all points.

Table 2.6: Activation parameters determined by chronoampero-metric methods, for charge transport through the metallopolymer films in sodium nitrate electrolytes (pH 3.0).

Electrolyte/ Polymer	E_a (CA) $kJ\ mol^{-1}$	$S^{\neq}$ (CA) $Jmol^{-1}K^{-1}$	$G^{\neq}$ (CA) $kJ\ mol^{-1}$
0.1 M NaNO$_3$			
Ru–PVP$_{100}$	17 (2)[a]	–109 (10)[a]	48 (2)[a]
Ru–PVP$_{75}$	25 (5)	–88 (18)	48 (5)
Ru–PVP$_{67}$	30 (4)	–65 (9)	47 (2)
Ru–PVP$_{50}$	21 (3)	–103 (8)	50 (3)
Ru–PVP$_{33}$	24 (4)	–87 (9)	47 (3)
1.0 M NaNO$_3$			
Ru–PVP$_{100}$	45 (5)	–8 (10)	43 (3)
Ru–PVP$_{75}$	48 (5)	11 (8)	42 (4)
Ru–PVP$_{67}$	34 (4)	–40 (6)	46 (4)
Ru–PVP$_{50}$	19 (5)	–93 (11)	44 (3)
Ru–PVP$_{33}$	21 (4)	–86 (9)	44 (3)

[a]Errors, ±, calculated from the standard deviation from the slope and the intercept of the best fit line of all points.

Table 2.7: Activation parameters determined by cyclic voltammetric methods, for charge transport through the metallopolymer films in perchloric acid electrolytes.

Electrolyte/ Polymer	E_a (CV) kJ mol^{-1}	$S^{\neq}$ (CV) $Jmol^{-1}K^{-1}$	$G^{\neq}$ (CV) kJ mol^{-1}
0.1 M $HClO_4$			
Ru-PVP$_{100}$	131 (11)[a]	230 (4)[a]	62 (7)[a]
Ru-PVP$_{75}$	56 (7)	−15 (3)	58 (4)
Ru-PVP$_{67}$	39 (9)	−77 (4)	59 (5)
Ru-PVP$_{50}$	33 (5)	−93 (3)	59 (2)
Ru-PVP$_{33}$	33 (7)	−87 (4)	57 (4)
1.0 M $HClO_4$			
Ru-PVP$_{100}$	65 (11)	20 (2)	68 (11)
Ru-PVP$_{75}$	43 (3)	−65 (1)	60 (1)
Ru-PVP$_{67}$	51 (7)	−41 (6)	60 (6)
Ru-PVP$_{50}$	28 (8)	−117 (4)	60 (4)
Ru-PVP$_{33}$	30 (3)	−102 (2)	58 (1)

[a]Errors, ±, calculated from the standard deviation from the slope and the intercept of the best fit line of all points.

83

Table 2.8: Activation parameters determined by chronoampero-metric methods, for charge transport through the metallopolymer films in perchloric acid electrolytes.

Electrolyte/ Polymer	E_a (CA) kJ mol^{-1}	$S^{\neq}$ (CA) Jmol^{-1}K^{-1}	$G^{\neq}$ (CA) kJ mol^{-1}
0.1 M HClO$_4$			
Ru-PVP$_{100}$	24 (7)[a]	-91 (4)[a]	49 (3)[a]
Ru-PVP$_{75}$	16 (2)	-112 (1)	47 (1)
Ru-PVP$_{67}$	15 (3)	-116 (4)	48 (3)
Ru-PVP$_{50}$	17 (3)	-106 (5)	46 (3)
Ru-PVP$_{33}$	13 (2)	-119 (5)	46 (3)
1.0 M HClO$_4$			
Ru-PVP$_{100}$	59 (4)	35 (4)	46 (3)
Ru-PVP$_{75}$	33 (4)	-20 (3)	45 (3)
Ru-PVP$_{67}$	30 (5)	-58 (6)	45 (3)
Ru-PVP$_{50}$	21 (3)	-88 (2)	44 (3)
Ru-PVP$_{33}$	11 (3)	-115 (4)	44 (3)

[a]Errors, $\pm$, calculated from the standard deviation from the slope and the intercept of the best fit line of all points.

2.3.2.1. Differences between D_{ct}(CA) and D_{ct}(CV)

The rate of charge transport through the
$[Ru(bpy)_2(Pol)_{10}Cl]Cl$ films, where Pol represents either PVP
or the copolymers, is clearly dependent on the timescale of the
method used to evaluate it, with short timescale potential step
experiments giving a consistently higher value of D_{ct}.
D_{ct}(CA) is also more sensitive to changes in the electrolyte
concentration, suggesting that the nature of the controlling
process may be time dependent. The thermodynamic data support
this interpretation, with E_a(CV) being typically larger than
E_a(CA).

The dependence of D_{ct} on the experimental timescale may be
due to different structural regions within the films, with the
ruthenium concentration adjacent to the electrode surface being
higher than that found near the film/electrolyte interface,
perhaps because of differences in the degree of swelling
throughout the film. However, the difference between D_{ct}(CA)
and D_{ct}(CV), typically of an order of magnitude, would require
differential swelling of over 300%. It is also possible that
only under the longer times of the cyclic voltammetry
experiments do all mobile species, electrons, ions and solvent
reach the populations dictated by the extent of film oxidation
[72]. An alternative explanation is that as the longer timescale
cyclic voltammetric experiments result in more complete
oxidation of the metallopolymer film (>80 %), it requires ion
diffusion to occur on a large scale both within the film and
across the film/electrolyte interface. In contrast, the
counterion diffusion requirements of the potential step
experiments can be localised within the film. The fact that ion
diffusion must occur on a larger scale and over a larger region
of the film may result in D_{ct}(CV) being suppressed compared to
D_{ct}(CA). A result that would seem to support this view is that
upon analysis of the current decay over a longer timescale
(20-100 ms) and the application of the Cottrell equation, a

85

D_{ct} value similar to that obtained from the CV experiments may be obtained.

2.3.2.2. Effect of the Nature and Concentration of the Electrolyte

The difference in charge transfer rates when the electrolyte solution was varied suggests that the contacting electrolyte directly influences counterion availability within the film and/or the polymer film morphology. For all of the polymers studied, a sharp increase in both Dct_{ct}(CA) and D_{ct}(CV) was obtained upon increasing the $NaNO_3$ concentration from 0.1 M to 1.0 M. Since $D_{ct}^{1/2}C$ is the experimentally determined parameter, where C represents the fixed site concentration in the film, the increase observed for D_{ct} may reflect a variation in either the charge transport rate or the fixed site concentration. In the $NaNO_3$ electrolyte, at pH 3.0, the increased electrolyte concentration is not expected to increase the fixed site concentration because of electrostatic repulsion between the protonated unbound pyridine units in the film. Thus it seems likely that the increase in D_{ct} seen with increasing electrolyte concentration reflects an increased charge transport rate. As the charge transport rate is governed by counterion diffusional limitations in these polymers (vide infra), any increase in the counterion concentration is likely to result in an increased charge transfer diffusion coefficient. It is postulated that, where the electrolyte concentration is above that of the fixed site concentration, the ion availability, or alternatively the ease of counterion diffusion within the film, is increased. This is most likely to arise as a result of increased swelling of the film at higher $NaNO_3$ concentrations, or because of an ion exclusion process occurring when the electrolyte concentration is below the fixed site concentration. This interpretation is supported by the relative insensitivity of D_{ct} to variations in the copolymer backbone composition in

the 0.1 M NaNO$_3$ electrolyte concentration, as this concentration is below the fixed site concentration for all of the polymers.

Activation energies ranging from 17 – 30 kJ mol^{-1}, together with negative entropy values, were obtained for the charge transport process in the 0.1 M NaNO$_3$ electrolyte. The negative entropy values are thought to be an indication of the increased order of the polymer film upon transport of charge compensating counterions and solvent. This transport requires a certain degree of expansion of the polymeric lattice which will result in a decreased polymeric chain mobility, and thus by implication, an increase in the order of the system. The activation parameters in the 0.1 M NaNO$_3$ electrolyte are consistent with ion transport control within the [Ru(bpy)$_2$(Pol)$_n$Cl]Cl films [16]. Activation parameters obtained in the 1.0 M NaNO$_3$ electrolyte solution will be discussed in the following section.

The dependence of D_{ct}(CV) on perchloric acid concentration is distinctly different to that discussed above, with D_{ct}(CV) decreasing as the perchlorate concentration was increased. This arises possibly because perchloric acid cannot swell these metallopolymers, as these polymers form highly insoluble salts with the perchlorate anion. The perchorate anion has also been reported to form ion-pairing crosslinks with PVP films, thus leading to highly compact film structures [14]. The decreasing D_{ct}(CV) value as the perchlorate concentration was increased is therefore likely to reflect an increasingly compact film, hindering counterion diffusion across the interface. This interpretation is consistent with recent reports on partially quaternised poly(4-vinylpyridine) films containing [Re(CO)$_3$(phen)], where phen is 1,10-phenanthroline, which suggested that nearly dehydrated, compact films are formed in perchlorate containing media [23]. Furthermore, quartz crystal microbalance studies carried out on the osmium anologue of the

87

Ru-PVP$_{100}$ metallopolymer [73] clearly showed that, unlike other anions, perchlorate enters the polymer layer in a dehydrated form.

The difference in the two experimental techniques of CV and CA are again illustrated by the differing trends seen for the metallopolymers upon increasing the perchlorate concentration. For the CV experiments D_{ct}(CV) decreases with increasing electrolyte concentration (Table 2.4), while D_{ct}(CA) increases with increasing electrolyte concentration. This supports the previous assumption that the D_{ct}(CA) value may reflect the localised motions of counterions within the polymer film, with D_{ct}(CV) reflecting the interfacial counterion transport required to maintain electroneutrality because of both the extent of reaction in the CV experiment and the timescale of the experimental technique.

Activation parameters determined for charge transport through the metallopolymer films in perchloric acdid electrolytes support the view of ion transport into or within the polymer being rate limiting. Activation energies of approximately 40 kJ mol^{-1} were obtained for all but the Ru-PVP$_{100}$ metallopolymer in both electrolyte concentrations, with little change in E_a upon increasing the electrolyte concentration. This reflects the assumption that the metallopolymers form highly insoluble compact layers in this electrolyte. The large activation energies together with positive entropy values obtained for the Ru-PVP$_{100}$ metallopolymer is associated with an increasing disorder within the film (hence the positive entropy terms), and probably represents polymer chain motion [14-16]. It seems that the film is so compact, from crosslinking, that only by polymer motion can counterions be transported across the film/electrolyte interface to maintain electroneutrality upon oxidation of the ruthenium redox centres. The activation parameters determined by the potential step chronoamperometric method indicate that in HClO$_4$ electrolytes, ion transport is the rate determining step

88

for these metallopolymers at the CA timescales. These activation
parameters will be discussed further in the following section,
with regard to their variations with changes in the polymeric
backbone.

2.3.2.3. Effect of Polymeric Backbone Composition

The effect of the styrene content in the polymeric backbone
in $NaNO_3$ electrolytes on both D_{ct}(CV) and D_{ct}(CA) is shown
in Figure 2.7 and Figure 2.8, respectively. For the D_{ct} values
determined in the 0.1 M $NaNO_3$ electrolyte, very little
variations were seen with varying polymeric compositions. This
is likely to be because of ion availability and/or ion
permeation limitations at this electrolyte concentration. This
invariance in D_{ct} with polymer composition supports the view
expressed in section 2.3.2.2., that an ion exclusion process
occurs where the electrolyte concentration is below that of the
fixed site concentration of electroactive species in the film.
The data obtained for D_{ct}(CV) in the 1.0 M $NaNO_3$
electrolyte (Figure 2.7) showed that a maximum D_{ct}(CV) value
was obtained for a styrene content of approximately 35% in the
polymer backbone. The initial increase in the D_{ct}(CV) values
upon addition of styrene to the polymer backbone may be the
result of an increase in the fixed site concentration within the
film. This possible increase may be attributed to a decrease in
protonated pyridine sites and also an increase in film
hydrophobicity associated with the styrene moieties, thus
resulting in decreased swelling of the polymeric film and a more
compact film. The subsequent decrease in D_{ct}(CV) observed with
the higher styrene content polymers could be a reflection of
film compaction to such an extent that ion transport across the
film/electrolyte interface becomes increasingly hindered.
Alternatively, the initial increase in D_{ct}(CV) values for the
higher styrene content polymers may be a reflection of a
decrease in the extent of coupling between the NO_3^- ion and

89

Figure 2.7: Variation of the charge transfer diffusion
coefficient, D_{ct}, with the mole fraction of PVP in the
metallopolymer films as determined from the anodic peak currents
of the cyclic voltammograms and the Randles-Sevcik equation. (■)
0.1 M $NaNO_3$ and (▲) 1.0 M $NaNO_3$. Ruthenium surface coverages
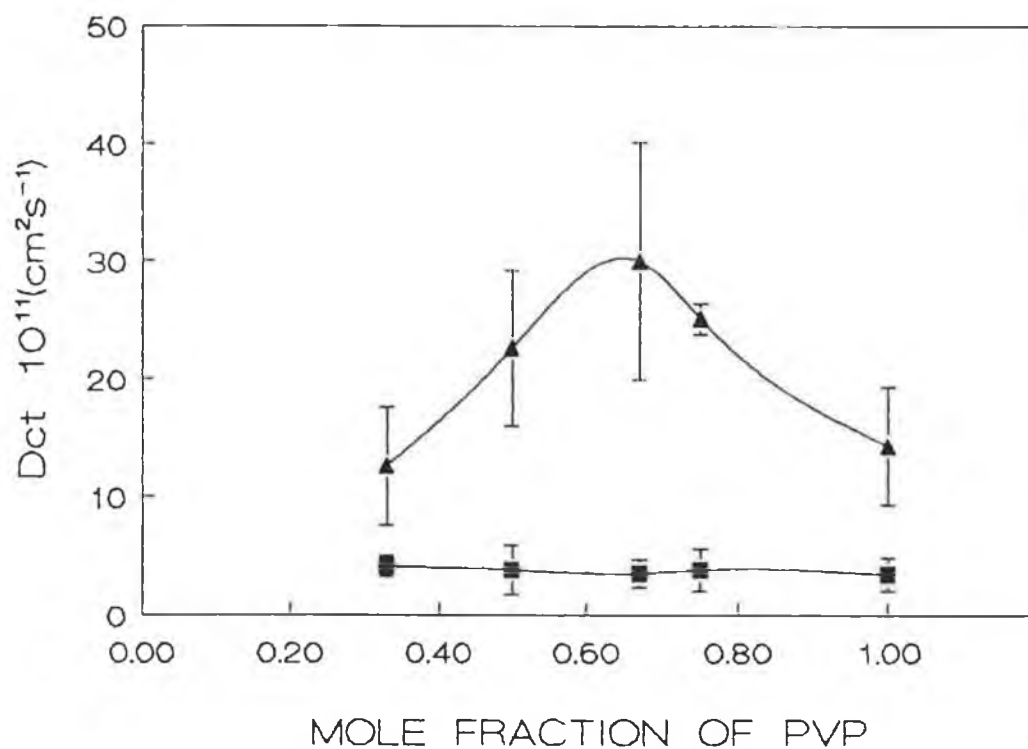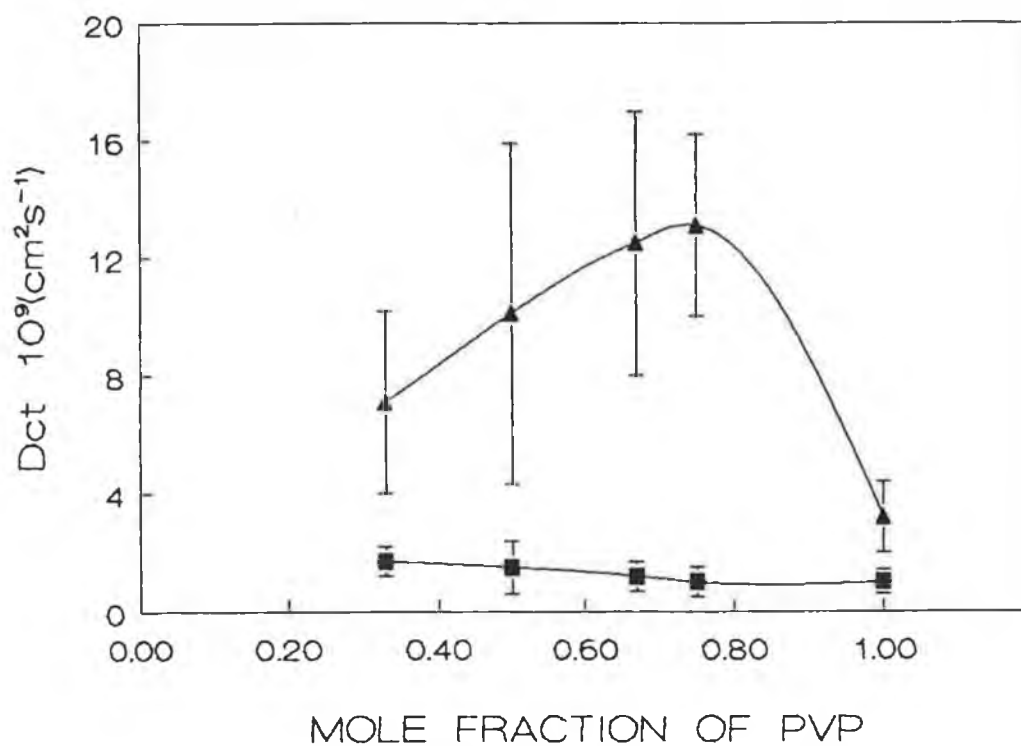are between 4 - 8 x 10^{-8}mol cm^{-2}.

Figure 2.8: Variation of the charge transfer diffusion coefficient, D_{ct}, with the mole fraction of PVP in the metallopolymer films as determined from the Cottrell equation. (■) 0.1 M $NaNO_3$ and (▲) 1.0 M $NaNO_3$. Ruthenium surface coverages are between $4 - 8 \times 10^{-8}$mol cm^{-2}.

the protonated pyridine groupings within the film thus leading to more facile ion transport [74].

The activation energies determined from the CV experiments (Table 2.5) are slightly higher than those obtained for the $[Ru(bpy)_2(PVP)_5Cl]Cl$ polymer films in HCl and $HClO_4$ electrolytes [16], possibly explained by the larger distances between the redox sites in the films. These activation energy values are thought to reflect interfacial ion motion limitations, with counterion transport into the film being hindered. Given the errors associated with the determination of these parameters, no significant trend with polymer backbone composition in those values in $NaNO_3$ electrolytes determined by CV methods were observed.

Activation energies obtained from the potential step results were generally lower than the corresponding CV values. This is most likely a result of the experimental timescale, with the short range localised ion motions of charge compensating counterions on the potential step timescale being more facile than the interfacial ion transport required in the CV experiments. Also, as mentioned previously, the extent of reaction for the CV methods will be much greater than for the potential step methods thereby requiring a much greater flux of counterions to maintain electroneutrality. The activation energies determined by potential step methods generally decrease with increasing styrene content in the polymeric backbone. This trend possibly reflects the reported coupling of the NO_3^- ion with protonated pyridine groupings [74] mentioned above, thus making the short range ion motions relatively more facile within polymer films of the higher styrene content polymers. The variation of $D_{ct}(CA)$ with styrene content for the 1.0 M $NaNO_3$ electrolyte (Figure 2.8) seems to reflect a trade off between the two factors involved in ion motion restriction at this timescale; that is, between film compaction with increasing styrene content, because of the increased hydrophobicity of the films, and ion motion restriction within the higher

92

4-vinylpyridine content films, because of ion coupling of the
nitrate with the protonated pyridine ions.

As mentioned previously, the perchlorate salts of the
ruthenium metallopolymers are highly insoluble and dehydrated,
and the perchlorate ion has been reported to act as a crosslink
within poly(vinylferrocene) (PVF) [9,15] and
$[Os(bpy)_2(PVP)_nCl]Cl$ [14] films because of ion-pair
interactions. D_{ct} values determined in the perchloric acid
electrolyte (Figure 2.9 and Figure 2.10 for CV and CA results
respectively) showed less variation with changes in the polymer
backbone styrene content than those seen in $NaNO_3$
electrolytes. The large errors assciated with the D_{ct} values
determined in this electrolyte make it difficult to establish
positively any definite trends in D_{ct} with variations in the
polymer backbone styrene content. The general trends in D_{ct}
seen for these metallopolymer films should still be valid, and
these trends are discussed below.

The trend seen for D_{ct}(CV) values is for an increase in
the charge transfer diffusion coefficient, with increasing
styrene content in the polymer backbone, in both 0.1 M and 1.0 M
$HClO_4$ electrolytes. This possibly reflects an increase in the
swelling capability of the polymer films upon addition of
styrene to the polymers and hence an increase in the ease of ion
motion within and permeation into the polymer films. This could
arise from the fact that there are less protonated pyridine
sites available for ion-pair formation and hence less
crosslinking of the polymer, giving the styrene-containing
metallopolymers a less rigid conformation. The activation energy
values determined in these electrolytes from CV results support
this view, with a decrease in E_a values with increasing
styrene content for both electrolyte concentrations. The high
activation energy value for the Ru-PVP_{100} metallopolymer films
in 0.1 M $HClO_4$ electrolyte can be associated with changeover
from ion permeation and motion control of the charge transport

93

Figure 2.9: Variation of the charge transfer diffusion
coefficient, D_{ct}, with the mole fraction of PVP in the
metallopolymer films as determined from the anodic peak currents
of the cyclic voltammograms and the Randles-Sevcik equation. (■)
0.1 M $HClO_4$ and (▲) 1.0 M $HClO_4$. Ruthenium surface coverages
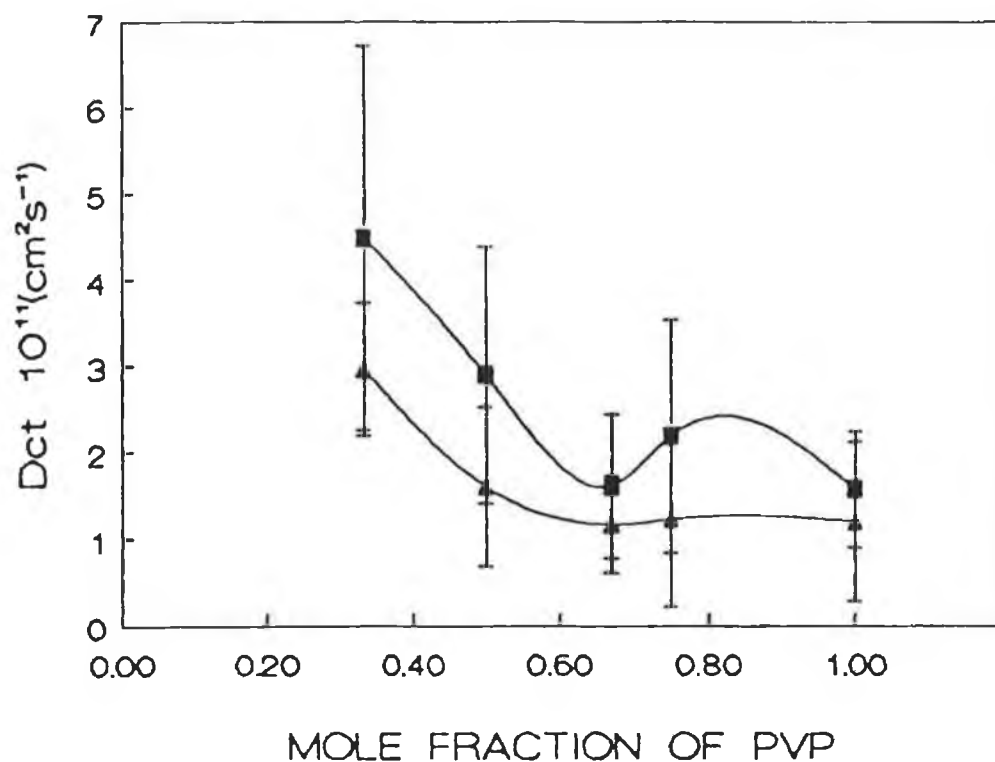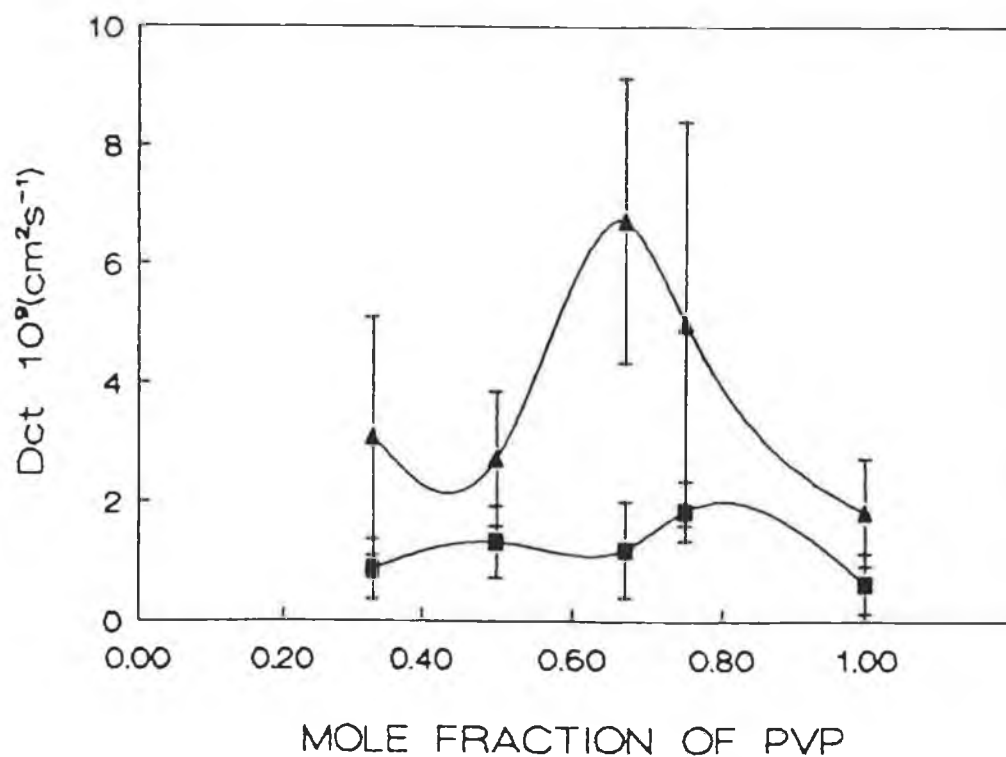are between $4 - 8 \times 10^{-8}$ mol cm^{-2}.

Figure 2.10: Variation of the charge transfer diffusion coefficient, D_{ct}, with the mole fraction of PVP in the metallopolymer films as determined from the Cottrell equation. (■) 0.1 M $HClO_4$ and (▲) 1.0 M $HClO_4$. Ruthenium surface coverages are between $4 - 8 \times 10^{-8}$ mol cm^{-2}.

process to one of polymer chain motions being rate limiting. The large positive entropy terms are a reflection of the increasing disorder within the films associated with these polymer motions [14,15]. It seems that only by polymer chain motion can counterions be transported across the film/electrolyte interface to maintain electroneutrality upon oxidation of the ruthenium redox centres.

The differences in profiles obtained for the variation of D_{ct} with styrene content by potential step (Figure 2.10) and CV (Figure 2.9) experiments again reinforces the opinions expressed earlier in this chapter on the timescale dependence of the results. The profile for $D_{ct}(CA)$ in 0.1 M $HClO_4$ electrolyte showed very little variation with styrene content in the polymer backbone, possibly indicative of ion transport limitations at this low electrolyte concentration. In the 1.0 M $HClO_4$ electrolyte, however, a peak-shaped profile was obtained, with a maximum $D_{ct}(CA)$ value at a PVP percentage concentration of approximately 65% in the polymer backbone. This behaviour may be attributed to a trade-off between the two factors which control the degree of polymer swelling, and thus ease of ion motion within the film. These are film compaction, because of increased ion pair associations, and thus increased crosslinks, and also film compaction, because of increased styrene content in the polymer backbone, and thus increased hydrophobicity of the films. The initial increase in $D_{ct}(CA)$ with increasing styrene content may thus be attributed to increased ease of ion motions within the polymer films due to a reduction in the extent of crosslinking of the films by the ion pair associations of the perchlorate anion and the protonated pyridines. The subsequent decrease in $D_{ct}(CA)$ values upon further increases in styrene content may be because of film compaction due to increased hydrophobicity associated with the styrene polymeric moieties, thus hindering ion motions.

Activation parameters determined for the potential step method indicate that in $HClO_4$ electrolytes, ion transport is

rate determining for these metallopolymers at the CA timescales. The activation energies determined by CA decrease in 1.0 M $HClO_4$ electrolyte with increasing styrene content in the polymer backbone. This decrease may be a reflection of increasing ease of ion motion in the films because of the more open structure of the films. Thus it is possible that the effect of styrene in perchlorate electrolyte is to improve ion transport in these films.

2.3.3. Heterogeneous Electron Transfer

The application of SCV techniques in the determination of heterogeneous electron transfer kinetics has been discussed previously. In this section, the heterogeneous electron transfer rates are discussed with regard to the rate limiting step for charge transport in the metallopolymer films studied above. A typical sampled current voltammogram for the Ru(II/III) oxidation within the $[Ru(bpy)_2(Pol)_{10}Cl]Cl$ films, where Pol is a 1:1 copolymer of 4-vinylpyridine and styrene in this case, in 0.1 M perchloric acid as electrolyte is shown in Figure 2.11. These sigmoidal shaped waves are similar to those observed at unmodified electrodes for solution phase reactants [75]. The anodic currents increase with increasing sampling times, and at the same time the half wave potentials of the voltammograms for the oxidation process shift to more positive potentials with decreasing sampling times. This behaviour is accepted as being indicative of Butler-Volmer kinetics [76]. In the previous sections it was seen that the charge transfer response through these films is diffusional in nature and that significant migration is absent. The conventional analysis for sampled current voltammograms as presented in section 2.1.1.4. was, therefore expected to be appropriate. The standard rate constant for heterogeneous electron transfer (k^o) was determined from the SCVs in perchloric acid electrolytes for electrodes modified
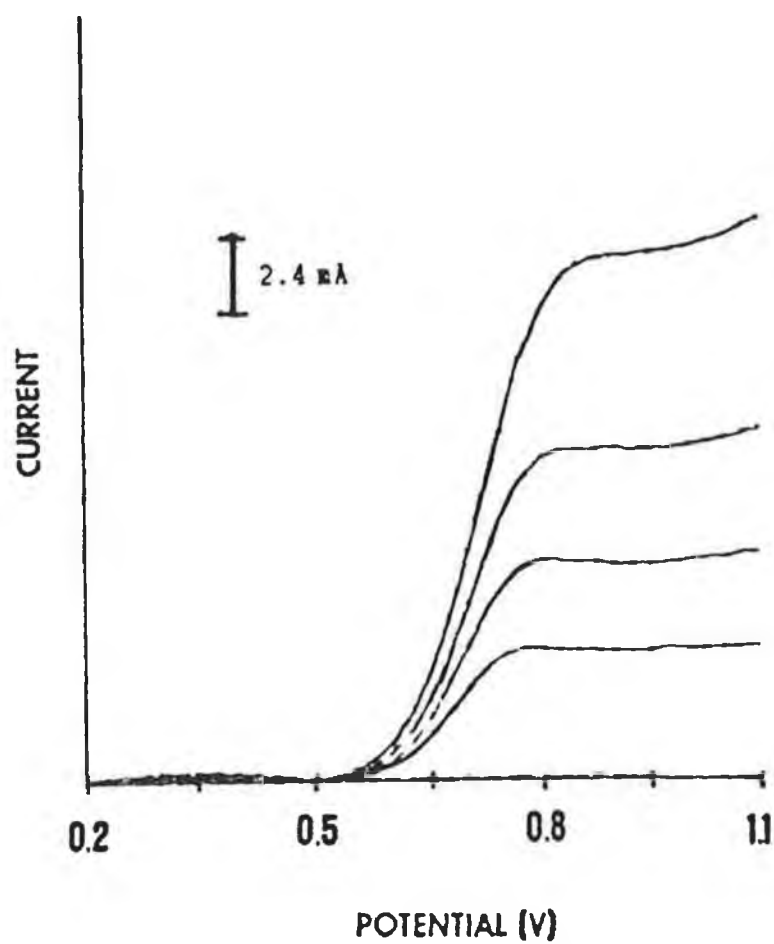
97

Figure 2.11: Sampled current voltammograms obtained for an Ru-PVP$_{50}$ metallopolymer film in 0.1 M HClO$_4$. Voltammograms represent, from the top, 1 ms, 2 ms, 4 ms and 10 ms sampling times.

with films of the ruthenium metallopolmyers presented in the previous sections. A large body of data was collected for the heterogeneous rate constant in perchloric acid electrolytes for all of the metallopolymer films on glassy carbon electrodes. The variations obtained from coating-to- coating for k^o values were large, with large variations in values also determined from repeated experiments at the same coating.

Rate constants in the order of 10^{-4} - 10^{-5} cm s^{-1} were obtained for all of the modified electrodes, with no systematic variations in k^o with electrolyte concentration or type. These values of k^o are at least an order of magnitude less than the values obtained for electroactive species in solution [77]. Such behaviour has been previously reported for several other systems [56,78,79]. Partial blocking of the electrode surface by the modifying film, as an explanation for the reduced k^o values, has been considered by Amatore et al. [80]. k^o for a modified electrode is considered to be the product of (1-θ) and k^o for the heterogeneous electron transfer at the active sites, where θ is the surface coverage of active sites. Since, for the polymers investigated in this study, the backbone is nonconducting, heterogeneous electron transfer can only occur between the electrode material and the ruthenium centres, thus leading to the decreased k^o values observed for the modified electrodes in comparison to solution values. Uncompensated resistance has also been reported to be responsible for reduced k^o values [81]. However, in this study, uncompensated resistance was routinely compensated for using positive feedback circuitry.

The values obtained for k^o for these modified electrodes were normally four orders of magnitude greater than the observed rates for homogeneous charge transfer within the polymer films as determined by CA methods. This confirms the view that the rate of heterogeneous electron transfer does not limit the charge transport process in these modified electrode films.

2.4. CONCLUSIONS

In conclusion to this chapter, it has been shown that the synthetic approach used has resulted in the preparation of various polymer backbones and their subsequent functionalisation with ruthenium redox centres, which were readily characterised. Physical measurements confirmed the retention of excited state and redox properties of the metal centres upon polymer attachment. Charge transfer diffusion coefficients and activation parameters for the charge transport process within the films on electrodes were shown to vary with electrolyte composition and concentration, as well as the polymer backbone composition, with ion transport limitations being the controlling factor in the process. The charge transfer diffusion coefficient was shown to vary in magnitude for different experimental techniques, with the short timescale potential step D_{ct} values being typically at least an order of magnitude greater than those obtained using longer timescale cyclic voltammetric procedures. An effect such as this for the charge transport process in PVF films has recently been reported [82], with the electrochemical quartz crystal microbalance being utilised to probe solvent and ion transport into and out of these films upon oxidation/reduction.

The results obtained in this section are of a fundamental importance in establishing a link between D_{ct} and the physical attributes of the polymer film. The successful sensor application of these metallopolymers as modifiers is also dependent on the optimisation of the rate of charge transport through these films. The application of these metallopolymer films as sensors will be presented and discussed in Chapter 3.

2.4.   REFERENCES

1.   C.P. Andrieux, O. Haas and J.M. Saveant, J. Am. Chem. Soc., (1986), 108, 8175.

2.   W.J. Albery and A.R. Hillman, J. Electroanal. Chem., (1984), 170, 27.

3.   D.A. Buttry and F.C. Anson, J. Am. Chem. Soc., (1982), 104, 4824.

4.   I. Rubinstein and A.J. Bard, J. Am. Chem. Soc., (1981), 103. 5007.

5.   C.E.D Chidsey and R.W. Murray, Science, (1986), 231, 25.

6.   F.B. Kaufmann and E.M. Engler, J. Am. Chem. Soc., (1980), 102, 483.

7.   R.J. Forster, Ph.D. Thesis, (1990), Dublin City University.

8.   M. Kaneko and D. Woehrle, Adv. Polymer Sci., (1988), 84, 142.

9.   G. Inzelt and L. Szabo, Electrochim. Acta, (1986), 31, 1381.

10.   A. Schroeder, F.B. Kaufmann, V. Patel and E.M. Engler, J. Electroanal. Chem., (1980), 113. 193.

11.   H. White, J. Leddy and A.J. Bard, J. Am. Chem. Soc., (1982), 104, 4811.

12.   T.P. Henning, H. White and A.J. Bard, J. Am. Chem. Soc., (1981), 103, 3937.

13.   S.B. Khoo, J.K. Foley and S. Pons, J. Electroanal. Chem., (1986), 215, 273.

14.   R.J. Forster, A.J. Kelly, J.G. Vos and M.E.G. Lyons, J. Electroanal. Chem., (1989), 270, 365.

15.   P. Daum, J.R. Lenhard, D. Rolison and R.W. Murray, J. Am. Chem. Soc., (1980), 102, 4649.

16.   M.E.G. Lyons, H.G. Fay, J.G. Vos and A.J Kelly, J. Electroanal. Chem., (1988), 250, 207.

17.   J.M. Clear, J.M. Kelly and J.G. Vos, Makromol. Chem., (1983), 184, 613.

18.   J.M. Clear, J.M. Kelly, G.M. O'Conell and J.G. Vos, J. Chem. Res.. (M), (1981), 3039.

19.   O. Haas and J.G. Vos, J. Electroanal. Chem., (1980), 113, 139.

20.   J.M. Calvert and T.J. Meyer, Inorg. Chem., (1981), 20, 27.

21.   S.M. Geraty and J.G. Vos, J. Chem. Soc., Dalton Trans., (1987), 3073.

22.   O. Haas, M. Kriens and J.G. Vos, J. Am. Chem. Soc., (1981), 103, 1318.

23.   S.M. Oh and L.R. Faulkner, J. Am. Chem. Soc., (1989), 111, 5613.

24.   K. Sumi and F.C. Anson, J. Phys. Chem., (1986), 90, 3845.

25.   J.N. Barisci, G.G. Wallace, E.A. Wilke, M. Meaney, M.R. Smyth and J.G. Vos, Electroanalysis, (1989), 1, 245.

26.   G.G. Wallace, M. Meaney, M.R. Smyth and J.G. Vos, Electroanalysis, (1989), 1, 357.

27.   R.W. Murray, Electroanalytical Chemistry, A.J. Bard (Ed.), M. Dekker, New York (1984), Vol 13.

28.   R.W. Murray, Ann. Rev. Mater. Sci., (1984), 14, 145.

29.   A.J. Bard and L.R. Faulkner, Electrochemical Methods, Wiley, New York (1980).

30.   P.N. Bartlett, Biosensors, Fundamentals and Applications, A.P.F. Turner, I. Karube and G.S. Wilson (Eds.), Oxford University Press, New York (1987), Ch. 13.

31.   R.S Nicholson and I. Shain, Anal. Chem., (1964), 36, 706.

32.   D.M. Mohilner, J. Electroanal. Chem., (1966), 1, 241.

33.   K. Aoki, K. Tokuda and H. Matsuda, J. Electroanal. Chem., (1983), 146, 417.

34.   K. Aoki, K. Tokuda and H. Matsuda, J. Electroanal. Chem., (1984), 160, 33.

35.   N. Oyama, S. Yamaguchi, Y. Nishiki, K. Tokuda, H. Matsuda and F.C. Anson, J. Electroanal. Chem., (1982), 139, 371.

36.   H. Matsuda, Bull. Chem. Soc. Jpn., (1980), 53, 3439.

37.   F.B. Kaufmann, A.H. Schroeder, E.M. Engler, S.R. Kramer

and J.Q. Chambers, J. Am. Chem. Soc., (1980), 102, 483.

38. G. Inzelt, J. Backsai, J.Q. Chambers and R.W. Day, J. Electroanal. Chem., (1987), 201, 301.

39. G. Inzelt, L. Szabo, J.Q. Chambers and R.W. Day, J. Electroanal. Chem., (1988), 242, 265.

40. E.F. Bowden, M.F. Dautartas and J.F. Evans, J. Electroanal. Chem., (1987), 219, 49.

41. M.F. Dautartas, E.F. Bowden and J.F. Evans, J. Electroanal. Chem., (1987), 219, 71.

42. E.F. Bowden, M.F. Dautartas and J.F. Evans, J. Electroanal. Chem., (1987), 219, 91.

43. W.J. Albery, M.G. Boutelle, P.J. Colby and A.R. Hillman, J. Electroanal. Chem., (1982), 133, 135

44. T. Ohsaka, N. Oyama, K. Sato and H. Matsuda, J. Electrochem. Soc., (1985), 132, 1871.

45. H. Daifuku, K. Aoki, K. Tokuda and H. Matsuda, J. Electroanal. Chem., (1985), 183, 1.

46. J.S. Facci, R.H. Schmehl and R.W. Murray, J. Am. Chem. Soc., (1982), 104, 4959.

47. K. Shigehara, N. Oyama and F.C. Anson, J. Am. Chem. Soc., (1981), 103, 2552.

48. N. Oyama, T. Ohsaka, M. Kaneko, K. Sato and H. Matsuda, J. Am. Chem. Soc., (1983), 105, 6003.

49. S.M. Oh and L.R. Faulkner, J. Electroanal. Chem., (1989), 269, 77.

50. N. Oyama, T. Ohsaka and T. Ushiroguchi, J. Phys. Chem., (1984), 88, 5274.

51. K. Chiba, T. Ohsaka and N. Oyama, J. Electroanal. Chem., (1987), 217, 239.

52. T. Ohsaka, S. Kunimara and N. Oyama, Electrochim. Acta, (1988), 33, 639.

53. T. Ohsaka, H. Yamamoto and N. Oyama, J. Phys. Chem., (1987), 91, 3775.

54. P.G. Pickup and R.A. Osteryoung, J. Electroanal. Chem., (1985), 186, 99.

103

55.   R.J. Forster and J.G. Vos, J. Electrochem. Soc.,
       submitted.

56.   R.J. Forster, M.E.G. Lyons and J.G. Vos, J. Chem. Soc.,
       Faraday Trans. 1, submitted.

57.   B.P. Sullivan, P.J. Salmon and T.J. Meyer, Inorg. Chem.,
       (1978), 17, 3334.

58.   E.M. Kober, J.V. Casper, R.S. Lumpkin and T.J. Meyer, J.
       Phys. Chem., (1986), 90, 3722.

59.   R.C. Sutton, L. Thai, J.M. Hewitt, C.L. Voycheck and J.S.
       Tan, Macromolecules, (1988), 21, 2432.

60.   D.P. Rillema, D.S. Jones and H.A. Levy, J. Chem Soc.,
       Chem. Commun., (1979), 849.

61.   J. Brandup and E.H. Immergut, Polymer Handbook, Wiley,
       New York (1975).

62.   R.J. Forster and J.G. Vos, Macromolecules, (1990), 23,
       4372.

63.   H.C. Haas and R.D. Moreau, J. Polym. Sci., (1977), 15,
       1225.

64.   F.E. Lytle and D.M. Hercules, J. Am. Chem. Soc., (1969),
       91, 253.

65.   T. Shimidzu, K. Izaki, Y. Akai and T. Iyoda, Polymer J.,
       (1981), 13, 889.

66.   B.A. Moyer and T.J. Meyer, Inorg. Chem., (1981), 20, 444.

67.   R. Lange and K. Doblhofer, J. Electroanal. Chem., (1987),
       237, 13.

68.   J.M. Saveant, J. Phys. Chem., (1988), 92, 4526.

69.   C.P. Andrieux and J.M. Saveant, J. Phys. Chem., (1988),
       92, 6761.

70.   W.T. Yap and R.A. Durst, J. Electroanal. Chem., (1987),
       216, 11.

71.   O. Haas, H.R. Zumbrunnen and J.G. Vos, Electrochim. Acta,
       (1985), 30, 1551.

72.   S. Bruckenstein, C.P. Wilde, M. Shay, A.R. Hillman and
       D.C. Loveday, J. Electroanal. Chem., (1989), 258, 457.

73.   A.J. Kelly, T. Ohsaka, N. Oyama, R.J. Forster and J.G.

Vos, <u>J. Electroanal. Chem.</u>, (1990), <u>287</u>, 185.

74.   P. Ferruti and R. Barbucci, <u>Adv. Polymer Sci.</u>, (1984), <u>58</u>, 55.

75.   T. Ohsaka, N. Oyama, S. Yamaguchi and H. Matsuda, <u>Bull. Chem. Soc. Jpn.</u>, (1981), <u>54</u>, 2475.

76.   K.J. Vetter, <u>Electrochemical Kinetics</u>, Academic Press, New York (1987).

77.   S. Yamaguchi, H. Matsuda, T. Ohsaka and N. Oyama, <u>Bull. Chem. Soc. Jpn.</u>, (1983), <u>56</u>, 2952.

78.   T. Ohsaka, T. Okajima and N. Oyama, <u>J. Electroanal. Chem.</u>, (1986), <u>215</u>, 191.

79.   T. Ohsaka, M. Nakanishi, O. Hatozaki and N. Oyama, <u>Electrochim. Acta</u>, (1990), <u>35</u>, 63.

80.   C. Amatore, J.M. Saveant and D. Tessier, <u>J. Electroanal. Chem.</u>, (1983), <u>147</u>, 39.

81.   L. Roullier and E. Laviron, <u>J. Electroanal. Chem.</u>, (1983), <u>157</u>, 193.

82.   A.R. Hilman, D.C. Loveday and S. Bruckenstein, <u>J. Electroanal. Chem.</u>, (1991), <u>300</u>, 67.

Chapter 3

The Application of the Mediated Oxidation

of Nitrite at $[Ru(bpy)_2(Pol)_{10}Cl]Cl$

Polymer Modified Electrodes

106

3.1.   INTRODUCTION

This chapter describes the optimisation of the mediated oxidation of the nitrite ion at the $[Ru(bpy)_2(Pol)_{10}Cl]Cl$ modified electrodes, where Pol represents the copolymers described in chapter 2. Mediated charge transfer forms the basis of many applications including electrochemical synthesis [1], photogalvanic display devices [2], oxygen reduction [3] and analytical applications [4]. For those applications involving charge mediation by the modifying layer between the underlying electrode material and a target analyte in solution, the theory of mediated charge transfer has been extensively studied by many authors and allows mechanistic elucidation and kinetic parameters to be evaluated [5-10]. With these theoretical models, both qualitative and quantitative information about these processes can be obtained; whereas in the field of analysis, it defines a means of optimising electrode response.

The first portion of this chapter involves the investigation into the mechanism of the mediated oxidation of the nitrite ion by the metallopolymer films on electrodes. These metallopolymers have been previously described in chapter 2. The effect of varying parameters such as background electrolyte, film thickness and the composition of the polymeric backbone on the mechanism and position of the mediating reaction within the films was studied. The second portion of this chapter describes the optimisation of sensor response for flow injection techniques, and an investigation into the stability of films of these metallopolymers on electrode surfaces under these vigorous hydrdynamic conditions. The anticipated increased stability of these polymer films, obtained by incorporating styrene into the polymeric backbone and comparing the response to that of the PVP homopolymer, was the aim of this study (encompassing this chapter and chapter 2) at the outset. The theory of flow injection techniques has been introduced previously in chapter 1, and will not be discussed further here. Finally the

107

application of the metallopolymer films to the analysis of nitrite levels in selected samples was investigated.

3.1.1. Theory of Mediation Processes at Modified Electrodes

The fundamental reactions which may occur between a solution species Y, with Z being the reduced product of Y, and a mediating layer containing the redox couple A/B are shown in Figure 3.1. The mediating process can be described by reactions (3.1) and (3.2);

$$A + e^- \longrightarrow B \qquad\qquad (3.1)$$
$$B + Y \longrightarrow A + Z \qquad\qquad (3.2)$$
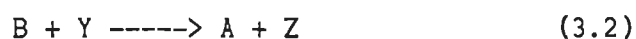
In this example the mediating process involves the reduction of the surface bound species A, but the same theories hold for the oxidation process also.

Depending on factors such as film morphology, film thickness, the diffusion rate of electroactive species through the film and electron transfer rates, four types of limiting cases may arise [11]:

- electron and substrate diffusion are so fast that the rate controlling step is the rate, k, of the catalytic reaction;

- the catalytic reaction is so fast that the rate is controlled by the two diffusion processes (diffusion of electrons and substrate);

- when diffusion of electrons is faster than diffusion of substrate a pure kinetic situation may arise by mutual compensation of the latter process and the catalytic reaction;

 in the opposite case a pure knetic situation may again

108

b = b₀ ... (figure diagram)

$$b = b_0 \qquad\qquad y_l = Ky_s$$

Electrode   Layer   Electrolyte

Figure 3.1: General model for the modified electrode showing the notation. Four processes are shown, electrode surface reaction (k'_E), partition of substrate into the film (K), mediated reaction within the film (k), and surface mediated reaction (k").

109

arise resulIting in the mutual compensation of electron
diffusion and catalytic reaction.

The fundamental processes involved in mediation are
identified as charge introduction at the modifying
layer/electrode interface, charge introduction at the
layer/solution interface and reaction of the target analyte with
the modifying layer. Coupled to these reactions one may observe
substrate diffusion into the film as dictated by the partition
coefficient, K. The diffusion rate of Y within the film, D_Y,
will, in all but a few cases, be considerably lower than the
solution value, D_S.

The analysis presented below is that developed by Albery,
Hillman and co-workers [5,12-14]. This model uses the notion of
"reaction layers" to describe two different reaction zones
within the film, one being a region where permeating Y is
converted to product Z, with the other being a region where
consumption of an electron or B occurs. In this analysis a rate
constant, k'_{ME}, for the modified electrode is utilised.
Alternative models have also been developed [11,15-20].

To analyse the mediating process for electrocatalytic
modified electrodes one has to solve equations (3.3) and (3.4)
below, given certain boundary conditions.

charge transport $\quad D_E \dfrac{\delta^2 b}{\delta x^2} - kby = 0 \qquad$ (3.3)

substrate diffusion $\quad D_Y \dfrac{\delta^2 y}{\delta x^2} - kby = 0 \qquad$ (3.4)

These equations describe the concentration profiles of both the
fixed redox couple and the substrate within the film, where b
and y represent the concentrations, in the coating, of B and Y,
respectively. D_E and D_y are the diffusion coefficients for
electron transport and substrate diffusion within the polymer

110

film, respectively. The boundary conditions are:

- charge introduction at the electrode/layer interface is
  assumed to be more rapid than charge propagation [21].
  Thus charge transfer to the electrode/layer interface is
  not expected to be rate limiting;

- the concentration of B at x = 0 is b_0, and is
  controlled by the electrode potential;

- the modifying layer acts in a catalytic manner, such that
  any substrate which permeates the layer and reaches the
  underlying electrode surface will not react there,
  therefore $(\delta y/\delta x)_0 = 0$. It is to be noted that, in their.
  treatment, Andrieux and Saveant [15] have included the
  reaction of the substrate directly at the electrode
  surface;

- the partitioning of the substrate Y between the solution
  and the modifying layer is given by:

$$y_L = Ky_S \qquad (3.5)$$

  where y_L and y_S are the concentration of Y within the
  layer and in solution, respectively, and K is the
  partition coefficient;

- the electron flux at the layer/solution interface is
  related to the kinetics by equation (3.6):

$$-D_E(\delta b/\delta x)_L = k''b_L Y_S \qquad (3.6)$$

  where b_L is the concentration of B at the interface (X
  = L).

The flux of electrons for the one-electron conversion of A

111

to B at the electrode surface is related to the current involved in the mediated transfer and to the concentration gradients by:

$$j_o = i/FA = -D_E (\delta b/\delta x)_o \qquad (3.7)$$

At this stage the electrochemical rate constant k'_{ME}, can be introduced [5], which relates the concentration of Y at the layer/solution interface to the electron flux, as in equation (3.8):

$$j_o = k'_{ME} y_s \qquad (3.8)$$

The rate constant, k'_{ME}, can be evaluated from the intercept of Koutecky-Levich plots using rotating disk electrode (RDE) studies, discussed later. The observed current is related to the sum of the fluxes of direct (j_y) and mediated (j_B) charge transfer and the concentration gradients at the electrode/film interface by:

$$(i/nFA) = j_o = j_B + j_y =$$
$$-D_E (\delta b/\delta x)_o + D_y (\delta y/\delta x)_o = k'_{ME} y_s \qquad (3.9)$$

As discussed earlier, an essential concept to be included in this analysis is that of the "reaction layer". The first reaction layer, X_L, defines the distance which Y can travel within the film prior to reaction with B, and is given by:

$$X_L = (D_Y/kb_L)^{1/2} \qquad (3.10)$$

The second reaction layer, X_o, defines the distance an electron can diffuse before reaction with Y:

$$X_o = (D_E/ky_o)^{1/2} \qquad (3.11)$$

where y_o is the concentration of Y at the film/electrolyte

112

interface.

With the concepts of the electrochemical rate constant and of the reaction layer now introduced, one can go back to reactions (3.3) and (3.4). Depending on the relative importance of electron and substrate diffusion, different approximations for k'_{ME} can be obtained. If $D_E b_o \gg D_y k y_s$, which arises from fast electron transport or slow permeation or ineffective partitioning of the substrate, then:

$$\frac{1}{k'_{ME}} \approx \frac{y_s L}{D_E b_o} + \frac{1}{k''b_o + kb_o KX_L \tanh(L/X_L)} \qquad (3.12)$$

$$\underset{\substack{\text{transport within} \\ \text{layer}}}{\text{electron}} \qquad \underset{\text{reaction}}{\text{surface}} \qquad \underset{\text{reaction}}{\text{layer}}$$

If permeation is very fast and/or electron transport within the film is relatively slower, then $D_E b_o \ll D_Y$ and:

$$\frac{1}{k'_{ME}} = \frac{L}{kD_Y} + \frac{k'' \tanh(L/X_o) + kKX_o}{kKX_o b_o \{k'' + kKX_o \tanh(L/X_0)\}} \qquad (3.13)$$

$$\underset{\substack{\text{transport} \\ \text{of Y across layer}}}{\text{}} \qquad \underset{\text{reaction}}{\text{surface}} \qquad \underset{\text{reaction}}{\text{layer}}$$

From the equations above it can be deduced that the slower contributions to the mediating reaction, which can be kinetic or diffusional in nature, will determine the magnitude of k'_{ME}. In the limiting case as represented by equation (3.12), the last term on the right hand side indicates the competition between the surface reaction (k'') and the layer reaction (k). The flux, however, may alternatively be limited to a value of $D_E b_o/L$ by electron transport through the film. The position of the reaction layer is reflected in the equation obtained for k'_{ME} in these limiting cases, and will depend on the ratio between

113

the reaction layer X_L and the layer thickness, L. For cases where $X_L \gg L$, the whole of the layer participates in the reaction and thus it is called a layer (L) case. In the reverse case the reaction occurs in a thin layer at the layer/solution interface, which is called the surface (S) case.

For the second limiting case, presented by equation (3.13), the position of the reaction layer may be determined by a similar method. If the layer thickness $L \gg X_O$, then the kinetic term on the right hand side reduces to kKX_Ob_O, and the reaction takes place in a layer adjacent to the electrode, which is called the layer/electrode (LE) case. In the reverse situation, when $L \ll X_O$, the reaction takes place at the layer/electrolyte interface, the so-called layer/surface (LS) case. For intermediate ratios of L and X_O, the reaction takes place throughout the layer.

If the electron and substrate diffusion contributions are of the same magnitude, another case arises, which can be described by equation (3.14) below.

$$\frac{D_E b_O}{K D_\gamma y_s} = \frac{X_O^2}{X_L^2} \approx 1 \qquad (3.14)$$

Under such conditions, and if X_O or X_L is less than L, then the reaction will take place somewhere in the middle of the layer, and will be controlled by the diffusion rates of both electrons and substrate. This is termed the layer/reaction zone (LRZ) case, with the solution for k'_{ME} being equation (3.15) given below.

$$\frac{1}{k'_{ME}} = \frac{L}{D_\gamma K + D_E b_O / y_s} \qquad (3.15)$$

From the equations above, it can be seen that the LE, LS and S cases can be controlled by either the transport or the kinetic term. Depending on the relative imortance of these two terms,

these cases can be subdivided into subclasses. These subclasses are either controlled by transport processes, in which case they are given the labels t_e or t_y, depending on whether electron or substrate diffusion are rate limiting, or by kinetic factors, in which case the labels are k or k". Using this notation, LEk denotes a mediated reaction that takes place in a layer close to the underlying electrode surface and is controlled kinetically, whereas in the LEt_y case the reaction takes place in the same part of the film but is controlled by substrate diffusion. These labels, together with the expression for their corresponding rate constants in the various limiting cases, are listed in Table 3.1. A diagram depicting the different positions and notations for the reaction layer is given in Figure 3.2.

The equations given above have been used to construct a kinetic zone diagram. An example of such a diagram is shown in Figure 3.3. "Surface" and "electrode" cases give a third dimension to the diagram but those cases are not of an interest in the design of three dimensional sensor devices.

The conditions for optimum efficiency of catalytic modified electrodes, that is a high value for k'_{ME}/k'_E, the ratio between the electrochemical rate constant for the modified and bare electrode, have been considered by Albery and Hillman [13] and by Andrieux et al. [11]. In these studies factors such as thickness of the modifying layer and limits for the kinetic parameters introduced above have been considered. Where the electrode response has been optimised with respect to electron transport and film morphology, it is usually found that electron diffusion is faster than substrate diffusion and that the concentration of the surface bound redox couple is to be larger than that of the substrate.

Because of the conditions discussed above, the number of limiting cases to be considered for optimisation of the modified electrode are limited, with the layer cases showing most promise. For the layer cases, the magnitude of k'_{ME} will initially increase with the layer thickness (all sites mediate

115

Table 3.1: Notation and expressions describing behaviour of different cases for Faradaic reactions at polymer modified electrodes.

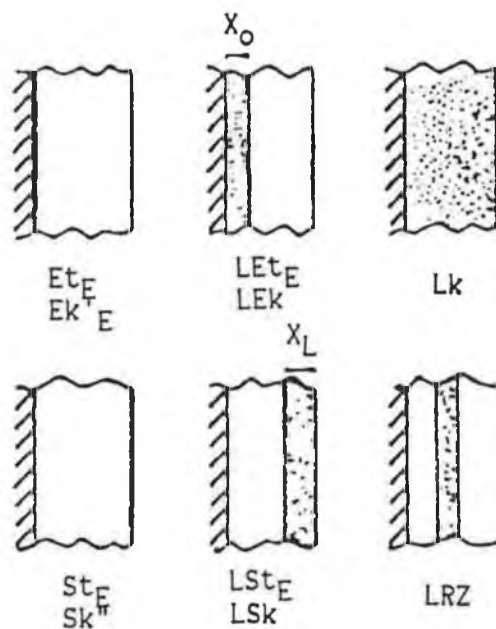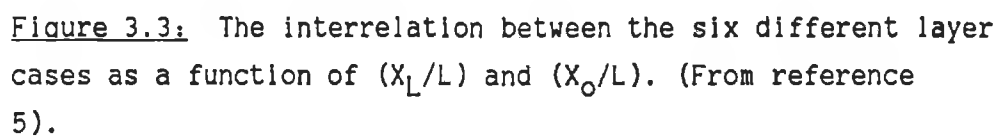| Case notation	Expression for charge transfer rate (k'_{ME})
Sk"	$k''b_o$
St_E	D_Eb_o/Ly_s
LSk	Kkb_oX_L
LSt_E	D_Eb_o/Ly_s
Lk	Kkb_oL
$LRZt_Et_Y$	$D_Eb_o/Ly_s + KD_y/L$
LEk	Kkb_oX_o
LEt_Y	KD_y/L
Ek'_E	Kk'_E
Et_Y	KD_y/L

116

Figure 3.2: The location of the reaction in the ten possible cases together with the notation used to distinguish them. The electrode is on the left in each case and the location of the reaction is shown by the shaded region. (From reference 5).

Figure 3.3: The interrelation between the six different layer
cases as a function of (X_L/L) and (X_o/L). (From reference
5).

electron transfer under kinetic control) then pass through a maximum before decreasing due to transport limitations of the substrate. These ideal cases correspond to a sufficient amount of mediation sites for substrate consumption combined with efficient substrate or charge diffusion and correspond to the ideal three dimensional modified electrode. For the LSk case the catalytic advantage becomes

$$k'_{ME}/k'_E = KX_L/l \qquad (3.16)$$

This can be very large, since the reaction layer thickness can be much greater than l, the distance over which electron transfer can take place. For reactions that exhibit slow homogeneous kinetics, a layer reaction is thus required where Y permeates the film rapidly.

For the two optimum surface and electrode cases, Sk" and Ek'$_E$, mediation does not occur throughout the layer, with the reaction taking place at the layer/solution and the electrode/layer interfaces, respectively. This reaction can not be described as three dimensional and these cases will thus find limited application in analysis. In the surface case, a practical application can only be envisaged if B is a specific catalyst for the oxidation or reduction of the substrate Y. The electrode case becomes applicable when favourable partition can be obtained. In that case, even as the reaction is taking place at the underlying electrode surface, a catalytic effect will be obtained because of the high value of the partition coefficient, K. This approach has been used in the development of sensors based on preconcentrating membranes.

The experimental determination of the parameters involved in the theoretical approach described above relies on the recognition of the appropriate limiting process. It is the use of rotating disk and rotating ring-disk electrodes which provides the means of analysing the kinetics of catalysis at the modified electrode surface. These techniques allow control of

119

the substrate diffusion in solution and thus permit the elucidation of the kinetics and mechanism of the catalytic reaction. By controlling the electrode potential, the surface concentration of the solution species can be reduced to zero, and the current response becomes limited by mass transport and is given by the Levich equation [22]:

$$i_{Lev} = 1.554nFAD^{2/3}\upsilon^{-1/6}y\,\omega^{1/2} \qquad (3.17)$$

where υ represents the kinematic viscosity of the substrate in the solution and ω the electrode rotation rate. Rotating disk measurements are ideal for the investigation of mediated reactions at electrode surfaces since the rate of mass transport of the substrate is calculable. This has lead to the widespread exploitation of this technique [23-26]. The modified electrode does not usually obey the simple Levich equation since mass transport may not represent the rate limiting process. In this case the limiting current is given by:

$$1/i_{Lim} = 1/i_F + 1/i_{Lev} \qquad (3.18)$$

or

$$1/i_{Lim} = 1/nFAk'_{ME}y + 1/1.554nFAD^{2/3}\upsilon^{-1/6}y\,\omega^{1/2} \qquad (3.19)$$

A plot of i_{Lim}^{-1} versus $\omega^{-1/2}$ gives a straight line, where the slope is the reciprocal of the Levich slope and the intercept yielding the value of k'^{ME}. Albery and Hillman [5] have published a useful flowchart for the diagnosis of reaction type based on this mode of analysis (Figure 3.4.). In this flowchart, the functional dependence of k'_{ME} on b_0, y_s and L allows classification of the process.
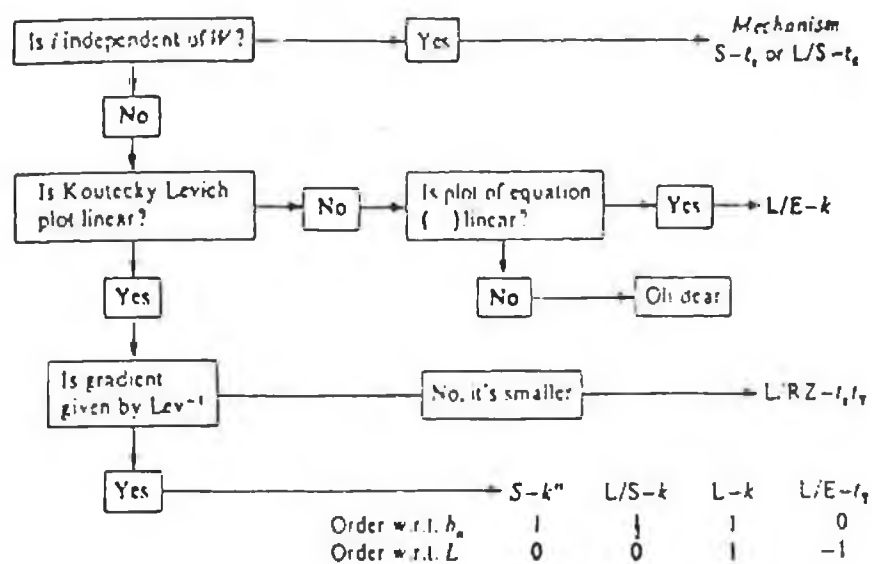
120

Is i independent of W? ⟶ Yes ⟶ *Mechanism*
$S-t_s$ or $L/S-t_s$

No

Is Koutecky Levich plot linear? ⟶ No ⟶ Is plot of equation ( ) linear? ⟶ Yes ⟶ $L/E-k$

Yes

No ⟶ Oh dear

Is gradient given by Lev^{-1} ⟶ No, it's smaller ⟶ $L'RZ-t_st_T$

Yes ⟶

	$S-k''$	$L/S-k$	$L-k$	$L/E-t_T$
Order w.r.t. h_n	1	1	1	0
Order w.r.t. L	0	0	1	-1

Figure 3.4: Diagnosis of mechanism for modified electrodes
(From reference 5).

121

3.2. EXPERIMENTAL

3.2.1. Materials

The metallopolymers were synthesised as described in Chapter 2. The electrolyte system used throughout, unless otherwise stated, was 0.1 M $NaNO_3$ at a pH of approximately 3.0.

NED reagent for the uv-visible spectrophotometric determination of nitrite was prepared by dissolving 0.2 g of N-(1-naphthyl) ethylenediamine.2HCl (Aldrich) in 150 cm^3 of 15% acetic acid. Sulfanilamide reagent was prepared by dissolution of 0.5 g of sulfanilamide (Aldrich) in 150 cm^3 of 15% acetic acid.

Stock solutions of $NaNO_2$ were prepared fresh every three days in 0.1 M $NaNO_3$ (pH 3.0) and stored in the dark.

3.2.2. Apparatus and Procedures

Rotating-disk electrodes constructed of glassy carbon or platinum of 3 mm diameter (Metrohm) were polished with a 0.3 um alumina slurry on a felt pad before use. Rotating disk voltammograms were recorded on an EG & G PAR Model 362 Scanning Potentiostat at a scan rate of 5 mV s^{-1} and using a Metrohm 628-10 Rotator and a Linseis LY17100 X-Y Recorder. The electrochemical cell in these experiments was of conventional design and was thermostatted at 25°C. All potentials are referenced with respect to the saturated calomel electrode. Metallopolymer deposition and surface coverage determinations of ruthenium were carried out as described in Chapter 2.

For the flow injection studies, an EG & G PAR Model 400 EC detector was utilised, with the electrochemical thin layer cell consisting of a 3 mm glassy carbon electrode (planar configuration), a stainless steel counter electrode and a Ag/AgCl reference electrode. The dual parallel electrode configuration was utilised for the comparison of currents at a

bare unmodified glassy carbon electrode and at the modified electrodes. Flow was controlled using a Waters 501 HPLC pump, in conjunction with a pulse dampener of 50 cm length of coiled tubing. i-t characteristics were recorded on a Philips PM8252 recorder.

Saliva was collected by expectoration into small vials. No sample pretreatment was carried out on the samples. Samples for electrochemical analysis were diluted 1:1 with 0.2 M $NaNO_3$, with all subsequent dilutions being carried out in 0.1 M $NaNO_3$, while samples for uv-visible spectrophotometric analysis were diluted with H_2O. Finely comminuted meat samples (5 g) were heated to $80^{\circ}C$ in 40 cm^3 of H_2O and mixed thoroughly with a glass rod. The samples were subsequently diluted with approximately 250 cm^3 of hot water and allowed to cool to room temperature. The total volume was then brought to 500 cm^3 and the solution was then filtered. Samples for electrochemical analysis were subsequently diluted 1:1 with 0.2 M $NaNO_3$.

Uv-visible spectrophotometric determination of nitrite levels was carried out by a standard procedure [27] using the NED and sulfanilamide reagents.

3.3. RESULTS AND DISCUSSION

3.3.1. General

Nitrite does not undergo a redox reaction at a bare glassy carbon electrode in the potential region of the Ru(II/III) (E^o = 700 mV vs SCE) oxidation, despite a formal potential of 590 mV (SCE) [28] for reaction (3.20) shown below:

$$NO_2^- + H_2O \iff NO_3^- + 2H^+ + 2e^{-1} \quad (3.20)$$
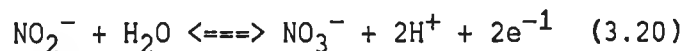
Given this formal potential of the nitrite/nitrate reaction, it was to be expected that electrodes modified with the

$[Ru(bpy)_2(Pol)_{10}Cl]Cl$ metallopolymers, described in Chapter
2, could mediate the NO_2^- oxidation with an approximately
110 mV driving force. Typical cyclic voltammograms obtained in
0.1 M $NaNO_3$ electrolyte at both the bare (A) and modified
(B,C) glassy carbon electrodes are depicted in Figure 3.5. The
bare glassy carbon electrode shows a broad irreversible wave for
the NO_2^- oxidation with an E_p of approximately 900 mV,
whereas the oxidation of the nitrite ion at the modified
electrode occurs at the potential for the onset of the oxidation
of the ruthenium metal centre, indicating mediation.

A $NaNO_3$ background electrolyte, adjusted to a pH of 3.0,
was utilised for all of the rotating disk experiments, as this
electrolyte had been shown to yield optimum charge transport
rates (see Chapter 2). Activation parameters determined for the
charge transport process in this electrolyte suggested that ion
diffusion limits D_{ct}. This fact, coupled to the "break-in"
effect observed in Chapter 2, suggests that, for some of the
metallopolymers, the films are swollen in this electrolyte. In
high concentrations of $NaNO_3$, this results in the
metallopolymer laterally diffusing across the glassy carbon
electrode surface in rotating disk experiments, leading to an
uneven film thickness. A 0.1 M $NaNO_3$ electrolyte was therefore
selected to produce films of the required stability for rotating
disk experiments.

In $NaClO_4$ electrolytes, charge compensating counterions
diffuse into the homopolymer film with little solvent transport
[29]. Furthermore, D_{ct} as measured by cyclic voltammetry
decreases with increasing $HClO_4$ concentration, suggesting the
formation of a highly dehydrated film. Studies into the
application of the 0.1 M $HClO_4$ electrolyte for the invest-
igation of the mediating capabilities of the metallopolymers
revealed that no mediation for the oxidation of NO_2^- was
obtained. This is not surprising given the dehydrated nature of
the film. From equation 3.20 above, it can be seen that
significant levels of solvent (H_2O) will be required within
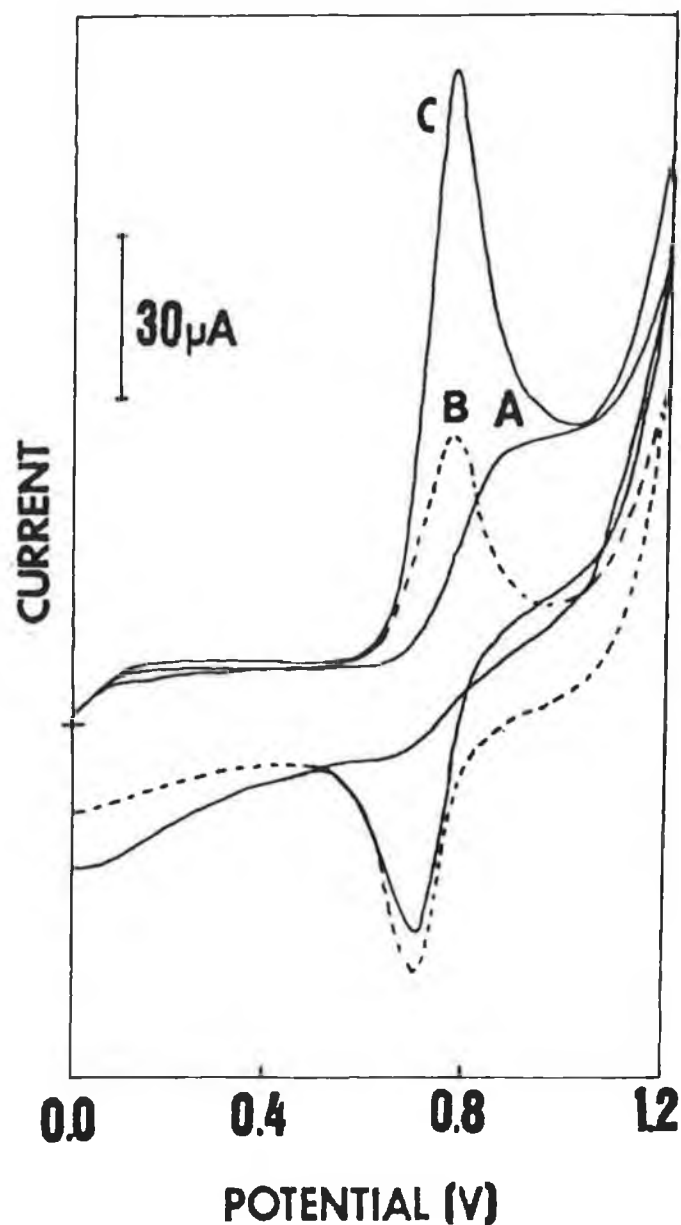
124

Figure 3.5: Cyclic voltammograms obtained for 2.5 mM NO_2^- in 0.1 M $NaNO_3$ electrolyte at the bare (A) and modified (C) glassy carbon electrodes. (B) represents the blank response at the $Ru-PVP_{50}$ modified electrode (surface coverage of 1.0 x 10^{-8}mol cm^{-2} ruthenium). Scan rate 100 mV s^{-1}

125

the film for the catalytic reaction to occur. The protonated pyridine moieties in the polymer backbone have also been reported to form ion pair associations with the perchlorate anion [30,31] in $HClO_4$ electrolytes. This would lead to a more compact structure for the films due to crosslinking and would also be expected to reduce the partitioning capability of the metallopolymer films for the incorporation of the nitrite ion into the film.

The remainder of this chapter will concentrate on the application of the metallopolymer films for the mediation of the NO_2^- oxidation in 0.1 M $NaNO_3$ (pH 3) electrolyte.

3.3.2. Rotating Disk Voltammetry

Rotating disk voltammetry was used in order to probe the mechanism and position of the reaction zone within the layer of the electrocatalytic reaction. This was carried out on films of two of the metallopolymers described in chapter 2. These were $Ru-PVP_{100}$, the 4-vinylpyridine homopolymer, and $Ru-PVP_{50}$, the metallopolymer consisting of the metal centre coordinated to a 1:1 copolymer of 4-vinylpyridine and styrene backbone composition.

Typical rotating disk voltammograms for the mediated oxidation of 0.1 mM NO_2^- in 0.1 M $NaNO_3$ electrolyte, at the $Ru-PVP_{50}$ metallopolymer modified electrode, are shown in Figure 3.6. It is evident from these plots that a mediated oxidation of NO_2^- appears in the potential region of the Ru(II/III) oxidation, and that i_{Lim} is dependent on the rotation rate, ω. Koutecky-Levich plots can then be used to analyse this data. Typical plots showing the dependence on layer thickness of the mediated oxidation of 0.25 mM NO_2^- at the $Ru-PVP_{100}$ films are shown in Figure 3.7. These plots are linear for the surface coverages examined, as are plots obtained at the $Ru-PVP_{50}$ modified electrode, giving a Levich slope of $3.7 \pm 0.4 \times 10^{-3}$ cm s$^{-1/2}$. This value is close to the

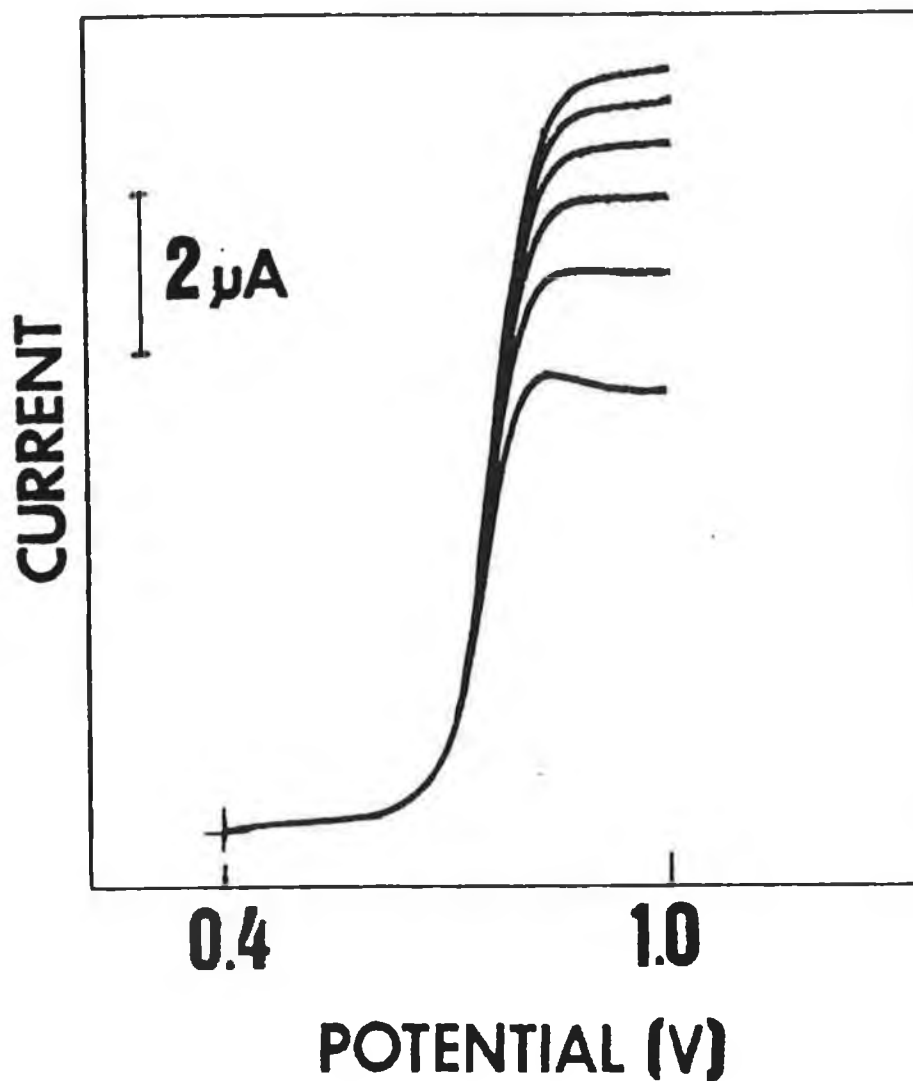Figure 3.6: Rotating disk voltammograms recorded at a Ru-PVP$_{50}$ modified glassy carbon electrode (surface coverage of 7.0 x 10^{-9}mol cm^{-2} ruthenium) for the mediated oxidation of 0.1 mM NO$_2^-$ in 0.1 M NaNO$_3$ electrolyte. Scan rate, 5 mV s^{-1}. Rotation rate, from top to bottom, 3000, 2500, 2000, 1500, 1000, and 500 rpm.

127

slope observed at a clean unmodified platinum electrode (4.0 $\pm$ 0.5 x 10^{-3} cm $s^{-1/2}$). The variations observed at the platinum electrode are attributed to surface poisoning of the electrode, thus necessitating polishing of the electrode surface between each scan. Since the limiting currents are dependent on rotation rate with all subsequent Koutecky-Levich plots being linear, the St_e, LSt_e and LEk cases can be eliminated (see Figure 3.4), and since the Levich slope is similar, within experimental error, to that obtained at a bare platinum electrode, the $LRZt_e t_y$ case can also be eliminated. Thus having excluded the above cases, the mediated reaction must lie within the Sk", LSk, Lk or LEt_y kinetic zones. These cases can be distinguished by examining the dependence of k'_{ME} on L.

The modified electrode rate constant, k'_{ME}, can be evaluated from the intercept of the Koutecky-Levich plot, as discussed earlier. The dependence of k'_{ME} on L, for the mediated oxidation of 0.25 mM NO_2^- for both of the metallopolymers examined, showed linear, first order behaviour up to a layer thickness of approximately 100 nm (surface coverage of approximately 8 x 10^{-9} mol cm^{-2}). For thicker films (surface coverages of greater 5 x 10^{-8} mol cm^{-2}) k'_{ME} was seen to be independent of film thickness. A similar behaviour was observed for other concentrations of NO_2^- (0.05 mM and 0.1 mM). The similarity of the reaction layer thickness, X_L, for the two metallopolymers examined, reflects the invariance of the charge transport diffusion coefficients determined for these metallopolymers in this electrolyte, as reported in Chapter 2. Since the dependence of k'_{ME} on L is first order, the kinetic zone can be assigned via the flowchart to be Lk. In order to confirm this diagnosis, the dependence of k'_{ME} on b_o, the concentration of mediator within the film, was investigated. For an Lk kinetic zone regime, k'_{ME} would be expected to have a first order dependence on b_o.

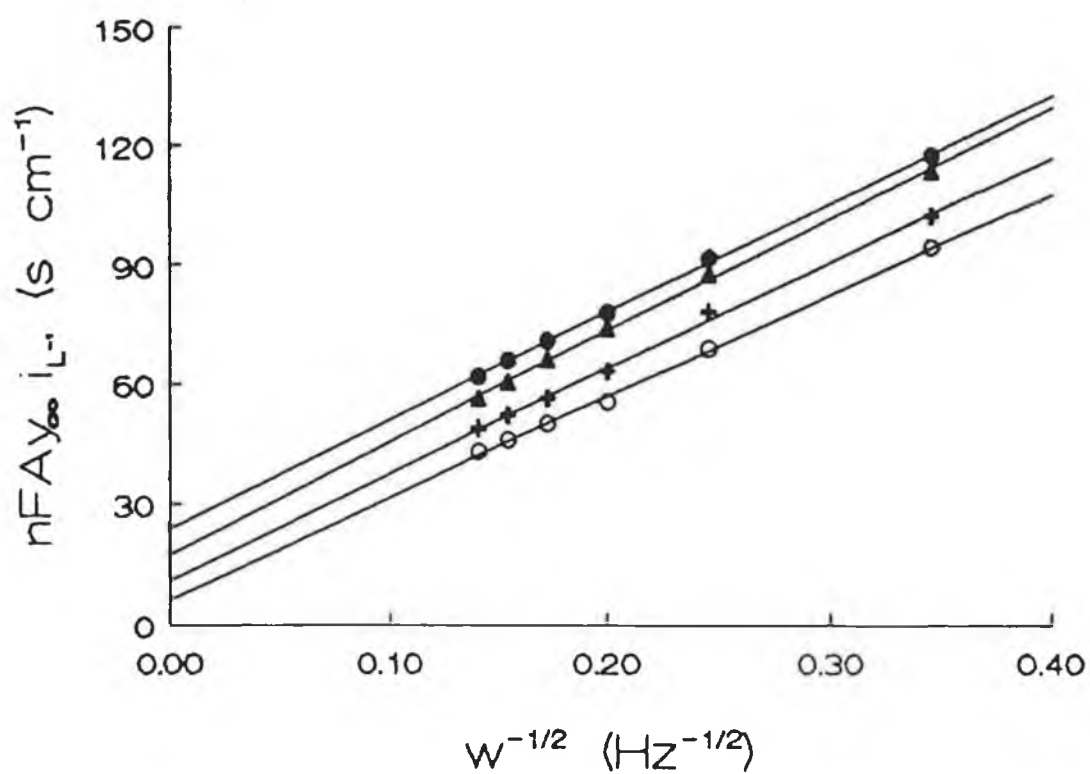In order to analyse the dependence on b_o, it is necessary to evaluate the concentration of Ru(III) within the film as a

128

Figure 3.7: Typical Koutecky-Levich plots for the mediated oxidation of 0.25 mM NO_2^- in 0.1 M $NaNO_3$ at an $Ru-PVP_{100}$ modified electrode. Surface coverages, from top to bottom are 8 x 10^{-10}, 1.9 x 10^{-9}, 3.5 x 10^{-9} and 1.15 x 10^{-8} mol cm^{-2}.

function of electrode potential. Films of the metallopolymers show classical surface-bound behaviour in this electrolyte at the sweep rates employed in the rotating disk voltammetric experiments (see Chapter 2). This strongly suggests that the Nernst equation is valid under these conditions. The observed response for slow sweep voltamograms of the metallopolymers films is shown in Figure 3.8 for Ru-PVP$_{100}$ films and in Figure 3.9 for the Ru-PVP$_{50}$ films. The super- Nernstian slopes upon oxidation of large proportions of the film may be attributed to a limiting interfacial charge transport of counterions into the film, as the charge compensating counterion diffusion process has been shown to limit charge transport, with this electrolyte, in these metallopolymer films (see Chapter 2). This portion of the plot was therefore not utilised further in the calculation. The linear portions of the plots gave slopes of 59 ± 3 mV decade^{-1} and 55 ± 4 mV decade^{-1} for the Ru-PVP$_{100}$ and Ru-PVP$_{50}$ metallopolymer films, respectively, in close agreement with the theoretical slope of 59.6 mV decade^{-1}. These data can thus be used to calculate the fraction, f, of the film which is oxidised via the relation:

$$\ln[f/(1-f)] = (F/RT)(E-E^O) \qquad (3.21)$$

and hence b$_o$ can be evaluated. By analysing the rising portion of the rotating disk voltammograms, k'$_{ME}$ can be evaluated at various fractions of Ru(II) oxidation. The plot of ln[k'$_{ME}$] versus ln[f] is shown in Figure 3.10, for the Ru-PVP$_{100}$ metallopolymer and in Figure 3.11, for the Ru-PVP$_{50}$ metallopolymer. These plots are linear, with slopes of 1.11 ± 0.20 and 1.02 ± 0.20, respectively. This agrees with the slope of unity expected for an Lk kinetic zone case.

Thus for surface coverages up to a value of approximately 8 x 10^{-9}mol cm^{-2}, for both of the metallopolymers examined, the kinetic zone is of the Lk type and the reaction is controlled by the polymer. For thicker films (> 5 x 10^{-8}mol

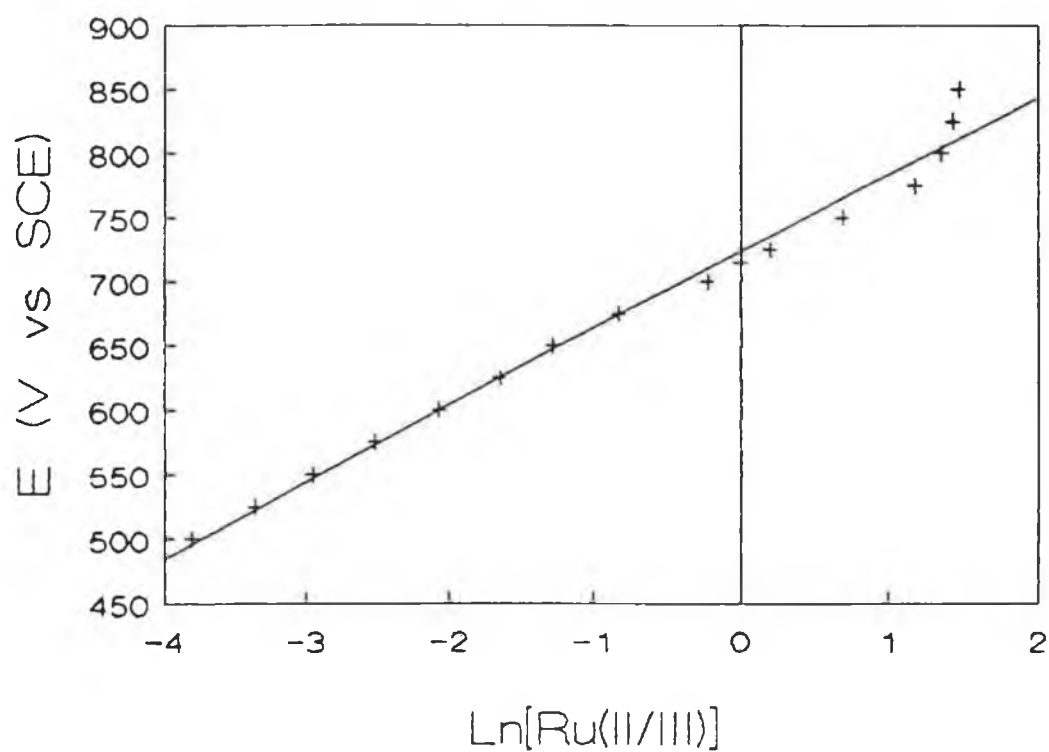**Figure 3.8:** Nernst plot for a Ru-PVP$_{100}$ modified electrode in 0.1 M NaNO$_3$. Surface coverage of ruthenium was 3.5 x 10^{-9}mol cm^{-2}.
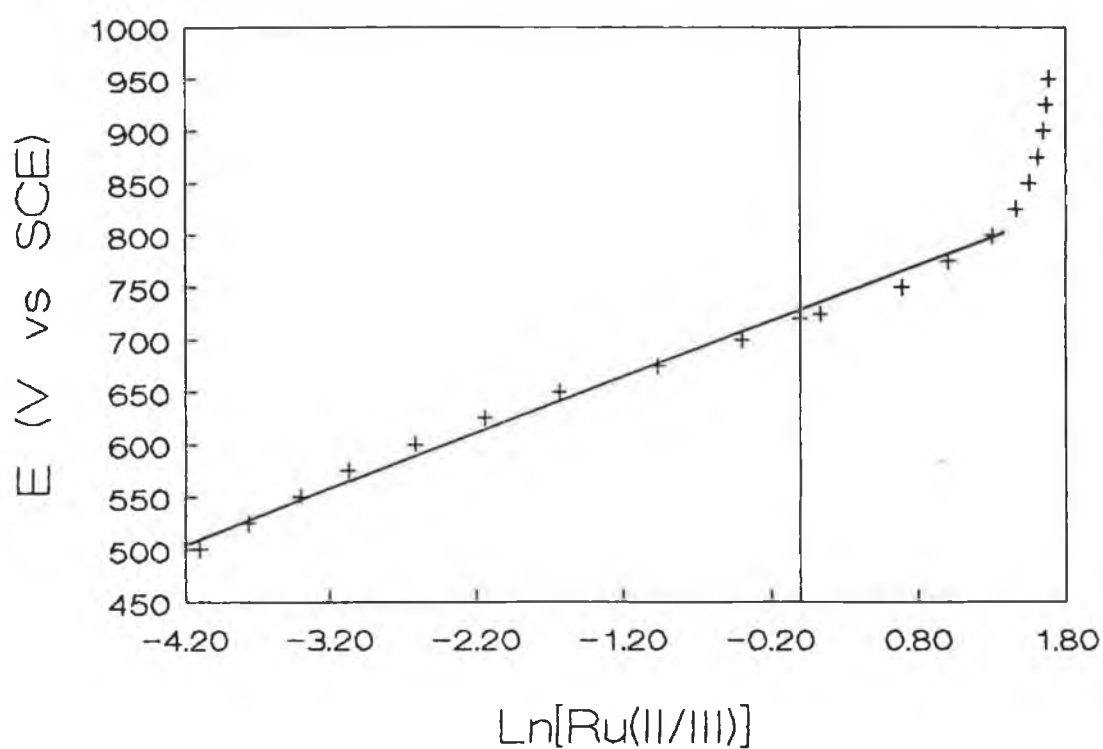
Figure 3.9: Nernst plot for a Ru-PVP$_{50}$ modified electrode in 0.1 M NaNO$_3$. Surface coverage of ruthenium was 5.5 x 10^{-9} mol cm^{-2}.
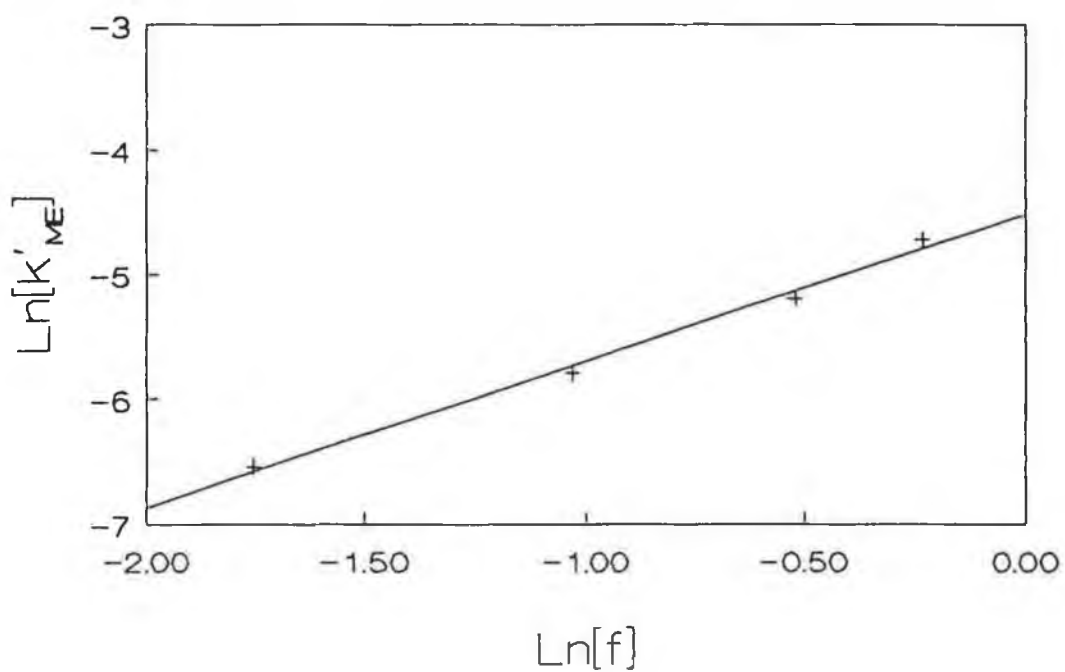
Figure 3.10: The effect of increasing the Ru(III) concentration within a film of Ru-PVP$_{100}$ on the modified electrode rate constant, k'$_{ME}$, for the reaction of 0.25 mM NO$_2^-$ in 0.1 M NaNO$_3$. Surface coverage 3.5 x 10^{-9}mol cm^{-2}.
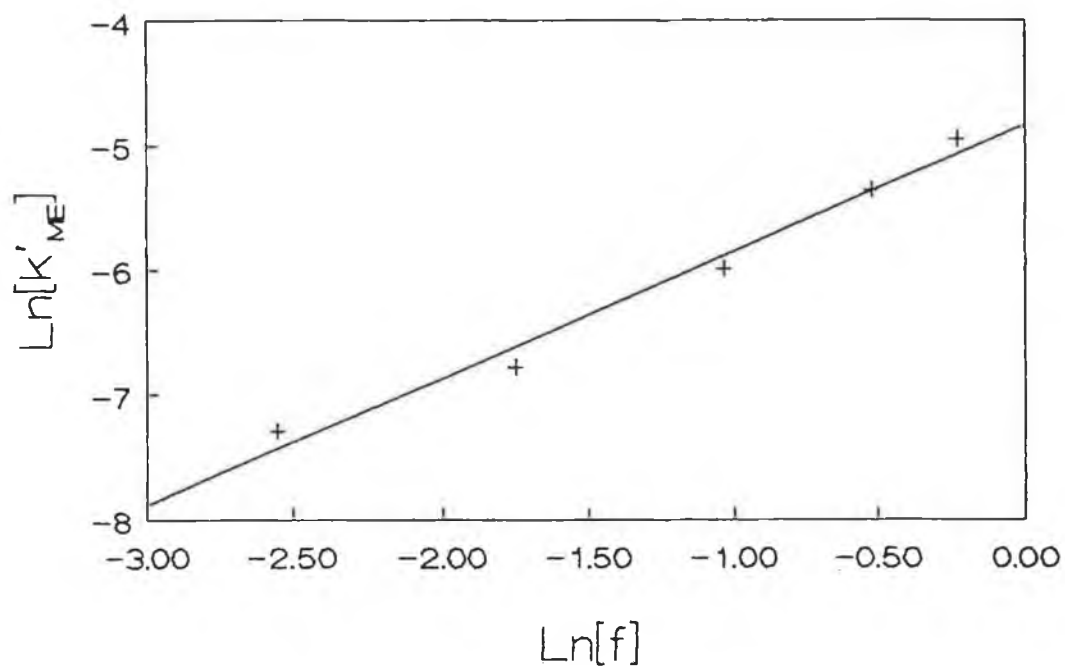
133

Figure 3.11: The effect of increasing the Ru(III) concentration within a film of Ru-PVP$_{50}$ on the modified electrode rate constant, k'$_{ME}$, for the reaction of 0.25 mM NO$_2^-$ in 0.1 M NaNO$_3$. Surface coverage 5.5 x 10^{-9}mol cm^{-2}.

cm^{-2}), k'_{ME} was shown to be independent of film thickness, and the mechanism corresponds to that of an LSk kinetic zone with diffusion of NO_2^- to the electrode surface controlling the process. For $HClO_4$ electrolytes no mediation of the oxidation of nitrite was observed. The observation that by varying the supporting electrolyte, optimal mechanisms for analysis can be obtained, has obvious implications for analytical applications of these modified electrodes. Variations in the polymeric backbone composition did not overly affect the mechanism of the mediating reaction in these metallopolymers, with the kinetic zone being the same for both the $Ru-PVP_{50}$ and $Ru-PVP_{100}$ modified electrodes. Further investigations into the analytical utility of this mediating reaction were carried out by flow injection analysis techniques, and will be discussed in the following section.

3.3.3.   Flow Injection Amperometric Detection of Nitrite

The analytical application of cyclic voltammetry and/or
rotating disk techniques to the routine analytical detection of
nitrite is limited; due, in part, to the presence of the
background ruthenium oxidation peak, and to the relatively long
timescales required for each analysis. Also, when the
metallopolymer-modified electrodes are used in stationary or
rotating disk cells, all responses for easily oxidised species
will occur at the potential of the Ru(II/III) transition, with
their oxidation mediated by the Ru(III) species. Consequently
this approach suffers from a lack of selectivity, making it
impossible to resolve the responses for two oxidisable species.
Perhaps more suited to analytical detection of nitrite,
therefore, is the technique of flow injection analysis using a
constant-potential detection mode (amperometric detection). Some
of the basic theory of flow techniques was introduced in Chapter
1. Flow injection techniques allow rapid analysis of multiple
samples, coupled with the convenience of adaptability for use as
detectors following chromatographic separation, while the
amperometric detection mode can offer increased signal-to-noise
ratios by virtue of the absence of a signal for the Ru(II/III)
oxidation.

A large number of analytical methods have been developed for
the determination of nitrite based principally on
spectrophotometric methods [32,33], but these have limited
sensitivity and linear ranges, involve long reaction times, and
frequently depend upon unstable coloured complexes. More
recently, several sensitive polarographic methods for the
determination of trace levels of nitrite have been reported
[34-36]. Methods based on solid electrodes are, however, more
desirable for sensing applications in flowing solutions. The
determination of nitrite by direct oxidation at a bare glassy
carbon electrode has been reported [37,38], but usually requires
prior chromatographic separation in order to eliminate

136

interferences observed due to the high overpotential at this electrode material. Cox and Kulesza [39] have described a platinum electrode modified by the deposition of iodine for the voltammetric detection of nitrite. This method was, however, limited by poor sensitivity. An alternative modified electrode for the determination of nitrite, based on anion exchange material incorporated into a carbon paste matrix, has been reported by Kalcher [40]. This method invloves relatively long analysis times, however, due to the preconcentration step requirement. Recently, a glassy carbon electrode coated with the Ru-PVP$_{100}$ metallopolymer described in Chapter 2, has been shown to mediate the nitrite oxidation in flowing solutions [41]. This material, as discussed previously in Chapter 2, suffers from a lack of long term stability in these flowing streams. This section describes the application of more stable metallopolymers, as described in Chapter 2, to the detection of nitrite in flowing solutions. The effect of varying levels of styrene in the polymer backbone on the stability and magnitude of the nitrite response are presented and discussed. The modified electrodes were utilised for the determination of nitrite levels in selected samples of cooked meat and saliva, with the response compared to that obtained by a standard spectrophotometric method [27].

3.3.3.1. Effect of Applied Potential

The effect of the applied potential (vs Ag/AgCl reference electrode) on the flow injection response at both the bare unmodified (+) and at a Ru-PVP$_{50}$-modified (o) glassy carbon electrode surface to the addition of 1 μg cm^{-3} concentration levels of nitrite into the flowing stream, using a constant-potential detection mode, is depicted in Figure 3.12. The applied potential was varied from +400 mV, where all of the surface ruthenium is present as Ru(II) and thus no mediation currents were observed, up to a value of +1000 mV, where the
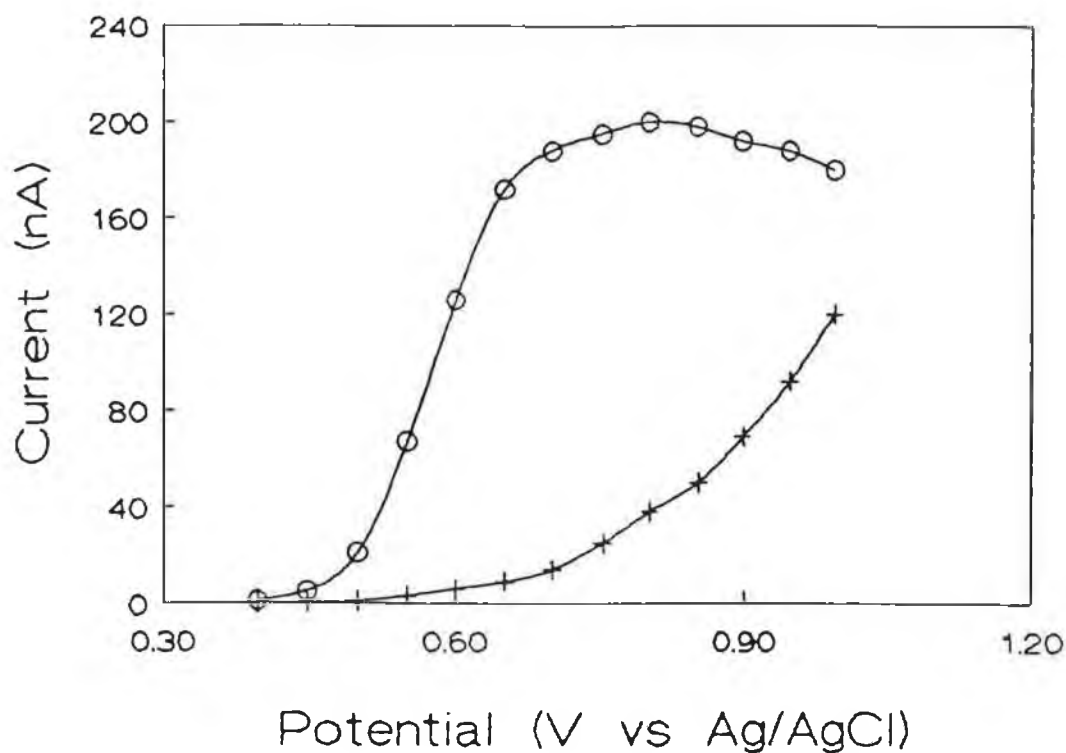
137

Figure 3.12: Hydrodynamic voltammograms obtained at the bare
(+) and the Ru-PVP$_{50}$-modified (o) electrodes for the injection
of 1 μg cm^{-3} nitrite. Background electrolyte, 0.1 M NaNO$_3$.
Flow rate of 1.0 cm^{3}min^{-1}. Surface coverage of ruthenium was
2.0 x 10^{-9}mol cm^{-2}.

surface ruthenium is present as Ru(III) and with mediation being limited either by substrate diffusion to the film/electrolyte interface or, alternatively, by substrate partition into the film, depending on factors such as the film thickness and background electrolyte flow rate. A plateau for the limiting current was attained at a potential of +800 mV for the Ru-PVP$_{50}$-modified electrode as shown in Figure 3.12, with no increase in response for subsequent increases in applied potential. Similar hydrodynamic voltammograms (HDVs) were obtained at electrodes modified with the Ru-PVP$_{100}$ homopolymer and the other styrene-containing metallopolymers, Ru-PVP$_{75}$, Ru-PVP$_{67}$ and Ru-PVP$_{33}$, the synthesis and characterisation of which are described in Chapter 2. Hydrodynamic voltammetric profiles for the oxidation of nitrite at the bare glassy carbon electrode in the flowing solutions exhibited an increased overpotential compared to the mediated oxidation at the modified electrodes, with a limiting current response not being attained within the potential window examined. An applied potential of +800 mV was selected for subsequent investigation into the application of the modified electrode for the detection of nitrite.

Representative responses to the injection of 1 µg cm^{-3} levels of nitrite at the bare and Ru-PVP$_{100}$-modified electrodes are shown in Figure 3.13, demonstrating the excellent peak shapes and relatively fast response times obtained at the modified electrode. A two to threefold enhancement in the current response at the modified electrode was normally obtained, in comparison to the response obtained at the bare electrode, with the magnitude of the enhancement depending on factors such as surface coverage of ruthenium (film thickness) and applied potential.
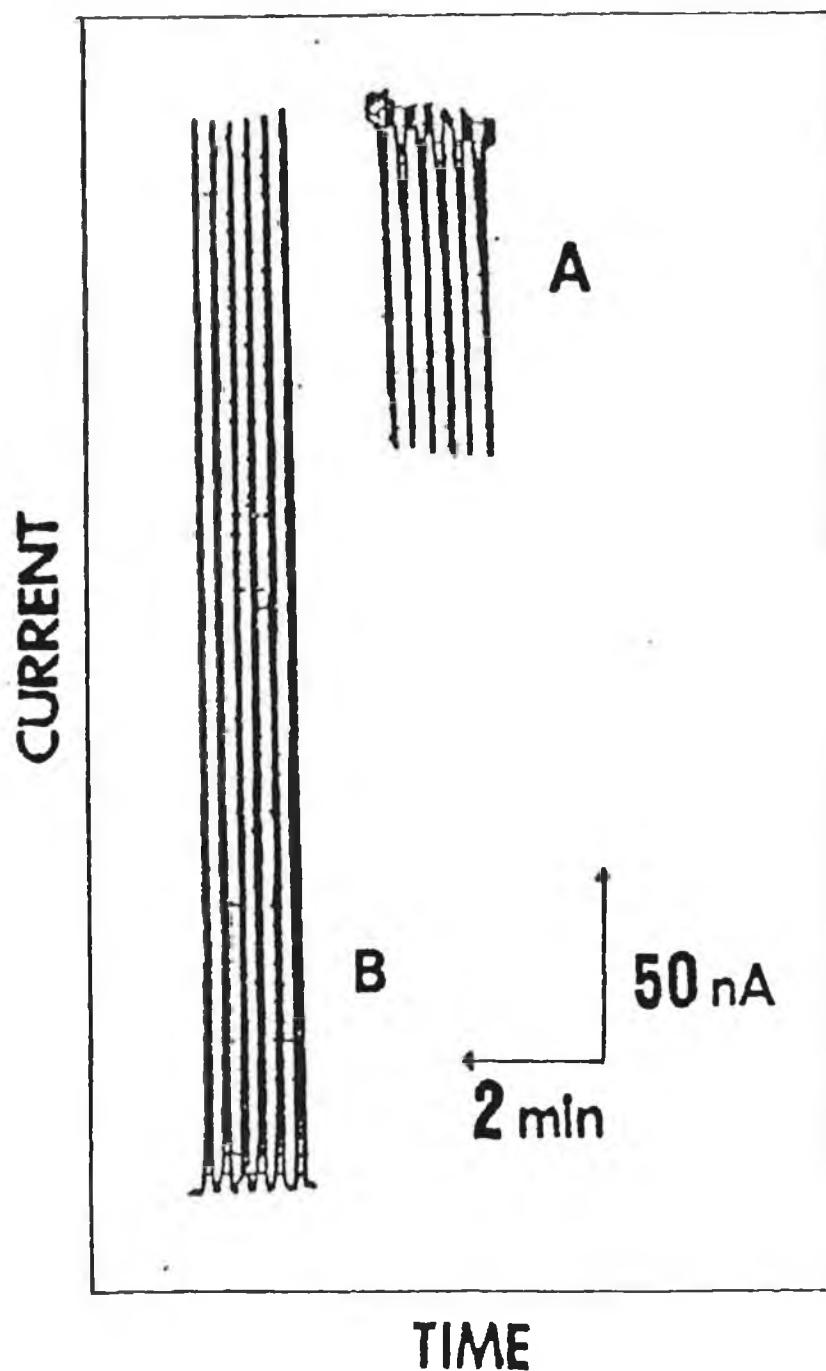
139

Figure 3.13: The flow-injection current response obtained at both the bare (A) and Ru-PVP$_{100}$-modified (B) glassy carbon electrodes to injections of 1 µg cm^{-3} levels of nitrite. Operating potential of +800 mV. 0.1 M NaNO$_3$ background electrolyte at a flow rate of 1.0 cm^{3}min^{-1}. Surface coverage of ruthenium was 3.5 x 10^{-9} mol cm^{-2}.

3.3.3.2. Effect of Flow Rate

The effect of flow rate on the magnitude of the response at
the Ru-PVP$_{50}$-modified electrode (surface coverage of 2.0 x
10^{-9} mol cm^{-2}) to injections of 1 µg cm^{-3} NO$_2^-$ was then
investigated. At very low flow rates (<0.4 cm^{3}min^{-1}), a
broad response was obtained, with the faster flow rates yielding
shorter response times. For example, peak widths at half height
of 22 sec and 3 sec were obtained for flow rates of 0.2
cm^{3}min^{-1} and 2.0 cm^{3}min^{-1}, respectively. Peak heights,
however, varied only slightly with variations in the flow rate,
with the faster flow rates (>1.2 cm^{3}min^{-1}) showing slight
diminutions in peak height with increasing flow rate. A flow
rate of 1.0 cm^{3}min^{-1} was therefore selected for further
research, in order to acheive a high sample throughput while
maintaining good sensitivities. Similar responses to variations
in flow rate were obtained at all of the metallopolymer-modified
electrodes for the surface coverages of ruthenium investigated.

3.3.3.3.   Effect of Film Thickness

The thickness of the metallopolymer films could be routinely
varied by variations in either the metallopolymer concentration
in the solutions used for the coating procedures, or by
variations in the volume of the metallopolymer solutions applied
to the electrode surface. Film thickness was estimated from a
knowledge of the metallopolymer dry densities (as described in
Chapter 2), and from the calculated surface coverage of
ruthenium on the electrode surface (see section 2.1.). However,
the film thickness, or surface coverages, for these
metallopolymers was found to be difficult to control and
reproduce, due, in part, to the photochemical instability of
these metallopolymers, as discussed in Chapter 2, and also due
to difficulties in reproducing the exact amount of
metallopolymer applied to the electrode surface. The trends

141

observed for a single metallopolymer with varying film
thickness, however, is still assumed to be valid. Further
difficulties occurred (vide infra) when attempting to compare
responses for the different metallopolymer films of the same
thickness, possibly because of slight variations in the
concentrations of the metallopolymer solutions prior to
drop-coating on the electrode surface.

The ratio of the current response at the modified electrode
(i_m) to that at the bare electrode (i_b), for the injection
of 1 µg cm^{-3} levels of nitrite was plotted as a function of
ruthenium surface coverage for the Ru-PVP$_{100}$ films and is
shown in Figure 3.14. The responses at both the bare and
modified electrodes were obtained from a dual electrode cell
configuration, in the parallel mode of operation, in order to
minimise variations that could be observed with varying
electrode surfaces and, possibly, variations in the
concentration of the samples injected with time [41]. It can be
seen from Figure 3.14 that large variations in response ratios
were obtained for different surface coverages. The results from
this study would seem to reflect those of the RDE results for
mediation in these metallopolymers. At the thicker films
(surface coverages of greater than approximately 8 x 10^{-9} mol
cm^{-2}), no enhancement in the response at the modified
electrode was obtained compared to that observed at the bare
electrode, probably because of a decreased partitioning of the
substrate within the film, thus leading to a surface reaction at
the film/electrolyte interface. The response ratio increased
upon decreasing the surface coverage possibly because of
increased partitioning of the substrate, thus leading to three
dimensional catalysis within the layer, with a maximum response
ratio being obtained for films of surface coverages of
approximately 1 x 10^{-9} mol cm^{-2}. This surface coverage most
likely represents the Lk case for the mediating reaction, as
described in the previous section, and therefore total
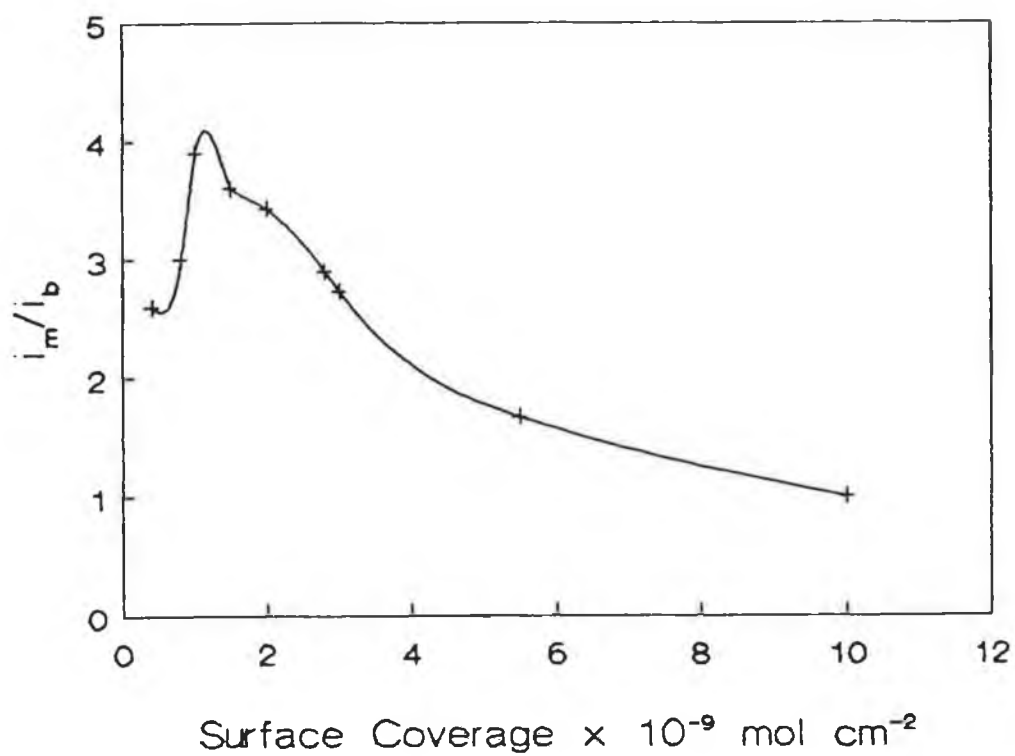catalysis, where the mediating reaction takes place throughout

142

Figure 3.14: The effect of variations in the surface coverage of the Ru-PVP$_{100}$ metallopolymer films on the ratio of the current response at the modified electrode (i_m) to that observed at the bare electrode (i_b) for injections of 1 µg cm^{-3} levels of nitrite to the flowing solutions. Other conditions as in Figure 3.13.

the entire film. The response ratio subsequently decreased with a further decrease in surface coverage, possibly because of the reduction in the total redox sites available for catalysis. Interestingly, the surface coverage observed for the Lk case in the flow cell configuration ($\sim$1 x 10^{-9} mol cm^{-2}) is considerably thinner than that observed in the RDE experiments ($\sim$8 x 10^{-9} mol cm^{-2}). This can be attributed to the different modes of mass transport that operate for the two experimental techniques and to the shorter residence times of the substrate in the flow injection manifold. From Figure 3.14, it can be seen that the optimum surface coverage for the Ru-PVP$_{100}$ metallopolymers was approximately 8 x 10^{-10} - 2 x 10^{-9} mol cm^{-2} of ruthenium, corresponding to approximate film thicknesses of 10 - 20 nm.

3.3.3.4. Effect of Polymeric Backbone Composition

The effect of the polymeric backbone composition on the FIA response to nitrite was investigated for the metallopolymers described in Chapter 2, and is presented in Figure 3.15. The errors associated with the values for the i_m/i_b factor at these metallopolymer films can be attributed to the difficulties in obtaining, reproducibly, the same surface coverages of ruthenium for the different metallopolymers. A surface coverage of approximately 2.0 x 10^{-9} mol cm^{-2} was selected for this investigation, in order to yield high catalytic (i_m/i_b) ratios. However, this can lead to further errors associated with the responses, as quite large differences in response ratios could be observed for only slight variations in surface coverages (see Figure 3.14). Taking the errors involved into account, it appears that no apparent differences exist in the magnitude of the response ratio for all of the metallopolymer films at this film thickness. Indeed, the response ratios obtained at the various metallopolymer films, for films of similar thicknesses, were very similar. This is contrary to what
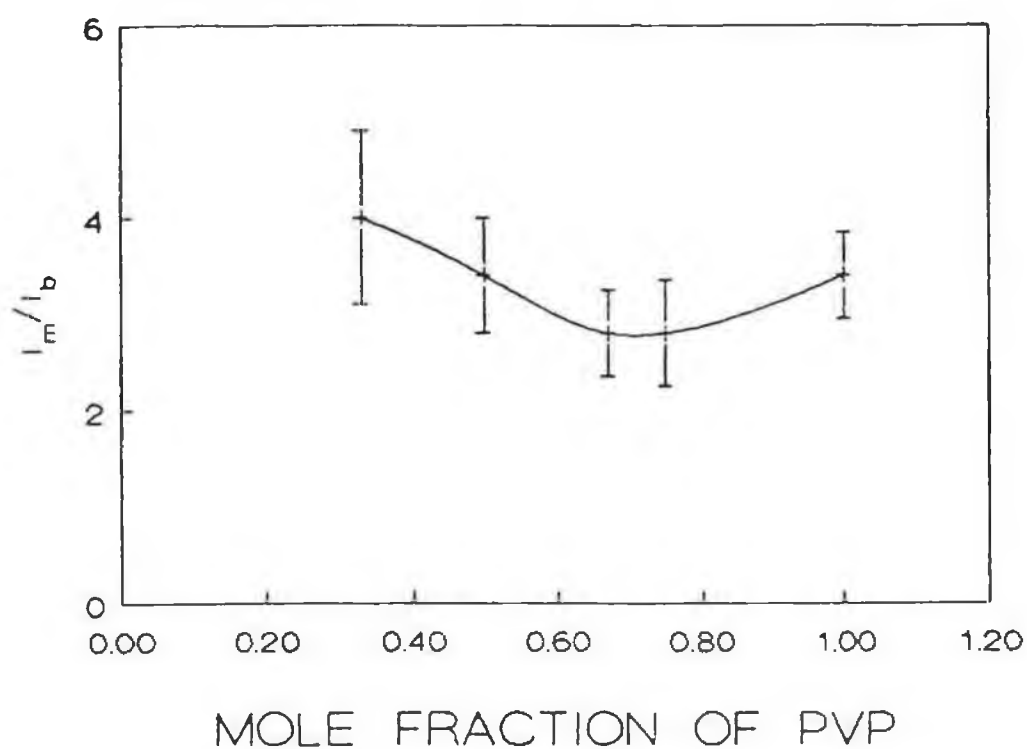
144

Figure 3.15: The effect of the composition of the polymeric backbone on the ratio of the current observed at the modified electrode to that observed at the bare unmodified electrode for repeated injections of 1 μg cm^{-3} levels of nitrite to the flow injection cell. Surface coverages of ruthenium were approximately 2.0 ± 0.5 x 10^{-9} mol cm^{-2} for all of the metallopolymer films. Other conditions as in Figure 3.13.

145

would be expected. Decreased permeation of the solvated nitrite ion into the styrene-containing polymer films would be expected, because of the increased hydrophobicity, and thus increased compaction of these films, thus leading to a decrease in the response ratio of the modified current to the bare electrode current. This trend was not observed, possibly because of the reported ion-coupling of the background electrolyte ion, i.e. the nitrate ion, with the protonated pyridine sites within the films [42]. This factor could lead to films with similar permeabilities to the nitrite ion because of a "trade-off" between compaction due to ion coupling, which would predominate for the high PVP content polymers, and film compaction due to styrene incorporation in the polymeric backbone. From Figure 3.15, it seems that the incorporation of styrene into the polymeric backbone does not result in a decreased sensitivity to the electrocatalytic oxidation of the nitrite ion at these modified electrodes in $NaNO_3$ background electrolyte. The styrene-containing metallopolymer films do, however, yield more stable films on the glassy carbon electrode surface in the flow-injection mode. This increased stability is demonstrated from a comparison of Figure 3.16, where the response ratio observed at the Ru-PVP$_{100}$ modified electrode with time is shown, and Figure 3.17, where the response ratio at the Ru-PVP$_{33}$ modified electrode with time is shown, for the detection of repeated injections of 1 µg cm^{-3} nitrite. The trend in the response ratio with time observed for the Ru-PVP$_{100}$ homopolymer reflects the trend seen for variations with surface coverages, with an initial increase in the response ratio, followed by a gradual decrease with time. This can be attributed to the slow stripping of the metallopolymer film from the electrode surface, with the initial increase due to increased mediation within the thinner films, followed by a decrease in response ratio because of the further decrease in available mediating sites. The practical application of these films, as mentioned previously [41], will therefore be limited
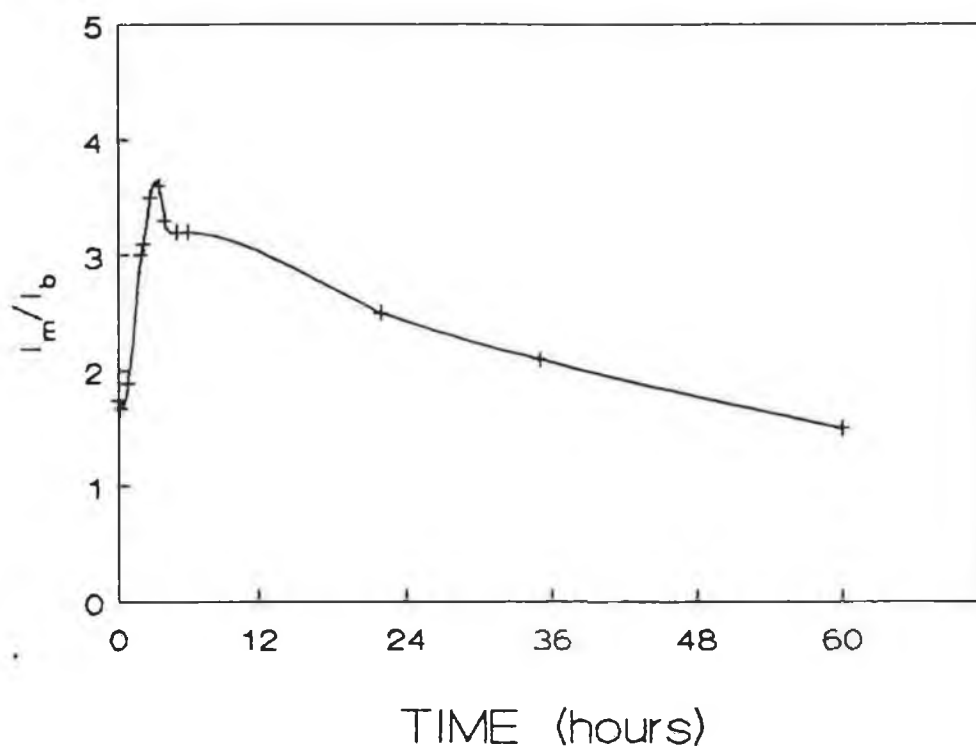
146

Figure 3.16: Variation of the ratio of the current response at the Ru-PVP$_{100}$ modified to the unmodified electrode with time for the repeated injection of 1 µg cm^{-3} levels of nitrite. Other conditions as in Figure 3.13.

Figure 3.17: Variation of the ratio of the current response at
the Ru-PVP$_{33}$ modified to the unmodified electrode with time
for the repeated injection of 1 µg cm^{-3} levels of nitrite.
Other conditions as in Figure 3.13.

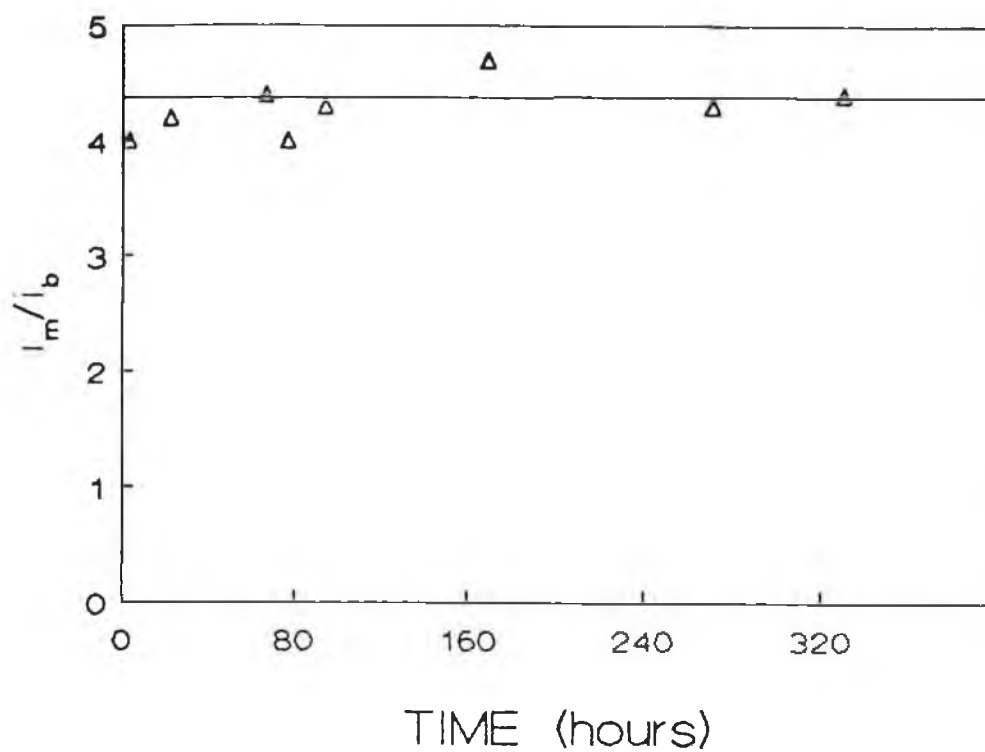because of the variability of the response with time. The data presented in Figure 3.17, however, for the response with time at the Ru-PVP$_{33}$ modified electrode, indicates the good stability obtained for these metallopolymer films upon incorporation of styrene into the polymeric backbone. The response observed at this modified electrode did not decrease significantly over the time period examined (13 days), with a 1.0% relative standard deviation obtained for the response ratio for this period.

The short term reproduciblity obtained at the modified electrodes is demonstrated in Figure 3.18. A mean current of 200 nA was obtained for the 50 injections of 1 μg cm^{-3} nitrite over a 20 min time period shown at the Ru-PVP$_{50}$-modified electrode, with a relative standard deviation of less than 1.0% calculated for these injections. The other metallopolymer films showed similar short term reproducibility. The response at the Ru-PVP$_{50}$-modified electrode in Figure 3.18 was linear with concentration in the 0 – 100 μg cm^{-3} range investigated, yielding a detection limit of 5 ng cm^{-3} (5.0 x 10^{-8} M, signal-to-noise ratio of 3). This represents a significant improvement compared to the detection limit observed at the unmodified electrode surface, and also compared to that observed at the modified electrode surface developed, for the detection of nitrite, by Cox and Kulesza [39].

The modified electrode surface also significantly inhibited the passivation of the underlying electrode surface by the SCN$^-$ ion. Repeated alternate injections of 1 μg cm^{-3} levels of both nitrite and SCN$^-$ at the bare electrode (not shown) resulted in a gradual decrease in the nitrite peak height at the bare electrode surface, whereas no decrease was observed for the nitrite peak obtained at the modified electrodes.

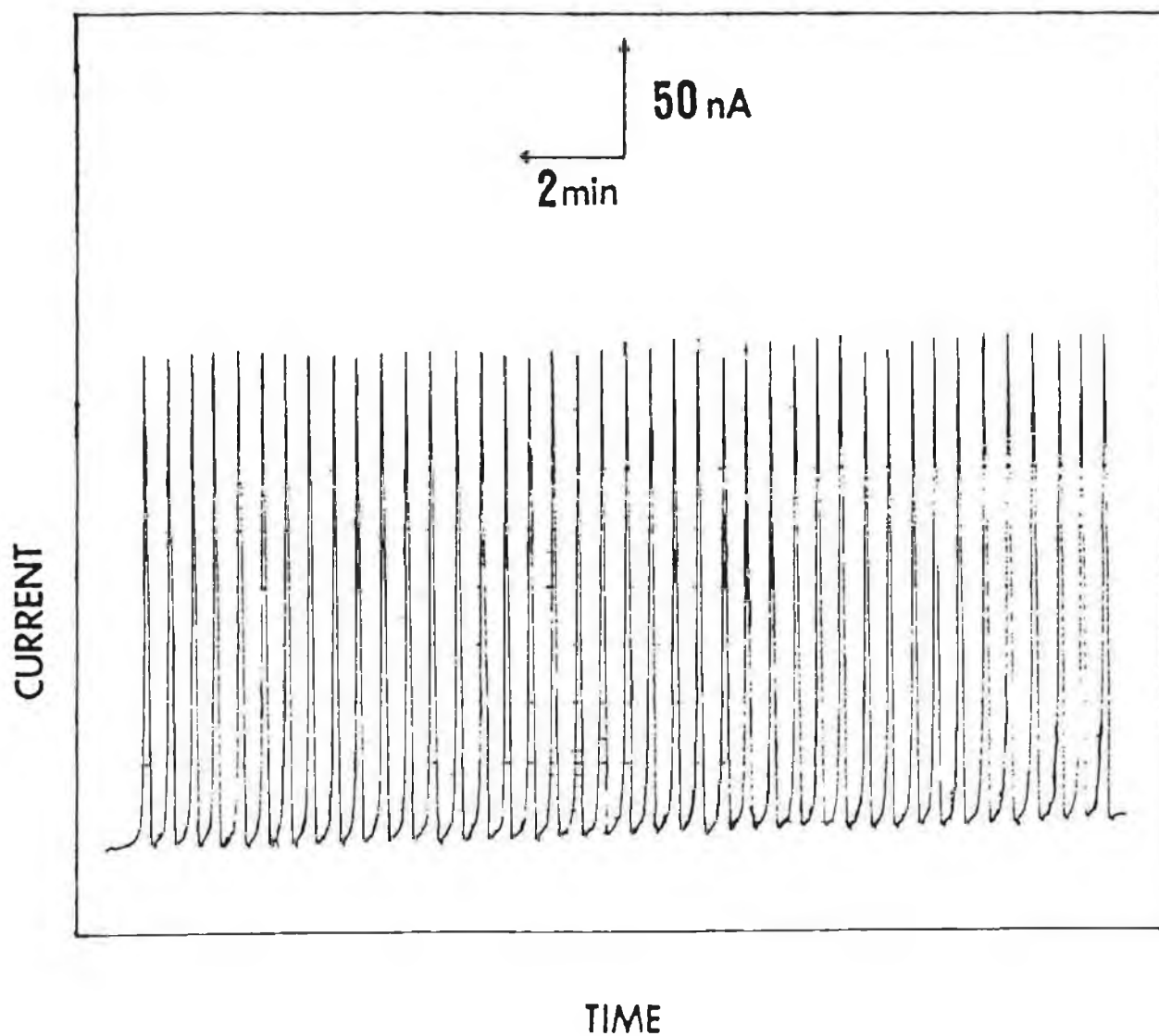Figure 3.18: Short-term reproducibility of 50 injections of 1 µg cm^{-3} nitrite over a 20 min time period at the Ru-PVP$_{50}$-modified electrode. Surface coverage of ruthenium of 3 x 10^{-9} mol cm^{-2}. Other conditions as in Figure 3.13.

3.3.3.5. The Determination of Nitrite Levels in Saliva and Meat Samples

The application of the $Ru-PVP_{33}$ metallopolymer-modified electrode to the determination of nitrite levels in saliva and cured meat samples was then investigated. The amperometric detection of nitrite in flowing solutions at the modifed electrode yielded values similar to those determined by a standard uv-vis spectrophotometric method [27] for the determination of nitrite, when utilised for five different determinations of the one sample. Average nitrite levels of 82 ± 6 µg cm^{-3} for the meat sample and 4.8 ± 0.8 µg cm^{-3} for the saliva samples were obtained. A slope of 0.94 was obtained for the correlation between the two techniques, with a correlation coefficient of 0.991. Furthermore, passivation of the electrode by other matrix components was prevented at the modified electrode surface. The nitrite levels found in the saliva samples were within the range previously reported for human saliva [43].

3.4. CONCLUSIONS

The rotating disk electrode was utilised to investigate the kinetics and mechanism of the mediation reaction of nitrite at the ruthenium metallopolymer-modified electrodes in both $NaNO_3$ and $HClO_4$ electrolytes for the different metallopolymers with varying styrene content in the polymeric backbone. No mediation currents were observed in the $HClO_4$ electrolyte, which correlated well with the results and opinions expressed in Chapter 2 as to the nature of the polymeric film in this electrolyte. The mediation reaction in $NaNO_3$ electrolyte was shown to be of the Lk type case for surface coverages of ruthenium less than approximately 8×10^{-9} mol cm^{-2}, while a surface LSk reaction mechanism was found for thicker ($> 2 \times 10^{-8}$ mol cm^{-2}) films.

The analytical application of the modified electrodes was investigated using constant-potential detection coupled to flow-injection analysis techniques. The flow-injection peak current at the modified electrodes was optimised with respect to applied potential, flow rate and film thickness. No significant trends were observed for the response at the modified electrodes with changing styrene content in the polymeric backbone. Considerably improved stability was, however, demonstrated for the Ru-PVP$_{33}$ metallopolymer film in comparison to the stability of the Ru-PVP$_{100}$ metallopolymer films in flowing streams. This represents a significant achievement for the area of modified electrodes, in that enhanced stabilities in flowing streams could be obtained via the copolymerisation of the PVP backbone with styrene, while maintaining the electrocatalytic activity of the resulting styrene-containing metallopolymers in comparison to that of the PVP homopolymer. The stable Ru-PVP$_{33}$ metallopolymer film was utilised for the determination of nitrite levels in saliva and cured meat samples, with good correlation being obtained between the amperometric detection of nitrite at the modified electrode

and a standard uv-visible spectrophotometric method for the determination of nitrite. The prevention of the passivation of the underlying bare electrode surface by the SCN^- ion, and by components in the matrix of the selected samples of meat and saliva, was also achieved.

In conclusion, electrodes modified with films of a ruthenium redox centre bound to copolymers of 4-vinylpyridine and styrene have been shown to be both sensitive and stable for the determination of nitrite in flowing solutions, offering a substantial decrease in overpotential for the oxidation of nitrite, with no decrease in the mediating capabilities of the metallopolymers upon incorporation of styrene into the polymeric backbone.

3.5. REFERENCES

1.   T. Komori and T. Nonaka, <u>J. Am. Chem. Soc.</u>, (1984), <u>106</u>, 2656.

2.   D.A. Buttry and F.C. Anson, <u>J. Am. Chem. Soc.</u>, (1983), <u>105</u>, 5690.

3.   K. Itaya, H. Akahoshi and S. Toshima, <u>J. Electrochem. Soc.</u>, (1982), <u>129</u>, 762.

4.   H.D. Abruna, <u>Coord. Chem. Rev.</u>, (1988), <u>86</u>, 135.

5.   W.J. Albery and A.R. Hillman, <u>R.S.C. Annual Report</u>, (1981), <u>78</u>, 377.

6.   F.C. Anson, J.M. Saveant and K. Shigehara, <u>J. Phys. Chem.</u>, (1983), <u>87</u>, 214.

7.   J. Leddy, A.J. Bard, J.T. Maloy and J.M. Saveant, <u>J. Electroanal. Chem.</u>, (1985), <u>187</u>, 205.

8.   K. Shigehara, N. Oyama and F.C. Anson, <u>J. Am. Chem. Soc.</u>, (1981), <u>103</u>, 2552.

9.   J.M. Saveant and K.B. Su, <u>J. Electroanal. Chem.</u>, (1984), <u>171</u>, 341.

10.   C.P. Andrieux, C. Blocman, J.M. Dumas-Bouchiat, F. M'Halla and J.M. Saveant, <u>J. Electroanal. Chem.</u>, (1980), <u>113</u>, 19.

11.   C.P. Andrieux, J.M. Dumas-Bouchiat and J.M. Saveant, <u>J. Electroanal. Chem.</u>, (1982), <u>131</u>, 1.

12.   W.J. Albery, A.W. Foulds, K.J. Hall and A.R. Hillman, <u>J. Electrochem. Soc.</u>, (1980), <u>127</u>, 654.

13.   W.J. Albery and A.R. Hillman, <u>J. Electroanal. Chem.</u>, (1984), <u>170</u>, 27.

14.   W.J. Albery, W.R. Bowen, F.S. Fisher, A.W. Foulds, K.J. Hall, A.R. Hillman, R.G. Edgell and A.F. Orchard, <u>J. Electroanal. Chem.</u>, (1980), <u>107</u>, 37.

15.   C.P. Andrieux and J.M. Saveant, <u>J. Electroanal. Chem.</u>, (1978), <u>93</u>, 163.

16.   C.P. Andrieux, J.M. Dumas-Bouchiat and J.M. Saveant, <u>J. Electroanal. Chem.</u>, (1984), <u>169</u>, 9.

17. C.P. Andrieux and J.M. Saveant, J. Electroanal. Chem., (1984) 171, 65.

18. C.P. Andrieux and J.M. Saveant, J. Electroanal. Chem., (1983), 142, 1.

19. C.P. Andrieux and J.M. Saveant, J. Electroanal. Chem., (1982), 134, 163.

20. K. Aoki, K. Tokuda and H. Matsuda, J. Electroanal. Chem., (1986) 199, 69.

21. F.C. Anson, J. Phys. Chem., (1980), 84, 3336.

22. V.G. Levich, Physicochemical Hydrodynamics, Prentice-Hall, Englewood Cliffs, New York, (1962).

23. T. Ikeda, C.R. Leidner and R.W. Murray, J. Electroanal. Chem., (1982), 138, 343.

24. T. Ik, R. Schmehl, P. Denisevich, K. Willman and R.W. Murray, J. Am. Chem. Soc., (1982), 104, 2683.

25. Y. Ohnuki, H. Matsuda, T. Ohsaka and N. Oyama, J. Electroanal. Chem., (1983), 158, 55.

26. F.C. Anson, J.M. Saveant and K. Shigehara, J. Electroanal. Chem., (1983), 145, 423.

27. W. Horowitz, Official Methods of Analysis of the Association of Official Analytical Chemists, AOAC, Washington D.C., (1980), 381.

28. G. Milazzo and S. Caroli, Tables of Standard Electrode Potentials, Wiley, New York (1978), 191.

29. A.J. Kelly, T. Ohsaka, N. Oyama, R.J. Forster and J.G. Vos, J. Electroanal. Chem., (1990), 287, 185.

30. R.J. Forster, A.J. Kelly, J.G. Vos and M.E.G. Lyons, J. Electroanal. Chem., (1989), 270, 365.

31. R.J. Forster, M.E.G. Lyons and J.G. Vos, J. Chem. Soc., Faraday Trans 1, submitted.

32. A. Chaube, A.K. Baveja and V.K. Gupta, Talanta, (1984), 1, 391.

33. S. Flamerez and W.A. Bashir, Analyst, (1985), 110, 1513.

34. S.K. Chang, R. Kozeniauskas and G.W. Harrington, Anal. Chem., (1977), 49, 2272.

155

35. C.M.G. Van den Berg and H. Li, <u>Anal. Chim. Acta,</u> (1988), <u>212,</u> 31.

36. Z. Gao, G. Wang and Z. Zhao, <u>Anal. Chim. Acta,</u> (1990), <u>230,</u> 105.

37. J.E. Newbery and M.P.L. de Haddad, <u>Analyst,</u> (1985), <u>110,</u> 81.

38. K. Ito, A. Ariyoshi, F. Tanabiki and H. Sunahara, <u>Anal. Chem.,</u> (1991), <u>63,</u> 273.

39. J.A. Cox and P.J. Kulesza, <u>J. Electroanal. Chem.,</u> (1984), <u>175,</u> 105.

40. K. Kalcher, <u>Talanta,</u> (1986), <u>33,</u> 489.

41. J.N. Barisci, G.G. Wallace, E.A. Wilke, M. Meaney, M.R. Smyth and J.G. Vos, <u>Electroanalysis,</u> (1989), <u>1,</u> 245.

42. P. Ferruti and R. Barbucci, <u>Adv. Polymer Sci.,</u> (1984), <u>58,</u> 55.

43. S.R. Tannenbaum, A.J. Sinskey, M. Weisman and W. Bishop, <u>J. Natl. Cancer Inst.,</u> (1974), <u>53,</u> 79.

CHAPTER 4

Ruthenium Dioxide-Modified Electrodes

for the Electrocatalytic Detection of

Hydroxylated Species

4.1. INTRODUCTION

At almost all catalytic modified electrodes, an immobilised reversible redox centre acts as a fast electron transfer mediator for a solution species, which is oxidised or reduced slowly or not at all at the underlying bare electrode surface. Despite the variety of reports in which redox polymer-coated electrodes have been exploited, the number of systems suitable for preparing stable electrode films remains relatively small. Furthermore, electrocatalysts as modifiers of electrode surfaces must be both highly reactive and capable of sustaining high rates of charge propagation within the coating. An appealing, but less explored, alternative is to consider inorganic matrices for creating microstructures on electrode surfaces, or within carbon paste electrodes. These inorganic modifiers may offer excellent stability, good conductivity, ease of preparation and specific reactivity.

Ruthenium dioxide (RuO_2) is of considerable interest as a corrosion-resistant material for electrocatalytic evolution of chlorine [1-4]. In the past two decades, the so-called dimensionally stable anodes (DSA) of RuO_2 and TiO_2 deposited on titanium substrates, developed by Beer in 1966-68 [5], have superseded carbon electrodes in the chlor-alkali industry. A significant decrease in the anodic oxygen overpotential has also been found for RuO_2 electrodes in comparison with other electrodes employed in today's electrometallurgic industries [6,7].

While most of the studies to date on this type of anode have been devoted to the chlorine evolution reaction, there has been some interest in extending its application to other areas such as electroorganic oxidations [8-11]. Relatively few studies have, as yet, appeared in the literature on the potential use of RuO_2-based electrodes for the electrocatalytic detection of various analytes [12,13].

In this chapter, the application of both carbon paste and

158

graphite-epoxy-modified ruthenium dioxide electrodes for the electrocatalytic oxidation and detection of selected analytes, such as simple alcohols and saccharide antibiotics, is described. Firstly, a review of the literature to date on the preparation procedures, surface morphology and electrochemical characteristics and reactions of RuO_2 anodes is presented. This review will illustrate the different characteristics observed for different anode preparations, and the various treatments of the electrochemical characteristics and reactions at these DSA electrodes.

4.1.1. Preparation and Morphology of RuO_2 Anodes

Research into the activity of RuO_2 electrodes towards oxygen and chlorine evolution has shown that the surface structure and method of preparation of the films influence the energetics and mechanisms of these reactions [14,15]. The techniques generally used have been established to achieve a highly conductive, low cost support onto which a layer of mechanically stable active material is deposited for industrial anodes. A number of methods can be used to grow oxides on different supports. The most frequently used method is the thermal decomposition at low temperature of suitable compounds. The basic method consists in dissolving the starting material, usually hydrated $RuCl_3$, in a suitable solvent or solution (isopropanol in most cases), spreading it on a support and firing at the selected temperature. The choice of firing temperature depends on the starting material and the nature of the support. Accordingly the oxide may present different features depending on the starting material. As a rule, the firing temperature must be high enough to ensure maximum decomposition of the reactant, but low enough so as to avoid excessive sintering and crystallisation of the final product. The thermogravimetric curve for the decomposition of $RuCl_3$ is shown in Figure 4.1. Decomposition can be seen to occur in
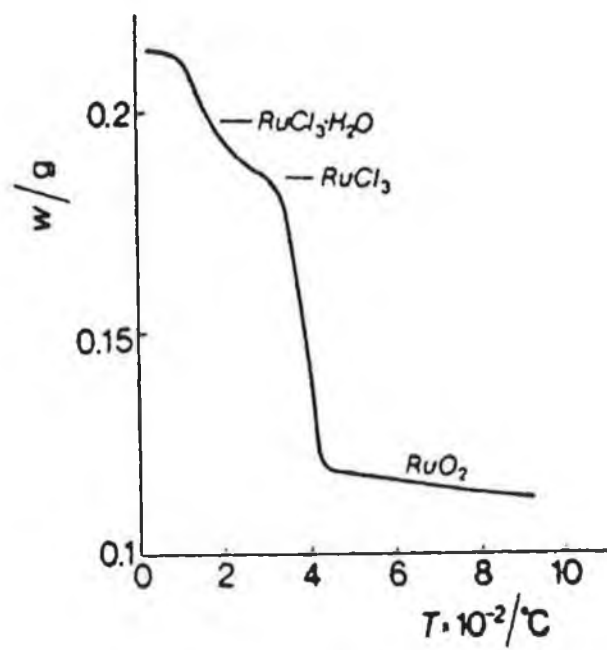
Figure 4.1: Thermogravimetric curve for the decomposition of
$RuCl_3.H_2O$. (From reference 1).

two steps. Water of hydration is lost first, then the salt decomposes to give the oxide [3]. Similar electrodes may also be prepared by chemical vapour transport techniques (CVT), which involves the deposition of RuO_2 from ruthenium metal and oxygen [3].

It is known that the decomposition temperature governs the crystallinity and crystal size of the layer. Several studies have shown that the support (usually titanium, tantalum or platinum) exerts little effect [3]. The possibility that some chloride remains in the lattice of RuO_2 prepared by thermal decomposition of $RuCl_3$ was first pointed out by Cotton and Hayfield [16] in 1971. This has since been confirmed by chemical analysis of powders [17] and films [3,18]. The chloride content of low temperature RuO_2 films depends on the firing temperature (with an increase in content occuring on decreasing temperature), on firing duration and on the decomposition atmosphere. The fact that the thickness of the layer has an effect in the sense that thinner films lose chloride more easily on annealing, suggests that the element probably remains trapped during decomposition.

The morphology of thermally prepared RuO_2 films depends on a number of factors: techniques of solution spreading on the support, solution concentration, film thickness, decomposition temperature and heating rate and atmosphere over the sample during firing. Solutions can be spread by brushing [3,6], immersion [6,18] or spraying [17,19]. The nature of the solvent has also some effect as non-aqueous solvents (usually isopropanol) spread out on the surface better than water, and evaporate at a lower temperature. It has been reported that final layers exhibit a cracked dried-mud look [17,21,22]. However, Lodi et al. [3,14,18] were able to prepare very compact layers by taking several precautions, such as spreading of the solution by immersion, preheating of the sample at 120°C, and gentle mechanical polishing of each layer after firing at a low heating rate. Typical electron micrographs of cracked and

161

smooth layers of RuO_2 are shown in Figure 4.2. It has been
suggested that parameters such as chloride content,
crystallinity, crystallite size, surface area and morphology are
all interdependent [3]. As the chloride content decreases, more
oxide is formed, with the possibility of improved crystal growth
and thus generation of lower specific surface area electrodes.

An alternative method of preparation of RuO_2 electrodes
are the hydrous oxide films grown by potential cycling of
ruthenium metal electrodes or ruthenised platinum electrodes
[22-25], which exhibit voltammograms similar to those recorded
for thermally prepared RuO_2 electrodes. Films formed by
cycling were found to have a smooth shiny appearance with an
underlying columnar structure, although films formed by
oxidation at a constant current were found to be more amorphous,
with higher O/Ru ratios. It should be noted that all of the
above electrode preparations are allegedly of nonstoichiometric
RuO_2, due to the presence of residual chloride in the layers.
Teflon-bonded RuO_2 electrodes on both glassy carbon and
platinum have also been prepared for use in electroorganic
reactions [10,26], although no details are available on the
surface structure or film morphology of these layers.

Stoichiometric single crystal RuO_2 electrodes have been
prepared from ruthenium powder and O_2 by the CVT method, and
have been used to examine chlorine evolution and hydrogen
adsorption reactions [27,28].

162

a
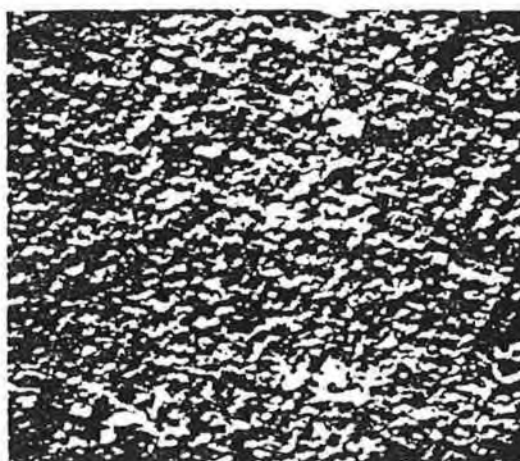
b

Figure 4.2: Morphology of RuO$_2$ films. (a) firing temperature of 450°C; silica glass support; x250 magnification. (b) firing temperature of 350°C; silica glass support; x300 magnification. Sample treatment for the films depicted in (b) involved spreading of solution by immersion, preheating the layers at 120°C and gentle mechanical polishing of each layer after firing. (From reference 1).

4.1.2. Electrical Characteristics

Although RuO_2 single crystals exhibit metallic behaviour, with a conductivity of approximately $2.5 \times 10^4 \Omega^{-1} cm^{-1}$, the nature of conduction in RuO_2 films has been under discussion [3,8,17]. Conductivity measurements with low temperature RuO_2 in the form of pressed pellets were first conducted by Pizzini et al. [17]. Results showed a conductivity about three orders of magnitude lower than that of single crystals. However, these results, pointing to semiconducting properties of RuO_2, have been disproved by measurements on compact films as opposed to pressed pellets or cracked layers, with these films exhibiting resistivity values and temperature coefficients of resistivity similar to those of single crystals [29]. Also Trasatti et al. have investigated the kinetics of electron transfer reactions at RuO_2 films deposited on tantalum and platinum supports, and reported reversible behaviour for the iron hexaquo redox system [30].

4.1.3. Electrochemical Properties

The current/potential curve obtained using cyclic voltammetry (CV) is apparently the best criterion to characterise RuO_2 electrodes. The most comprehensive treatment, in basic solutions, where the higher oxidation states of ruthenium exist, has been published by Lam et al. [31]. These workers investigated the redox reactions of both ruthenate (RuO_4^{2-}) solutions at a platinum working electrode, and RuO_2 electrodes prepared by the thermal decomposition method, in NaOH. Four pairs of peaks were observed and the composite diagram drawn from different cyclic voltammograms of ruthenate is depicted in Figure 4.3. The oxidation states of the electrolysis products were evaluated by coulometry and absorption spectra, and the redox reactions have been assigned as follows:
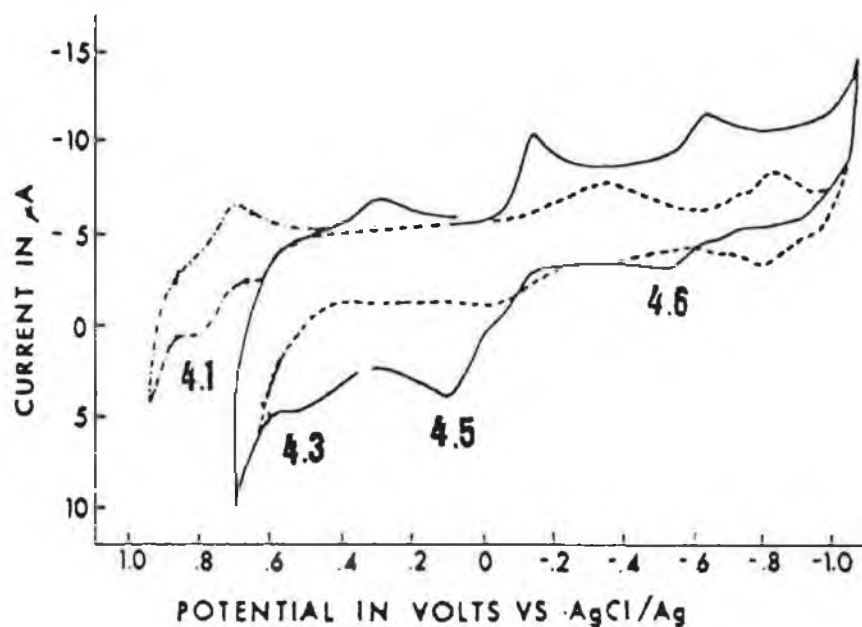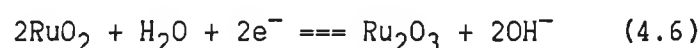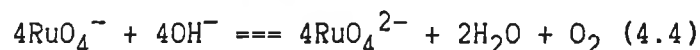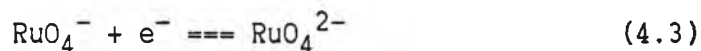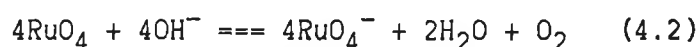
164

Figure 4.3: Composite diagram drawn from cyclic voltammograms of ruthenate. Scan rate was 50 mV s^{-1}; (_____) ruthenate concentration of 0.256 mM in 2 M NaOH; (------) blank, 2 M NaOH; (_._._._) ruthenate concentration of 0.256 mM in 8.5 mM NaOH. The numbers at the anodic peaks represent the reactions shown on the next page. (From reference 31).

$$RuO_4 + e^- === RuO_4^- \qquad (4.1)$$

$$4RuO_4 + 4OH^- === 4RuO_4^- + 2H_2O + O_2 \qquad (4.2)$$

$$RuO_4^- + e^- === RuO_4^{2-} \qquad (4.3)$$

$$4RuO_4^- + 4OH^- === 4RuO_4^{2-} + 2H_2O + O_2 \qquad (4.4)$$

$$RuO_4^{2-} + 2H_2O + 2e^- === RuO_2 + 4OH^- \qquad (4.5)$$

$$2RuO_2 + H_2O + 2e^- === Ru_2O_3 + 2OH^- \qquad (4.6)$$

Sullivan et al. [18,10] and Burke et al. [9,22,32] have also investigated reactions in basic solutions at thermally prepared RuO_2 and RuO_2/TiO_2 electrodes, and at electrochemically grown hydrous oxide RuO_2 electrodes on ruthenium metal, and have confirmed the assignments of Lam et al. [31]. The voltammogram obtained for RuO_2 anodes in acidic solution is shown in Figure 4.4, where indications of two reasonably reversible pairs of peaks are seen. These are postulated as being the redox reactions relating to equations (4.5) and (4.6) above. Similar wave shapes were observed by other workers for thermally prepared RuO_2/TiO_2 and $RuO_2/SnO_2/TiO_2$ and electrochemically grown films [11,19,20,23,33].

There has been some considerable discussion regarding the extent of the contribution of bulk redox processes, with associated proton diffusion, for example along grain boundaries, to the non-faradaic currents observed in voltammograms of RuO_2 electrodes. Burke et al. [34,35] have generally maintained that the voltammetric charge is due to surface processes only, on the basis of detailed BET surface area and electrochemical analysis, and have suggested that the redox transitions above may occur over a range of potentials, thus causing the large background currents [9]. Cyclic voltammetry was also proposed as a technique for estimating the real surface area of the RuO_2
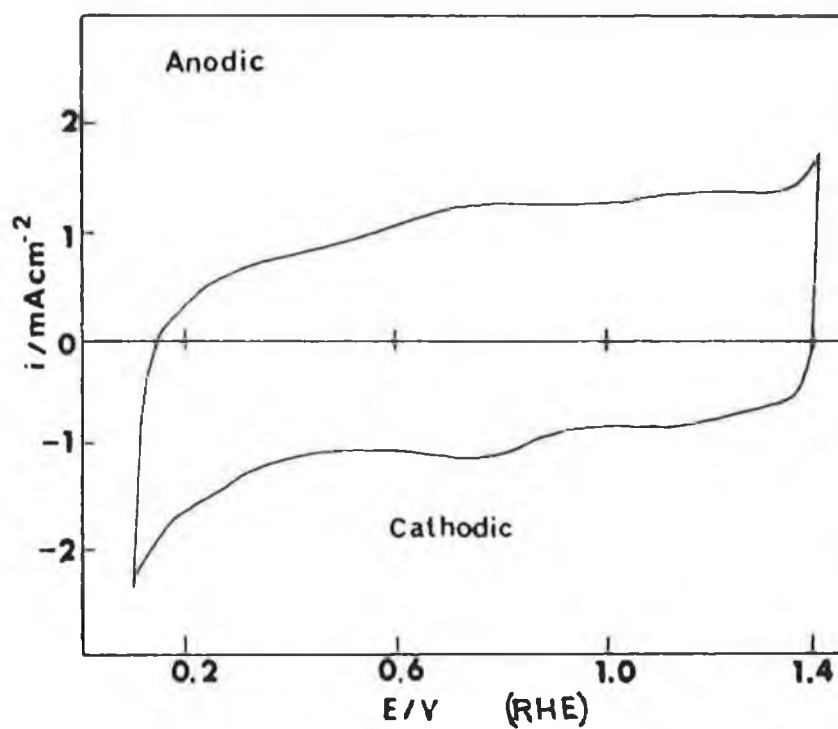
166

Figure 4.4: Cyclic voltamogram recorded under continuous
potential cycling conditions for a ruthenised platinum electrode
in 0.5 M H_2SO_4. Scan rate of 50 mVs^{-1}. (From reference
23).

electrode on the basis of BET surface area and CV charge correlation studies [35,36]. However, it has been maintained that not all surface ruthenium species participate in the redox processes [9]. It has been estimated that the ruthenium species that react according to equation (4.2) correspond to only about 12% of the number of apparent surface species [9,35]. In general, however, the electrochemical studies of ruthenium species on platinum by Lam et al. [31] support the assignments of Burke et al. and Doblhofer et al. [19] for the oxidation state changes of ruthenium on thermally prepared RuO_2 surfaces. The discrepancies between the results of various groups may be due to the variability in preparation from laboratory to laboratory, and the absence of a sharp cut-off point between the internal surface and bulk electrode material, or grain boundary and defect regions [8]. The direct correlation of BET surface area with voltammetric charge [35,36] is attractive and simple. However, there may still be uncertainties in this approach; for example sweep rate dependence or preparation method. Furthermore, there may be charge associated with electrochemical reactions occurring in regions of the RuO_2 layers not accessed in gas adsorption experiments [8]. There will probably continue to be more discussion on this topic in the literature.

A rest potential of 0.95V (vs. RHE) has been reported for RuO_2 films with a pH dependence of 59 mV pH^{-1} [37]. Safonova et al. [38] observed that the electrode potential at constant total surface charge showed a pH dependence of 59 mV pH^{-1} in the range 0.3-0.9 V (vs. RHE). Burke et al. [9,32], on the other hand, have reported that the voltammetric peak potentials for RuO_2 at 0.5 V and 1.1 V (vs. RHE) in 1.0 M NaOH, which correspond to reactions (4.6) and (4.5) above respectively, exhibit a pH dependence of 75 mV pH^{-1} rather than the Nernstian 59 mV value. Burke and Healy [32] used the electrooxidation of benzaldehyde as a probe reaction in studying the pH dependence of the voltammetric peak corresponding to

equation (4.5) (Figure 4.5). The oxidation of benzaldehyde coincides with the Ru(IV)/Ru(VI) transition. The authors suggested that surface oxycomplexes may be formed such that equation (4.5) may best be written in the form

$$RuO_2(OH)_{2.5}^{0.5-} + 2e^- === RuO_2 + 2.5OH^- \qquad (4.7)$$

The species on the left of equation (4.7), though speculative, may be part of a polymeric or interlinked system of otherwise anhydrous RuO_2 [32]. A somewhat greater pH dependence of 88 mV pH^{-1} has been observed for redox transitions in the case of hydrous, electrochemically grown oxide films [39,40]. The discrepancies between the different groups working in this area are difficult to rationalise, especially since different experimental approaches were employed by the different groups. It seems that the pH-dependence of the electrode potential of the RuO_2 films is likely to remain a topic of discussion for some time.
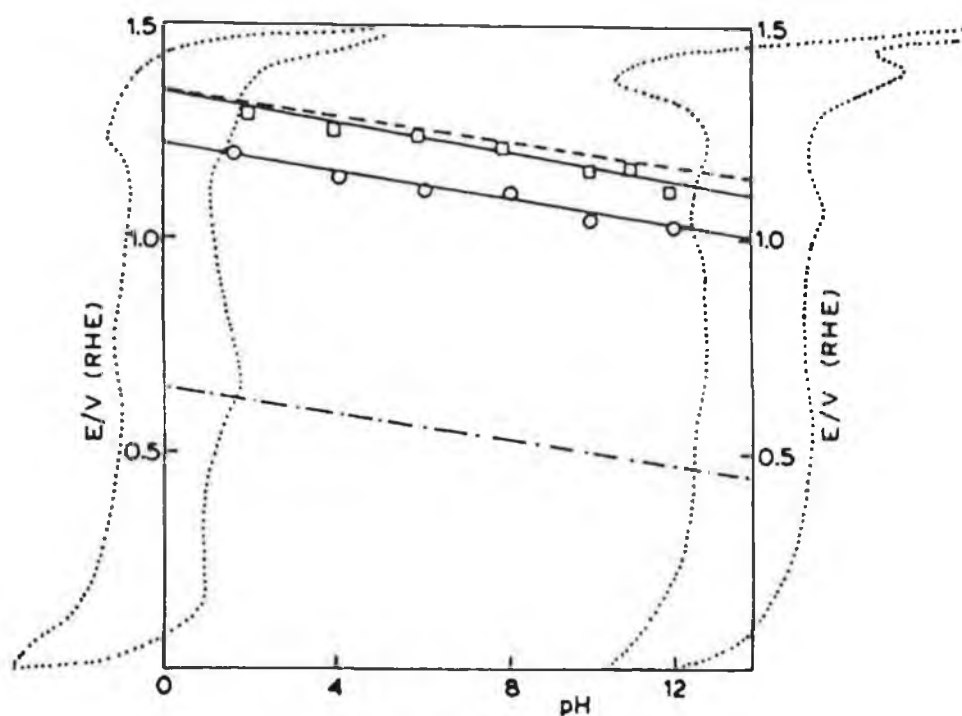
Figure 4.5: Effect of solution pH on the behaviour of an
RuO$_2$-aqueous solution interface. (_._._), RuO$_2$/TiO$_2$ film.
The upper lines are for the Ru(IV)/Ru(VI) transition as obtained
from voltammograms for pure RuO$_2$ (on Ti) in a range of borate
(pH > 8) and phthalate (pH < 8) buffer solutions.: o and □ refer
to the cathodic and anodic peak maxima, respectively. (----):
Variation of the half-wave potential for benzaldehyde oxidation
(0.1 M, scan rate of 1.5 mV s^{-1}) on pure RuO$_2$ in buffered
10% t-butanol in water mixtures. (From reference 32).

4.1.4. Oxygen Evolution

RuO_2 exhibits a very good electrocatalytic activity for O_2 gas evolution in both acid and base. Oxygen evolution on RuO_2 and RuO_2/TiO_2 mixed oxide electrodes is characterised by a relatively low Tafel slope (40 mV decade^{-1}) at low current densities. The method of preparation of the RuO_2 influences the current density for oxygen evolution, with the current density decreasing with increasing firing temperature [41]. This is readily explained in terms of a surface area effect. As discussed above, the surface area of the films and the voltammetric charge decrease with increasing firing temperature. Oxygen evolution current densities (geometric area) increase with oxide loading. However, a log of current density vs. potential plot of oxygen evolution for different RuO_2 loadings [8] shows that the current densities estimated using BET surface areas are essentially independent of the weight of RuO_2. Another complication is that Lodi et al. [7] have suggested that effects such as degree of compactness, or the defect nature of the RuO_2 films, can influence electrochemical parameters, including the Tafel slope for oxygen evolution. The mechanism of O_2 evolution at RuO_2 electrodes is a complicated area and will not be discussed here. Excellent reviews of the various theories and proposals have appeared over the years [8,15,42].

RuO_2 single crystals have been subjected to a limited amount of electrochemical investigation to date [27,28,43]. Hepel et al. [27] observed significant differences in electrochemical behaviour for the hydrogen absorption region for various single crystal faces and a correlation was found between the hydrogen absorption/desorption regions of the cyclic voltammograms and the composition and structure of the idealised surface of the rutile structure of RuO_2. Shafer et al. [43] observed that the Tafel slope for O_2 evolution in acid was, for the most part, independent of the crystal face. The Tafel

slope for oxygen evolution was higher, approximately 80 mV decade^{-1}, for all the faces studied, than that which is usually reported for the thermally prepared RuO_2 films.

4.1.5. Chlorine Evolution

The chlorine-chloride reaction, shown in equation (4.8), is fairly reversible

$$Cl_2 + 2e^- === 2Cl^- \qquad (4.8)$$

with a standard potential of 1.358 V (vs. RHE). Although the thermodynamic potential for the oxygen electrode reaction (1.229 V (vs. RHE)) is lower than that of the chlorine electrode, in practice the kinetics of the chlorine electrode reactions are substantially faster than those of the oxygen electrode reactions [8]. Thus chlorine tends to evolve preferentially in the electrolysis of aqueous Cl^--containing solutions. Since the chlorine evolution reaction usually exhibits a lower Tafel slope than the oxygen evolution reaction, quite high efficiences of Cl_2 evolution are observed at high current densities in relatively concentrated chloride solutions [8].

Thermally prepared, mixed oxide DSA, containing RuO_2 as the catalytically active component, have been employed with considerable success in chlor-alkali cells [44]. Despite its success in anodes for chlorine evolution, RuO_2 is an appreciably poorer catalyst than platinum [45]. However, it is well established that Pt electrodes exhibit passivation phenomena at moderately high current densities [46]. Furthermore, noble metal catalysts are known to degrade due to contact with Hg in amalgam cells [47]. Thus RuO_2-based anodes are good catalysts for practical Cl_2 evolution cells.

Owing to the success of RuO_2-based DSA in the chlor-alkali industry, a significant amount of study has been carried out on the kinetics and mechanism of chlorine evolution at these

172

electrodes over the past 15 years or so. A considerable body of experimental data has therefore been accumulated regarding the chlorine evolution reaction at RuO_2 anodes. However, despite the amount of research that has been conducted, it seems premature to state that the kinetics and mechanism of this reaction are understood. There is considerable disagreement between the results of the various workers in the field. A detailed review and discussion of the entire body of literature will not be attempted here. There are several relatively recent articles available which deal with this subject [1-4,8,15]. A few general observations regarding the reported results for the chlorine evolution at RuO_2 electrodes will be made in the following section.

Chlorine is evolved in practical chlor-alkali cells at about pH 2-3 and with NaCl concentrations of approximately 5 M [8], and many authors have employed such electrolytes in studies of chlorine evolution. Most authors quote Tafel slopes of 30-40 mV decade^{-1} for chlorine evolution at RuO_2 electrodes [14,48-50]. However, the Tafel slope has been reported by other authors to vary from as low as 20 mV decade^{-1} [51] to even as high as 108 mV decade^{-1} [52]. As has been pointed out by Yorodetskii et al. [53], and in several recent reviews [3,8,15], the Tafel slope obtained in concentrated chloride solutions is sometimes less than 2.3RT/2F. This theoretical value represents the lowest possible slope which can be obtained under conditions where the electrode reaction is limited by an electrochemical or subsequent diffusion step. Losev [54] has confirmed that anomalously low Tafel slopes can arise in fast electrochemical gas evolution reactions due to rate-limiting transport of gas away from the electrode surface.

In general, the Tafel slope value has been found to be independent of Cl^- ion concentration, although a decrease in slope with increase in Cl^- concentration has been reported in at least one instance [55]. The effect of electrolyte pH on the kinetics of chlorine evolution has not been considered in detail

173

in the literature, and it has been suggested that there is no pH effect in the case of RuO_2/TiO_2 electrodes [49]. However, Arikado et al. [56] and Erenburg et al. [57] have reported a pH effect, and have attributed this effect to surface oxyruthenium species which they suggested play a role in the mechanism of chlorine evolution. The activity of RuO_2/TiO_2 electrodes for Cl_2 evolution decreases only a little on decreasing the RuO_2 content from 100% down to 20-30% [58], at which point a rapid fall-off with further decrease in RuO_2 content occurs. A few studies have been carried out on the effect of preparation temperature on the activity of RuO_2 and RuO_2/TiO_2 electrodes. Kalinovskii et al. [59] observed, in the case of pure RuO_2, that the potential of constant current increased only slightly as the preparation temperature was increased from 350-600°C. Burke and O'Neill [60], on the other hand, have reported a slight increase in Cl_2 evolution activity with increase in electrode preparation temperature for RuO_2 in the range 350-500°C. In the case of RuO_2/TiO_2 electrodes, it has been shown that catalytic activity for chlorine evolution remains virtually unchanged as electrode temperature is increased [8], but Jannsen et al. [50] have seen a slight decrease in the activity of their mixed oxide electrodes. This general relative insensitivity of the catalytic activity towards preparation temperature of electrodes indicates that internal surface area is not a critical factor in the chlorine evolution process. However, Ardizzone et al. [14] observed differences in the kinetics of chlorine evolution between "cracked" (highly defective) and "compact" (low-defect) layers of pure RuO_2. A Tafel slope of 30 mV decade^{-1} was observed for the former type of electrode, while a slope of 40 mV decade^{-1} was found for the latter type.

4.1.6. Electroorganic Reactions

There has been considerable interest in the application of
RuO_2-based anodes in electroorganic synthesis and reactions. A
review of relevant selected examples of reactions at these
anodes will be presented here.

The use of RuO_4 as an organic oxidant is well documented,
and a review of its application in this area is available [61].
RuO_4 is generally regarded as a powerful, non-selective and
rather destructive oxidant. It does, however, have some uses in
organic chemistry, mainly in the oxidation of secondary hydroxyl
groups of carbohydrates to carboxyl functions [61]. Recently,
Griffith et al. have developed new oxidants based on the
ruthenate and perruthenate ions for the mild and selective
oxidation of alcohols to carbonyl compounds [62-64], and have
succeeded in preparing a number of organic soluble Ru(VII)-oxo
catalysts. These workers have also reported the catalytic
oxidation of primary and secondary halides to their respective
aldehydes and ketones by a Ru(VI) oxidant in the presence of
N-methylmorpholine-N-oxide as co-oxidant [65]. Burke and Healy
have also reported the catalytic oxidation of alcohols, in basic
solutions, by perruthenate ions in the presence of
peroxodisulphate [66], while Kaneda et al. have used a
RuO_2-methanol system for the selective catalytic oxidative
cleavage of carbon-carbon double bonds of alkenes using oxygen
[67]. This oxidation of alkenes has been carried out
electrochemically by Van Veen et al. using non-stoichiometric
lead and bismuth ruthenates, and these workers have concluded
that the catalytically active species is Ru(VI) [68]. Horowitz
et al. [69] also studied the oxidation of a number of organic
compounds at high surface area lead ruthenate in aqueous alkali.
These workers observed that lead ruthenate catalyses the
electrooxidation of primary alcohols to acids, secondary
alcohols to ketones, and the cleavage of ketones and alkenes to
carboxylic acids. It was tentatively suggested that the active

moieties were Ru(IV) groups which formed cyclic complexes with olefinic double bonds, leading to their cleavage.

Burke and Healy [9] observed that the oxidation of benzaldehyde, in basic solutions at thermally prepared RuO_2 electrodes, commences in the region where RuO_2 is converted to RuO_4^{2-}, while the oxidation of benzyl alcohol occurs where RuO_4^- is found on the surface of the ruthenium dioxide electrodes. Burke and Murphy have reported the rapid oxidation of methanol to formaldehyde, formic acid and CO_2 at RuO_2/TiO_2 electrodes in acid solutions [11], and have also reported the activity of these electrodes towards carbon-carbon cleavage of higher alcohols. These workers have postulated that the mechanism for the oxidation of methanol at RuO_2 electrodes involves the generation of species such OH_{ads} and H_{ads}. A similar theory was invoked by Watanabe and Motoo [70] to account for the enhanced oxidation of methanol on platinum by ruthenium ad-atoms. In a recent study, however, Kennedy and Smith [71] have concluded that RuO_2 is a poor promoter for the methanol oxidation at platinised carbon electrodes, and have postulated that the oxygen atoms needed to complete the methanol oxidation reaction are too tightly held in their RuO_2 electrodes to participate in the reaction.

O'Sullivan and White have investigated formaldehyde oxidation at thermally prepared RuO_2 electrodes in alkaline solution [10]. Two waves were observed for this reaction, with the first wave coinciding with the peak associated with the Ru(IV)/Ru(VI) couple, and the second coinciding with the peak usually associated with the Ru(VI)/Ru(VII) couple [31]. Formate was observed to be the primary product of HCHO oxidation in the first wave, while oxidation of HCHO to carbonate was observed in the second wave. Despite these interesting features, however, RuO_2 was not as active as the noble metal catalysts Pt and Pd for this reaction.

Laule et al. [21], in an interesting publication, have reported preliminary results on the application of "cracked"-

type RuO_2 electrodes for the electrochemical oxidation of a polychlorinated biphenyl (PCB) compound, 4,4'-dichlorobiphenyl, in the presence of persulphate, although no determination of the relative toxicity of the product, 2-acetoxy-4,4'-dichlorobiphenyl, was made.

In general, all of the work above highlights the important role that electrochemically generated higher oxide species can play in electrocatalysis at these RuO_2-based electrodes. It will be demonstrated in the following sections that electrodes prepared by simple mixing of hydrated RuO_2 with carbon paste or graphite-loaded epoxy matrices can be used to detect alcohols, carbohydrates and various antibiotic drugs via electrocatalytic oxidation of hydroxyl groups.

4.2. ELECTROCATALYTIC DETECTION OF ALCOHOLS AT RUO$_2$-MODIFIED ELECTRODES

The quantitation of low relative molecular mass alcohols is of great importance due to their widespread use in various industries. In addition, the detection of ethanol is of tremendous clinical and forensic importance. Direct electrochemical measurements of alcohols have been limited, in part, by the large overvoltage for their electro-oxidation at bare carbon electrodes. The development of novel electrode materials for use in the detection of alcohols is thus an active area of investigation. The most important and commercially successful approach to date utilises metallic electrode substrates to obtain enhanced oxidation over that seen at common carbon electrodes . Metallic sensing electrodes such as platinum [72-74], gold [75-77], nickel [78-81] and copper [82,83] have all been used for the direct electrochemical detection of alcohols and carbohydrates. However, with Pt or Au, where the electrocatalysis proceeds via the adsorption of the substrate or of resulting oxidation products, a stable response is only obtained if appropriate cycles of oxidative cleaning of adsorbed material and subsequent reductive removal of the oxide layer are applied between detection intervals. Thus, the use of a dual- or triple-pulse potential waveform is generally required for operation of these electrode materials [72-77]. With Ni and Cu electrodes, where electrocatalysis proceeds with the formation of an active oxide formed in situ on the electrode at the detection potential, simple constant-potential operation is possible [78-83].

An alternative approach for the electrochemical detection of alcohols has been the use of enzymes as oxidising agents of primary alcohols with the subsequent electrochemical monitoring of the products of these reactions, usually of H$_2$O$_2$ or NADH [84-88]. The problems associated with these enzyme systems, however, are numerous. The application of these biosensors is

178

limited by the difficulty in selecting appropriate enzyme supports, the time needed to attain a steady-state signal, and most significantly, the inherent lack of stability of these systems due to loss of enzyme activity.

In this work, highly stable electrocatalytic oxidation of several important alcohols based on the use of ruthenium dioxide-modified carbon paste electrodes is described. The analytical advantages that accrue from the low fixed-potential amperometric detection of alcohols at the RuO_2-chemically modified electrodes (CMEs) are illustrated in the following sections. Recent research by Wang and Taha [13] has indicated the use of such electrodes for the detection of carbohydrates.

4.2.1. EXPERIMENTAL

4.2.1.1. Apparatus

Cyclic voltammetry was performed using an EG & G PAR Model 264A voltammetric analyzer, in conjunction with a Houston Omniscribe X-Y recorder. A 10 cm^3 Bioanalytical Systems (BAS) Model VC-2 electrochemical cell was employed in these experiments with the working electrode, reference electrode (Ag/AgCl, Model RE-1, BAS) and platinum wire auxiliary electrode inserted into the cell through holes in its Teflon cover.

The flow injection system consisted of the carrier reservoir, a Rainin Model 5041 sample injection valve (20μL loop), interconnecting Teflon tubing, and the thin layer electrochemical detector (Model T1-4, BAS). An EG & G PAR Model 364 polarographic analyzer and a Houston Omniscribe Strip-chart recorder were used in the flow injection experiments.

4.2.1.2. Reagents and Procedures

Ruthenium dioxide-modified carbon pastes (usually 40:40:20 w/w graphite:oil:RuO_2) were prepared by adding weighed amounts

of RuO_2 (Aldrich) and graphite powder (Acheson 38, Fisher) to 10 cm ^{3} of diethyl ether, and sonicating the slurry until the ether had evaporated. The desired amount of mineral oil (Aldrich) was then added and thoroughly hand-mixed with the RuO_2-coated graphite. Portions of the resulting paste were then packed into the end of a glass tube (4mm i.d.) or within the cavity of the flow detector. The surface was then smoothed on a weigh paper.

Amperometric detection was used for both batch and flow injection systems, using convective mass transport of 600 rpm and 0.5 cm^3min^{-1}, respectively. The desired working potential (usually +0.4 V) was applied and transient currents were allowed to decay. All measurements were made at room temperature.

4.2.2. RESULTS AND DISCUSSION

4.2.2.1. Cyclic Voltammetry

Preliminary experiments to investigate the nature of the electrocatalytic activity of the RuO_2-CME towards alcohol oxidation were performed by cyclic voltammetry. Typical cyclic voltammograms obtained with the RuO_2-CME in 1.0 M NaOH, both with and without added alcohols (solid and broken lines, respectively) are shown in Figure 4.6. The voltammograms obtained in blank NaOH exhibit a well defined cathodic and anodic peak, with a formal potential of +0.43 V (vs. Ag/AgCl). It has been suggested that the transition evident at this potential is due to the Ru(IV)/(III) transition shown in equation (4.6) [13]. Previous studies on RuO_2 electrodes, and that of Lam et al. [31] in particular, have indicated however that the redox transition next to the oxygen evolution wave, in basic solutions, is that of the RuO_4^{2-}/RuO_4^- couple shown in equation (4.3). Burke et al. [9,22,23] and Trasatti et al. [1,2] have reported wave shapes similar to those in Figure
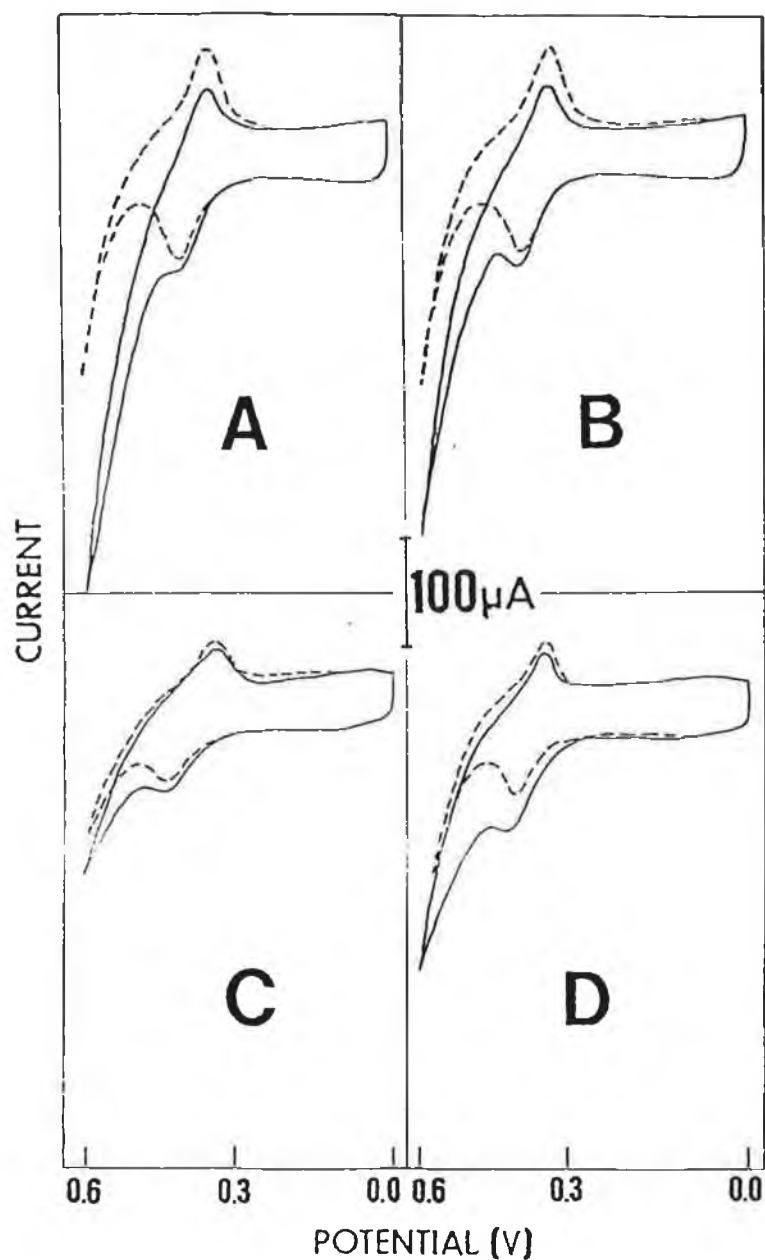
180

Figure 4.6: Cyclic voltammograms for 1 M methanol(A), 1 M ethanol (B), 10 mM glycerol (C) and 10 mM ethylene glycol (D) recorded at the 20% w/w RuO_2-modified carbon paste electrode. Supporting electrolyte, 1.0 M NaOH. Scan rate, 20 mV s^{-1}. Dotted lines represent the blank, alcohol free, solutions.

4.6 and have also attributed the transition next to the oxygen evolution wave to the ruthenate/peruthenate transition shown above. Further evidence that this transition is involved is presented in the following sections, where the electrocatalytic oxidation of alcohols is seen to occur at the onset of this transition. It has been found that, for both solution catalysis and electrocatalysis at RuO_2 electrodes, a Ru(VII) species has been attributed to be the active component in the catalytic oxidation of both primary and secondary alcohols [62-67], thus indicating that the couple at +0.43 V in Figure 4.6 is a Ru(VI)/Ru(VII) transition. The wave seen at +0.43 V for the RuO_4^{2-}/RuO_4^{-} transition, showed the peak current vs sweep rate linearity, characteristic of a surface redox reaction [89], up to sweep rates of 50 mV s^{-1}.

The voltammograms obtained upon addition of the alcohols to the electrolyte, exhibit classic electrocatalytic behaviour, with an increase in anodic and a decrease in cathodic peak currents, although the electrodes showed more specific catalytic activity for alcohol oxidation than simple redox mediation [90]. The anodic peak potentials obtained for the electrocatalysis of methanol, ethanol, ethylene glycol and glycerol oxidations are +0.43 v, +0.43 V, +0.41 V and +0.42 V, respectively, which agree with the potential for the oxidation of the surface ruthenate species. The cyclic voltammetric responses for the electrooxidation of the various alcohols all showed the peak current vs square root of scan rate linearity associated with a diffusion controlled process. All of these cyclic voltammetric responses were extremely stable, with no apparent change in the peak currents upon extended cycling over a 60 min period.

4.2.2.2. Amperometry

Constant-potential amperometric detection was employed in the investigation of the analytical utility of the RuO_2-modified electrodes for the electrocatalytic oxidation of the
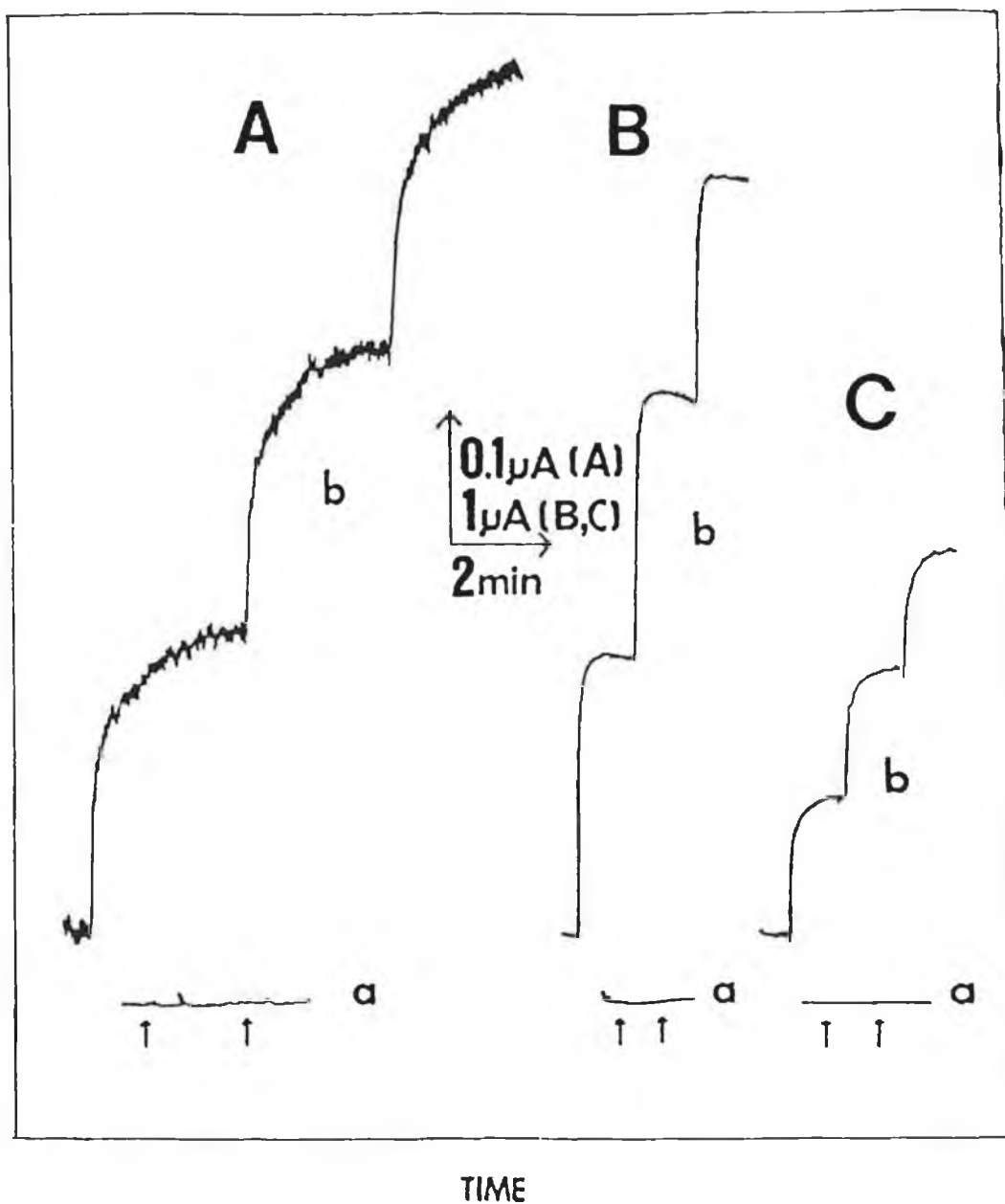
Figure 4.7: Standard additions of 5 mM methanol (A), 1 mM glycerol (B) and 1 mM ethylene glycol (C) at the bare (a) and 20% RuO_2-modified (b) electrodes. Batch operation with +0.4 V potential and 600rpm stirring. Electrolyte 1.0 M NaOH.

183

alcohols. Typical responses obtained for several alcohols at both the modified and unmodified electrode surfaces in 1.0 M NaOH electrolyte, with batch addition of aliquots of the alcohol and constant-potential operation at +0.4 V are shown in Figure 4.7. From this, the absence of a response at +0.4 V, at the plain unmodified carbon paste electrode, as compared to the fast achievement of a large steady-state current at the modified surface, can be seen.

The effect of the RuO_2 content of the paste on the analytical signal was investigated by successive additions of 2 mM glycerol to the cell, with batch operation at a potential of +0.4 V and mass transport controlled by stirring at 400 rpm with a magnetic stirrer. Calibration plots yielding slopes of 0.34 mA mol^{-1}, 0.87 mA mol^{-1} and 2.19 mA mol^{-1} were obtained for the 5%, 10% and the 20% w/w RuO_2-modified electrodes, respectively (correlation coefficients of 0.995, 0.997 and 0.997). A similar increase in response with increasing modifier content was observed for the electrocatalytic detection of carbohydrates at a RuO_2-carbon paste electrode (RuO_2-CPE) [13]. A RuO_2-CPE consisting of 20% w/w RuO_2 was selected for further experiments in order to minimise higher background currents that would be associated with larger percentage modifier concentrations, while maximising the electrocatalytic current for alcohol oxidation.

The hydrodynamic voltammograms (HDV) obtained under flow injection conditions for ethylene glycol (A), 1,3-propanediol (B) and glycerol (C) are shown in Figure 4.8. The response at the modified electrode is of the order of ten times larger than the peak obtained at the unmodified carbon paste in the thin layer detector. This response at the unmodified electrode is attributed to a conductivity effect associated with the passage of the sample plug in the flow-injection manifold. The plateau shapes seen in Figure 4.8, for the HDVs at the modified electrodes, are those expected for a diffusion limited electrode process. Although the HDVs show a maximum response at potentials
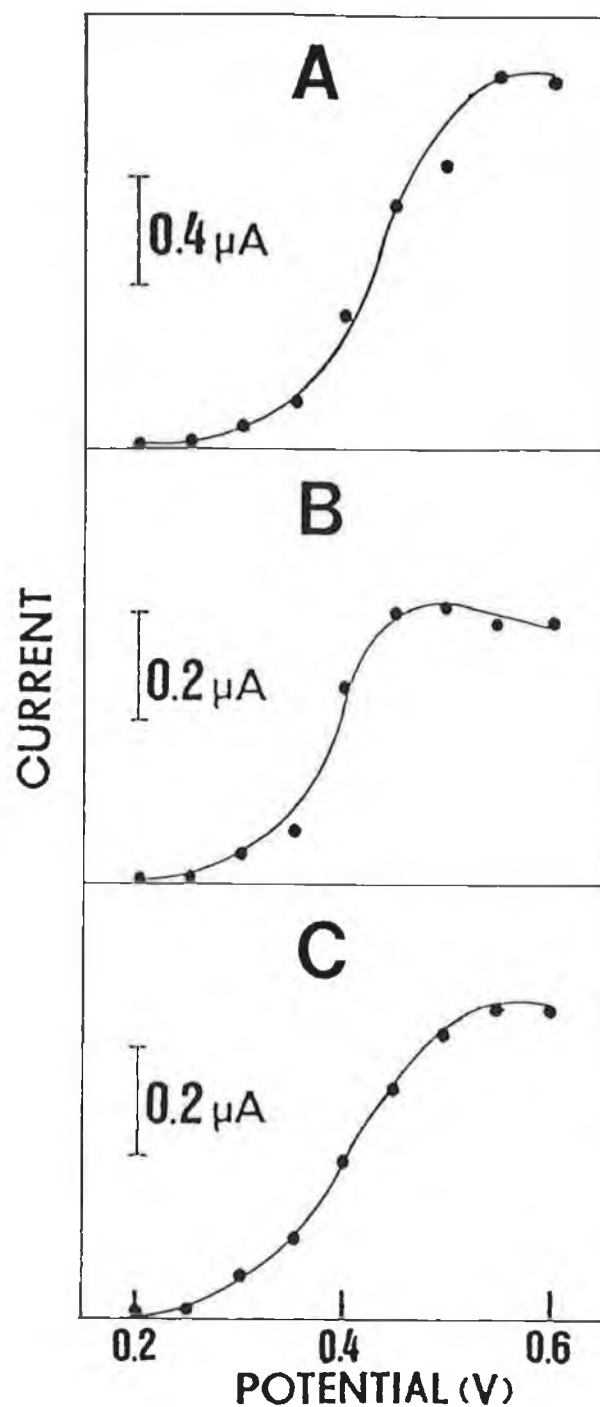
184

Figure 4.8: Hydrodynamic voltammograms obtained for 10 mM ethylene glycol (A), 10 mM 1,3-propanediol (B) and 1 mM glycerol (C) injection concentrations at the modified electrode. Flow rate, 0.5 $cm^3 min^{-1}$. Electrolyte and carrier, 1.0 M NaOH.

above approximately +0.5 V, an operating potential of +0.4 V was selected for further experiments. This lower potential both minimises potential interferents and also has a lower background current associated with it, relative to the higher operating potentials.

Other parameters investigated, which affect the catalytic response, were the NaOH electrolyte concentration and the flow rate in FIA. The effect of both of these experimental variables on the flow injection response for the electrocatalytic oxidative detection of methanol are shown in Figure 4.9. The effect of NaOH concentration (curve A) was investigated over the 0.1-1.5 M range. The FIA peak current increased steadily with increasing NaOH concentration up to approximately 1.0 M, after which it leveled off. A similar profile for response versus base concentration was observed for carbohydrate oxidation at RuO_2-modified carbon paste electrodes [13] and other electrode systems [73,83,91]. This dependence of response on base concentration may be attributed to the availability of the adsorbed radical species OH_{ads}, which is thought to participate in the electrooxidation of alcohols and carbohydrates at RuO_2-based electrodes [11,70], and/or to the requirement of high pH for the formation of the higher valency ruthenium-oxy species known to be the catalytically active surface components [31]. The flow injection peak current was also strongly affected by changes in the electrolyte flow rate (curve B, Figure 4.9), showing a sharp decrease with increasing flow rates. Apparently, the electrocatalytic reaction is too slow to produce appreciable currents during faster passage of the sample plug in the flow injection manifold, and mass transfer to the surface has a negligible effect on the current. Similar flow rate dependence curves were reported for carbohydrate detection at Cu-CMEs [83] and RuO_2-CPEs [13]. Significant broadening of the methanol peak was observed, in this investigation, at the lower flow rates, and this can be attributed to sample dispersion in the flow injection manifold.
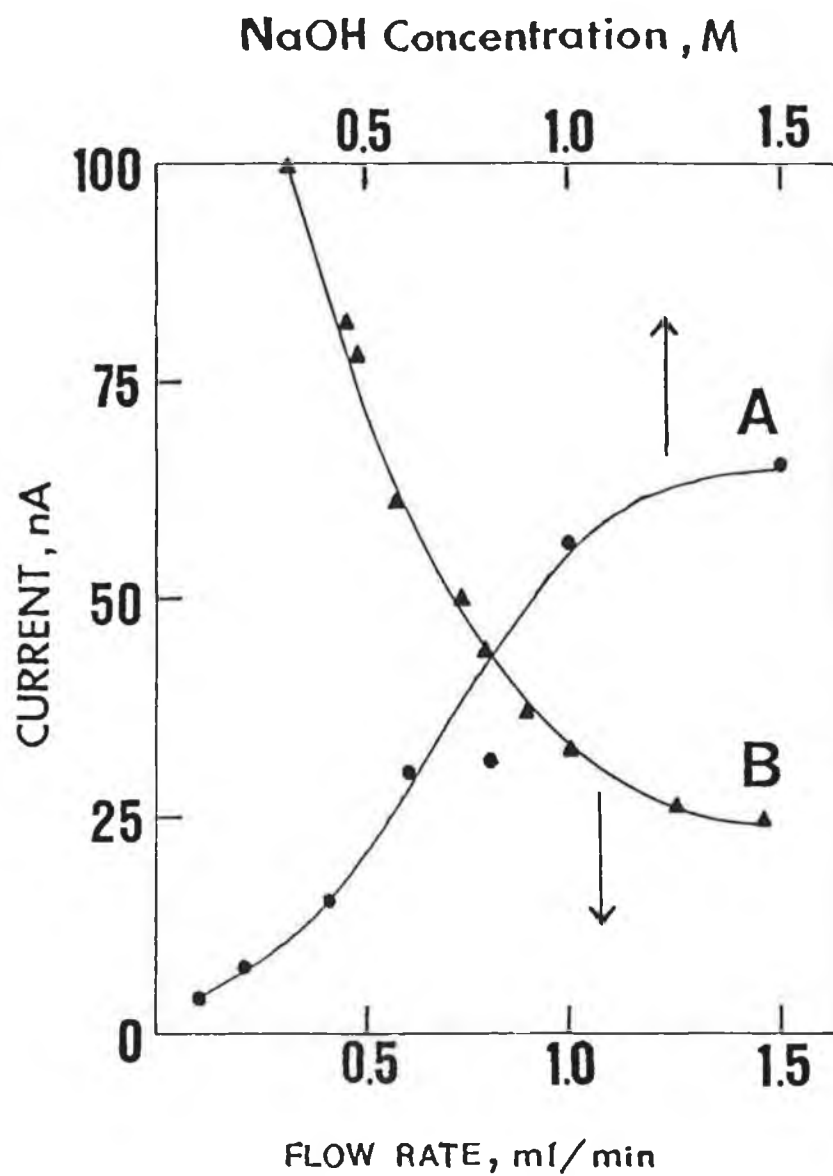
186

Figure 4.9: Effect of NaOH concentration (A) and flow rate (B) on the flow injection response for 20 mM methanol at the modified electrode. Applied potential, +0.4 V. Other conditions as in Figure 4.8.

For example, peak widths of 20 seconds and 52 seconds were obtained at flow rates of 1.45 cm^3min^{-1} and 0.3 cm^3min^{-1}, respectively, allowing sample throughput of 90 and 45 injections per hour. A flow rate of 0.5 cm^3min^{-1} was selected for subsequent flow injection analyses as a compromise between reasonable sample throughput and good detection limits.

The FIA peak currents obtained for increasing levels of different alcohols are shown in Figure 4.10. These peaks are part of a wider study of the linear range and detection limits attained for the various alcohols. Excellent linearity was observed for the different alcohols, although the slope (sensitivity) varied according to the number and position of the hydroxyl groups in the alcohol structures. This aspect will be discussed in more detail in section 4.4. Linear peak current-concentration plots were obtained over the 0.25 - 2.5 mM range for glycerol and ethylene glycol yielding slopes of 0.114 mA mol^{-1} and 0.038 mA mol^{-1}, respectively (correlation coefficients of 0.999 and 0.998). Slopes of 1.86 μA mol^{-1} and 0.91 μA mol^{-1} (correlation coefficients of 0.999 and 0.998) were obtained for methanol and ethanol, respectively, over the 5 - 50 mM concentration range. Based on the flow injection peaks shown in Figure 4.10, detection limits (signal-to-noise ratio of 3) of 16 μM, 45 μM, 1.2 mM and 2.4 mM were determined for glycerol, ethylene glycol, methanol and ethanol, respectively. These detection limits are higher than those reported for pulsed amperometric detection at platinum electrodes [72] or for enzyme- or yeast-based biosensors for ethanol [84-87]. However, the RuO_2-modfied carbon paste electrode offers advantages over these electrode systems, such as its simple methodology, fast response time and long-term stability.

As mentioned above, the main feature of RuO_2-CMEs in comparison to other amperometric systems for the detection of alcohols, is their inherent electrocatalytic stability. The short-term stability of the modified electrodes was assessed by measuring the flow injection peak currents for repeated
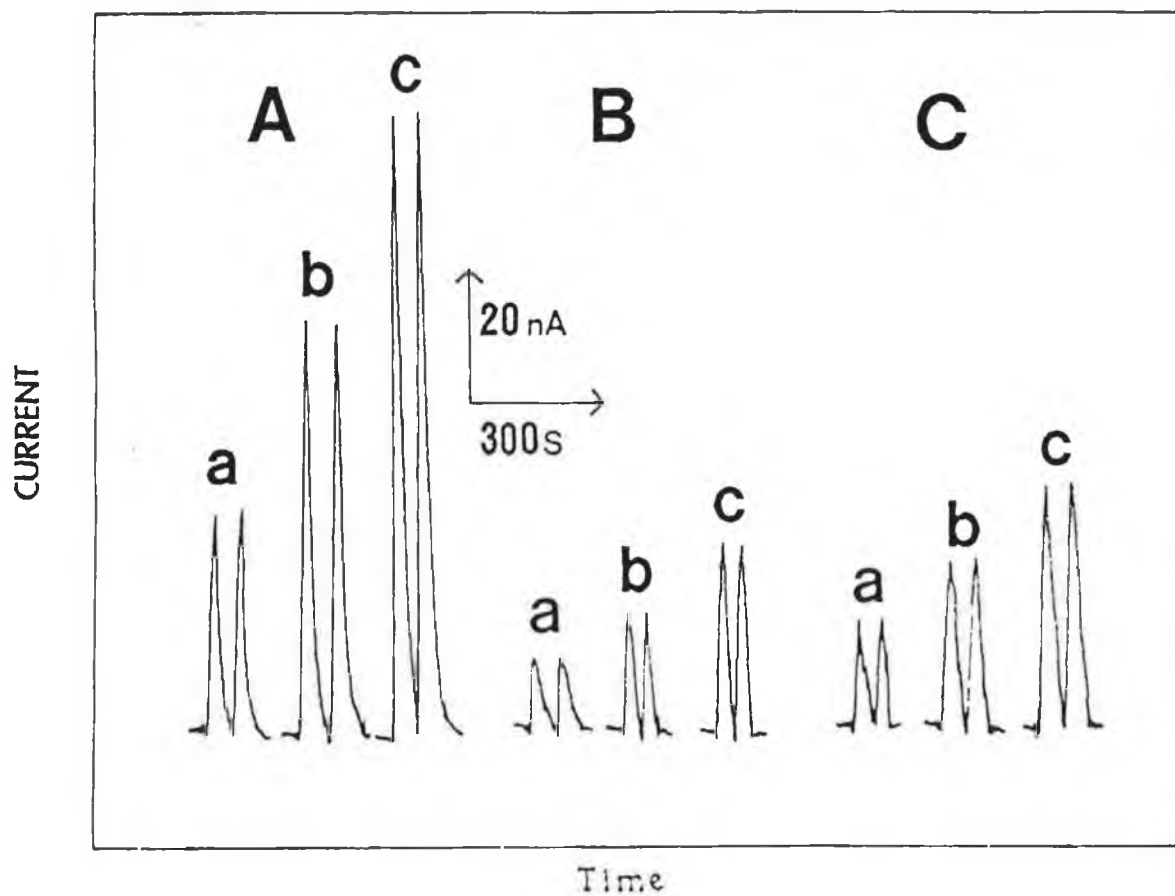
Figure 4.10: Amperometric detection for injections of glycerol (A), ethylene glycol (B) and methanol (C) solutions from 0.25 mM to 0.75 mM (a-c) concentration for (A) and (B), and from 5 mM to 15 mM (a-c) concentration for (C) at the modified electrode. Applied potential, +0.4 V. Other conditions as in Figure 4.8.
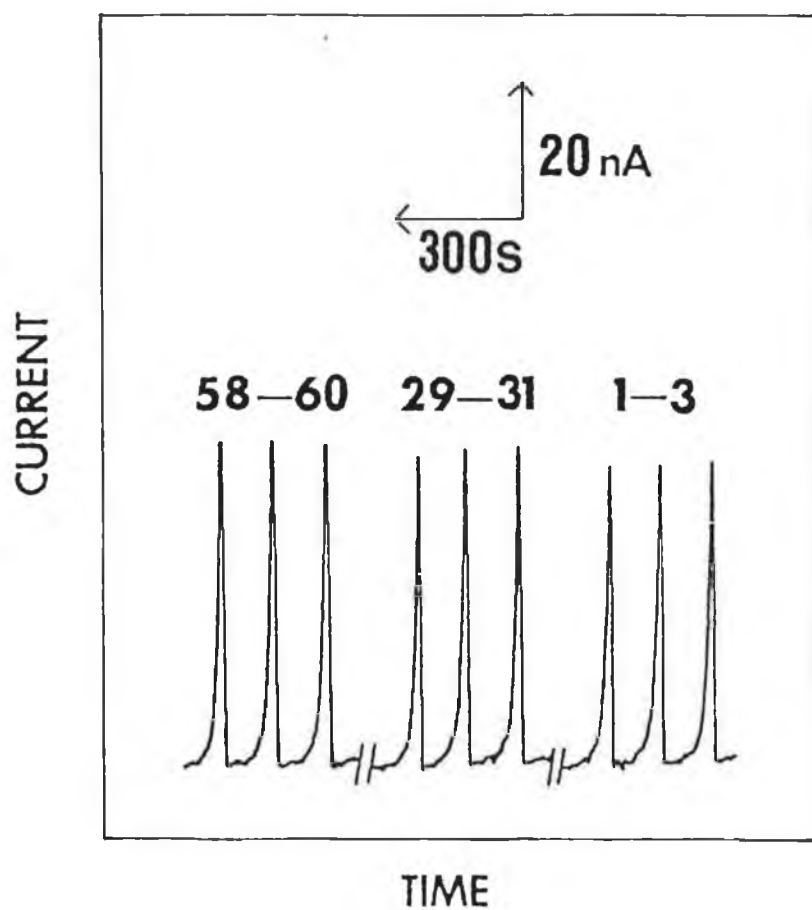
Figure 4.11: Time dependence of electrode sensitivity over a 120 min period to repeated injections (60 in total) of 20 mM methanol. Other conditions in as in Figure 4.8.
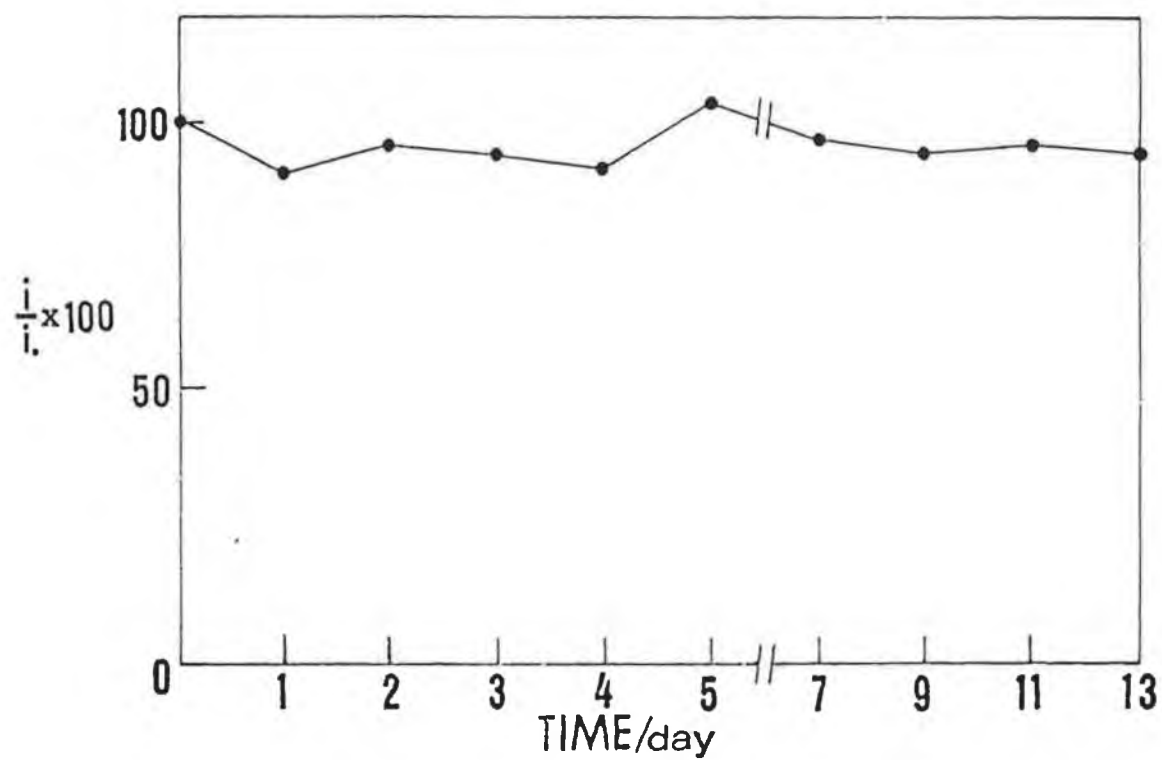
190

Figure 4.12: Long-term stability of the modified electrode.
Batch operation with additions of 10 mM methanol. Other
conditions as in Figure 4.7.

191

injections of 20 mM methanol over a 120 minute time period as shown in Figure 4.11. The relative standard deviation of the resulting 60 injections was determined to be 3.4%. The stability of these electrodes over longer time periods was monitored, as shown in Figure 4.12, by measuring the steady-state current recorded upon addition of 10 mM of ethanol to the electrochemical cell, over a 13-day period, using the same electrode surface throughout. The electrode was left standing in the 1.0 M NaOH electrolyte between each batch experiment. The RuO_2-CME functioned in a normal fashion throughout this series of experiments, showing a slight decrease (approximately 6%) in response with a relative standard deviation of 4.0%, over the 13-day period. Overall, the data shown in Figures 4.11 and 4.12 indicate that the electrocatalytic activity of these modified carbon paste electrodes is maintained over relatively long time periods, showing good reproducibility and little deterioration in the current response.

In summary, the analytical utility of the RuO_2-modified carbon paste electrodes for the detection of various alcohols has been demonstrated. These electrocatalytic surfaces offer marked decrease in overpotentials for alcohol oxidation. Due to their ease of preparation, long-term stability and simple, fixed-potential operation, it is envisaged that the RuO_2-CME could be a valid alternative to the pulsed amperometric detection of alcohols and other species. These electrodes also offer increased stability over enzymatic sensors for ethanol.

192

4.3. ELECTROCATALYTIC DETECTION OF SACCHARIDE ANTIBIOTICS AT RUO₂-MODIFIED GRAPHITE-EPOXY COMPOSITE ELECTRODES.

Streptomycin is a trisaccharide derivative that is important in tuberculosis therapy and in the treatment of other infectious diseases, such as tularemia and plague. The electrochemical reduction of streptomycin, involving the aliphatic aldehyde group, has been exploited for polarographic measurements of the drug using various mercury electrodes [92-95]. With d.c. polarography, mM concentrations of streptomycin can be quantified [92,93]. Differential pulse polarography permits detection of μM levels [94], while adsorptive stripping voltammetry of the drug offers detection limits in the nM range [95]. The related saccharide antibiotics, neomycin and novobiocin, have also been quantitatively determined using polarographic techniques [95,96].

Methods based on solid electrodes may be more desirable for sensing and flow (FIA) applications. In particular, constant-potential amperometric monitoring of these antibiotics offers a more attractive and simpler approach to various batch or flow quantitations. Unfortunately, the anodic oxidation of saccharide antibiotics suffers from high overvoltages and poor reproducibility at solid electrodes.

In section 4.2, carbon paste electrodes modified with a RuO_2 catalyst were shown to be effective for the electrocatalytic oxidation of various alcohols, allowing their quantitation via fixed-potential amperometry. In this section, electrodes modified with RuO_2 are shown to lower the overvoltage for the oxidation of the hydroxylated antibiotics discussed above, with their structures being depicted in Figure 4.13. The use of graphite-epoxy modified electrodes was exploited in order to obtain a renewable electrocatlytic response upon polishing of the electrode surface. Other recent studies have demonstrated the improved stability and reproducibility that composite graphite-epoxy electrodes

193

NH

H₂NCNH

NH

NHCNH₂

H

OH H

HO

H

H

OH

H

H

O

H

O

H₃C

CHO H

HO

R = CH₂OH

R' = CH₃NH

HO

R

R'

H

H

H

H

HO

H

A

CH₂NH₂

O

HO

H₂N

HO

H₂N

O

H₂N

NH₂

OH

O

HOH₂C

O

H

H

H

H

HO

O

O

HO

NH₂

HO

CH₂NH₂

C

CH₃

O

O

CH₃O

CH₃

O

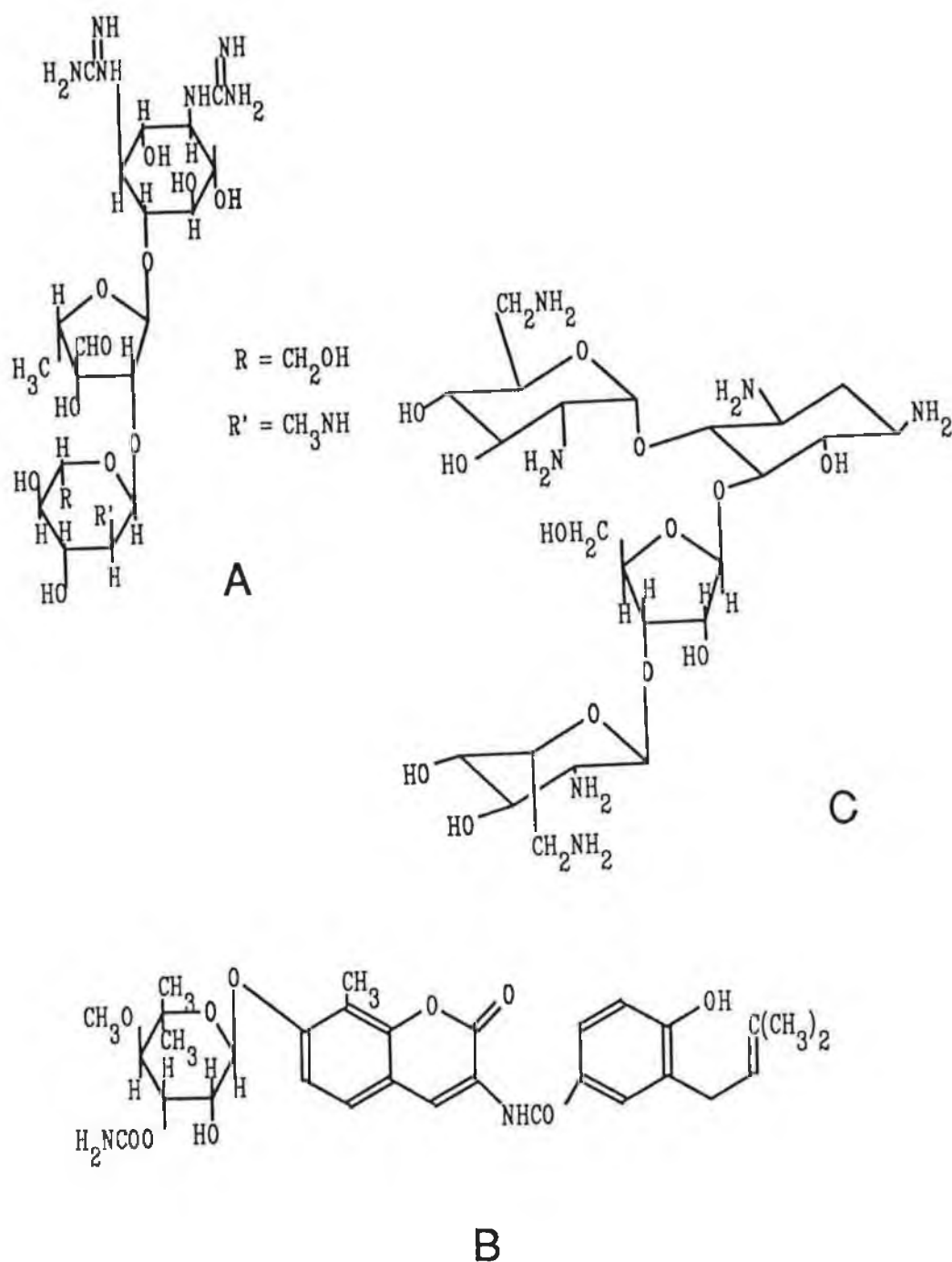CH₃

H

H

H

H

CH₃

O

OH

C(CH₃)₂

H₂NCOO

HO

NHCO

B

Figure 4.13: Chemical structure of steptomycin (A), novobiocin (B) and neomycin (C).

containing electrocatalysts can offer over their carbon paste counterparts [97-100]. These electrodes showed similar analytical attributes as their carbon paste counterparts, while offering benefits of increased mechanical stability, versatility and renewability. Polishable graphite-epoxy electrodes modified with metal catalysts [97,99,100] and biological entities [98] have been successfully used.

4.3.1. EXPERIMENTAL

4.3.1.1. Apparatus

The apparatus employed in these experiments has been previously described in section 4.2.1.1..

4.3.1.2. Reagents and Procedures

Standard solutions of streptomycin sulfate, neomycin sulfate and novobiocin sodium salt were prepared fresh daily in the 0.5 M NaOH background electrolyte.

The graphite-epoxy electrodes were prepared by mixing equal amounts of the epoxy-bonded graphite (Dylon) resin and accelerator components. Ruthenium-dioxide modified graphite epoxy electrodes were prepared by the subsequent addition and thorough hand-mixing of the required amount of RuO_2 (usually 80:20 graphite epoxy:RuO_2) to the graphite paste. Portions of the resulting paste were then packed into the end of a glass tube (3 mm i.d.) and allowed to cure at room temperature for 48-72 hours. The hardened electrode surface was then polished with wet and dry emery paper (1200 grade), rinsed with deionised water, polished with a 0.05 m alumina slurry, rinsed with water once more and finally ultrasonicated for 3 min to remove any residual alumina.

RuO_2-modified carbon paste electrodes for flow analysis were prepared as described in section 4.2.1.2.

195

4.3.2. RESULTS AND DISCUSSION

4.3.2.1. Cyclic Voltammetry

Cyclic voltammograms similar to those seen for the
RuO_2-carbon paste modified electrodes were observed for the
graphite-epoxy modified electrodes, as shown in Figure 4.14,
confirming the retention of the ruthenium redox characteristics
in the rigid graphite-epoxy matrix. The blank signal in 0.5 M
NaOH electrolyte shows the wave previously attributed to the
RuO_4^-/RuO_4^{2-} transition at +0.45 V and shown in equation
(4.3). Also apparent, at a potential of 0.0 V, is the
RuO_4^{2-}/RuO_2 transition shown in equation (4.5). The
electrocatalytic behaviour of these electrodes towards the
oxidation of the saccharide antibiotics is similar to that seen
for the oxidation of alcohols at the RuO_2-CPE. The oxidation
of novobiocin seems to be catalysed by both of the ruthenium
couples, with an increase in the anodic peak currents at the
RuO_4^{2-}/RuO_2 transition at 0.0 V and the
RuO_4^-/RuO_4^{2-} transition at +0.45 V. In contrast, the
unmodified graphite-epoxy or the glassy carbon electrodes do not
respond to a solution containing 5 mM novobiocin. No transitions
were evident in the voltammograns obtained for the three drugs
at the unmodified graphite-epoxy electrodes. Broad,
irreversible, oxidation waves at potentials of +0.75 V and +0.80
V were observed, respectively, for streptomycin and novobiocin
at the glassy carbon electrode. Surface poisoning of the glassy
carbon electrode resulted in a gradual decrease in these
oxidation currents. The peaks obtained at the RuO_2-modified
electrodes, however, were similar to those seen for alcohol
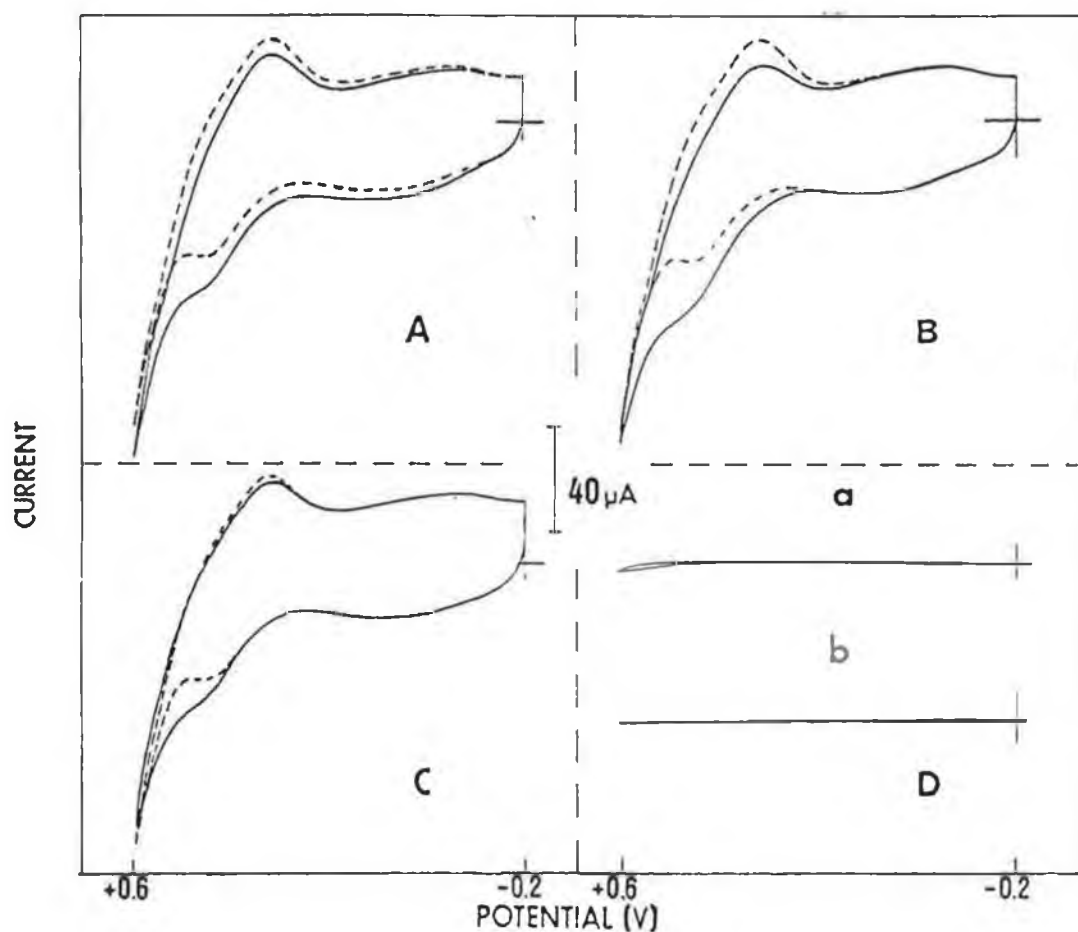oxidation and showed good stability upon extended cycling.

Figure 4.14: Cyclic voltammograms obtained at the RuO$_2$modified graphite-epoxy electrode in blank 0.5 M NaOH electrolyte (dotted lines) and upon the addition of 5 mM novobiocin (A), 5 mM streptomycin (B) and 20 mM neomycin (C). Also shown (D) is the response for 5 mM novobiocin at a bare glassy carbon electrode (a) and at an unmodified graphite-epoxy electrode (b). Scan rate, 20 mVs^{-1}.

4.3.2.2. Amperometry

Batch, fixed-potential amperometry was utilised to further investigate the analytical utility of the RuO_2-graphite epoxy electrodes. The hydrodynamic voltammetric profiles for batch additions of streptomycin (A), novobiocin (B) and neomycin (C) at both the unmodified (▲) and modified (●) electrodes are shown in Figure 4.15. The unmodified electrode does not permit convenient quantitation of these analytes over the potential window studied. In contrast, distinctly peak-shaped HDVs, with a maximum response in the vicinity of +0.45 V, were observed at the modified electrodes. These profiles do not have the expected plateau shape usually expected (and seen for alcohol oxidation at the carbon paste modified electrodes in the previous section) for diffusion limited processes. Similar peak-shaped HDVs have been seen for carbohydrate detection at both RuO_2-CPEs and at Cu-modified glassy carbon electrodes. This peak profile may be attributed to the formation of intermediates in the electrocatalytic reaction which poison the electrode surface at the higher potentials. The HDV obtained for the oxidation of novobiocin shows a catalytic current even at a potential as low as 0.0V. This confirms the behaviour seen using CV and allows the convenient monitoring of novobiocin at lower potentials, hence minimising interferences and the background currents associated with the RuO_2-graphite epoxy electrodes. A potential of +0.35 V was selected for detection of both streptomycin and neomycin. A potential of +0.2 V was selected for the determination of the analytical parameters for novobiocin in the batch cell. Subsequent experiments on novobiocin were carried out at a fixed-potential of 0.0 V in order to minimise interference from carbohydrates and alcohols, which do not give catalytic currents at this potential.

The batch amperometric detection of 50 μM (final cell concentration) novobiocin (A) and streptomycin (B) at the modified and unmodified electrodes is shown in Figure 4.16.
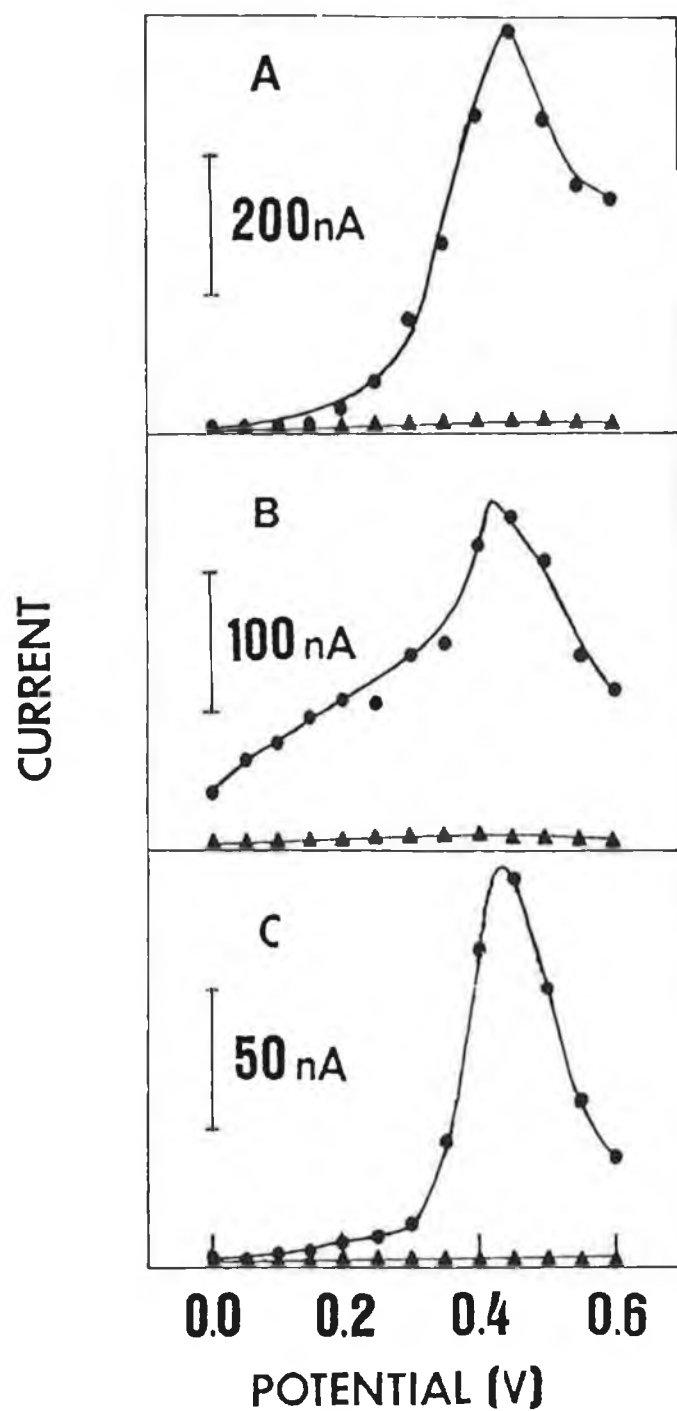
198

Figure 4.15: Hydrodynamic voltammograms obtained at the modified (●) and unmodified (▲) graphite-epoxy electrodes for the batch addition of 50 μM streptomycin (A), 5Γ M novobiocin (B) and 0.5 mM neomycin (C). 0.5 M NaOH electrolyte with 500rpm stirring.

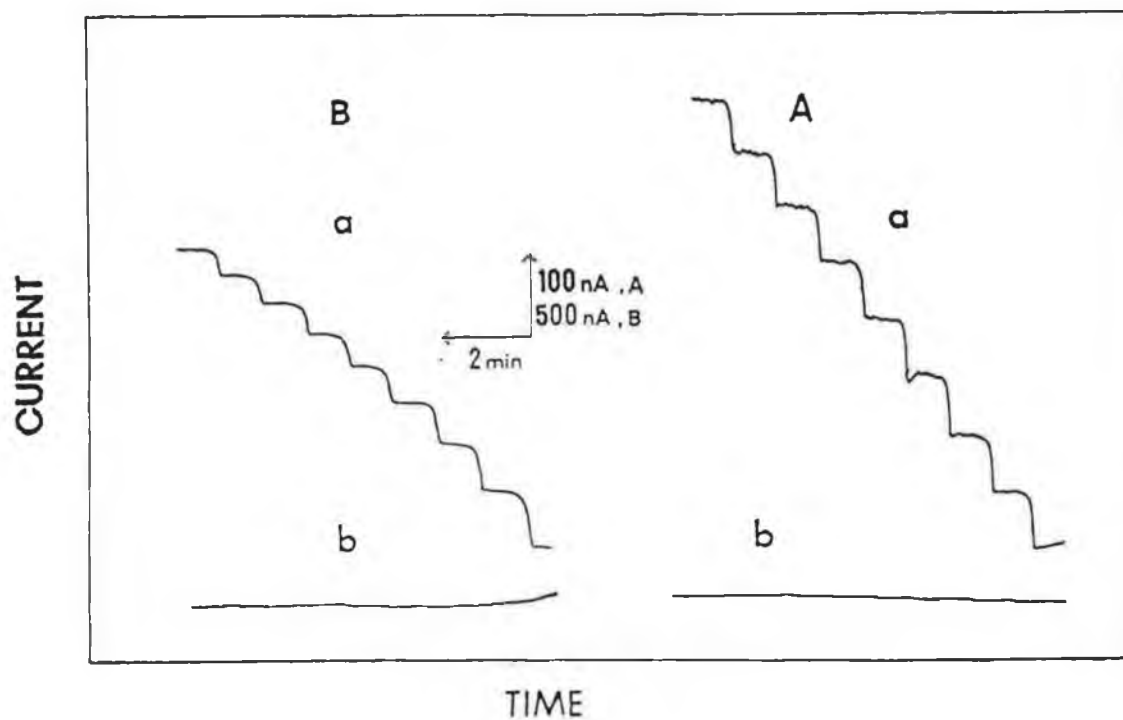Figure 4.16: Batch additions of 50 μM novobiocin (A) and
streptomycin (B) at the modified (a) and unmodified (b)
graphite-epoxy electrodes with constant-potential detection at
+0.2 V (A) and +0.35 V (B). Other conditions as in Figure 4.15.

Table 4.1: Analytical parameters calculated for the antibiotics fom batch additions at fixed-potentials. Background electrolyte, 0.5 M NaOH; 400rpm stirring.

Parameter	Streptomycin[a]	Neomycin[a]	Novobiocin[b]
Linear range	1.5 – 250 μM	0.01 – 2 mM	6 – 400 μM
Sensitivity	4.43mA mol^{-1}	0.08mA mol^{-1}	1.31mA mol^{-1}
Correlation	0.996	0.998	0.999
L.O.D. (s/n=3)	1.5 μM	10 μM	6 μM

[a]Fixed-potential detection at +0.35 V.
[b]Fixed-potential detection at +0.2 V.

Excellent response times and signals are observed for both of these drugs at the monitoring potentials used. The analytical characteristics obtained at the 20% RuO_2-modified graphite-epoxy electrodes for the three antibiotics are listed in Table 4.1. Good sensitivities with detection limits of 6 μM and 1.5 μM were obtained for novobiocin and streptomycin (at +0.2 V and +0.35 V monitoring potentials), respectively. Neomycin gave a detection limit of 10 μM. These detection limits are higher than those seen for adsorptive stripping voltammetric measurements of these antibiotics at mercury electrodes [95,96]. However, as previously mentioned, methods based on mercury may be undesirable for many practical applications, including flow analysis. A significant advantage of these graphite-epoxy modified electrodes over other modified electrode systems, however, is the stability and renewability associated with the response.

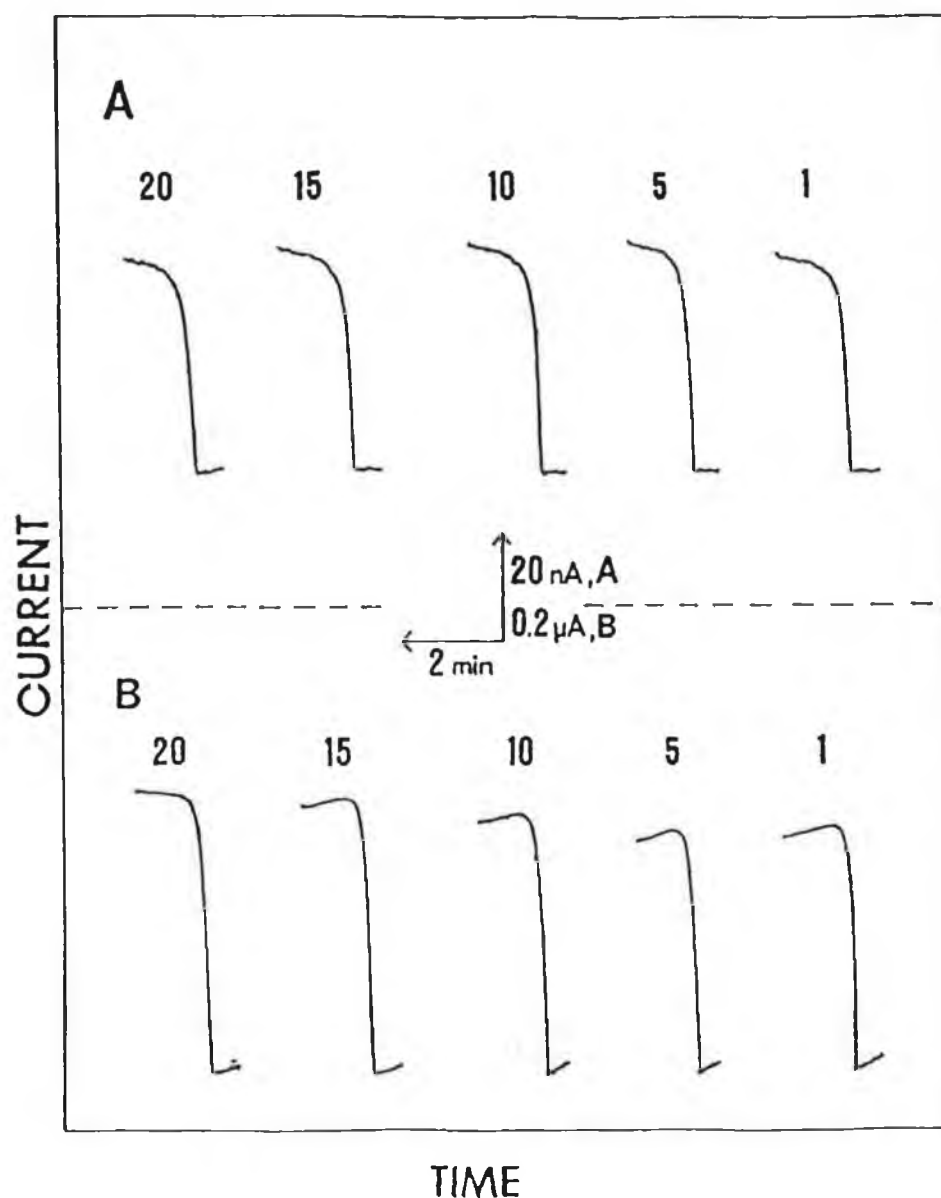The stability and precision of the RuO_2-graphite epoxy

Figure 4.17: Same-surface precision for repeated batch additions of 50 μM novobiocin (A), with 0.0 V constant-potential detection, and surface-to-surface precision for repeated batch additions of 50 μM streptomycin (B), with +0.35 V constant-potential detection, at the graphite-epoxy modified electrode. Other conditions as in Figure 4.15.

modified electrodes towards the electrooxidation of the saccharide antibiotics is demonstrated in Figure 4.17. Figure 4.17(A) represents the precision of the electrode at the same electrode surface for the oxidation of 50 μM novobiocin with the electrode being removed and rinsed with deionised water between injections. From the 20 repetitive injections made, a mean current of 40.1 nA, with a relative standard deviation of 3.7% was established. Figure 4.17(B) shows the surface-to-surface precision of the electrodes to streptomycin oxidation at the 50 μM level. Between measurements, the electrode was removed from the cell, polished for 30 s with a 0.05 μm alumina slurry and rinsed with deionised water. For the series of 20 consecutive measurements at different surfaces, a mean current of 486 nA, with a relative standard deviation of 6.5% was calculated. The data reported above demonstrates the very good stability and reproducibility that the polishable, graphite-epoxy modified electrode can offer. The success of the modified graphite-epoxy electrode fabrication technique also compares favourably with other techniques for the incorporation of modifiers into polishable, robust electrodes [101-103]. All of the RuO_2-modified graphite epoxy electrodes prepared functioned in a reproducible ($\pm$ 10%) fashion, whereas methods such as the copolymerisation of styrene and divinylbenzene, in the presence of the modifier and carbon black [101,102] to form polishable modified electrodes, are less successful.

The practical application of the RuO_2-modified electrodes to antibiotic, or indeed alcohol, monitoring in complex matrices is hampered by the general catalytic activity of these electrodes towards the oxidation of hydroxylated compounds, such as alcohols (see previous section), carbohydrates [13] and other potential interferents. The application of the RuO_2-modified electrodes to constant-potential detection of the saccharide antibiotics in flowing streams, with a view to LCEC applications, was therefore investigated. For these experiments,
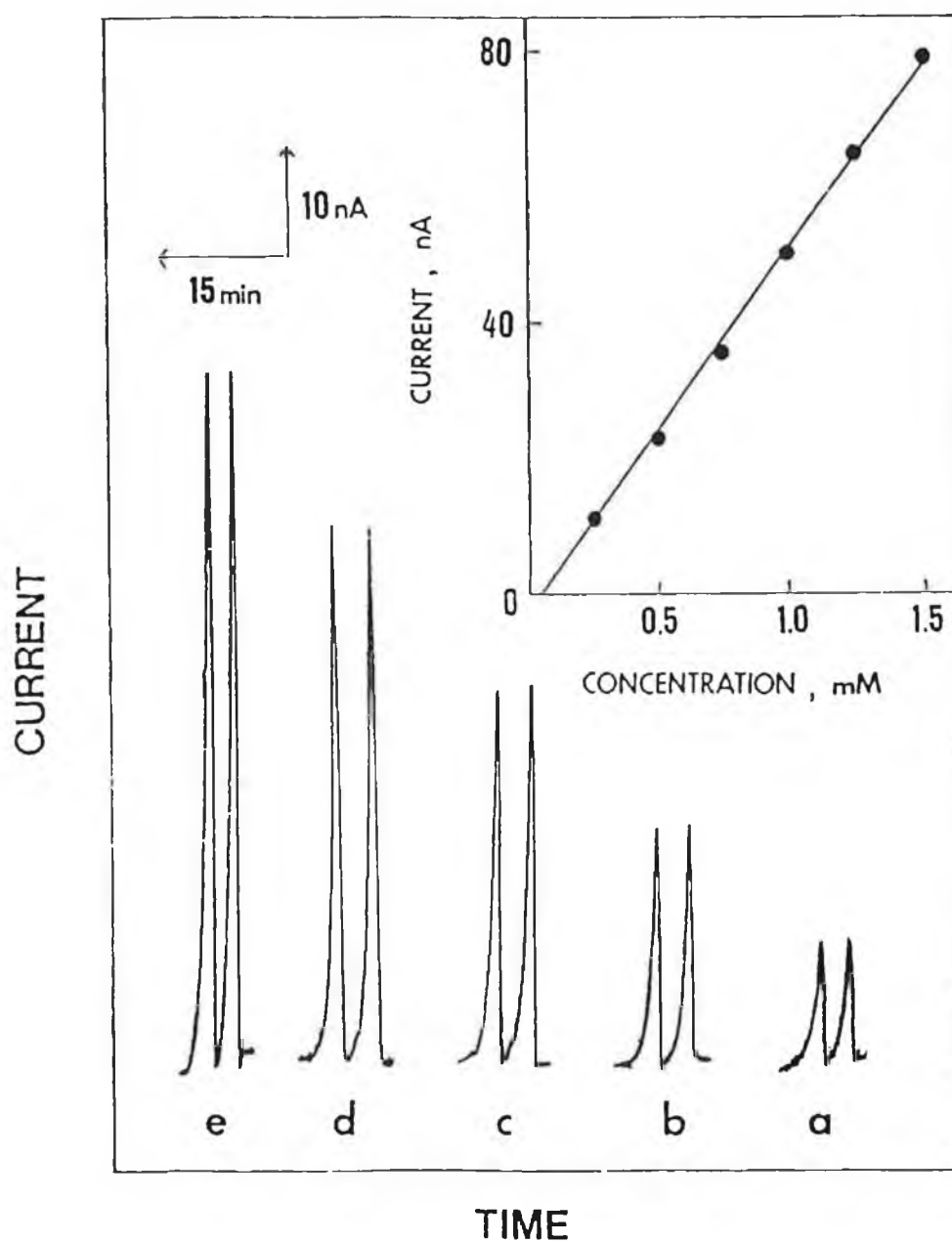
Figure 4.18: Flow injection response at the RuO$_2$-modified carbon paste electrode to injections of 0.25 (a), 0.5 (b), 0.75 (c), 1.0 (d) and 1.25 mM (e) novobiocin. Constant-potential operation at 0.0 V. Flow rate, 1.0 cm^{3}min^{-1} and electrolyte, 0.5 M NaOH. Inset shows the i-C calibration curve obtained for novobiocin up to a concentration of 1.5 mM.

204

carbon paste modified electrodes were utilised.

The short-term stability of the RuO_2-CPE in the flow system was investigated. A series of 60 repeated injections of 0.1 mM streptomycin, over a 110min period yielded a mean current of 62.5 nA with a relative standard deviation of 3.1%, demonstrating the stability of these electrodes for the oxidation of these drugs in flowing streams.

The current-concentration profile of novobiocin at the RuO_2-CPE is shown in Figure 4.18. Excellent linearity was observed over the 0 - 1.5 mM concentration range, with a slope of 52 nA mmol^{-1} (correlation coefficient of 0.998). Detection limits (S/N=3) of 8 μM and 60 μM were calculated for streptomycin and novobiocin, respectively, under the conditions used here.

The results reported above indicate that the RuO_2- based modified electrodes may be used for the LCEC determination of saccharide antibiotic levels. Future applications of these electrodes in the LCEC separation and detection of carbohydrates, alcohols and various other components, such as the saccharide antibiotics, are envisaged.

4.4. MECHANISTIC ASPECTS OF OXIDATION AT RUO$_2$-CMEs

The approximate relative responses of the alcohols normalised to the glucose response (from reference 13) at the RuO$_2$-modified electrodes in flowing 1.0 M NaOH solutions with constant-potential detection at +0.4 V are listed in Table 4.2. The normalised responses for the saccharide antibiotics are not given because of the slightly different conditions used for their detection, namely a lower NaOH concentration and lower operating potentials. These variations would make the detection limits for the antibiotics higher than if the conditions used for alcohol detection were utilised. However, in general, the normalised response of the saccharide antibiotics can be considered to be approximately 30-50% that of the glucose response based on comparison of the detection limits obtained for the alcohols and the drugs. Although the exact electrocatalytic mechanism of the RuO$_2$-based electrodes remains to be elucidated, some relevant parameters can be gathered from the data shown in Table 4.2.

The effect of hydroxyl group number on the electrocatalytic response is evident from a comparison of the response obtained for the alcohols. The response increases upon increasing number of the hydroxyl groups, as seen from comparison of the responses of methanol, ethylene glycol and glycerol. The significant difference in the response obtained for ribose and deoxyribose also indicates the important role of hydroxyl groups in the electrocatalytic reaction. The position of the hydroxyl group also greatly affects the electrocatalytic response, with no response obtained for t-butanol, 2-butanol or 2-propanol, while 1-propanol can be detected at these electrodes. Comparison of the relative responses of 1,3-propanediol and ethylene glycol also gives an indication of the effect the hydroxyl group position has on the signal magnitude. Finally, the carbon chain length or substrate size also appears to play a role in determining the magnitude of the electrocatalytic response. A

206

Table 4.2: Flow injection responses of RuO_2-modified carbon
paste electrodes to various hydroxy-containing compounds.

Compound	% response with respect to glucose
glucose	100
galactose	87
ribose	96
deoxyribose	20
maltose	64
sucrose	20
glycerol	22
ethylene glycol	11
1,3-propanediol	4.5
methanol	2.3
ethanol	1.2
1-propanol	0.8
2-propanol	negligible
1-butanol	0.4
2-butanol	negligible
t-butanol	negligible

significant decrease in activity of the RuO_2-modified
electrodes towards oxidation of longer chain alcohols is evident
from a comparison of the responses obtained for methanol,
ethanol, 1-propanol and 1-butanol. Decreases in response of
these electrodes to the oxidation of disaccharides as compared
to monosaccharide oxidation is also apparent with steric
hindrance of the more bulky sugars likely affecting the
sensitivity [13]. This steric hindrance effect is also evidently
important in the detection of the antibiotics reported in the
previous section, with the more bulky neomycin yielding reduced

207

sensitivity compared to either streptomycin or novobiocin. Similar dependences on hydroxyl group number and position have been reported for alcohol and carbohydrate oxdations at Cu-modified glassy carbon electrodes [82,83].

The response for all of the compounds described above, as reported for other metal electrodes, is strongly dependent on the hydroxide ion concentration (see section 4.2.3.2.). This is probably because of the postulated mechanism of oxidiation at these electrodes. Burke's group have maintained that methanol oxidation, which is catalytically mediated in a heterogeneous manner by the perruthenate species, involves the adsorption of hydroxy radical species on the metal oxide. The mechanism presented below is based on this groups work, and assumes that the chemical reaction between the surface species and the alcohol, rather than electron transfer, is the rate–determining step.

$$H_2O === OH_{ads} + e^- \qquad\qquad (4.9)$$

$$RCH_2OH + OH_{ads} === RCHO + H_3O^+ + e^- \qquad (4.10)$$
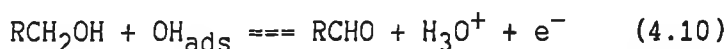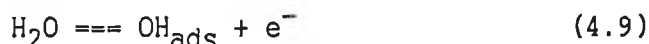
Further steps involving the oxidation of the aldehyde to the carboxylic acid and carbon dioxide may also occur. This group, and other workers, have reported findings similar to that in Table 4.2 [9,13,82,83]. Burke and Healy [9] observed that perruthenate was active in the presence of peroxodisulphate towards oxidation of primary and secondary alcohols but did not oxidise t-butanol.

4.5   CONCLUSIONS

In conclusion, the RuO_2-modified electrodes have been shown to be capable of electrocatalytically oxidising species such as alcohols, carbohydrates and selected antibiotics, which can not be oxidised at common bare carbon electrodes. The electrocatalytically active species at the electrode surface is proposed to be electrochemically generated RuO_4^-. The electrodes therefore only operate at high, extremely basic, pH where this species can be formed. Although the mechanistic details of the electrocatalytic reaction are unclear, the RuO_2-modified carbon paste or graphite-epoxy electrodes have been shown to yield highly stable, reproducible responses for the various analytes. In the case of the graphite-epoxy modified electrodes, it has been demonstrated that reproducible repsponses could also be obtained after polishing of the electrode surface, thus leading to a polishable, renewable modified electrode. Future application of these RuO_2-modified electrodes in the routine detection of the various alcohols, carbohydrates and other hydroxylated species following prior chromatographic separation is envisaged.

4.6. REFERENCES

1. S. Trasatti and W.E. O'Grady, _Advances in Electrochemistry and Electrochemical Engineering_, H. Gerischer and C.W. Tobias (Eds.), Wiley, New York (1981), _Vol 12_, 177.

2. D.M. Novak, B.V. Tilak and B. E. Conway, _Modern Aspects of Electrochemistry_, J.O.M. Bockris and B.E. Conway (Eds.), Plenum Press, New York (1982), _Vol 14_, 195.

3. S. Trasatti and G. Lodi, _Electrodes of Conductive Metallic Oxides_, S. Trasatti (Ed), Elsevier, Amsterdam (1980), _Part A_, Chapter 7, 301.

4. S. Trasatti, _Electrochim. Acta_, (1987), _32_, 369.

5. H.D. Beer, _South African Pat._ 662,667 (1966); 680,034 (1968).

6. R.S. Yeo, J. Orehotsky, W. Visscher and S. Srinivisan, _J. Electrochem. Soc._, (1981), _128_, 1900.

7. G. Lodi, E. Sivieri, A De Batisti and S. Trasatti, _J. Appl. Electrochem._, (1978), _8_, 135.

8. E.J.M. O'Sullivan and E.J. Calvo, _Comprehensive Chemical Kinetics_, R.G. Compton (Ed), (1987), _Vol 27_, 247.

9. L.D. Burke and J.F. Healy, _J. Electroanal. Chem._, (1981), _124_, 327.

10. E.J.M. O'Sullivan and J.R. White, _J. Electrochem. Soc._, (1989), _136_, 2576.

11. L.D. Burke and O.J. Murphy, _J. Electroanal. Chem._, (1979), _101_, 351.

12. P.K. Ghosh, A.W.-H. Mau and A.J. Bard, _J. Electroanal. Chem._, (1984), _169_, 315.

13. J. Wang and Z. Taha, _Anal. Chem._, (1990), _62_, 1413.

14. S. Ardizzone, A. Carugati, G. Lodi and S. Trasatti, _J. Electrochem. Soc._, (1982) _129_, 1689.

15. S. Trasatti and G. Lodi, _Electrodes of Conductive Metallic Oxides_, S. Trasatti (Ed), Elsevier, Amsterdam (1981), _Part B_, 521.

16. J.B. Cotton and P.C.S. Hayfield, _Brit_, (1971), _1_, 408.

17. S. Pizzini, G. Buzzanca, C. Mari, L. Rossi and S. Torchio, Mat. Res. Bull., (1972), 7, 449.

18. G. Lodi, C. Bighi and C deAsmundis, Mater. Chem., (1976), 1, 177.

19. K. Doblhofer, M. Metikos, Z. Ogumi and H. Gerischer, Ber. Bunsenges. Phys. Chem., (1978), 82, 1046.

20. D. Gallizoli, F. Tantardini and S. Trasatti, J. Appl. Electrochem., (1974), 4, 57.

21. G. Laule, R. Hawk and D. Miller, J. Electroanal. Chem., (1986), 213, 329.

22. L.D. Burke and D.P. Whelan, J. Electroanal. Chem., (1979), 103, 179.

23. L.D. Burke and M.E.G. Lyons, Modern Aspects of Electro-chemistry, R.E. White, J.O.M. Bockris and B.E. Conway (Eds.), Plenum Press, New York, (1986), Vol. 18, 169.

24. V. Birss, R. Myers, H. Angerstein-Kozlowska and B.E. Conway, J. Electrochem. Soc., (1984), 131, 1502.

25. L.D. Burke and K.J. O'Dwyer, Electrochim. Acta, (1989), 34, 1659.

26. A Hamnett and B.J. Kennedy, Electrochim. Acta, (1988), 33, 1613.

27. T. Hepel, F.H. Pollak and W.E. O'Grady, J. Electrochem. Soc. , (1984), 131, 2094.

28. T. Hepel, F.H. Pollak and W.E. O'Grady, J. Electrochem. Soc. , (1986), 133, 69.

29. S.R. Butler and J.L. Golson, Mat. Res. Bull., (1971), 6, 81.

30. D. Gallizoli, F. Tantardini and S. Trasatti, J. Appl. Electrochem., (1975). 5, 203.

31. K.W. Lam, K.E. Johnson and D.G. Lee, J. Electrochem. Soc., (1978), 125, 1069.

32. L.D. Burke and O.J. Murphy, J. Electroanal. Chem., (1980), 109, 199.

33. A Bandi, J. Electrochem. Soc., (1990), 137, 2157.

34. L.D. Burke, O.J. Murphy and J.F. O'Neill, J. Electroanal.

Chem., (1977), 81, 391.

35. L.D. Burke and O.J. Murphy, J. Electroanal. Chem., (1979), 96, 19.

36. L.D. Burke and O.J. Murphy, J. Electroanal. Chem., (1980), 112, 39.

37. G. Lodi, G. Zucchini, A. deBatisti, E. Sivieri and S. Trasatti, Mater. Chem., (1978), 3, 179.

38. T.Y. Safonova, O.A. Petrii and E.A. Gudkova, Elektrokhim-iya, (1980), 16, 1607.

39. L.D. Burke and M. McRann, J. Electroanal. Chem., (1981), 125, 387.

40. L.D. Burke, M.E.G. Lyons, E.J.M. O'Sullivan and D.P. Whelan, J. Electroanal. Chem., (1981), 122, 403.

41. L.D Burke, O.J. Murphy, J.F. O'Neill and S. Venkatesan, J. Chem. Soc., Faraday Trans. 1, (1977), 73, 1659.

42. W.E. O'Grady, C Iwakura, J. Huang and E. Yeager, Electrocatalysis, M.W. Breiter (Ed.), Electrochemical Society, Princeton, NJ, (1974), 286.

43. M.W. Shafer, R.A. Figat, R. Johnson and R.A. Pollack, Extended Abstracts 30th ISE Meeting, Trondheim, (1979), 313.

44. A. Nidola, Electrodes of Conductive Metallic Oxides, S. Trasatti (Ed), Elsevier, Amsterdam (1981), Part B, 627.

45. I.R. Burrows, D.A Denton and J.A Harison, Electrochim. Acta, (1978), 23, 493.

46. B.E. Conway and D. M. Novak, J. Electroanal. Chem., (1979), 99, 133.

47. R.T. Atanasoski, B.Z. Nikolic, M.M. Jaksie and A.R. Despic, J. Appl. Electrochem., (1975), 5, 155.

48. B.V. Tilak, J. Electrochem. Soc., (1979), 126, 1343.

49. D.A. Denton, J.A. Harrison and R.I. Knowles, Electrochim. Acta, (1979), 24, 521.

50. L.J.J. Janssen, L.M.C. Starmans, J.G. Visser and E. Barendrecht, Electrochim. Acta, (1977), 22, 1093.

51. I.E. Veselovskaya, E.K. Spasskaya, V.A. Sokolov, V.I.

Tkachenko and L.M. Lakimenko, <u>Elektrokhimiya</u>, (1974), <u>10</u>, 70.

52. A.T. Kuhn and C.J. Mortimer, <u>J. Electrochem. Soc.</u>, (1973), <u>120</u>, 231.

53. S.V. Evdokimov, V.V. Gorodetskii and V.V. Losev, <u>Elektrokhimiya</u>, (1985), <u>21</u>, 1427.

54. V.V. Losev, <u>Elektrokhimiya</u>, (1981), <u>17</u>, 733.

55. G. Faira and G. Fiori, <u>J. Electrochem. Soc.</u>, (1973), <u>120</u>, 1702.

56. T. Arikado, C Iwakura and H. Tamura, <u>Electrochim. Acta</u>, (1978), <u>23</u>, 9.

57. R.G. Erenburg, L.I. Krishtalik and N.P. Rogozhina, <u>Elektrokhimiya</u>, (1984), <u>20</u>, 1183.

58. E.K. Spasskaya, Y.B. Makarychev, A.A. Yakovleva and L.M. Yakimenko, <u>Elektrokhimiya</u>, (1977), <u>13</u>, 327.

59. E.A. Kalinovskii, R.U. Bondar and N.N. Meshkova, <u>Elektrokhimiya</u>, (1972), <u>8</u>, 1468.

60. L.D. Burke and J.F. O'Neill, <u>J. Electroanal. Chem.</u>, (1979), <u>101</u>, 341.

61. D.G. Lee. M. van der Engh, <u>Oxidation in Organic Chemisrtv</u>, W.S. Trahanowsky (Ed.), Academic Press, London (1973), <u>Vol. B</u>, 177.

62. M. Schroder and W.P. Griffith, <u>J. Chem. Soc.. Chem. Commun.</u>, (1979), 58.

63. W.P. Griffith, S.V. Ley, G.P. Whitcombe and A.D. White, <u>J. Chem. Soc.. Chem. Commun.</u>, (1987) 1625.

64. W.P. Griffith and S.V. Ley, <u>Aldrichim. Acta</u>, (1990), <u>23</u>, 13.

65. W.P. Griffith, J.M. Joliffe, S.V. Ley and D.J. Williams, <u>J. Chem. Soc.. Chem. Commun.</u>, (1990), 1219.

66. L.D. Burke and J.F. Healy, <u>J. Chem. Soc.. Dalton Trans.</u>, (1982), 1091.

67. F. Kaneda, S. Haruna, T. Imanaka and K. Kawamoto, <u>J. Chem. Soc.. Chem. Commun.</u>, (1990), 1467.

68. J.A.R. van Veen, J.M. van der Eijk, R. de Ruiter and S.

Huizinga, Electrochim. Acta, (1988), 33, 51.

69. H.H. Horowitz, H.S. Horowitz and J.M. Longo, Electrocatalysis, W.E. O'Grady, P.N. Ross, Jr. and F.G. Will (Eds.), Electrochemical Society, Pennington, NJ (1982), 285.

70. M. Watanabe and S. Motoo, J. Electroanal. Chem., (1975), 60, 267.

71. B.J. Kennedy and A.W. Smith, J. Electroanal. Chem., (1990), 293, 103.

72. S. Hughes, P.L. Meschi and D.C. Johnson, Anal. Chim. Acta, (1982), 132, 1.

73. S. Hughes and D.C. Johnson, Anal. Chim. Acta, (1981), 132, 11.

74. S. Hughes and D.C. Johnson, Anal. Chim. Acta, (1983), 149, 1.

75. G.G. Neuberger and D.C. Johnson, Anal. Chem., (1987), 59, 203.

76. G.G. Neuberger and D.C. Johnson, Anal. Chem., (1987), 59, 150.

77. D.S. Bindra and G.S. Wilson, Anal. Chem., (1989), 61, 2566.

78. M. Fleischmann, K. Korinek and D. Pletcher, J. Electroanal. Chem., (1971), 31, 39.

79. K.G. Schick, V.G. Magearu and C.O. Huber, Clin. Chem., (1978), 24, 448.

80. T.N. Morrison, K.G. Schick and C.O. Huber, Anal. Chim. Acta, (1980), 120, 75.

81. R.E. Reim and R.M. van Effen, Anal. Chem., (1986), 58, 3203.

82. S.V. Prahbu and R.P. Baldwin, Anal. Chem., (1989), 61, 852.

83. S.V. Prahbu and R.P. Baldwin, Anal. Chem., (1989), 61, 2258.

84. G.G. Guilbault and G.J. Lubrano, Anal. Chim. Acta, (1974), 69, 189.

85. E.L. Gulberg and G.D. Christian, Anal. Chim. Acta, (1981), 123, 125.

86. H. Belghith, J.L. Romette and D. Thomas, Biotech. and Bioeng., (1987), 1001.

87. W.W. Kubiak and J. Wang, Anal. Chim Acta, (1989), 221, 43.

88. Y. Kitigawa, K. Kitibatake, I. Kubo, E. Tamiya and I. Karube, Anal. Chim. Acta, (1989), 218, 61.

89. E. Laviron and L. Roullier, J. Electroanal. Chem., (1980), 115, 65.

90. P.J. Kulesza, J. Electroanal. Chem., (1987), 220, 295.

91. L.M. Santos and R.P. Baldwin, Anal. Chem., (1987), 59, 1766.

92. G.B. Levy, P. Schwed and J.W. Sackett, J. Am. Chem. Soc., (1946), 68, 528.

93. L. Doan and B.E. Reidel, Can. Pharm. J. Sci., (1963), 96, 109.

94. H. Siegerman, Electroanalytical Chemistry, A.J. Bard (Ed.), M. Dekker, New York (1979), Vol. 11, 291.

95. J. Wang and J.S. Mahmoud, Anal. Chim. Acta, (1986), 186, 31.

96. H. Siegerman, J.B. Flato and G.W. O'Dom, Automation in Microbiology and Immunology, C.G. Heden and T. Illeni (Eds.), Wiley, New york (1975), 306.

97. J. Wang, T. Golden, K. Varughese and I. El-Rayes, Anal. Chem., (1989), 61, 508.

98. J. Wang and K. Varughese, Anal. Chem., (1990), 62, 318.

99. S.A. Wring, J.P. Hart and B.J. Birch, Analyst, (1989), 114, 1563.

100. S.A. Wring, J.P. Hart and B.J. Birch, Analyst, (1989), 114, 1571.

101. B.R. Shaw and K.E. Creasy, J. Electroanal. Chem., (1988), 243, 209.

102. B.R. Shaw and K.E. Ceasy, Anal. Chem., (1988), 60, 1241.

103. J.Park and B.R. Shaw, Anal. Chem., (1989), 61, 848.

215

CHAPTER 5

The Development and Application of Some

Novel Glucose Sensors

216

5.1. INTRODUCTION

Because of the clinical and industrial significance of measuring glucose levels, the development of biosensors for glucose detection continues to attract considerable interest. This chapter deals with the development of two biosensors for glucose detection. Firstly, however, the term "biosensor" has to be explained and qualified. A review of recent literature on the various methods available for the amperometric sensing of glucose will then be presented.

The term "biosensor", as it is widely used in the scientific literature today, can represent two different, partly overlapping, categories of sensors. In the first category the term "bio" refers to the field of application of the sensor. For instance, sensors that are used in clinical analysis, in physiological and pharmacological studies or in other areas of experimental life science are all biosensors of the first category. In biosensors belonging to the second category, the operation of the sensor involves a biological or biochemical recognition process directly linked to a transducer. Sensors based on enzymes, tissues or immunochemicals are part of this category. Nagy and Pungor [1] have recently offered a means of separating these two categories. These workers have designated sensors of the first category as "biomatrix sensors", while those of the second category have been termed as "biomimetic sensors".

The first section of this chapter involves the use of a RuO_2-modified electrode for the detection of glucose. This electrode is thus an example of a biomatrix sensor, and the application of glucose sensors of this type is reviewed.

The second section of the chapter concerns the development of a novel and simple, one-step fabrication method of an amperometric enzyme electrode for glucose and is thus an example of a biomimetic sensor. The application of such enzyme-based sensors for glucose will also be reviewed.

217

5.1.1. Biomatrix Sensors for Glucose

Amperometric biomatrix sensors for glucose are generally developed so that the analyte is oxidised directly at solid electrode surfaces. The voltammetric response for glucose at carbon electrodes is limited by the rather large overvoltage associated with its oxidation at these electrode surfaces. Various other electrode materials have thus been investigated for their application in this area. The most relevant electrode materials used for the direct electrochemical detection of glucose are gold and platinum [2-7]. Oxidation of glucose at these electrodes results, however, in the poisoning of the electrode surface. Thus a stable response at these electrodes is only obtained if appropriate potential cycles are utilised to clean and condition the electrodes between sensing intervals. This usuallly involves the use of a dual or triple-pulse potential waveform involving oxidative cleaning of adsorbed marterial with subsequent reductive removal of the oxide layer. The use of electrocatalytic chemically modified electrodes for the detection of glucose has also been described. Santos and Baldwin [8] have utilised a cobalt phthalocyanine-modified carbon paste electrode for the detection of picomolar levels of carbohydrates. This electrode requires a pulsed potential waveform similar to that of the gold and platinum electrodes in order to obtain reproducible signals.

Nickel or copper electrodes [9-14] are also capable of oxidising glucose at low potentials and have been used for the direct electrochemical detection of glucose and other carbohydrates using a constant-potential waveform. A recent alternative modified electrode for carbohydrate detection has been described by Wang and Taha [15]. A carbon paste electrode modified with ruthenium dioxide was utilised for flow injection analysis of various carbohydrates. This electrode has been shown to be effective in the detection of alcohols and various saccharide antibiotics [Chapter 4]. An investigation into the

218

application of this modified electrode as a biosensor for
glucose was therefore undertaken.

5.1.2. Biomimetic Sensors for Glucose

Biocomponents, which function as biochemical recognition
systems in biomimetic sensors, can be as varied as enzymes,
tissues, bacteria, yeast, antibodies/antigens, organelles or
receptors [16]. A typical biomimetic sensor configuration is
shown in Figure 5.1. The biomimetic configurations which have
received the greatest attention to date are electrochemical
(amperometric) transducers used in conjunction with enzymes.
Enzyme electrodes were the earliest biomimetic sensors reported
in the literature [17,18] and have been the first to be
developed to the stage of a commercially available product [19].
The most studied system involving enzyme electrodes is the
assay of glucose using glucose oxidase (GOD):

$$\text{glucose} + O_2 \xrightarrow{\text{GOD}} \text{gluconolactone} + H_2O_2 \quad (5.1)$$
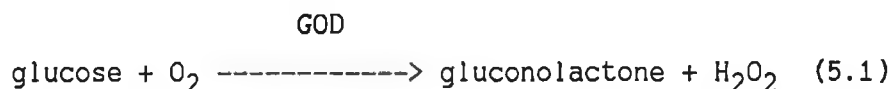
The change in the concentration of oxygen may be monitored using
a Clark oxygen electrode. Alternatively, the change in hydrogen
peroxide concentration can be monitored by following its
oxidation at a platinum electrode as shown below.

$$H_2O_2 \xrightarrow{\hspace{2cm}} O_2 + 2\ H^+ + 2\ e^- \quad (5.2)$$
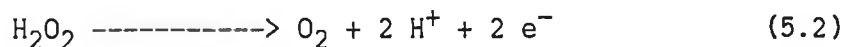
In this section, the three most important aspects in the design
and operation of a biomimetic biosensor will be reviewed. These
are: immobilisation of the enzyme/biocomponent, enhancement of
the electrode response and prevention of interferences and
electrode fouling. The application of amperometric enzyme
electrodes have been reviewed previously by several authors
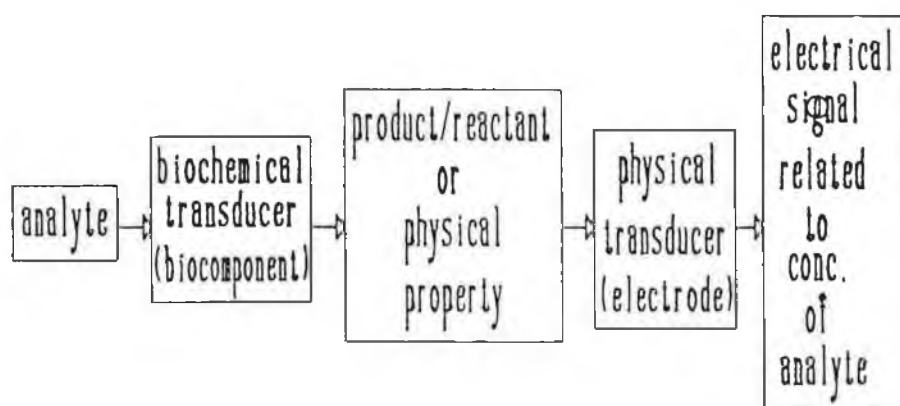[16,20-23].

219

Figure 5.1: Schematic diagram of a biomimetic biosensor.

5.1.2.1. Immmobilisation of Biocomponents

Immobilised enzymes confined to an electrode surface offer attractive advantages over utilising solution species [16]. An immobilised enzyme can de readily separated from the reaction mixture and can be reused. Other properties such as increased stability, high sensitivity, fast response, high sampling rate (in flow injection applications), and prevention of interferences or electrode fouling can also be achieved with immobilised enzyme electrodes. The most common methods of enzyme immobilisation include adsorption, covalent attachment, gel/polymer entrapment and crosslinking. Combinations of these methods are also used to enhance electrode stabilities and activities.

Physical adsorption of the enzyme on the electrode is a popular technique [16,20]. However, several disadvantages such as greater susceptibility to pH, temperature and ionic strength changes and leaching of the enzyme from the surface are associated with this technique. Ikariyama et al. [24] have shown that the platinisation of platinum, to form platinum black, provides a good substrate for adsorption of enzymes. A thin film can be made by crosslinking with glutaraldehyde and bovine serum albumin (BSA). Ikeda et al. [25] have adsorbed GOD onto the surface of carbon paste electrodes and have covered this with a thin film of nitrocellulose to enhance stability. Gorton et al. [26] have shown that the order of adsorption of the mediator, Meldola blue, and the enzyme can affect the electrode response. When the mediator is adsorbed first, a greater response to glucose is observed in comparison to when the enzyme is adsorbed first. Several workers have examined the use of a carbon paste matrix for the immobilisation of enzymes [27-30]. Graphite paste electrodes containing GOD have been developed for use in flow injection systems [27], while an amperometric biosensor for glucose has been constructed using carbon paste modified with GOD and a ferrocene mediator (1,1'-dimethylferrocene) [30].

221

Covalent attachment of an enzyme to an electrode surface provides a more stable sensor than adsorption. The attachment involves several stages, including activation of the support, enzyme coupling and removal of unbound enzyme [16,20]. Activation of the support is usually accomplished with chemicals such as silanes [31] or cyanuric chlorides [32]. Pretreatment of platinum electrodes also has an effect on the covalent attachment of enzymes [33,34]. Thomas et al. have studied the differences in electrodes formed with covalent attachment to anodised platinum and platinum black and thermally oxidised platinum electrodes [33,34]. Anodised platinum black proved to be superior to platinum due to increased available surface areas for silanisation. Narasimhan and Wingard [35] have reported a method for the covalent attachment of GOD which uses an (aminophenyl)boronic acid-modified glassy carbon electrode as support. Yacynych et al. [36] have covalently attached GOD to the surface of anodised reticulated vitreous carbon (RVC) and have used this electrode for the flow-through detection of glucose. GOD has also been immobilised by covalent attachment to a polypyyrole modified electrode via a carbodiimide activation of the enzyme with subsequent attachment to the functionalised amino groups of the polypyrrole [37].

By far the most popular technique is the use of gel/polymer entrapment. Most enzymes can be easily incorporated into several different polymers, with the entrapment being improved by using other immobilisation techniques such as crosslinking. Foulds and Lowe [38] have developed an interesting immobilisation method based on the coimmobilisation of GOD and polypyyrole onto a platinum electrode using electropolymerisation. The important aspect of this method is that redox mediators [39] or platinum microparticles [40] may also be entrapped in the polypyyrole thus leading to enhanced responses for glucose. The electropolymerisation of aniline in the presence of GOD has also been shown to be an effective means for immmobilisation of the enzyme [41]. The polyaniline film also helps protect the

222

electrode surface from interferences. O-phenylenediamine has been used for GOD immobilisation on platinum electrodes by electrochemical polymerisation [42]. This procedure produced a glucose sensor with a response time of less than 1 s and also offered favourable rejection of interferences such as ascorbate.

Physical adsorption and gel/polymer entrapment are often supplemented with crosslinking to prevent leaching of the enzyme. Crosslinking alone can also be used for the immobilisation of enzymes [16]. The most popular method is to create enzyme membranes, by employing bifunctional agents, which can crosslink the enzyme to either the gel/polymer, other species or the electrode surface. The difficulty associated with this method is that several factors must be controlled, including pH, ionic strength, temperature and reaction time. In addition, the thickness and glutaraldehyde content of the crosslinked membranes can also have an effect on sensor response [16]. Many researchers have been using crosslinking agents along with BSA to create enzyme membranes [43-45]. The use of BSA is believed to allow more inter-molecular bonding and less crowding of the enzyme. Most of the methods used are modification of a procedure developed by Mascini and Guilbault [46]. Crosslinked membranes may be attached to the electrode surface by covalent attachment or adsorption. Covalent attachment can be achieved through procedures similar to that developed by Yao [47], where a bifunctional agent can crosslink the enzyme and attach it to the activated electrode surface.

5.1.2.2. Enhancement of Response at Enzyme Electrodes

Enhancement of the electrode response has taken a variety of forms. Electron mediators can be used to shuttle electrons between the electrode and a species which is difficult to electrolyse directly, such as hydrogen peroxide or NADH. The emergence of new electrode materials, such as the organic metals, can also improve electron tansfer. Direct electron

223

transfer is the most elegant approach, but has yet to reach its full capability.

The GOD enzyme electrode system normally relies upon oxygen to act as an electron acceptor to recycle the the enzyme after conversion of substrate to product, as shown in Figure 5.2. This limits biosensor operation at the higher substrate levels as oxygen may not be sufficiently soluble in the electrolyte. One approach to alleviate this problem is to replace oxygen with an artificial mediator for electron transfer. This approach has been used successfully, with a ferrocene derivative as the mediator, in a range of applications [48-53]. Green and Hill [54] have noted that positively charged ferrocenes are better mediators for GOD than negatively charged ones. Several approaches have been devised for the immobilisation of these mediators, but will not be dealt with here. Other mediators which have been successfully used include quinones [55], ruthenium amines [56], octacyanotungstates [57] and Meldola blue [26,58]

Another approach is to use organic metals as mediators, or as the electrode material itself. The mechanism of the reaction of the enzyme at the organic metal electrodes is not well understood [59-61], but it is believed that mediation, accomplished by the dissociated ions of the organic metal, and direct electron transfer from the GOD($FADH_2$) enzyme can both occur. Organic metal electrodes made from N-methylphenazinium (NMP^+) and tetracyanoquinodimethanide ($TCNQ^-$) or tetra thiafulvalinium (TTF^+) and $TCNQ^-$ salts are useful for the oxidation of both NADH and GOD [59, 62-64].

Direct electron transfer between an enzyme and the electrode is the most elegant approach for biosensors, because of its directness and simplicity. Studies by Hill [65], Degani and Heller [66-68], and others [53,69,70], have shown that direct oxidation of the flavin centre of GOD at unmodified electrodes can be achieved if the enzyme is first modified by the covalent attachment of electron shuttles, such as ferrocenes.
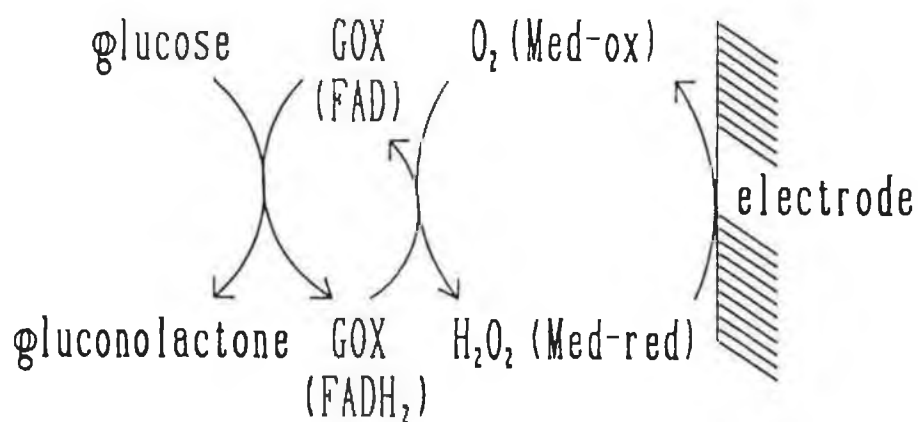
224

Figure 5.2: Example of an oxidoreductase enzyme process showing
the possible substitution of oxygen (O_2) by a mediator (Med),
where GOX(FAD) and GOX(FADH$_2$) represent the oxidised and
reduced forms of the flavin prosthetic group of the glucose
oxidase enzyme, respectively.

225

5.1.2.3. Prevention of Interferences and Electrode Fouling

Electrodes can be protected by several procedures, including chemical removal of interferences, and the use of polymer films as barriers. Polymer films have emerged as the predominant method, because they provide both protection from fouling and interferences. Fouling of the electrode surface by the adsorption of matrix species, such as proteins, is a major problem in the analysis of biological samples. Protection against electroactive interferences is more difficult to achieve than protection against fouling due to their lower relative molecular weights. The combination of electrode fouling and interferences are a major challenge in the design of a successful biosensor.

Chemical removal of interferences can sometimes be achieved, although the best operating conditions will always be a compromise for each enzyme used in these multi-enzyme systems. Wollenberger et al. [71] have demonstrated a laccase/GOD system which allows for the elimination of up to 20 mM ascorbic acid.

Polymer films have the advantage of usually providing protection from both fouling and interferences. Polymer films have also been known to increase the stability of the immobilised enzyme. Cellulose acetate coating of platinum electrodes [72,73] is a common way to eliminate protein adsorption and interferences, as is the use of polyurethane or polypropylene dialysis membranes. Electrostatic repulsion of anionic interfering species can be achieved with electrodes modified with a Nafion polymer layer [8,74,75] or alternative perfluorosulfonic acid polymers [58,76] or other polymer layers [77]. These membranes are normally applied to the surface of a membrane that contains the enzyme and thus lead to practical difficulties in controlling film thicknesses and substrate diffusion. Recently, a glucose biosensor composed of GOD immobilised in electropolymerised poly(o-phenylenediamine), has been shown to be effective as a protection from fouling and

226

interferences [42]. This system is the first sensor based on a one-step fabrication technique, where the polymer layer performs the functions of enzyme immobilisation and protection from fouling and interferences. In this Chapter, an alternative method for the one-step fabrication of a glucose sensor is demonstrated. This fabrication method is simpler than that of electropolymerisation, does not denature the enzyme, and proves to be a convenient, fast and simple technique to prepare stable reproducible glucose sensors.

5.2. RUTHENIUM DIOXIDE-MODIFIED GRAPHITE-EPOXY ELECTRODE FOR THE DETECTION OF GLUCOSE

The application of RuO_2-modified carbon paste electrodes in the electrocatalytic oxidation of alcohols and various other hydroxy-containing species was demonstrated in chapter 4. The enhanced stability and applicability of this modifier, upon incorporation into a graphite-epoxy electrode matrix, was also demonstrated.

The aim of the present study was to illustrate the application of the RuO_2-modified graphite-epoxy electrodes in the detection of glucose. Attempts to lower the NaOH concentration, and pH, required for the electrocatalytic reaction to occur are also presented. Selective detection of glucose at these modified electrodes was attempted by the application of various polymer films to the electrode surface.

5.2.1. EXPERIMENTAL

5.2.1.1. Apparatus

The apparatus used for both the batch and flow experiments has been described previously in section 4.3.1.1.

5.2.1.2. Reagents and Procedures

RuO_2-modified graphite-epoxy electrodes were prepared as described previously in section 4.2.1.2.

All solutions were prepared from doubly-distilled deionised water. Standard solutions of glucose (Sigma) were prepared fresh daily in the 0.5 M NaOH electrolyte.

All potentials are quoted with respect to the Ag/AgCl reference electrode.

228

5.2.2. RESULTS AND DISCUSSION

5.2.2.1. Voltammetry

Preliminary experiments, to confirm the retention of electrocatalytic activity of the RuO_2-modified electrodes, were performed using cyclic voltammetry. Typical cyclic voltammograms obtained with the RuO_2-modified electrodes, in 0.5 M NaOH electrolyte, both with and without added glucose (solid and broken lines, respectively) are shown in Figure 5.3. Similar profiles to those shown in chapter 4 were observed, with peak potentials of +0.40 V (anodic) and +0.35 V (cathodic) obtained for the ruthenate/peruthenate transition, in this electrolyte. The RuO_2-modified electrodes exhibited classic electrocatalytic behaviour, with an increase in anodic and a decrease in cathodic peak currents, upon addition of glucose to the cell, as seen for the RuO_2-modified carbon paste and graphite-epoxy electrodes for alcohol detection, discussed in chapter 4. These currents were extremely stable with no apparent decrease upon extended cycling over a 60 min period, illustrating the highly stable nature of both the modifying matrix and modifier.

5.2.2.2. Amperometry

The effect of the RuO_2 loading within the graphite epoxy matrix on the response to glucose was investigated by constant-potential (+0.35 V) batch additions of 1 mM glucose levels to a stirred (400 rpm) cell. The current-time profiles observed at the 5(a), 10(b) and 20% w/w (c) RuO_2-modified graphite-epoxy electrodes are shown in Figure 5.4. Also shown (inset) is the corresponding current-loading curve determined for these modified electrodes. A similar, linear correlation between response and RuO_2 loading in the electrode matrix, was observed at RuO_2-modified carbon paste electrodes [15] used
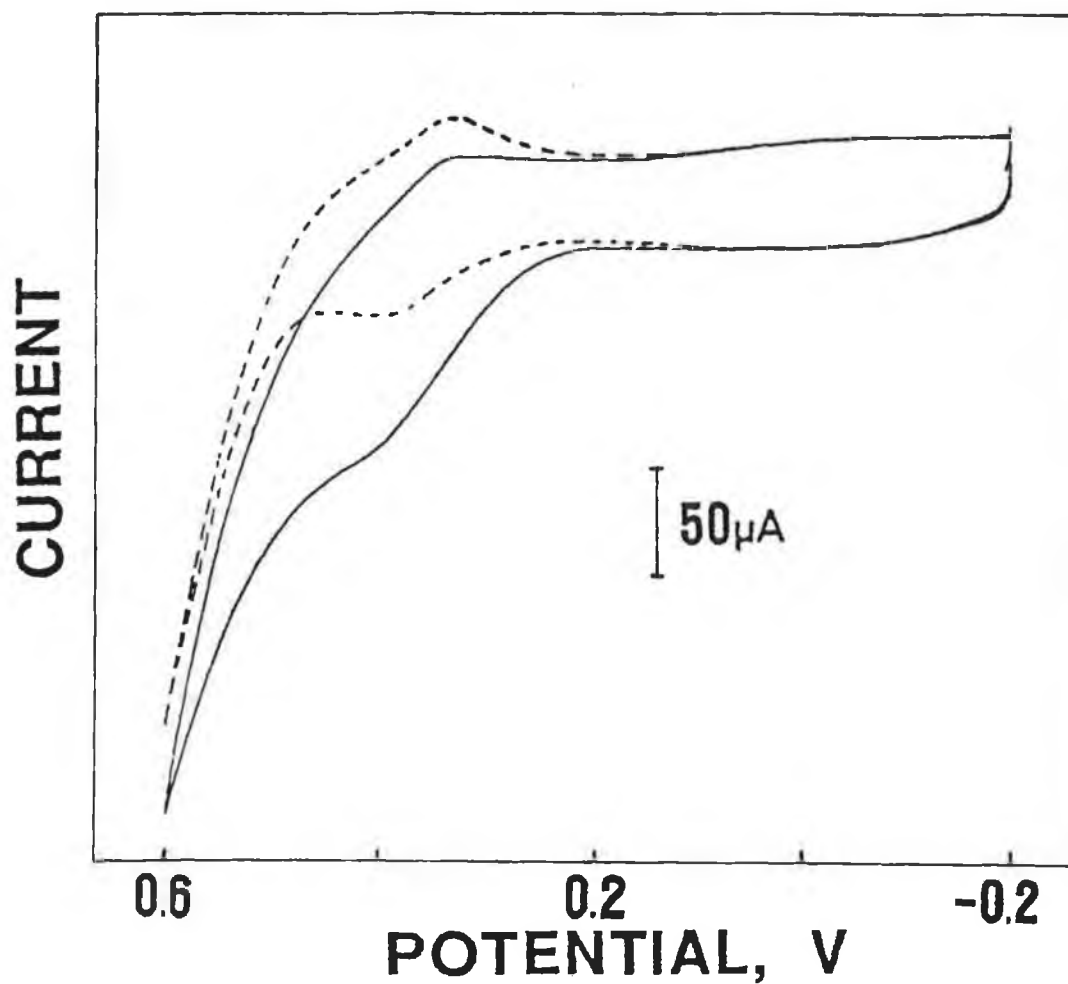
Figure 5.3: Cyclic voltammograms at the 20% w/w RuO$_2$-modified electrode. Dotted line represents the blank 0.5 M NaOH solution response. Solid line represents the voltammetric response upon addition of 2.5 mM glucose to the cell. Scan rate of 20 mV s^{-1}.
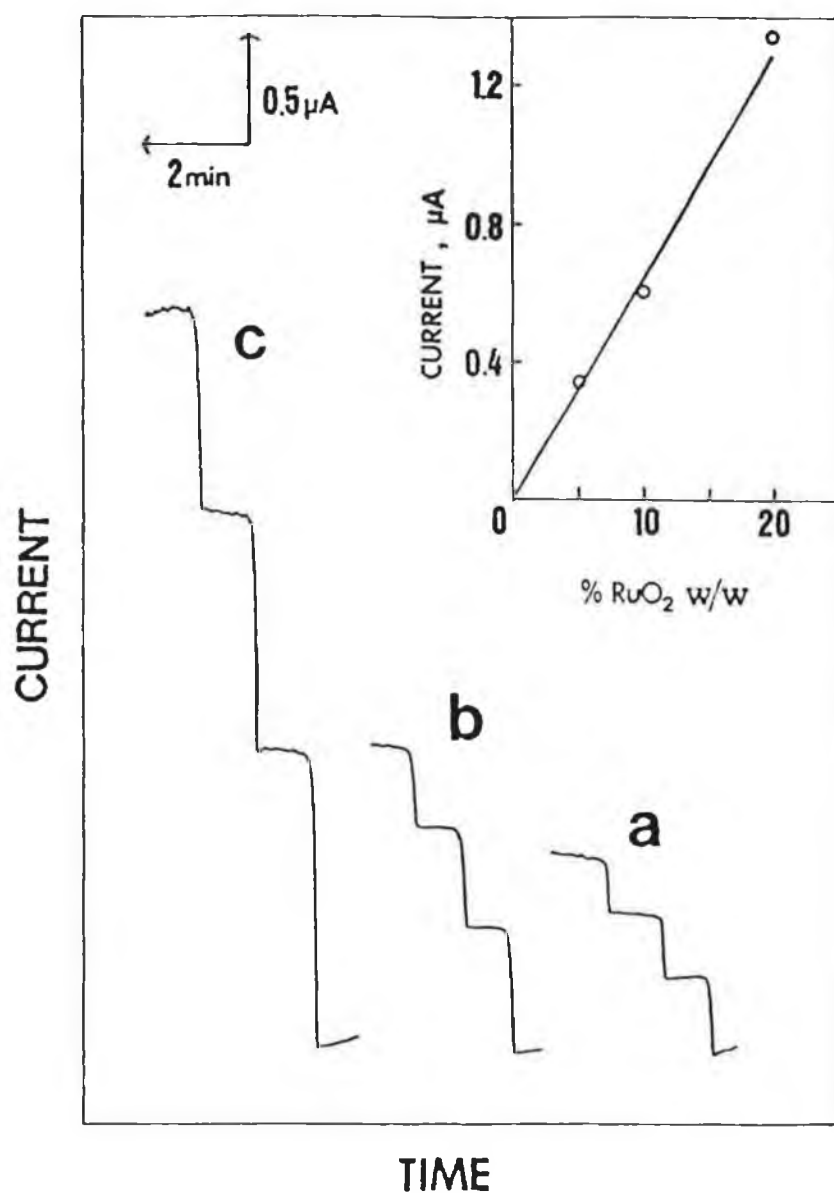
Figure 5.4: The effect of RuO_2-loading in the graphite-epoxy electrode matrix on the batch adition of 1 mM glucose levels to (a) 5%, (b) 10% and (c) 20% RuO_2-modified electrodes. Inset shows the plot of current versus loading. Constant-potential detection at +0.35 V, 400rpm stirring and 0.5 M NaOH electrolyte.

231

for the electrooxidation of carbohydrates. A RuO_2 loading of 20% w/w was selected for futher investigations in order to achieve the highest electrocatalytic response while minimising the higher background currents associated with the higher loadings (not shown).

A hydrodynamic voltammogram similar to those obtained in section 4.2.3.2, for antibiotic oxidation at RuO_2-modified graphite-epoxy electrodes, was obtained for glucose oxidation. A monitoring potential of +0.35 V was selected for subsequent investigations in order to minimise interferences at the higher potentials and to maintain lower background currents.

Attempts to lower the relatively high NaOH concentrations and pH levels required for the electrocatalytic reaction to occur proved unsuccessful. The currents obtained in low (<0.1 M) NaOH concentrations, upon addition of glucose to the cell, were negligible but rose sharply to a plateau upon increasing the NaOH concentration, reaching maximum levels at approximately 0.5 M NaOH concentration. Experiments conducted in 0.05 M phosphate buffer, using NaOH for adjustment of pH, showed that negligible currents were obtained upon addition of glucose to the cell, below a pH of 10. Above this pH a sharp rise in current obtained for glucose additions with pH was observed, corresponding to the increase in NaOH concentration. This requirement of high NaOH concentrations has been discussed in chapter 4. A NaOH concentration of 0.5 M was selected for subsequent investigations. This high pH level precluded the addition of a modifying polymer layer onto the surface of the RuO_2-modified graphite-epoxy electrode, that would be required in order to exclude interferences such as proteins and other biological entities. All polymers investigated for this purpose (Nafion, cellulose acetate, PVP, AQ55-D and AQ29-D) proved to be unstable on the electrode surface in this electrolyte.

The response at the 20% w/w RuO_2-modified graphite-epoxy electrode to the repeated addition of 0.5 mM levels of glucose is depicted in Figure 5.5. A slope of 1.06 mA mol^{-1}
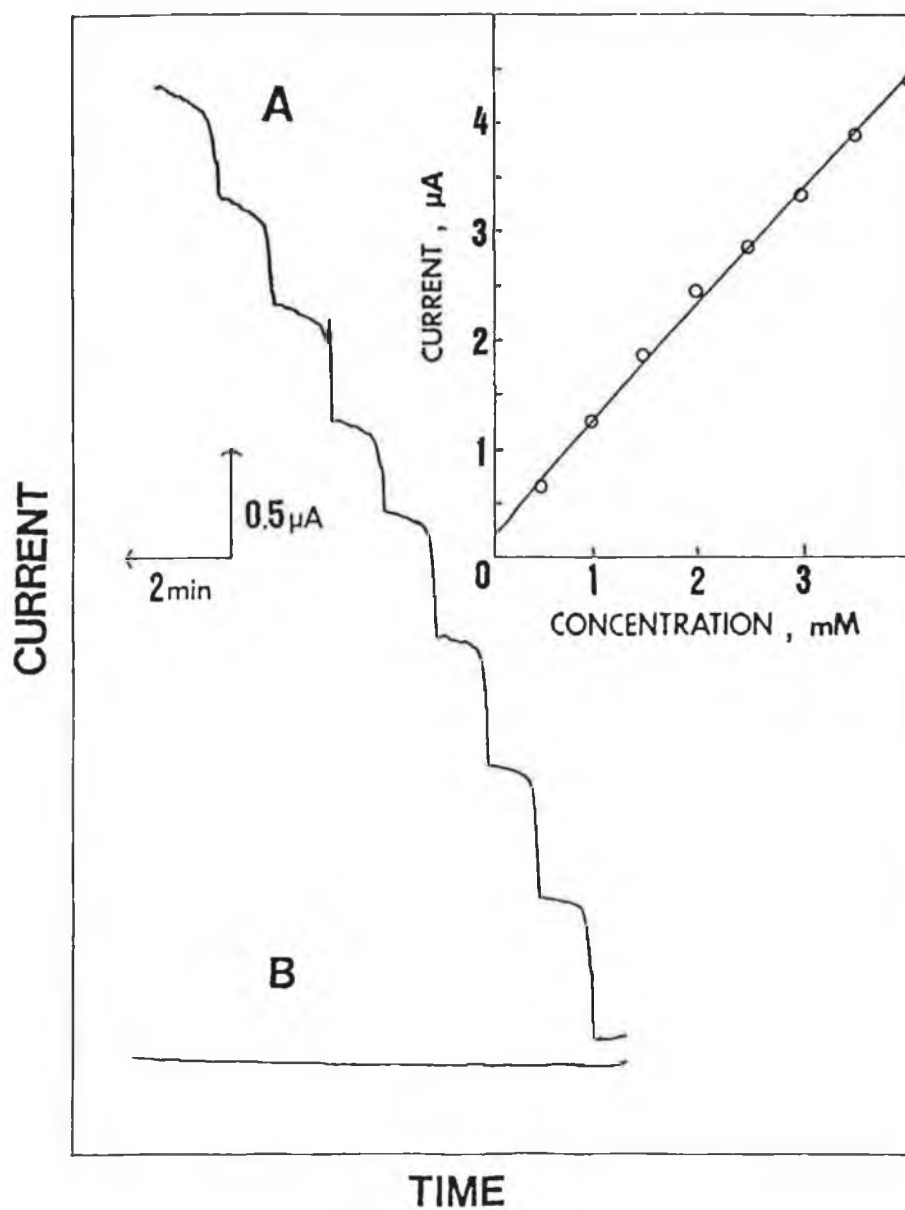
232

Figure 5.5: Current-time recording obtained at (A) the 20% w/w RuO_2-modified and (B) the unmodified graphite-epoxy electrodes upon the batch addition of glucose in 0.5 mM increments to the stirred (400rpm) cell. Other conditions as in Figure 5.4. Inset shows the corresponding I-C calibration curve.

233

(correlation coefficient of 0.999) was obtained, with the electrode displaying linearity over the 0.5 - 5 mM concentration range. All of the 20% w/w RuO_2-modified electrodes prepared functioned in a similar manner, yielding calibration curves with slopes of approximately 1 mA mol^{-1} ($\pm$ 10%) over the linear range. The success of this electrode fabrication technique (100% success rate for the 15 electrodes prepared) compares favourably with other techniques for the incorporation of modifiers into polishable, robust electrodes [67-70].

The stability and precision associated with the detection of glucose using these RuO_2-modified electrodes is demonstrated in Figure 5.6. Figure 5.6(A) represents the precision of the electrode response from surface-to-surface, with the electrode being polished for 30 sec with a 0.05 μm alumina slurry between additions. For the series of 8 determinations shown, a mean current of 1.98 μA, with a relative standard deviation of 3.75%, was obtained for the addition of 2.5 mM glucose to the cell. Figure 5.6(B) shows the repeated addition of 2.5 mM glucose to the cell, with the electrode being rinsed with distilled water between experiments. A mean current of 1.72 μA with a relative standard deviation of 2.1% was obtained for this series. These results combined illustrate the extreme stability and reproducibiity that inorganic modifiers of graphite-epoxy electrodes can achieve.
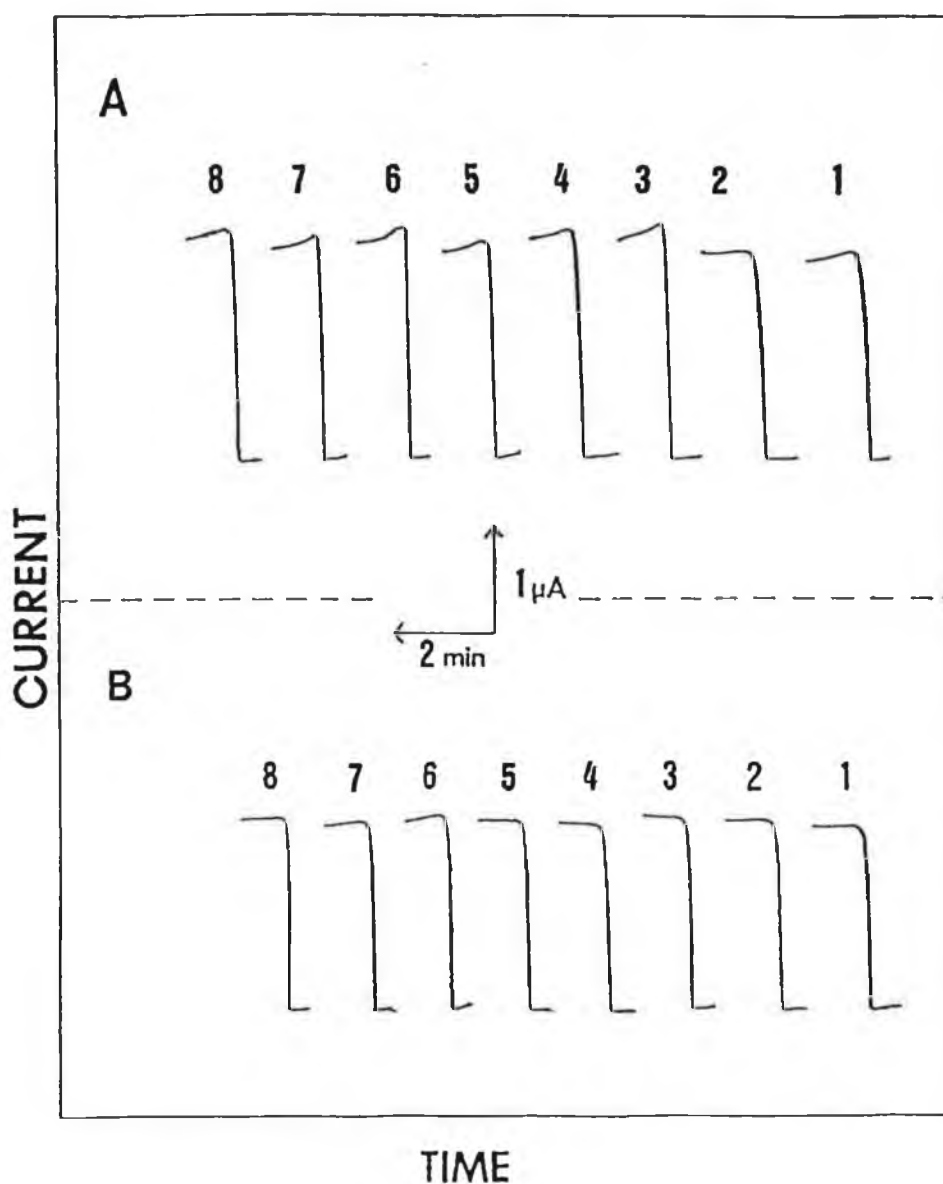
Figure 5.6: Precision experiments for the 20% RuO_2-modified electrode upon addition of 2.5 mM glucose. (A): surface-to-surface precision; polishing with 0.05 μm alumina slurry for 30 secs and rinsing with distilled water. (B): precision obtained for one electrode surface; rinsing with distilled water between additions. Other conditions as in Figure 5.4.

5.2.3.   CONCLUSIONS

In conclusion to this section, it has been shown that the RuO_2-modified graphite-epoxy electrodes are capable of glucose detection, yielding stable, reproducible and renewable responses for mM levels of glucose. Attempts to reduce the high pH level and NaOH concentration required for the electrocatalytic oxidation of glucose were unsuccessful, however, as were attempts to modify the electrode surface with polymer films to confer a degree of selectvity on these modified electrodes. It would seem, therefore, that the practical application of these modified electrodes will be in the non-selective detection of hydroxyl-containing species (alcohols, carbohydrates and selected pharmaceuticals) following chromatographic separation. It is envisaged that the RuO_2-modified graphite-epoxy electrodes may offer a viable alternative to the commercially available pulsed amperometric detection systems for carbohydrate detection.

5.3. ONE-STEP FABRICATION OF A GLUCOSE SENSOR BASED ON THE ENTRAPMENT OF GLUCOSE OXIDASE WITHIN POLY(ESTER-SULFONIC ACID) COATINGS

Various approaches, as described in section 5.1.2., have been proposed for incorporating the enzyme glucose oxidase (GOD) on electrode surfaces. Most commonly GOD is held physically, behind a membrane or via adsorption, or chemically, via an intermediate linkage, onto the surface [82]. Combinations of several membranes, including polyurethane, cellulose acetate or Nafion are commonly employed in the former case. Direct incorporation, by mixing the enzyme within carbon paste matrices [83] or by electrodeposition during the anodic growth of polymers [84], or in the presence of chloro-platinum complexes [24], have also been reported.

The aim of the present study was to illustrate a one-step immobilisation of GOD from a solution of a poly(ester-sulfonic acid) cation exchanger. Aqueous solutions of this polymer, which is composed of a hydrophobic polyester backbone and sulfonated exchanged sites, are available commercially under the trademark Eastman AQ polymers [85]. The complete structure of the AQ polymer used in this study, AQ55D, is not known; however the proposed backbone [86] is shown in Figure 5.7.

Recent work has demonstrated the effective permselective (charge exclusion) and antifouling properties and uptake of cations at Eastman AQ polymers [58,76,87-89]. Gorton et al. [58,76] recently illustrated the improved stability and protection associated with coverage of mixed enzyme/carbon paste electrodes with Eastman AQ polymer films. As reported in the following sections, casting mixed GOD/Eastman AQ (water-based) solutions onto platinum surfaces offers a rapid, simple and reproducible approach for immobilising the enzyme. The resulting enzyme electrodes exhibit a very fast and sensitive response to glucose, while excluding potential interferences. Such simultaneous performance of the enzyme entrapment and
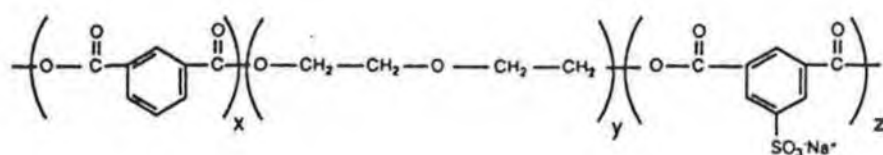
237

Figure 5.7: The proposed structure of the poly(ester sulfonic
acid) backbone of the Eastman AQ-55D polymer.

permselective and protective tasks, eliminates the need for multilayer membrane systems and makes the Eastman AQ films very attractive and versatile for biosensor work.

5.3.1. EXPERIMENTAL

5.3.1.1. Apparatus

The apparatus used for both the batch and flow experiments has been described previously in section 4.2.1.1., with the exception of the working electrodes. These were a platinum working electrode (1.5 mm diameter, BAS) and platinum in a thin-layer electrochemical detection system (Model MF1012, BAS), respectively.

5.3.1.2. Reagents and Procedures

All solutions were prepared using doubly-distilled deionised water. Glucose oxidase (Type X-S, EC 1.1.3.4.), ascorbic acid, uric acid and acetaminophen were all purchased from Sigma. Stock solutions of D-glucose (Sigma) were prepared in the 0.05 M phosphate buffer and allowed to stand overnight to allow muta-rotational equilibrium. The poly(ester sulfonic acid) cation-exchanger polymer (Eastman AQ-55D, Eastman Chemical Products) was used as obtained, dissolved (28% w/v) in water. The supporting electrolyte was a 0.05 M phosphate buffer solution (pH 6.5).

Modification of the platinum electrode was achieved by covering the surface with a 10 μL drop of the mixed polymer/GOD aqueous solution (1.4% polymer and 1 mg cm^{-3} enzyme usually). The coatings were then thoroughly dried for 15 min with a heat gun, held 40 cm above the surface. Once dried, the films were water insoluble. In most experiments, the working electrode was held at +0.7 V (vs. Ag/AgCl) and transient currents were allowed to decay. Batch experiments were performed in stirred (400 rpm)

solution and all measurements were taken at room temperature.

5.3.2. RESULTS AND DISCUSSION

5.3.2.1. Amperometry

The preparation procedure devised for the mixed enzyme/polymer films on the platinum electrode yielded the most stable and reproducible films. It has been reported [86], in a systematic investigation of the drying temperature and time for obtaining stable AQ-55D polymer films, that a drying temperature above that of the T_g of the polymer (where T_g represents the polymer glass transition temperature; T_g= 55°C for the AQ-55D polymer) gave optimum film stability. This is in agreement with our observations of mixed enzyme/polymer films. A drying time of 15 min with a heat gun held approximately 40 cm above the electrode was found to be sufficient in the present study. The variation in the physical properties of the membranes caused by the high temperature solution processing procedures are likely to be a result of a combination of changes in water content and/or the supermolecular structure of the nonionic and ionic domains within the ionomer [86].

Investigations of the response of the mixed polymer/GOD modified electrodes to glucose and interferences were performed using batch additions of aliquots of the analyte to a stirred electrochemical cell. The characteristic current-time data for additions of glucose (A), ascorbic acid (B), uric acid (C) and acetaminophen (D) at both the bare (a) and poly(ester-sulfonic acid)/GOD modified (b) electrodes are shown in Figure 5.8. These easily prepared poly(ester-sulfonic acid)/GOD electrodes effectively couple the enzymatic selectivity with discrimination against these potential interferences. GOD is confined in an active form within the polymer matrix. The modified electrode exhibits a fast and sensitive response to glucose (A(b)), indicating a facile transport of this substrate towards the
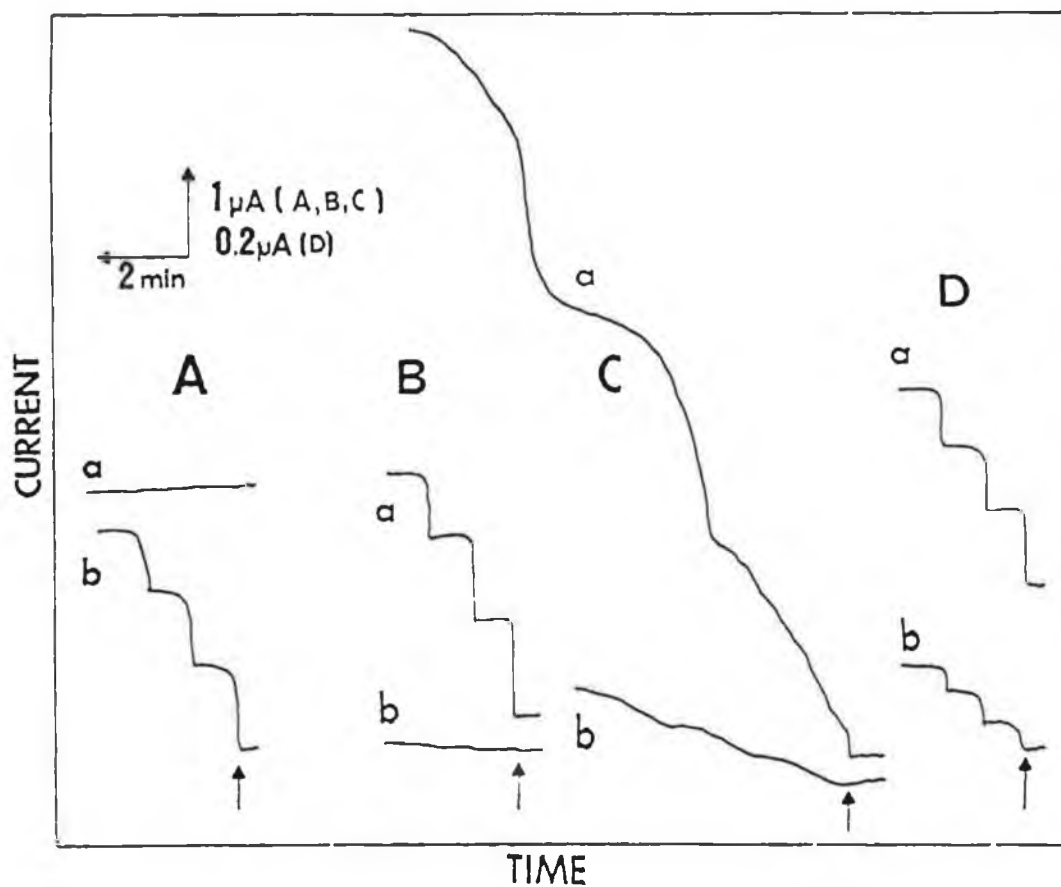
Figure 5.8: Current-time recording on increasing the glucose
(A), ascorbic acid (B), uric acid (C) and acetaminophen (D)
concentrations in 1 mM, 0.1 mM, 0.25 mM and 0.05 mM steps,
respectively. Bare (a) and poly(ester sulfonic acid)/GOD
modified (b) electrodes. Batch experiment with 400rpm stirring
and +0.7 V (A-C) and +0.5 V (D) operating potentials.
Electrolyte, 0.05 M phosphate buffer solution (pH 6.5).

241

enzymatic sites and of the peroxide product, which is detected oxidatively at the electrode surface, to the sensing sites. A steady-state current was achieved within 15-20 s. In contrast, the negatively-charged film hinders the transport of the anionic ascorbic and uric acids, leading to decreased current responses for these substrates in comparison to the response observed at the bare unmodified electrode (i_m/i_b of 0.03 and 0.10, respectively). Some discrimination against acetaminophen, leading to a i_m/i_b ratio of 0.37, was also observed. It should be noted, however, that all of the interferents above were added at concentrations that are at the highest range of their normal physiological levels, whereas the 1 mM glucose addition is at the lower range of the physiological level normally expected for blood glucose. The permselective response is illustrated also from the potential-dependent experiments of Figure 5.9. The effective exclusion of ascorbic acid is maintained over the entire potential window of +0.3 to +0.9 V (curve A vs. dotted line). In contrast, the response to glucose increased with increasing potential, reaching a maximum at +0.7 V (B), which was the potential used in subsequent experiments. In addition to the rejection of anionic interferences, the glucose response was not affected by the presence of large biomacromolecules. For example, no change in the response for 0.1 mM glucose was observed in the presence of 500 ppm albumin during a prolonged (30 min) stirring operation. Hence the single ionomeric coating effectively performs the immobilisation, permselectivity and antifouling functions, providing an interferent-free environment at the surface. In addition, such minimisation of membrane barriers, and the close proximity of the biocatalytic and sensing sites, offer extremely short response times. The commercial availability of poly(ester-sulfonic acid) in aqueous solutions of pH 5-6 makes it attractive for casting of enzymes, as compared to other ionomers, such as Nafion, which are available only in organic media. The casting of mixed enzyme/polymer solutions films from
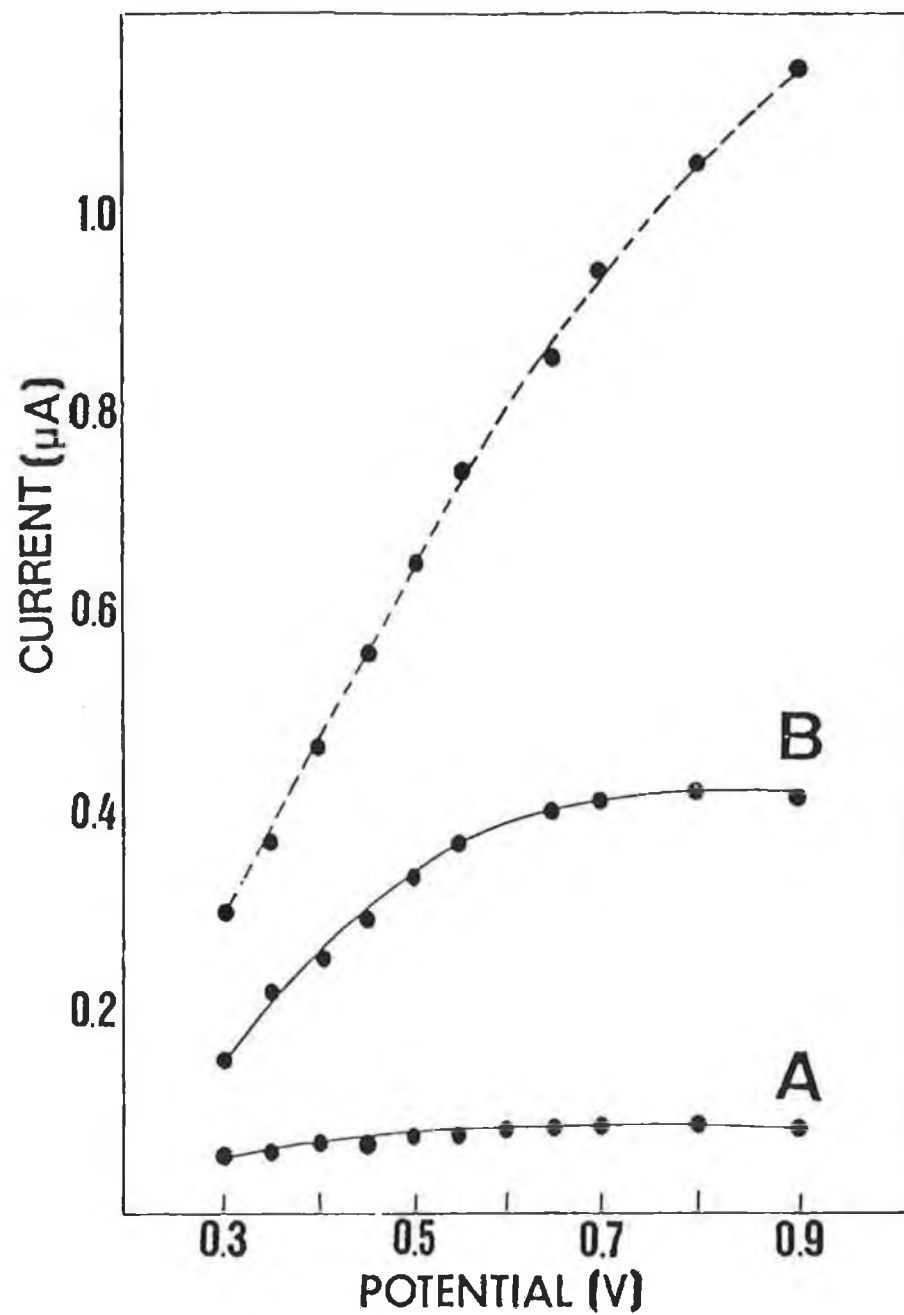
Figure 5.9: Variation in response to 0.1 mM ascorbic acid (A) and 0.5 mM glucose (B) with applied potential. Other conditions as in Figure 5.8. Also shown (dotted line) is the analogous resonse to ascorbic acid at the bare electrode.

these organic solutions may lead to denaturation of the enzyme and/or low enzyme activities. Furthermore, Nafion-based glucose probes have been reported to require an intermediate linkage between the enzyme and polymer for stability of response [74]. No such linkage is required for the Eastman AQ-55D ionomers.

Mell and Malloy [90] reported a model for an amperometric immobilised enzyme electrode (obtained through digital simulation), in flow injection analysis, that dealt with both the steady-state and the transient part of the current-time curve. According to the authors, the time required to reach a current that is half of the steady-state current is roughly given (at high substrate concentration) by:

$$t_{1/2} = 0.1d^2/D \qquad\qquad (5.3)$$

where d is the thickness of the film and D is the diffusion coefficient of glucose within the film. An accurate estimation of $t_{1/2}$ cannot be done for the system considered here, mainly due to the "mixing" time contribution after glucose injection. If an overestimate of 10 s for $t_{1/2}$ is assumed, as inferred from the curves in Figure 5.8, a value for d^2/D of approximately 100 s can be calculated. If an estimated d value of 10-100 nm is used, a D value of the order of 1×10^{-13} $cm^2 s^{-1}$ for the diffusion of glucose within the film can be calculated. This value, however, must be correctly considered as the product kD, where k is the partition coefficient of glucose between the film and the solution [42]. These kD values are highly dependent on the nature of the film, and indeed on its thickness. For glucose in a poly(acrylamide) gel, a value of 2.4 $\times 10^{-6} cm^2 s^{-1}$ was found [91], while a value of 4×10^{-12} $cm^2 s^{-1}$ was calculated for glucose in an electrosynthesised poly(N-methylpyrrole) film through a different approach [92]. kD values of the order of $1 \times 10^{-13} cm^2 s^{-1}$ have also been estimated for glucose partition and diffusion in an o-phenylenediamine/GOD film formed via electrochemical

244

polymerisation [42].

The dependence of the sensitivity of the poly(ester-sulfonic acid)/GOD electrode on the pH of the electrolyte is shown in Figure 5.10(A). A slight increase in the response was observed over the 5 to 6 pH range, with a levelling off at higher values. All subsequent investigations were carried out using a pH of 6.5. The dependence of the glucose response on the composition of the mixed polymer/GOD coating is shown in Figure 5.10(B). The amperometric response rapidly increased upon increasing the enzyme loading to 0.25 mg cm^{-3}, after which it remained constant. The 1.0 mg cm^{-3} concentration of GOD was subsequently used, as it offered the best rejection of anionic interferences. Various levels of the cation-exchanger in the casting solution (ranging from 0.5 to 7.0% w/v) were also evaluated. Maximum response for glucose was obtained using the 1.4% w/v polymer solution, obtained by 20-fold dilution of the commercial product (28% dispersion). The smaller signals observed at higher levels (i.e. thicker films) are attributed to hindered transport of the glucose substrate and/or the peroxide.

Additions of glucose, each effecting a 0.5 mM increase in concentration, were used to estimate the linear range. A typical calibration curve obtained at an electrode cast from a 1 mg cm^{-3} solution of GOD and 1.4% w/v AQ-55D mixture is shown in Figure 5.11. Castner and Wingard [93] have shown that for enzymes immobilised on a rotating electrode, or with mass transport to the electrode controlled by stirring, as it was in this study, the Eadie-Hofstee form of the Michaelis-Menten equation applies under conditions were the enzymatic reaction is rate controlling

$$i_{ss} = i_{max} - K'_m i_{ss}/C \qquad (5.4)$$

where i_{ss} is the steady-state current, i_{max} is the maximum current under saturating substrate conditions, K'_m is the apparent Michaelis-Menten constant (which can differ
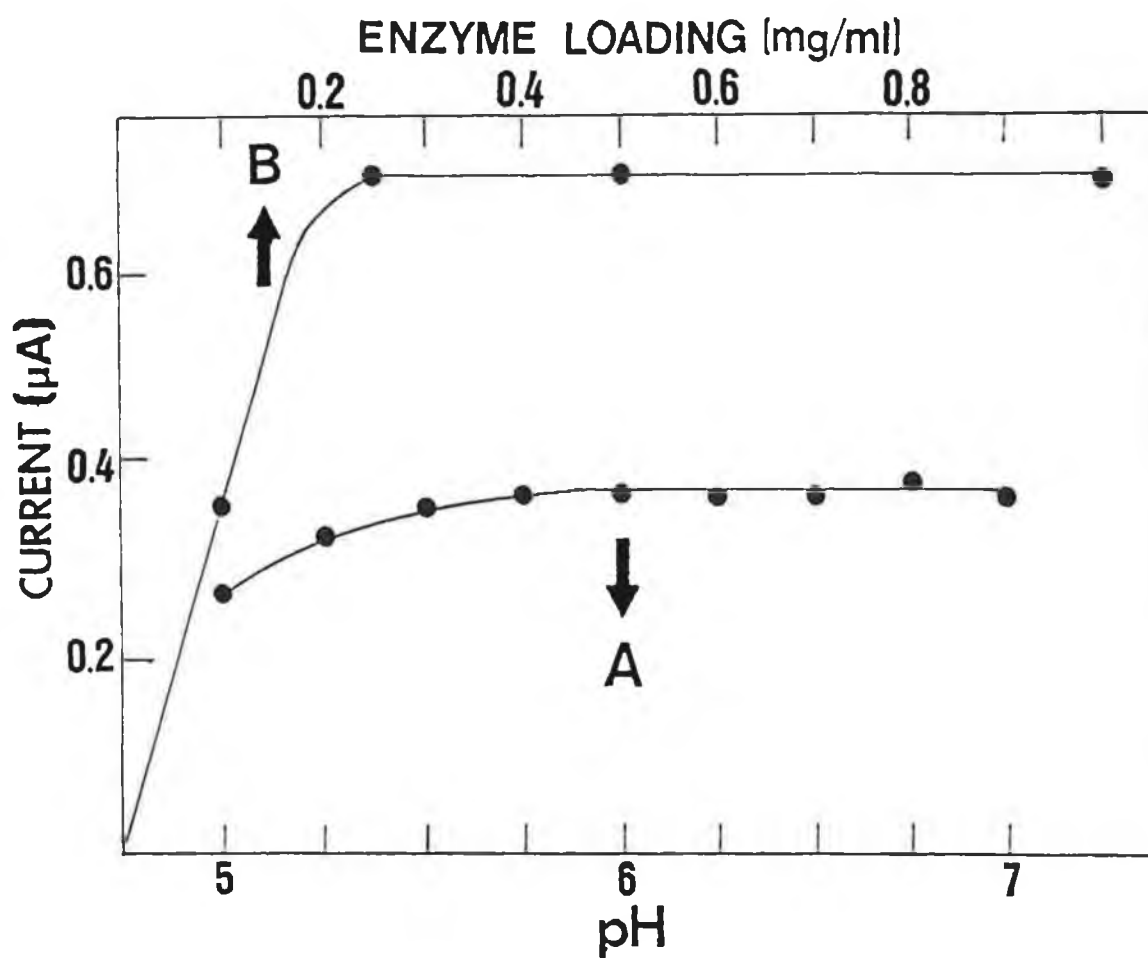
245

Figure 5.10: Effect of pH (A) and enzyme loading (B) on the
amperometric response. Glucose concentration, 0.5 mM (A) and 1.0
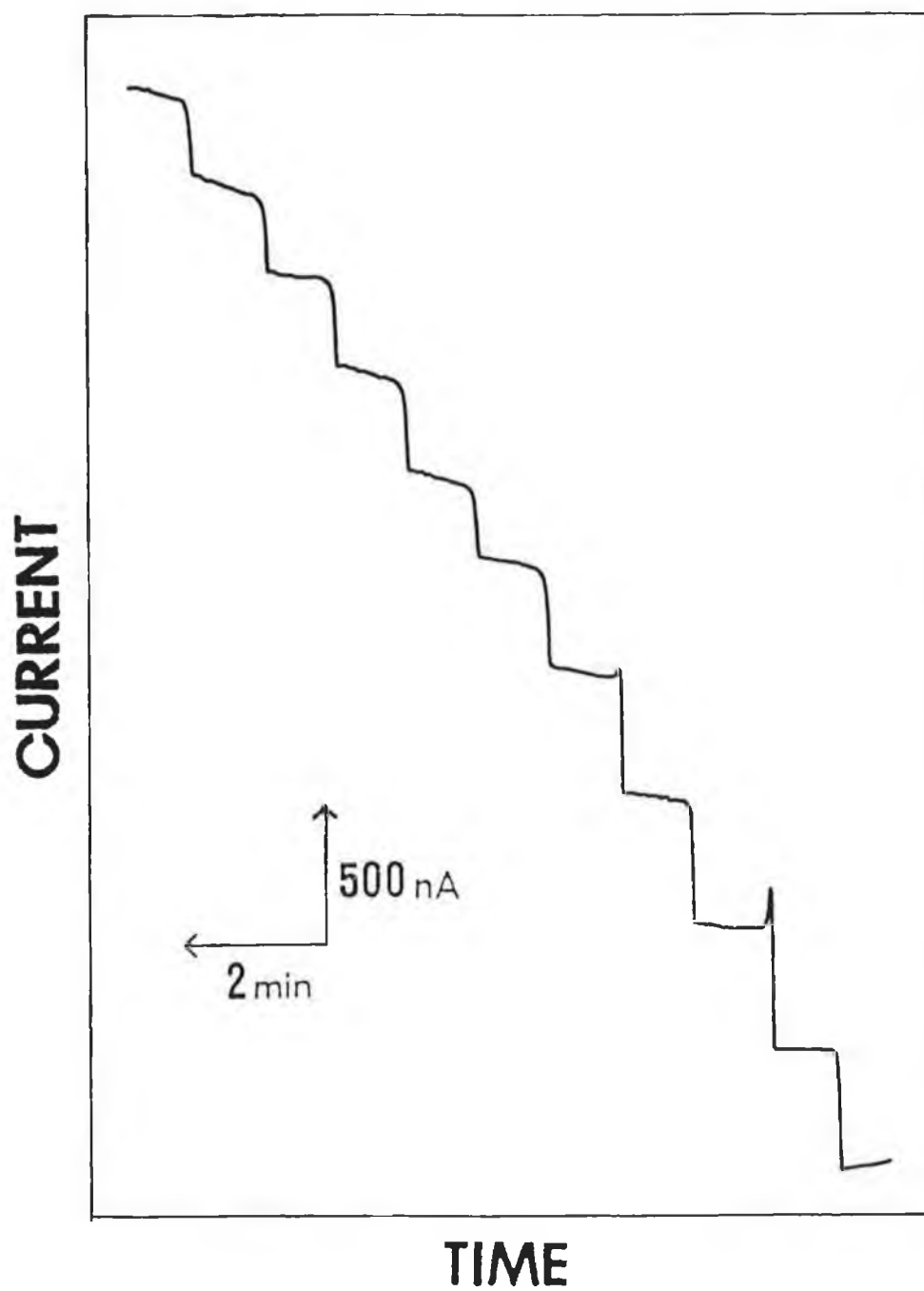mM (B). Operating potential +0.7 V. Other conditions as in
Figure 5.8.

Figure 5.11: Current-time response obtained upon the repeated addition of 0.5 mM glucose to the cell. Other conditions as in Figure 5.8.

247

significantly from that measured in homogeneous solution, and is not an intrinsic property of the enzyme but of the system), and C is the concentration of glucose in the solution. The data shown in Figure 5.11, when plotted according to equation (5.4) are shown in Figure 5.12. As can be seen, a deviation from linearity at low substrate concentrations is observed, indicating a mass-transfer limitation. Due to the fact that the H_2O_2 must diffuse through the film before being detected at the platinum electrode, it can not be ascertained, at least under the experimental conditions used in this study, whether the overall current appears mass transport limited due to diffusional limitations of substrate, H_2O_2 or both. From the best-fit line for all of the points of the Eadie-Hofstee plot, a K'_m of 3.7 mM and an i_{max} of 4.3 μA were estimated. Calculations on the linear portion of the calibration curve depicted in Figure 5.11 (0 - 4 mM) yielded a slope of 0.8 mA mol^{-1} with a correlation coefficient of 0.999. Using 0.1 mg GOD cm^{-3} casting solutions, with 1.4% w/v of the ionomer present, linearity prevailed up to approximately 8 mM glucose (slope, 0.38 mA mol^{-1}; correlation coefficient, 0.999). This demonstrates the facile expansion of the linear range of these modified electrodes via a judicious choice of enzyme loading. Extended linearity could also be achieved by increasing the proportion of the AQ-55D polymer in the casting solution (leading to increased film thicknesses).

In addition to its simplicity and speed, the poly(ester-sulfonic acid) immobilisation approach is very reproducible. Figure 5.13 illustrates the surface-to-surface reproducibility obtained for eight repetitive castings of the polymer/enzyme solution (1 $mg\,cm^{-3}$ GOD, 1.4% w/v polymer). The relative standard deviation for the 0.5 mM glucose response over this series is 7%. An even better precision (relative standard deviation of 2%) was obtained for 16 repetitive measurements of 0.5 mM glucose at the same electrode surface, when the electrode was dipped in distilled water for 30 s between measurements.
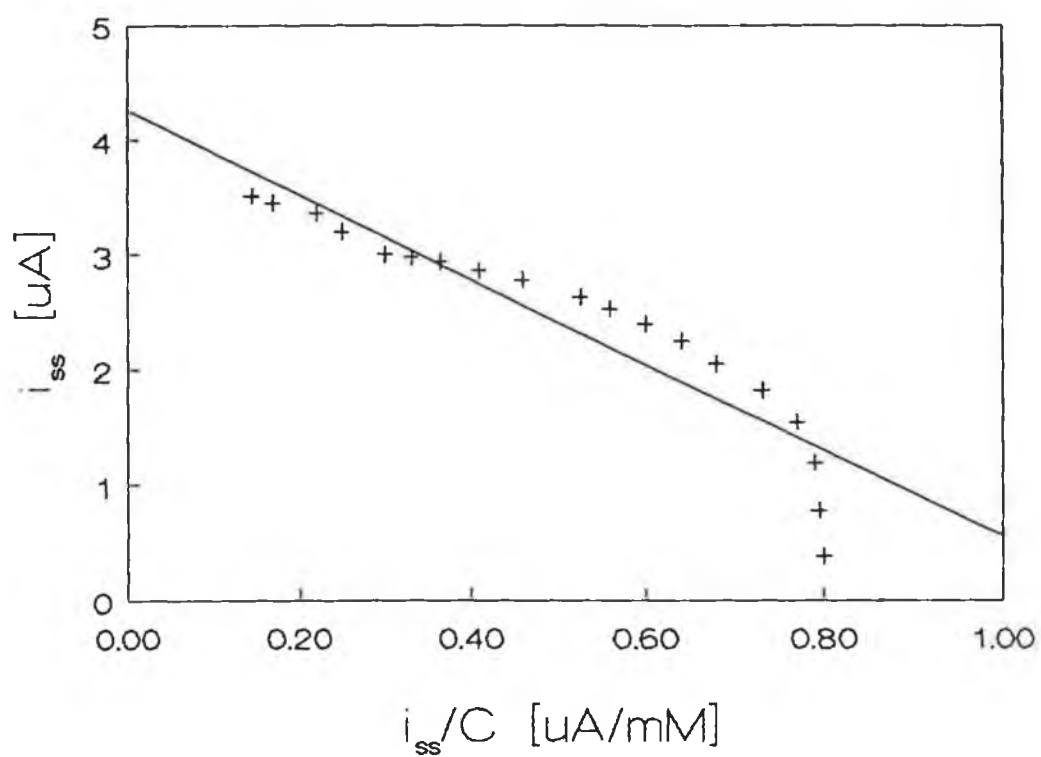
248

Figure 5.12: A plot of the data taken from Figure 5.11
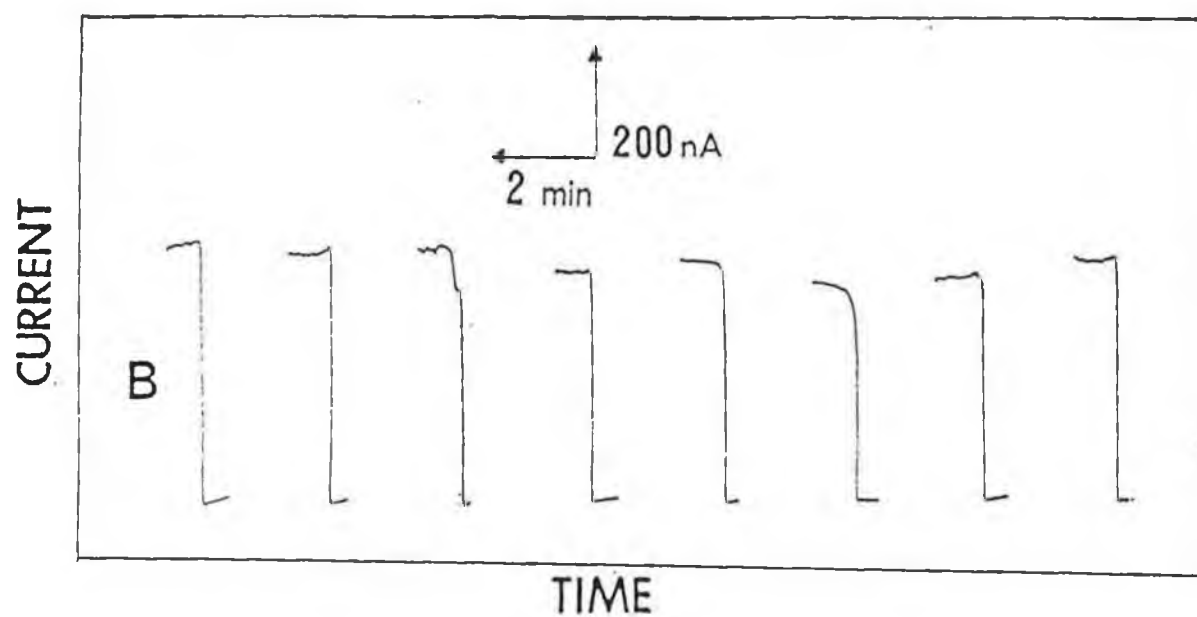according to equation 5.4 (Eadle-Hoftsee plot).

Figure 5.13: Precision between surfaces (different coatings) for addition of 0.5 mM glucose. Other conditions as in Figure 5.8.

5.3.2.2. Flow-Injection Analysis

The fast response of the poly(ester-sulfonic acid)/GOD electrode makes it suitable for use in dynamic flow systems. Typical flow injection response peaks at the modified thin-layer flow electrode for glucose solutions of increasing concentration (50-150 μM, a-c) are shown in Figure 5.14. Short response times and a rapid return to the baseline were observed, indicating facile transport of the substrate, H_2O_2 and removal of the products. The peak half-width observed was 6.5 s, allowing a high sample throughput of 120 samples per hour. A detection limit (based on a signal-to-noise ratio of 3) of 3 μM was estimated from the flow injection peaks shown. The three measurements shown in Figure 5.14 are part of a series of eight concentration increments over the 25-250 μM range. The resulting calibration plot is also shown in this figure. A linear relationship was observed, yielding a slope of 942 μA mol^{-1}, intercept of 5 nA and correlation coefficient of 0.998, respectively. Increasing the flow rate between 0.5 and 2.0 cm^{-3}min^{-1} did not affect the peak height, indicating that mass transfer to the electrode is not a limiting factor. The increase in flow rates did yield shorter response times, with improved "wash-out" characteristics, and hence very high injection rates of up to 180 samples per hour.

The flow injection peaks depicted in Figure 5.15(B) illustrate that the response is retained over relatively long time periods. These peaks are part of a series of 120 repetitive injections over a 40 min period. Despite the vigorous hydrodynamic conditions prevailing in the flow cell, the response remained essentially unchanged throughout this series. This is attributed to the good mechanical stability and surface adherence of the poly(ester-sulfonic acid) films. Only 5% and 18% decreases of the flow injection peak were observed upon 48 and 96 hour storages respectively, of the coated electrode at room temperature. Such losses do not represent major problems

251
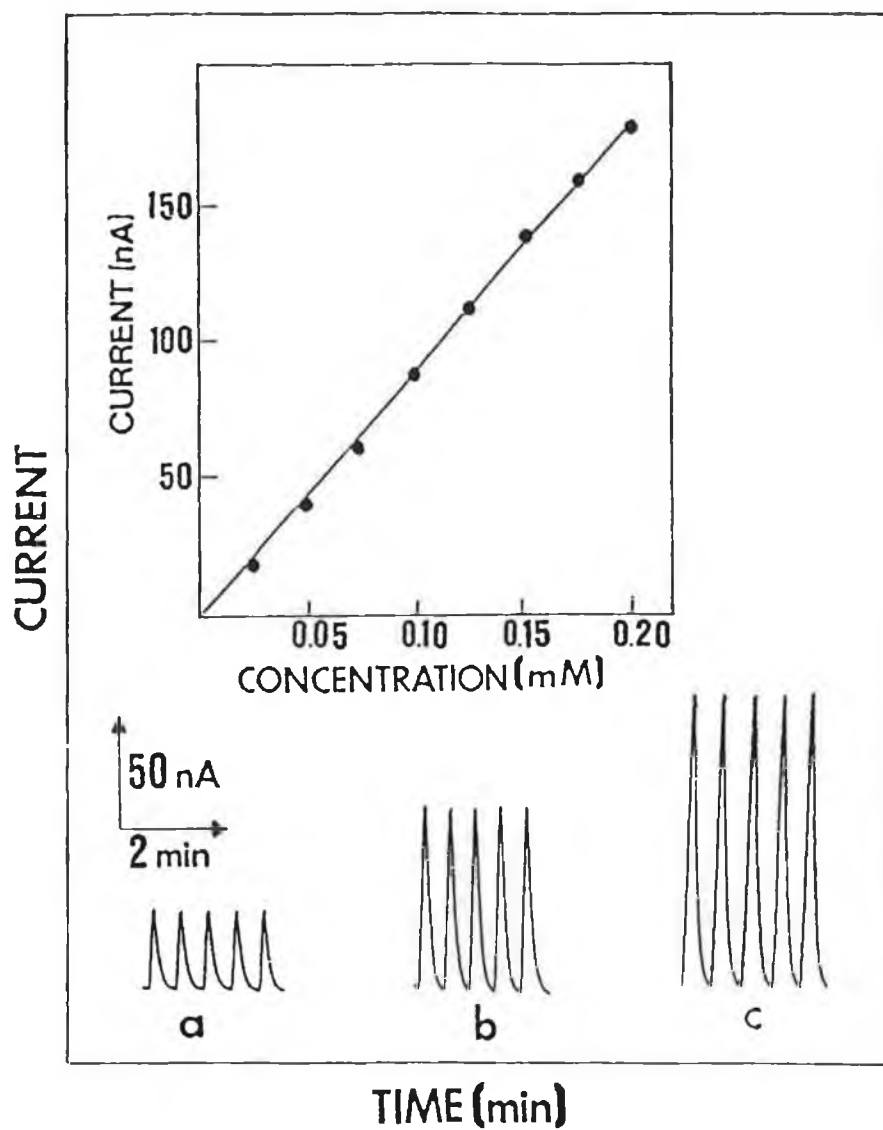
Figure 5.14: Flow injection peaks for solutions containing increasing glucose concentrations of 50 (a), 100 (b) and 150 (c) μM. Flow rate, 1.1 cm^3min^{-1}; sample volume 20 μL. Other conditions as in Figure 5.8.
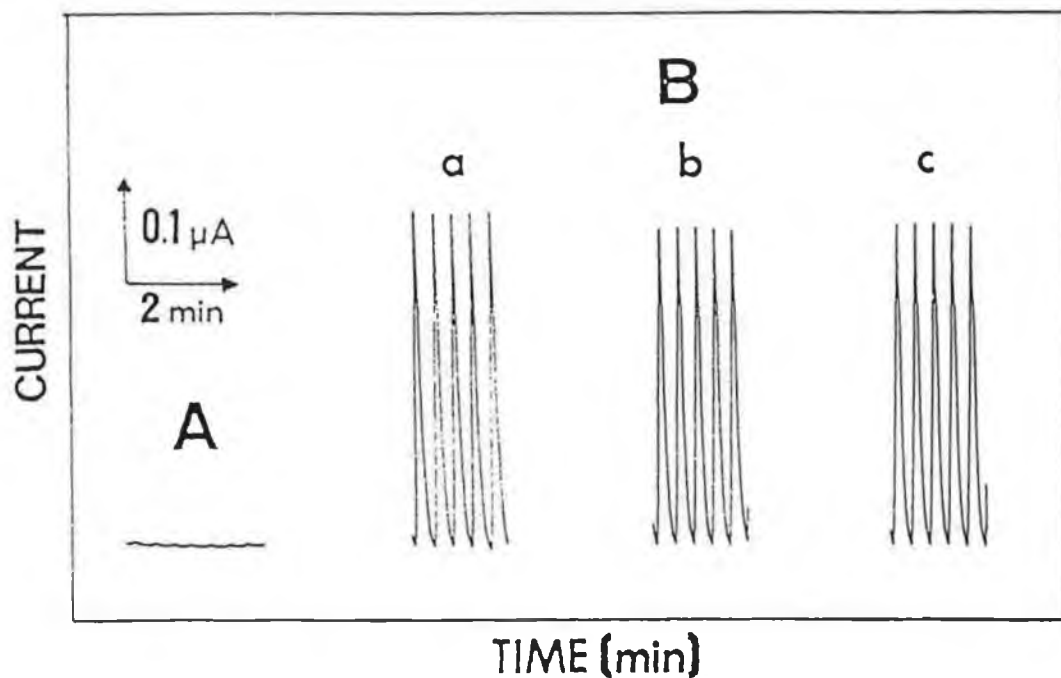
Figure 5.15: Stability of the flow injection response to 0.4 mM glucose over a total time period of 120 min (B). Peaks recorded during the first (a), 60th (b) and 120th (c) min of operation. Also shown (A), analogous measurements at the bare electrode. Flow rate, 0.7 cm^3min^{-1}. Other condtions as in Figure 5.14..

given the speed and reproducibility of the immobilisation procedure.

5.3.3.   CONCLUSIONS

In conclusion to this section, the experiments described above illustrate an attractive avenue for fabricating glucose sensors based on casting GOD from water-based poly(ester-sulfonic acid) solutions. This versatile polymer serves for entrapping the enzyme as well as for excluding potential interferences. The resulting sensor yields a very fast and sensitive response to glucose. Simultaneous incorporation of several enzymes and/or of a redox mediator should further enhance the power of these devices. As demonstrated recently, electrocatalytic metal complexes, such as $Ru(bpy)_3^{2+}$, can be held electrostatically by the sulfonated groups of the polymer [89]. This simple method of biosensor construction should be applicable to other enzyme-substrate systems, supportive surfaces (such as disposable strips), and for a variety of practical situations.

5.4. REFERENCES

1.   G. Nagy and E. Pungor, <u>Bioelectrochem. and Bioenerg.</u>, (1988), <u>20</u>, 1.

2.   S. Hughes, P.L. Meschi and D.C. Johnson, <u>Anal. Chim. Acta</u>, (1982), <u>132</u>, 1.

3.   S. Hughes and D.C. Johnson, <u>Anal. Chim. Acta</u>, (1982), <u>132</u>, 11.

4.   S. Hughes and D.C. Johnson, <u>Anal. Chim. Acta</u>, (1983), <u>149</u>, 1.

5.   G.G. Neuberger and D.C. Johnson, <u>Anal. Chem.</u>, (1987), 59, 203.

6.   G.G. Neuberger and D.C. Johnson, <u>Anal. Chem.</u>, (1987), 59, 150.

7.   D.S. Bindra and G.S. Wilson, <u>Anal. Chem.</u>, (1989), <u>61</u>, 2566.

8.   L.M. Santos and R.P. Baldwin, <u>Anal. Chem.</u>, (1987), <u>59</u>, 1766.

9.   M. Fleischmann, K. Korinek and D. Pletcher, <u>J. Electroanal. Chem.</u>, (1971), <u>31</u>, 39.

10.   K.G. Schick, V.G. Magearu and C.O. Huber, <u>Clin. Chem.</u>, (1978), <u>24</u>, 448.

11.   T.N. Morrison, K.G. Schick and C.O. Huber, <u>Anal. Chim. Acta</u>, (1980), <u>120</u>, 75.

12.   R.E. Reim and R.M. van Effen, <u>Anal. Chem.</u>, (1986), <u>58</u>, 3203.

13.   S.V. Prahbu and R.P. Baldwin, <u>Anal. Chem.</u>, (1989), <u>61</u>, 852.

14.   S.V. Prahbu and R.P. Baldwin, <u>Anal. Chem.</u>, (1989), <u>61</u>, 2258.

15.   J. Wang and Z. Taha, <u>Anal. Chem.</u>, (1990), <u>62</u>, 1413.

16.   P.W. Stoecker and A.M. Yacynych, <u>Sel. Electrode Rev.</u>, (1990), <u>12</u>, 137.

17.   L.C. Clark and C. Lyons, <u>Anns. N.Y. Acad. Sci.</u>, (1962), <u>29</u>, 102.

18. S.J. Updick and G.P. Hicks, Nature, (1967) 214, 986.

19. L.C. Clark, Biosensors: Fundamentals and Applications,
     A.P.F. Turner, I. Karube and G.S. Wilson (Eds.), Oxford
     Univ. Press, Oxford, (1987), 3.

20. A.P.F. Turner, I. Karube and G.S. Wilson, Biosensors:
     Fundamentals and Applications, Oxford Univ. Press, Oxford,
     (1987).

21. P.W. Carr and L.D. Bowers, Immobilized Enzymes in
     Analytical and Clinical Chemistry, Wiley, New York,
     (1980).

22. J.E. Frew and H.A.O. Hill, Anal. Chem., (1987), 59, 933A.

23. F. Scheller, F Schubert, D. Pfeiffer, R. Hintsche, I.
     Dransfeld, R. Renneberg, U. Wollenberger, K. Riedel, M.
     Pavlova, M. Kuhn, H-G. Muller, P. Tan, W. Hoffmann and W.
     Moritz, Analyst, (1989), 114, 653.

24. T. Ikariyama, S. Yamauchi T. Yukiashi and H. Ushioda,
     Anal. Lett., (1987), 20, 1791.

25. T. Ikeda, H. Hamada, K. Miki and M. Senda, Agric. Biol.
     Chem., (1985), 49, 541.

26. G. Marko-Varga, R. Appelquist and L. Gorton, Anal. Chim.
     Acta, (1986), 179, 371.

27. W. Matuszewski and M. Trojanowicz, Analyst, (1988), 113,
     735.

28. J. Wang and M.S. Lin, Electroanalysis, (1989), 1, 43.

29. M. Bonakdar, J.L. Vilchez and H.A. Mottola, J.
     Electroanal. Chem., (1989), 266, 47.

30. A. Amine, J-M Kauffmann and G.J. Patriarche, Talanta,
     (1991), 38, 107.

31. M. Masoom and A. Townshend, Anal. Chim. Acta, (1984), 166,
     111.

32. R.M. Ianniello and A.M. Yacynych, Anal. Chem., (1984), 53,
     2090.

33. G.J. Moody, G.S. Sanghera and J.D.R. Thomas, Analyst,
     (1986), 111, 1235.

34. S.K. Beh, G.J. Moody and J.D.R. Thomas, Analyst, (1989),

<u>114</u>, 29.

35. K. Narasimhan and L.B. Wingard, Jr., <u>Anal. Chem.</u>, (1986), <u>58</u>, 2984.

36. H.J. Wieck, G.H. Heider, Jr. and A.M. Yacynych, <u>Anal. Chim. Acta</u>, (1984), <u>158</u>, 137.

37. W. Schuhmann, R. Lammert, B. Uhe and H-L. Schmidt, <u>Sens. Actuators B1</u>, (1990), 537.

38. N.C. Foulds and C.R. Lowe, <u>J. Chem. Soc., Faraday Trans. 1</u>, (1986), <u>82</u>, 1259.

39. N.C. Foulds and C.R. Lowe, <u>Anal. Chem.</u>, (1988), <u>60</u>, 2473.

40. D. Belanger, E. Brassard and G. Fortier, <u>Anal. Chim. Acta</u>, (1990), <u>228</u>, 311.

41. H. Shinohara, T. Chiba and M. Aizawa, <u>Sens. Actuators</u>, (1988), <u>13</u>, 79.

42. C. Malitesta, F. Palmisano, L. Torsi and P.G. Zambonin, <u>Anal. Chem.</u>, (1990), <u>62</u>, 2735.

43. N.J. Szuminskt, A.K. Chen and C.C. Liu, <u>Biotech. and Bioeng.</u>, (1984), <u>26</u>, 642.

44. N. Oyama, T. Ohsaka, M. Mizunuma and M. Kobayashi, <u>Anal. Chem.</u>, (1988), <u>60</u>, 2536.

45. H. Fu, J. Anzai, T. Osa and T. Matsua, <u>Chem. Pharm. Bull.</u>, (1988), <u>36</u>, 119.

46. M. Mascini and G.G. Guilbault, <u>Anal. Chem.</u>, (1977), <u>49</u>, 795.

47. T. Yao, <u>Anal. Chim. Acta</u>, (1983), <u>148</u>, 27.

48. A.E.G. Cass, G. Davis, M.J. Green and H.A.O. Hill, <u>J. Electroanal. Chem.</u>, (1985), <u>190</u>, 117.

49. A.E.G. Cass, G. Davis, G.D. Francis, H.A.O. Hill, W.J. Aston, I.J. Higgins, E.V. Plotkin, L.D.L. Scott and A.P.F. Turner, <u>Anal. Chem.</u>, (1984) <u>56</u>, 667.

50. A.E.G. Cass, G. Davis, H.A.O. Hill and D.J. Nancarrow, <u>Biochim. Biophys. Acta</u>, (1985), <u>828</u>, 51.

51. E.G. D'Costa, I.J. Higgins and A.P.F. Turner, <u>Biosensors</u>, (1986), <u>2</u>, 71.

52. J.M. Dicks, W.J. Aston, G. Davis and A.P.F. Turner, <u>Anal.</u>

257

Chim. Acta, (1986), 182, 103.

53. P.N. Bartlett, V.Q. Bradford and R.G. Whitaker, Talanta, (1991), 38, 57.

54. M.J. Green and H.A.O. Hill, J. Chem. Soc., Faraday Trans. 1, (1986), 82, 1237.

55. J.J. Kulys and N.K. Cenas, Biochem. Biophys. Acta, (1983), 744, 57.

56. A.L. Crumbliss, H.A.O. Hill and D.J. Page, J. Electroanal. Chem., (1986), 206, 327.

57. I. Taniguchi, S. Miyamoto, S. Tomimura and F.M. Hawkridge, J. Electroanal. Chem., (1988), 240, 33.

58. G.Bremle, B. Persson and L. Gorton, Electroanalysis, (1991), 3, 77.

59. W.J. Albery, P.N. Bartlett and D.H. Craston, J. Electroanal. Chem., (1985), 194. 223.

60. M.S. Freund and A. Brajter-Toth, Anal. Chem., (1989), 61, 104.

61. N.K. Cenas and J.J. Kulys, Bioelectrochem. Bioenerg., (1981), 8, 103.

62. W.J. Albery, P.N. Bartlett, A.E.G. Cass, D.H. Craston and B.G.D. Haggett, J. Chem. Soc., Faraday Trans. 1, (1986), 82, 1033.

63. J.J. Kulys and A.S. Samalius, Bioelectrochem. Bioenerg., (1983), 10, 385.

64. J.J. Kulys, Biosensors, (1986), 2, 3.

65. H.A.O. Hill, European Patent Application, (1984), 84303090.

66. Y. Degani and A. Heller, J. Phys. Chem., (1987), 91, 1285.

67. Y. Degani and A. Heller, J. Am. Chem. Soc., (1988), 110, 2615.

68. Y. Degani and A. Heller, J. Am. Chem. Soc., (1989), 111, 2357.

69. B.A. Gregg and A. Heller, Anal. Chem., (1990), 62, 258.

70. P.N. Bartlett, R.G. Whitaker, M.J. Green and J. Frew, J. Chem. Soc., Chem. Commun., (1987), 103.

71. U. Wollenberger, F. Scheller, D. Pfeiffer, V.A. Bogdanovskaya, M.R. Tarasevich and G. Hanke, <u>Anal. Chim. Acta,</u> (1989), <u>187,</u> 39.

72. D.R. Thevenot, <u>Diabetes Care,</u> (1982), <u>5,</u> 174.

73. D.A. Gough, J.Y. Luciano and P.H.S. Tse, <u>Anal. Chem.,</u> (1985), <u>57,</u> 2351.

74. D.J. Harrison, R.F.B. Turner and H.P. Baltes, <u>Anal. Chem.,</u> (1988), <u>60,</u> 2002.

75. J. Wang and T. Golden, <u>Anal. Chim. Acta,</u> (1989), <u>217,</u> 343.

76. L. Gorton, H.I. Karan, P.D. Hale, T. Inagaki, Y. Okamoto and T.A. Skotheim, <u>Anal. Chim. Acta,</u> (1990), <u>228,</u> 23.

77. L.A. Coury, Jr., E.W. Huber, E.M. Birch and W.R. Heineman, <u>J. Electrochem. Soc.,</u> (1989), <u>136,</u> 1044.

78. J.A. Cox and K.R. Kulkarni, <u>Talanta,</u> (1986), <u>33,</u> 911.

79. B.R. Shaw and K.E. Creasy, <u>J. Electroanal. Chem.,</u> (1988), <u>243,</u> 209.

80. B.R. Shaw and K.E. Creasy, <u>Anal. Chem.,</u> (1988), <u>60,</u> 1241.

81. J. Park and B.R. Shaw, <u>Anal. Chem.,</u> (1989), <u>61,</u> 848.

82. L.D. Bowers and P.W. Carr, <u>Anal. Chem.,</u> (1976), <u>48,</u> 544A.

83. J. Wang, L.H. Wu, Z. Lu, R. Li and J. Sanchez, <u>Anal. Chim. Acta,</u> (1990), <u>228,</u> 251.

84. M. Umana and J. Waller, <u>Anal. Chem.,</u> (1986), <u>58,</u> 2679.

85. <u>Kodak Laboratory and Research Product News,</u> Eastman Kodak, Rochester, New York, 1988.

86. T. Gennett and W.C. Purdy, <u>Anal. Chem.,</u> (1990), <u>62,</u> 2155.

87. J. Wang and T. Golden, <u>Anal. Chem.,</u> (1989), <u>61,</u> 1397.

88. J. Wang and Z. Taha, <u>Electroanalysis,</u> (1990), <u>2,</u> 383.

89. J. Wang and Z. Lu, <u>J. Electroanal. Chem.,</u> (1989), <u>266,</u> 287.

90. L.D. Mell and T.J. Maloy, <u>Anal. Chem.,</u> (1975), <u>47,</u> 299.

91. L. Gorton, <u>Anal. Chim. Acta,</u> (1985), <u>178,</u> 247.

92. P.N. Bartlett and R.G. Whitaker, <u>J. Electroanal. Chem.,</u> (1987), <u>224,</u> 37.

93. J.F. Castner and L.B. Wingard, <u>Biochemistry,</u> (1984), <u>23,</u> 2203.

APPENDIX A: PUBLICATIONS

1. Electrocatalysis and flow detection of alcohols at ruthenium dioxide-modified electrodes, D. Leech, J. Wang and M.R. Smyth, Electroanalysis, (1991), 3, 37.

2. Electrocatalytic detection of streptomycin and related antibiotics at ruthenium dioxide modified graphite-epoxy electrodes, D. Leech, J. Wang and M.R. Smyth, Analyst, (1990) 115, 1447.

3. One step fabrication of glucose sensors based on entrapment of glucose oxidase within poly(ester-sulfonic acid) coatings, J. Wang, D. Leech, M. Ozsoz, S. Martinez and M.R. Smyth, Anal. Chim. Acta, (1991), 245, 139.

4. Polishable glucose sensors based on ruthenium dioxide-modified graphite-epoxy electrodes, D. Leech, J. Wang and M.R. Smyth, Anal. Proc., submitted.

5. The effect of the composition of the polymer-backbone on some spectroscopic and electrochemical properties of ruthenium(II) bis(2,2'-bipyridyl) containing 4-vinylpyridine/styrene copolymers, D. Leech, R.J. Forster, M.R. Smyth and J.G. Vos, J. Mats. Sci., (1991), 1, 629.

6. The optimisation and application of 4-vinylpyridine/styrene copolymers containing a coordinated ruthenium(II) bis(2,2'-bipyridyl) metal centre to the stable electrocatalyic detection of nitrite in flowing solutions, D. Leech, M.R. Smyth and J.G. Vos, to be submitted.

7. Voltammetric and amperometric sensors, D. Leech, M.R. Smyth and J.G. Vos, Sensors and Signals, D. Diamond (Ed.), Wiley and Sons, London, Chapter 3, manuscript in preparation.

A1